STRUCTURE AND FUNCTION OF POTASSIUM AND CALCIUM CHANNELS

Louisa Rebecca Stevens

Submitted in accordance with the requirements for the degree of Doctor of Philosophy

The University of Leeds

School of Biomedical Sciences

July 2005

Acknowledgements

I would first like to thank Prof. Dennis Wray for his supervision and encouragement during the course of my studies. I would also like to thank Drs. Malcolm Hunter, Dan Donnelly, Asipu Sivaprasadarao and Debra Gawler for their expert assistance during the course of this work, and the many people in the department whom I have regularly got support and assistance from. I would also like to thank the BBSRC and the University of Leeds for financial support throughout the duration of this work.

Special thanks go to my husband and family for their encouragement, love, putting up with the tantrums, support, (and proof-reading!) over the many years. A thanks also goes to the members of the lab past and present (especially Kate, Min and Emma) that have given me endless support, laughter and encouragement for many, many hours. I could not have done this without any of you.

Abstract

In this thesis, potassium channels human Kv2.1 and rat Kv2.1, along with calcium channels $Ca_v1.2$, $Ca_v3.1$, and chimeras have been studied. These channels were expressed in *Xenopus* oocytes for electrophysiological experiments using two-electrode voltage clamp. For protein expression studies, DNA was expressed in BL21 or COS-7 cells and purified using glutathione or an ID4 affinity column.

Firstly, the roles of the N- and C- terminal domains in the activation kinetics of rat and human forms of Kv2.1 were investigated. A mutant in the N- terminal domain and chimeras between the rat and human forms were constructed. All clones were expressed in *Xenopus* oocytes and activation times obtained. The results suggested that key residues in the N- and C- terminal domains are involved in determining the activation kinetics of rat and human Kv2.1.

Further experiments were carried out using GST fusion proteins, Biacore surface plasma resonance, and FRET investigations. These confirmed that the N- and C- terminal domains are important in determining activation kinetics, and that these regions interact.

To determine the positions of both the N- and C- terminal domains in the folded channel, rat Kv2.1 and a C-terminal deleted protein were expressed, purified, and shown to have correct protein folding. These samples were sent for electron microscopy experiments and a preliminary picture obtained.

No studies of S4 movement in calcium channels have been reported previously. Cysteine residues were substituted into the domain I S4 of a calcium channel chimera (with domain I of $Ca_v3.1$ replaced by $Ca_v1.2$). Cysteine residues at positions 263, 265, 266, 268, 269 and 271 were characterized by electrophysiology. Cysteine mutants at residues 263, 265, 266 and 268 reacted when extracellular PCMBS was applied, but mutants at residues 269 and 271 did not. This suggests that under depolarising conditions the S4 segment is exposed to the extracellular environment up to and including residue 268, with residues 269 and 271 remaining buried. Further investigation of residue 263 indicated that this movement occurs at potentials more negative than the resting membrane potential of -80mV. The data suggests that under depolarisation, the S4 becomes exposed to the extracellular solution and this movement of the S4 occurs before the ionic flow.

Contents

Chapter 2. Materials and methods

List of figures

Chapter 1.

Chapter 2.

Chapter 3.

Chapter 4.

Chapter 5.

Chapter 6.

List of tables

Chapter 1.

Chapter 2.

Chapter 5.

Abbreviations

µA	microamps
AS	anti-sense
ATP	adenosine 5'triphosphate
BK	large conductance K_{Ca} channel
bp	base pair
°C	degrees centigrade
CFP	cyan fluorescent protein
cGMP	cyclic GMP (nucleotide of guanosine)
CNG	cyclic nucleotide gated
cRNA	complimentary ribonucleic acid
CTA	residues 740-853 in Kv2.1
DEPC	diethyl pyrocarbonate
DNA	deoxyribonucleic acid
DTT	dithiothreitol
EAG	ether-a-go-go channel
EDTA	ethyldiamine tetra-acetate
elk	eag-like channel
EM	electron microscopy
FRET	fluorescence resonance energy transfer
g	gram
GMP	guanosine monophosphate
GST	glutathione S-transferase
HEPES	N-2-hydroethyl piperazine-N'-2-thane sulphonic acid
hKv2.1	human Kv2.1
HVA	high voltage activated
Hz	Hertz
IK	intermediate conductance K_{Ca} channel
IPTG	isopropyl-β-D-galactopyranoside

I/V	current-voltage
k	slope parameter (Boltzmann)
KCNQ	a voltage gated channel family
kDa	kiloDalton
kHz	kiloHertz
Kir	inward rectifier potassium channel family
Kv	voltage-gated potassium channel family
LB	Luria-Bertani liquid broth
LVA	low voltage activated
M	molar
μM	micromolar
MΩ	megohm
mg	milligram
min	minutes
mM	millimolar
ml	millilitre
ms	milliseconds
MTSET	methanethiosulphonate ethyl trimethyl ammonium
mV	milliVolt
P	pore region
PAGE	polyacrylamide gel electrophoresis
PBS	phosphate buffered saline
PCMBS	parachloromercuribenzenesulphonate
PCR	polymerase chain reaction
rKv2.1	rat Kv2.1
RNA	ribonucleic acid
rpm	revolutions per minute
S	sense or Siemens
s	seconds
SDS	sodium dodecyl sulphate
SK	small conductance K_{Ca} channel

SNAREs	soluble N-ethyl-maleimide sensitive attachment proteins
T1	tetramerisation domain
TAE	tris acetate EDTA buffer
TASK	twik-related acid-sensitive K channel family
TM	transmembrane
Tris	2-amino-2-(hydoxymethyl)-1, -3-propanediol
TRP	transient receptor potential K channel
TWIK	tandem pore, weak inward rectifier K channel family
UV	ultra violet
V	Volts
$V_{0.5}$	potential for half-maximal activation
YFP	yellow fluorescent protein
YT	yeast tryptone liquid broth

Amino acid abbreviations

Amino acid	One-letter abbreviation	Three-letter abbreviation
Alanine	A	Ala
Cysteine	C	Cys
Aspartate	D	Asp
Glutamic acid	E	Glu
Phenylalanine	F	Phe
Glycine	G	Gly
Histidine	H	His
Isoleucine	I	Ile
Lysine	K	Lys
Leucine	L	Leu
Methionine	M	Met
Asparagine	N	Asn
Proline	P	Pro
Glutamine	Q	Gln
Arginine	R	Arg
Serine	S	Ser
Threonine	T	Thr
Valine	V	Val
Tryptophan	W	Trp
Tyrosine	Y	Tyr

CHAPTER 1

GENERAL INTRODUCTION

1. Introduction

Ion channels are situated in the membranes of cells and selectively allow a particular ion to pass through them, from one side of the membrane to the other. All are composed of protein molecules and contain a central aqueous pore that can be opened by conformational change, to allow the flow of ions.

Studies by Hodgkin and Huxley on the action potential of the squid giant axon provided a mathematical description of the flow of sodium and potassium ions through the membrane (Hodgkin and Huxley, 1952). Currents produced by ion movement were observed, and Hodgkin and Huxley proposed that ionic movement was localized at particular sites that later became known as ion channels.

Ion channels have an important range of functions, which include the determination of the resting membrane potential, and modulation of neurotransmitter release. The movement of Na^+, K^+, Ca^{2+} and Cl^- through their respective ion channels controls electrical signalling and excitation in the nervous system. These ion channels are all important for maintaining proper cellular functions.

1.1 Potassium channel families

Potassium channels are broadly diversified and contribute to many tasks; for instance they may depolarize or polarize the cell, set the resting membrane potential, and alter the function of the cell (Hille, 2001).

The potassium channel family can be divided into voltage gated, calcium activated, inward rectifier, tandem pore, and ligand-gated sub-families. The different potassium channel types are defined and distinguished by their selectivity to potassium, their structure, gating and pharmacological characteristics. A brief outline of the different types of potassium channel families follows in this section.

1.1.1 Inward rectifier (Kir) and bacterial (KcsA) potassium channels – two transmembrane domains

For the Kir inward rectifying potassium channel family, the inward flow of potassium ions is greater than the outward flow (Nichols and Lopatin, 1997). The channels' main function is to stabilise the resting membrane potential, and they are essential in cells that have action potentials with long plateaus. For instance in cardiac cells, they enable cardiac repolarisation thus maintaining the resting membrane potential (Zitron *et al,* 2004).

Six sub-families have been identified; Kir1 to Kir6, which have a structure as shown (Fig. 1.1). They comprise two transmembrane domains (M1 and M2) linked by a conserved pore domain, and intracellular N- and C- terminal domains (Bichet *et al,* 2003). Four monomers assemble to form functional Kir channel tetramers (Abraham *et al,* 1999).

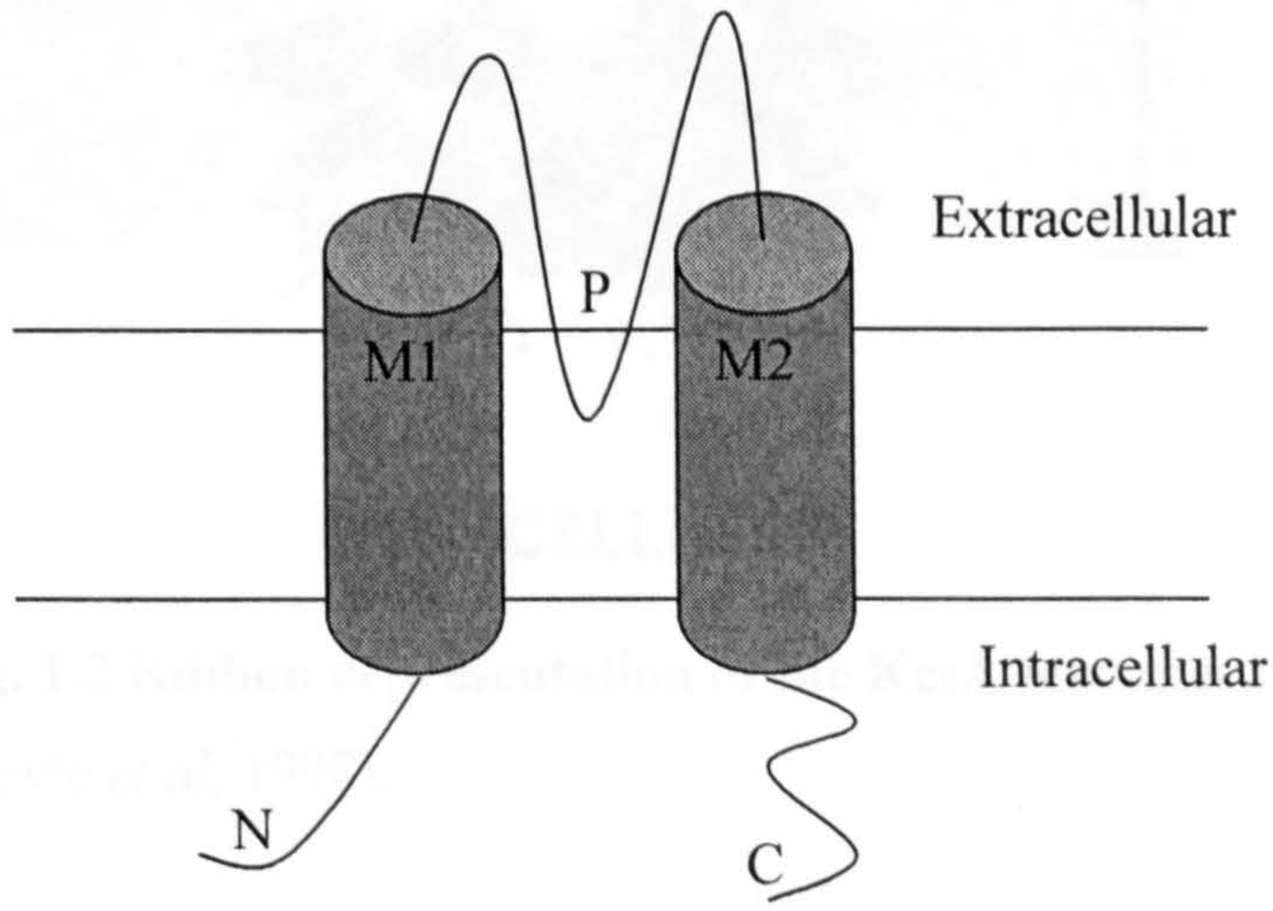

Fig. 1.1 Schematic diagram of a potassium channel with two transmembrane domains. The pore region (P) is labelled.

Another channel family that has two transmembrane domains is the bacterial channel KcsA of the eubacterium, *Streptomyces lividans*. The crystal structure has been solved by MacKinnon's laboratory (Doyle *et al,* 1998), and the gene encodes a two transmembrane domain potassium channel of only 160 residues. This structure was important, as it was the first structural view of an ion

channel. The crystal structure revealed a highly ordered compact structure where a functional channel is a tetramer, typically of four identical subunits (Doyle *et al,* 1998). The pore region is similar with that of *Shaker* and other potassium channels, with residues –TVGYG- lining the pore.

The structure (Fig. 1.2) was found to possess four pore helices, which point towards the centre of the cavity. This ensures that the potassium ion remains in the correct trajectory when the channel is in the open state (Doyle, 2004).

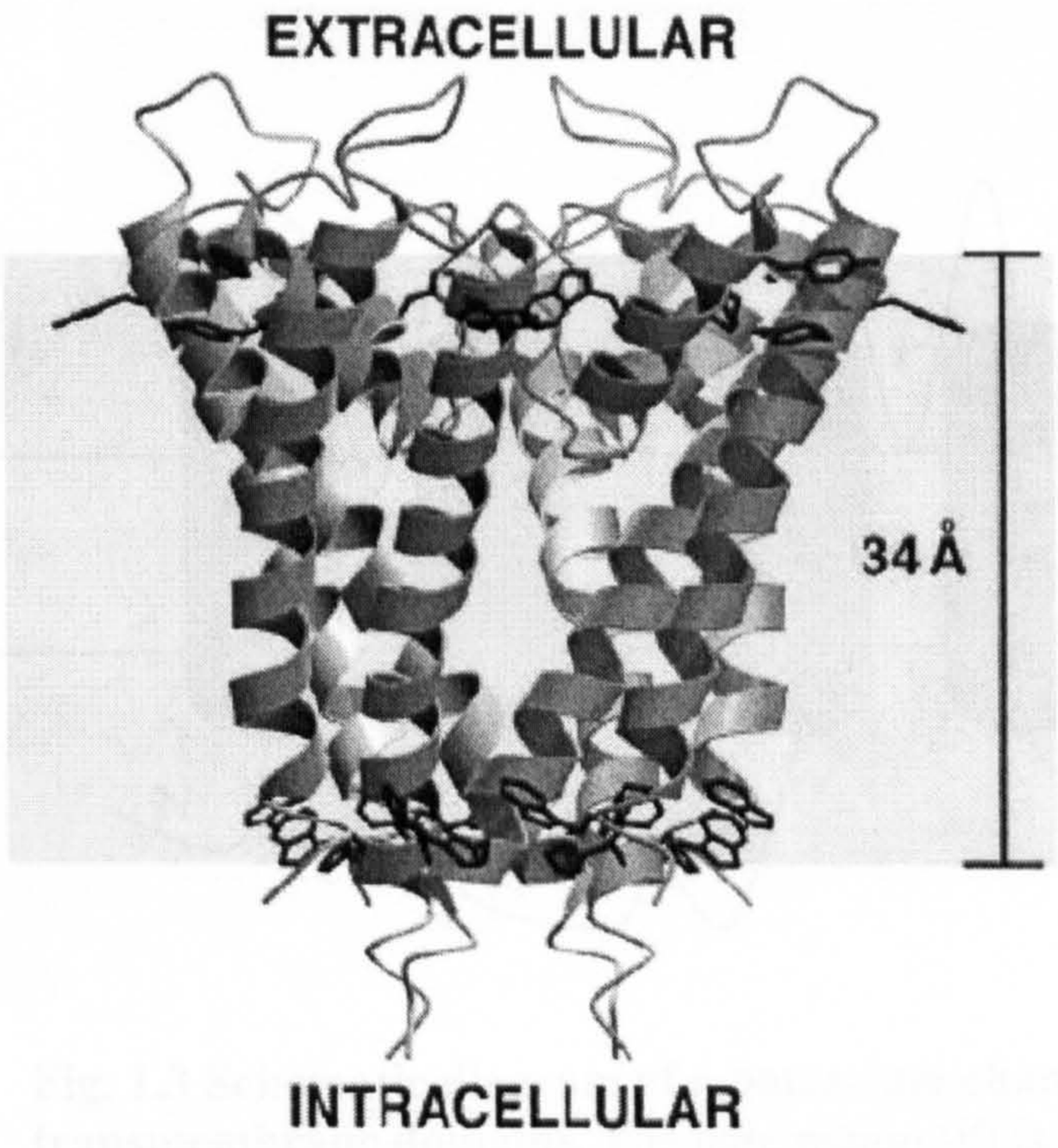

Fig. 1.2 Ribbon representation of the KcsA tetramer.

(Doyle *et al,* 1998).

Opening of this channel *in vivo* occurs upon lowering of the pH on the intracellular side (Heginbotham *et al,* 1999), although the channel does also show weak voltage dependence.

1.1.2 Tandem pore potassium channels (TWIK) – four transmembrane domains

Tandem or twin pore potassium channels were cloned only recently. Study of the *C. elegans* genome has revealed that this family of proteins is more diverse than previously imagined (Salkoff and Jegla, 1995). The potassium channel monomers have four transmembrane domains and two pore regions, and assemble as functional dimers (Fig. 1.3).

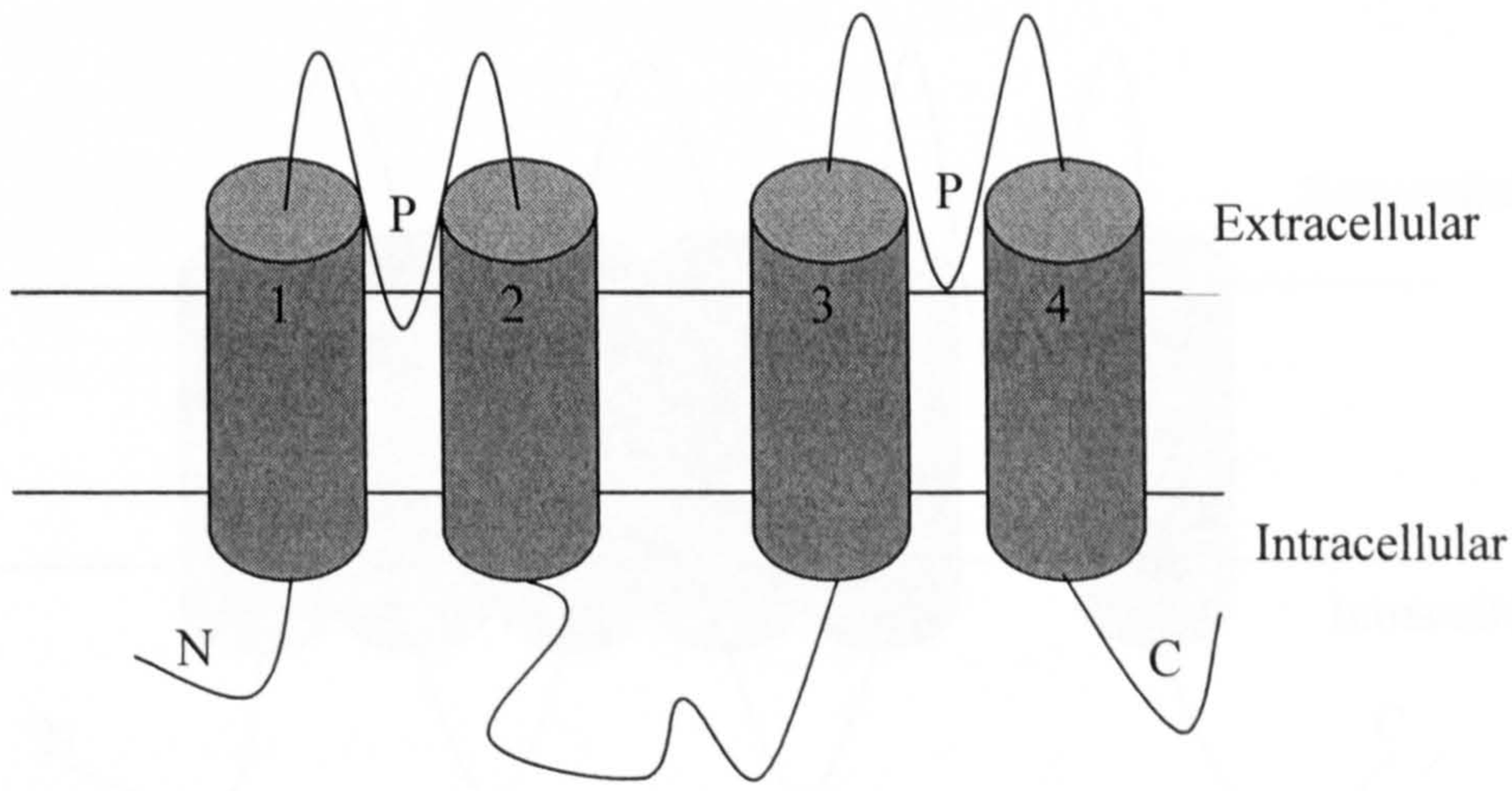

Fig. 1.3 Schematic diagram of a potassium channel with four transmembrane domains. The pore region (P) is labelled.

Twin pore channels have small rectification but no voltage dependent gating, as they lack a voltage-sensing domain, and can exhibit inwardly (TWIK), or outwardly (TASK) rectifying currents (Hille, 2001). Some of these channels are sensitive to second messenger signal or to changes in pH.

The physiological role of twin pore channels is not as yet clear, but it is thought that they may have a role in setting the resting membrane potential (Brown, 2000). It is known that they are opened by anaesthetics, leading to depressed brain activity under general anesthesia (Sirois *et al,* 2000).

1.1.3 Kv, KCNQ, EAG, CNG, TRP potassium channels - six transmembrane domains

Several sub-families with six transmembrane domains have been defined. These include Kv channels, (which will be discussed in section 1.2), KCNQ, EAG, CNG and TRP sub-families. All have a common structure including intracellular N- and C- termini, as can be seen in Fig.1.4.

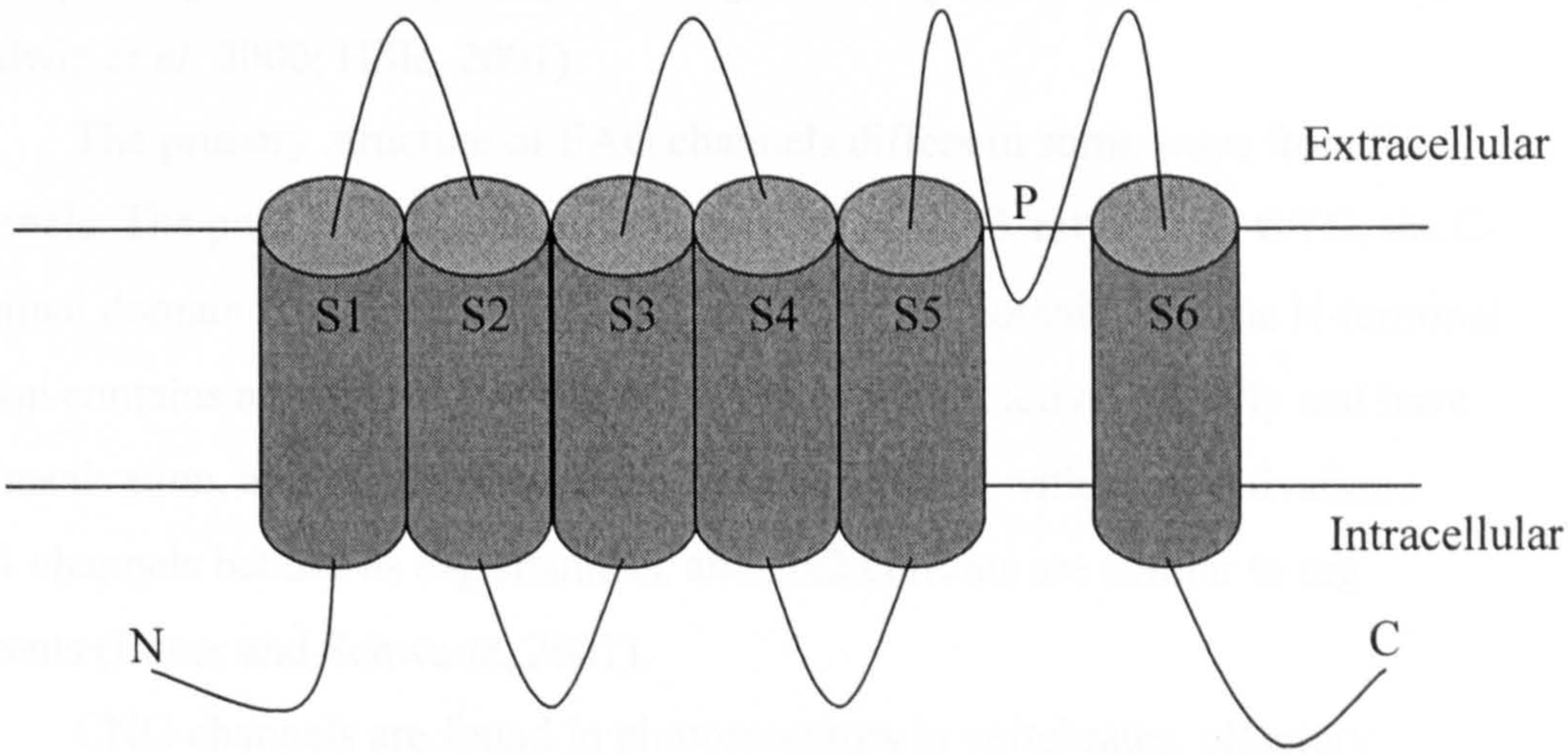

Fig. 1.4 Schematic diagram of a potassium channel with six transmembrane domains. The pore region (P) is labelled.

KCNQ channels are voltage gated, show outward rectification, and do not inactivate. The first member of this family to be cloned was KCNQ1, which was isolated by gene mutations which give rise to the long QT syndrome (Wang *et al*, 1996; Sanguinetti *et al*, 1996; Ashcroft, 2000). These channels differ from Kv channels by the lack of the tetramerisation domain that is known to mediate subunit association (see section 1.2.3), and interact with accessory subunits such as MinK (Yamada *et al,* 2002). Five members of this family have been cloned, KCNQ1, KCNQ2, KCNQ3, KCNQ4 and KCNQ5. mRNA for KCNQ1 channel is distributed strongly in the heart and brain with lower levels in the placenta, pancreas, gastrointestinal tract, kidney, ear and lung (Ashcroft, 2000; Dedek and

Waldegger, 2001; Yamada *et al,* 2002). KCNQ2, and KCNQ3 channels have distributions that largely overlap, being widely distributed in the brain (Yang *et al*, 1998; Ashcroft, 2000; Robbins, 2001). KCNQ4 channels are found largely in the auditory pathway (Kharkovets *et al*, 2000; Wong *et al,* 2004), and KCNQ5 are found mostly in the central nervous system (Robbins, 2001; Yus-Najera *et al*, 2003).

EAG potassium channels were discovered following the isolation of mutant fruit flies which shook their legs when exposed to ether; the gene responsible was called the ether-a-go-go gene (Drysdale *et al,* 1991). Other genes isolated subsequently have been sub-classified into three subfamilies; eag (eag1 and eag2), eag-related (erg1, erg2, and erg3) and eag-like (elk1, elk2 and elk3) (Ludwig *et al,* 2000; Hille, 2001).

The primary structure of EAG channels differs in some ways from Kv channels. The pore contains the structural motif of GFG, rather than GYG, the C-terminal domain contains a cyclic-nucleotide binding domain, and the N-terminal region contains a so-called PAS domain. Eag channels activate slowly and have no inactivation, and erg channels have fast inactivation with slow activation. Elk1 channels behave as eag channels, and elk2 currents are similar to erg currents (Bauer and Schwartz, 2001).

CNG channels are found in photoreceptors in vertebrates, olfactory neurones, cardiac cells and the kidney (Kaupp, 1995). In the eye, they are responsible for the flow of ions in the dark, and they open in the presence of intracellular cGMP which binds the C- terminal domain (Kaupp *et al,* 1989). These channels also form tetramers, (resembling Kv channels), of two homologous subunits, α and β. Both the forms together are able to form functional channels, with characteristics of the native channel (Broillet and Firestein, 1997). Native channels are cyclic-nucleotide gated, and sodium and potassium selective; these channels only discriminate slightly between these ions. The channels are also permeable to calcium but this ion also acts as a blocker of monovalent ions (Ashcroft, 2000).

The TRP extended family comprises many channels found in flies, worms, and mammals. The first member to be cloned was discovered in a mutant *Drosophila melanogaster* whose photoreceptors failed to maintain a response to a stimulus of light (Minke, 1977). In specialised cells, they participate in vision,

hearing, temperature, pain, and pheromone perception (Clapham, 2003). TRP proteins can be classified into three sub-families: TRPM, TRPV, and TRPC (Gudermann and Flockerzi, 2005). More than 100 TRP protein sequences are present in database sets from *Dictyostelium discoideum*, *D. melanogaster*, *C. elegans*, and mammals, although the physiological roles for most of the channels are not known (Padinjat and Andrews, 2004). Interestingly the S4 region does not contain charged amino acids proposed to be required for the voltage sensor in voltage gated channels (Wes *et al*, 1995).

1.1.4 Calcium activated potassium channels (BK, SK and IK) – seven transmembrane domains

This family of potassium channels are structurally similar to voltage-gated six transmembrane channels, but have an extra transmembrane domain on the N-terminal side of the channel (Fig. 1.5; Vergara *et al,* 1998). Channels in this family are sensitive to calcium, where an increase in intracellular Ca^{2+} ions causes the channel to open. They are also activated by depolarisation.

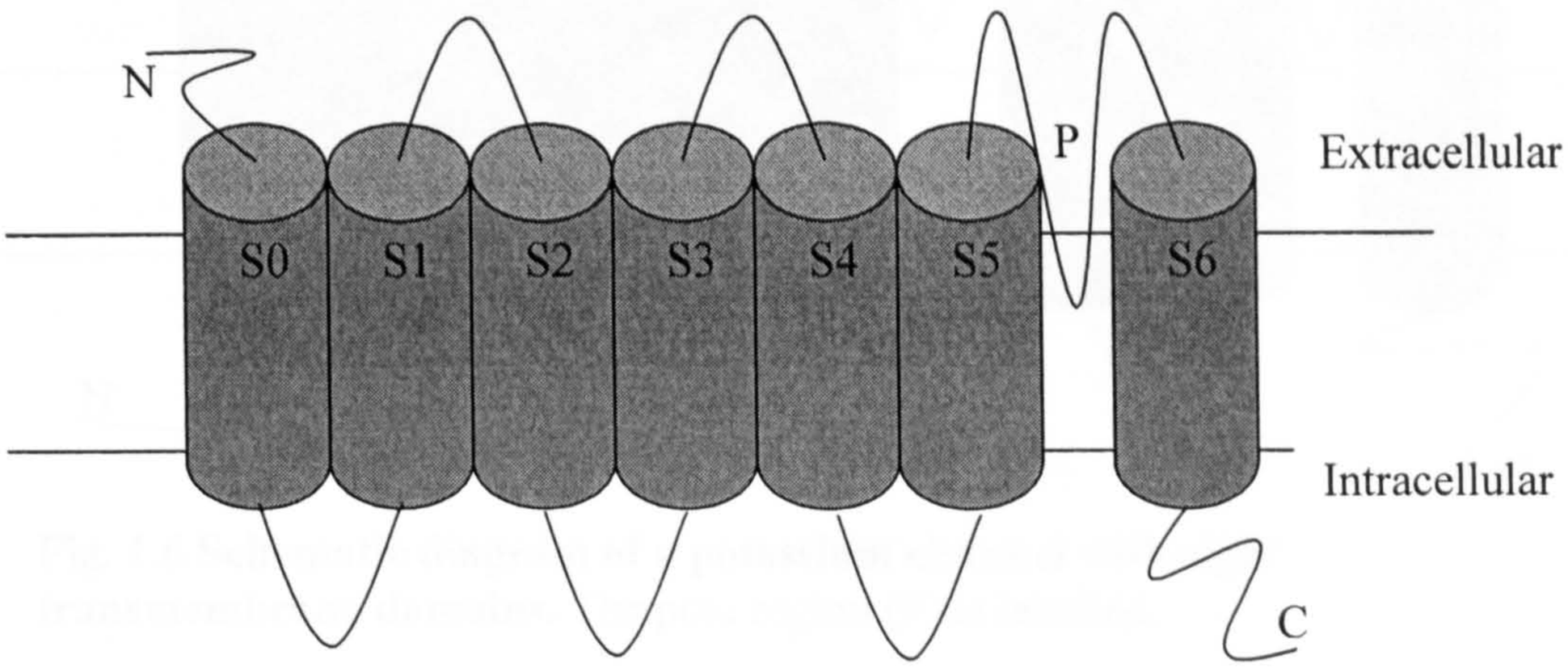

Fig. 1.5 Schematic diagram of a potassium channel with seven transmembrane domains. The pore region (P) is labelled.

This family comprises three subfamilies, SK (which have small conductance), IK (with intermediate conductance), and BK (with big

conductance). They are found in many tissues, including neurons, where they are thought to be involved in regulation of the frequency of action potentials, in β-cells of the liver where they are involved in both hormone secretion, and in depolarisation of the membrane after depolarisation (Wu, 2003; Yost, 1999).

1.1.5 Yeast TOK potassium channels – eight transmembrane domains

The eight transmembrane channel of yeast is one of its few channels serving a role in K^+ transport. It has a structure as shown below (Fig. 1.6), which contains two pore domains in each subunit. The TOK1 channel was identified in *Saccharomyces cerevisae;* it possesses eight predicted transmembrane domains and encodes a non-voltage gated outward rectifier. It has been proposed to function as a potassium selective 'leak' channel involved in the control of the membrane potential (Roberts, 2003).

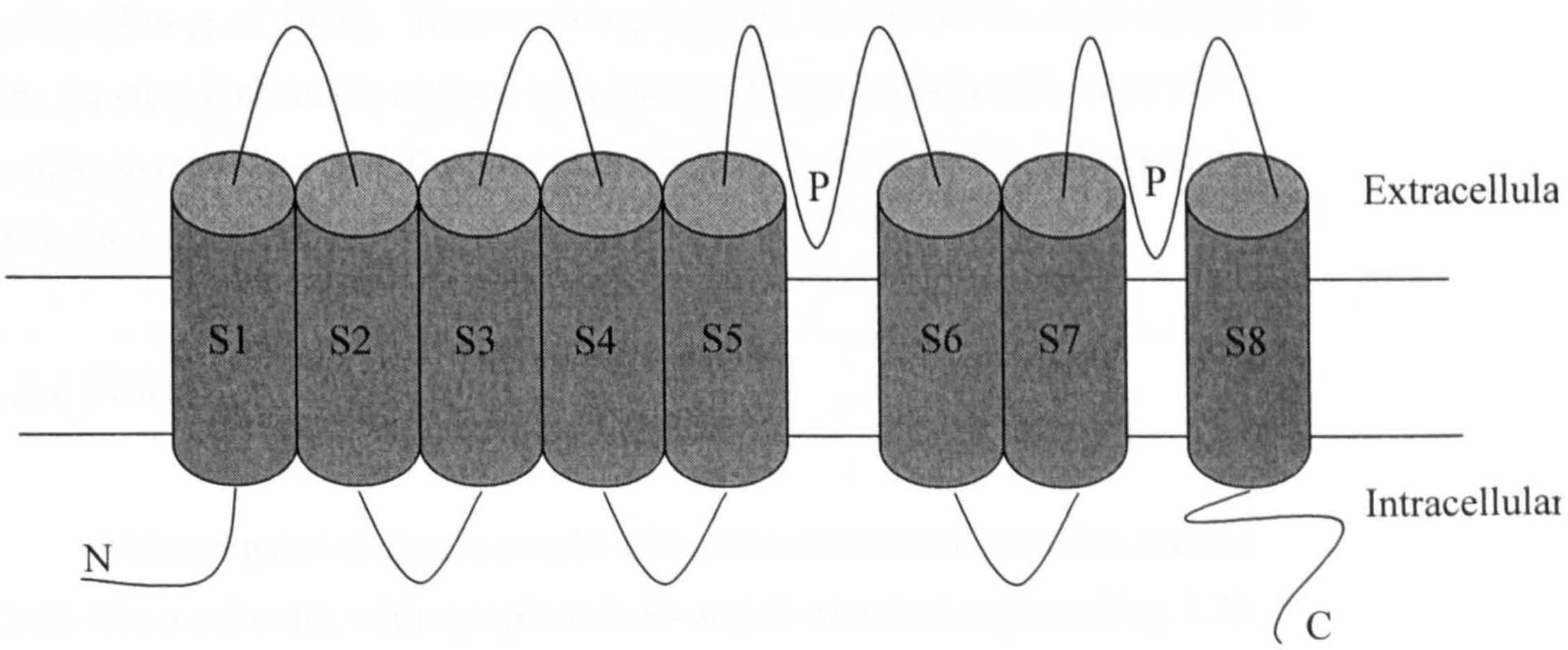

Fig. 1.6 Schematic diagram of a potassium channel with eight transmembrane domains. The pore region (P) is labelled.

This channel conducts an outward current; opening is favoured by low extracellular K^+ and depolarisation. A voltage dependent block is seen with Mg^{2+} ions (Ketchum *et al,* 2002). Again, unusually, the S4 domain contains no charged amino acids.

1.2 Voltage gated potassium channels

Voltage gated potassium or Kv channels activate upon depolarisation of the membrane potential, and deactivate upon repolarisation. They are found in a large number of excitable tissues (MacKinnon, 2003). The first Kv channel was cloned from Drosophila (Kamb *et al,* 1987), and many members of this family have since been cloned and characterised according to their physiological characteristics, and amino acid sequences (Albrecht *et al,* 1993).

The official nomenclature for vertebrate Kv channels is Kv*m.n* where *m* and *n* are numbers denoting families and sub–families respectively. Kv1.1 to 1.8 are *Shaker* related and most activate and inactivate quickly (Dolly and Parcej, 1996). Kv2.1, 2.2, and 2.3 are *Shab* related; they activate and inactivate slowly (Albrecht *et al*, 1993). Kv3.1 to 3.4 are *Shaw* related; they activate slowly, have a fast rate of deactivation upon repolarisation, and show no inactivation (Ruby and McBain, 2001). Kv4.1 and 4.2 are *Shal* related, and activate and inactivate rapidly (Zhu *et al*, 1999). The remaining families, Kv5 to Kv10, do not appear to form functional channels on their own, but can form channels with other sub-families to modulate their function (Kerschensteiner *et al,* 2003; Salinas *et al,* 1997; Sano *et al,* 2002).

1.2.1 Voltage gated channel structure

Voltage gated channels consist of six transmembrane domains, termed S1-S6 (the α subunit), with cytoplasmic N- and C- terminal regions (Fig. 1.7). Four of these α subunits are needed to form a functional channel (reviewed in Mackinnon, 1991). When a tetramer assembles, an aqueous pore is formed by the P loops. Each P loop is approximately twenty amino acids long, and enters (and exits) the membrane from the extracellular side. The P region forms both the selective pore and the outer vestibule (P helix) of the potassium channel. At the N- terminus, the T1 domain is located, which is discussed further below.

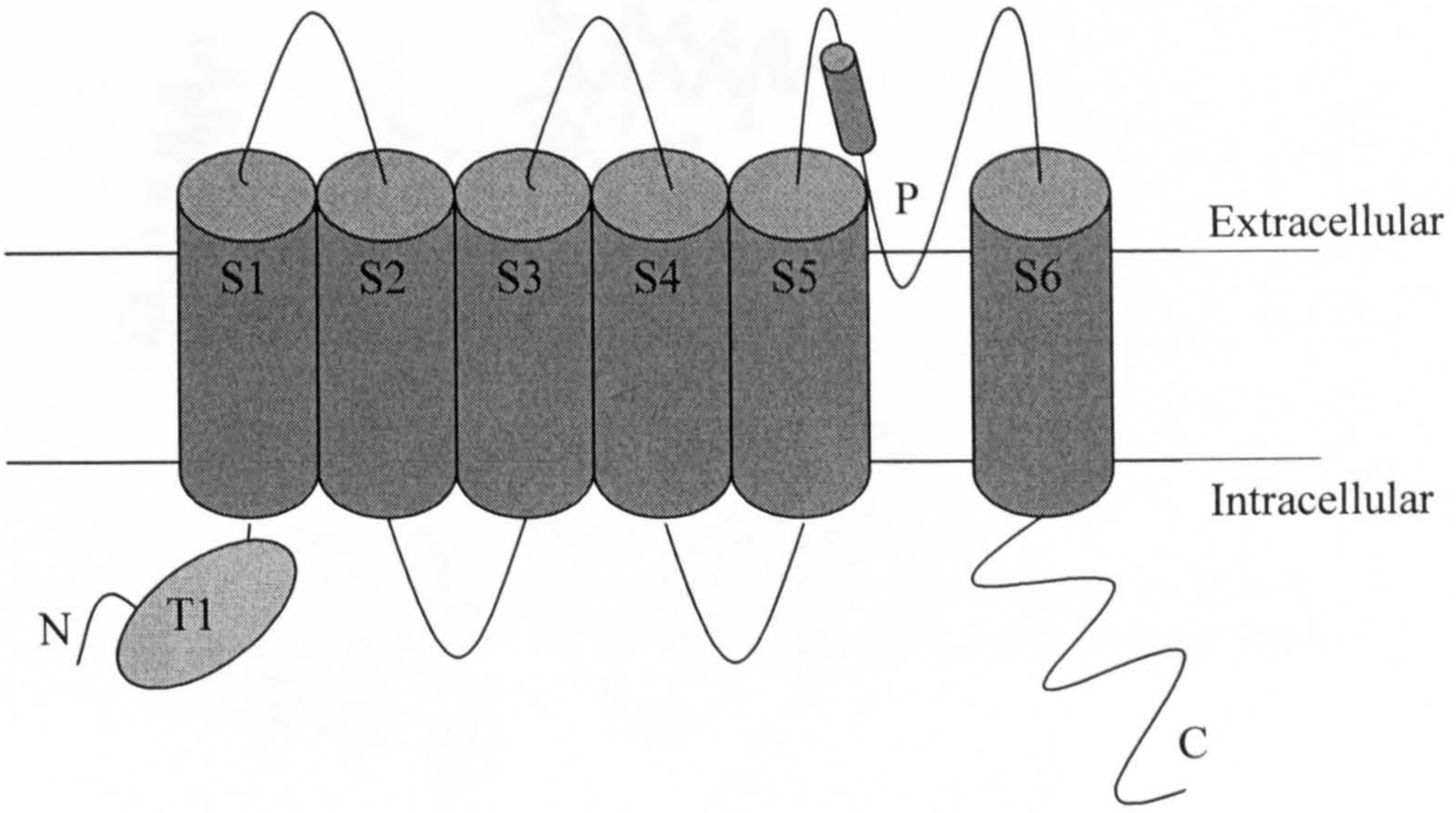

Fig. 1.7 Schematic diagram of an α subunit of a voltage gated potassium channel.

The P region and T1 domain are labelled.

The structure of a voltage gated potassium channel from *Aeropyrum pernix*, KvAP has recently been solved at a resolution of 1.9Å. It can be see from the structure (Fig. 1.8) that the channel contains a central pore surrounded by a voltage sensor (S4) transmembrane domain from each of the four subunits. Although this structure is from an archaebacterium, the channel sequence is closely related to eukaryotic Kv channel sequences. For the pore helices the structure is also similar to the KcsA crystal structure (Fig. 1.2), where the selectivity filter and the pore can be directly superimposed on one another (Jiang *et al,* 2003).

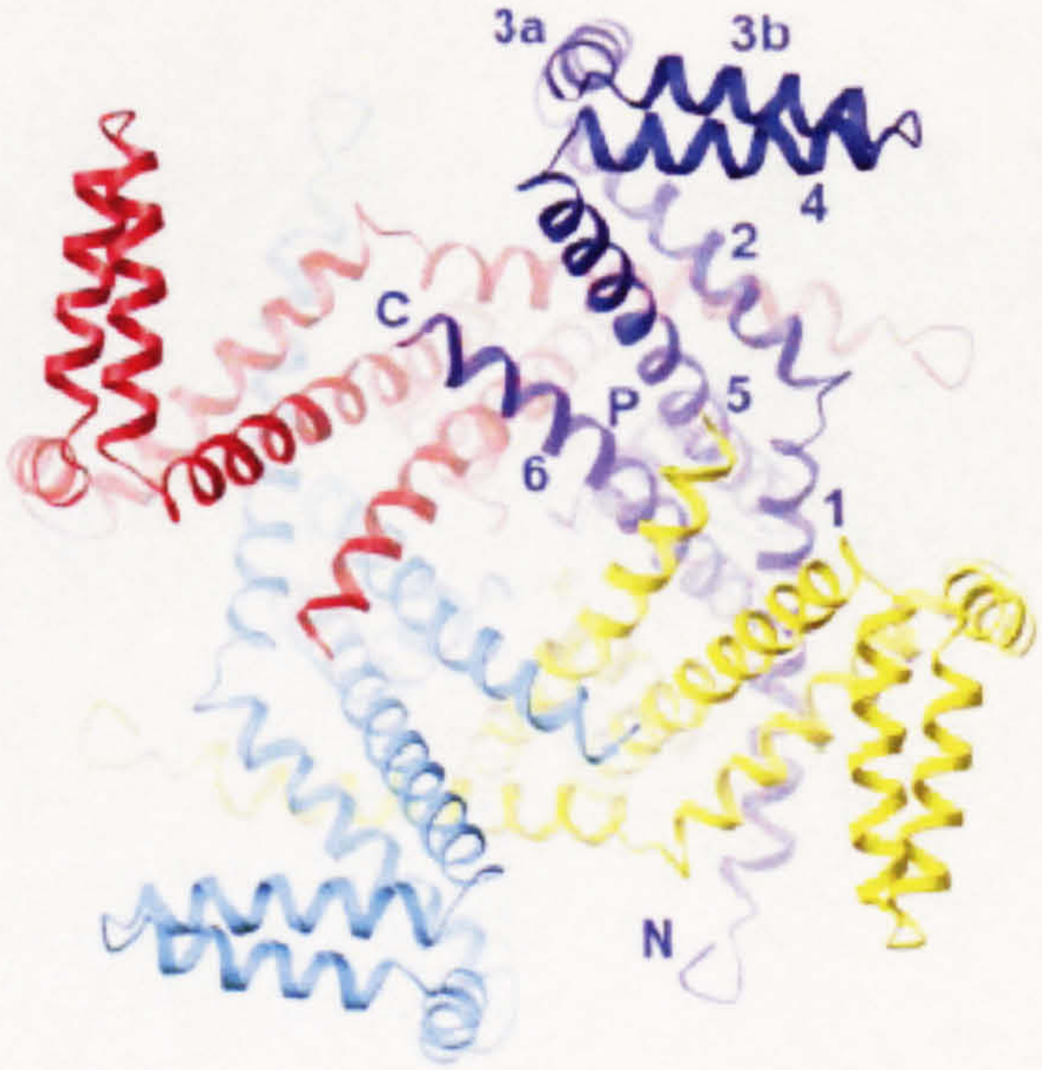

Fig. 1.8 Crystal structure of the KvAP channel, as viewed from the intracellular side of the membrane.
Each subunit is shown as a different colour, with the S1-S6 transmembrane domains and P region labelled. (Jiang *et al,* 2003).

Contained within the P-region is the selectivity filter. Recent work on the KcsA and MthK channels (Jiang *et al*, 2002b) has advanced our structural understanding of this region greatly. The sequence alignment of the P region shows strong sequence conservation at the selectivity filter (TXGYG), and in the inner helix where a conserved glycine in the centre of the helix and five amino acids near the C-terminal end of this region are thought to increase flexibility of the structure. Crystal structures have shown that the GYG signature sequence forms an hourglass shape, with the narrowest part forming the main section of the selectivity filter.

Electron microscope single particle structures have been obtained for *Shaker* (Sokolova *et al,* 2001; Sokolova *et al,* 2003), Kv1 (Orlova *et al,* 2003) and KvAP (Jiang *et al,* 2004) potassium channels. The *Shaker* structure includes the T1 domain discussed further below. It shows a four fold symmetrical structure with a large and small domain linked by connectors (Fig. 1.9, and Sokolova *et al*, 2001). The upper part of the structure shows the membrane spanning regions, and the lower part is the T1 domain. However, the structure of the C- terminal domain has not yet been determined.

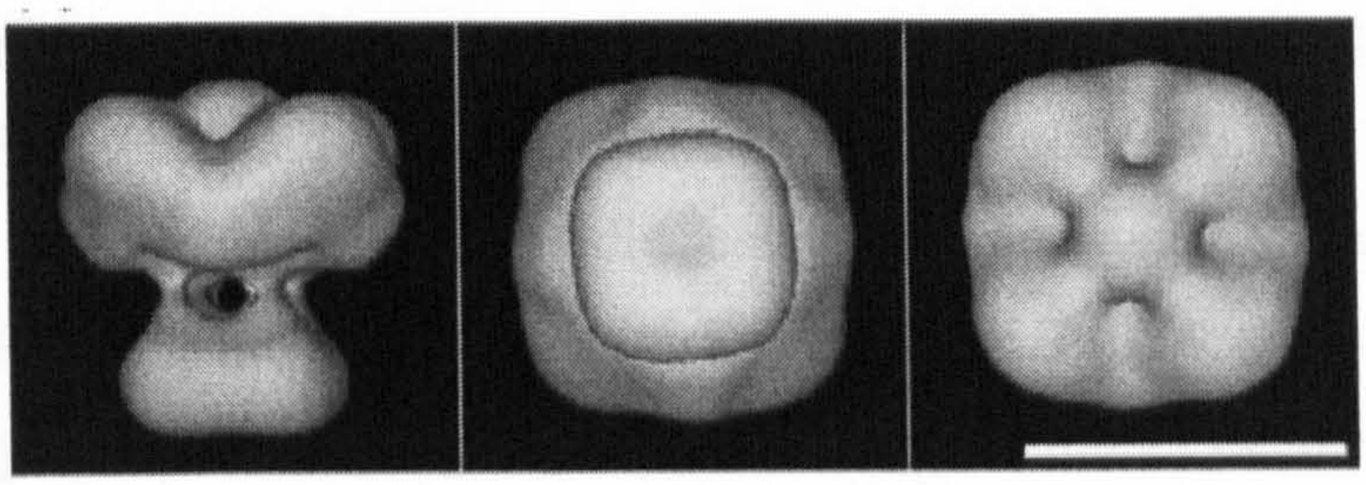

Fig. 1.9 3D structure of the *Shaker* potassium channel.
Three views of the channel in different orientations. The left picture shows the side view, the middle shows the bottom view, and the right picture shows the top view. (Sokolova *et al,* 2001).

No structures have yet been obtained for the potassium channels investigated in this thesis, although an abstract has recently been published of the human Kv2.1 structure (Adair *et al*, 2005).

1.2.2 Voltage sensor and channel gating

Gating mechanisms control the voltage at which channels open and become active. In voltage gated potassium channels, this gating mediates the response to changes in the membrane potential. Hodgkin and Huxley (1952) predicted the existence of gating currents, and that they would occur on activation of a channel by a rearrangement in the voltage sensor. These have been detected as the currents produced by the movement of gating charges prior to the ionic flow (e.g. Fedida and Hesketh, 2001; Bezanilla and Stefani, 1994). In order to demonstrate the relatively small gating currents it is necessary to block the ionic current with toxins, leaving just the gating current. The measurement of these gating currents has been carried out on cloned and native channels in this way.

The S4 domain is thought to be the voltage sensor in voltage gated K^+ channels (reviewed in Bezanilla, 2000). It has positively charged amino acids at every third position in the helix; thus charged residues lie in a stripe within the α helix. The S4 region is highly conserved. Replacement of these positively

charged residues in voltage gated potassium channels with neutral amino acids leads to altered voltage dependence of activation, and in some cases prevents channel formation (Liman *et al*, 1991; Papazian *et al*, 1991; Logothetis *et al*, 1992; Shao and Papazian, 1993; Papazian *et al*, 1995).

S4 accessibility studies using parachloromercuribenzenesulphonic acid (PCMBS) have shown that the S4 domain of *Shaker* moves out of the membrane upon depolarisation. The side chains of substituted cysteine residues react with extracellular PCMBS under depolarising but not hyperpolarising conditions, suggesting a net movement of these residues out of the membrane (Yusaf *et al*, 1996). Others, (e.g. Larsson *et al*, 1996) have used other cysteine binding reagents (e.g. MTSET) with similar results

Analysis of mutant channels that have retained their gating property suggests that upon depolarisation, 12 to 16 charges per channel move across the transmembrane region in *Shaker* (Zagotta *et al*, 1994). Extensive studies of potassium and sodium channels have suggested that the S4 segment rotates as well as moves outwards during depolarisation (Gandhi and Isacoff, 2002; Sheets and Hanck, 2002; Bezanilla, 2002; Glauner *et al*; 1999; Cha *et al*, 1999a; Cha *et al*, 1999b). X-ray crystallography studies have recently been interpreted to propose a paddle-like motion, where a coupling mechanism between the paddle motion of the S3-S4 segments and channel opening has been proposed (Monticelli *et al*, 2004). However, such apparent coupling is likely to be an artefact of distortion due to the channel being co-crystallised with an antibody (Jiang *et al*, 2003; Shrivastava *et al*, 2004).

It is now known that other transmembrane domains are also involved in gating. These include the S2 and S3 domains (Cha *et al*, 1999a; Milligan and Wray, 2000) which are thought to interact with the S4 domain. Neutralising the negative charges in these domains has shown that some residues contribute significantly to the overall gating charge, and so are a major component of the voltage sensor (Planells-Cases *et al*, 1995; Seoh *et al*, 1996). Other recent structural and functional studies in potassium channels have indicated that the intracellular regions also have a fundamental role in channel gating and regulation (Jiang *et al*, 2002; Nishida and MacKinnon, 2002; Kuo *et al*, 2003; Sokolova *et al*, 2003).

1.2.3 T1 domain

Assembly of Kv channels into tetramers is thought to be controlled by the highly conserved T1 or tetramerisation recognition domain. It is located within the intracellular N- terminal region (Fig. 1.7; Kobertz and Miller, 1999). This domain is thought to be attached by thin connectors to the membrane spanning region.

The crystal structure of the T1 domain has been solved in Kv1 and Kv3 families (Bixby *et al*, 1999; Gulbis *et al*, 2000; Kreusch *et al*, 1998). It comprises a rotationally symmetrical tetramer with a small central channel, approximately 20Å in length (Kreusch *et al*, 1998). Fig. 1.10 shows the crystal structure of the T1 domain; the N- and C- termini of each subunit are located at opposite faces of the tetramer. The T1 domain is also though to be the docking region for the β subunit, through which a $T1_4$ β_4 complex can be formed. This complex is orientated with the T1 domains facing the transmembrane pore interacting with the β subunits in the cytoplasm (Gulbis *et al*, 2000).

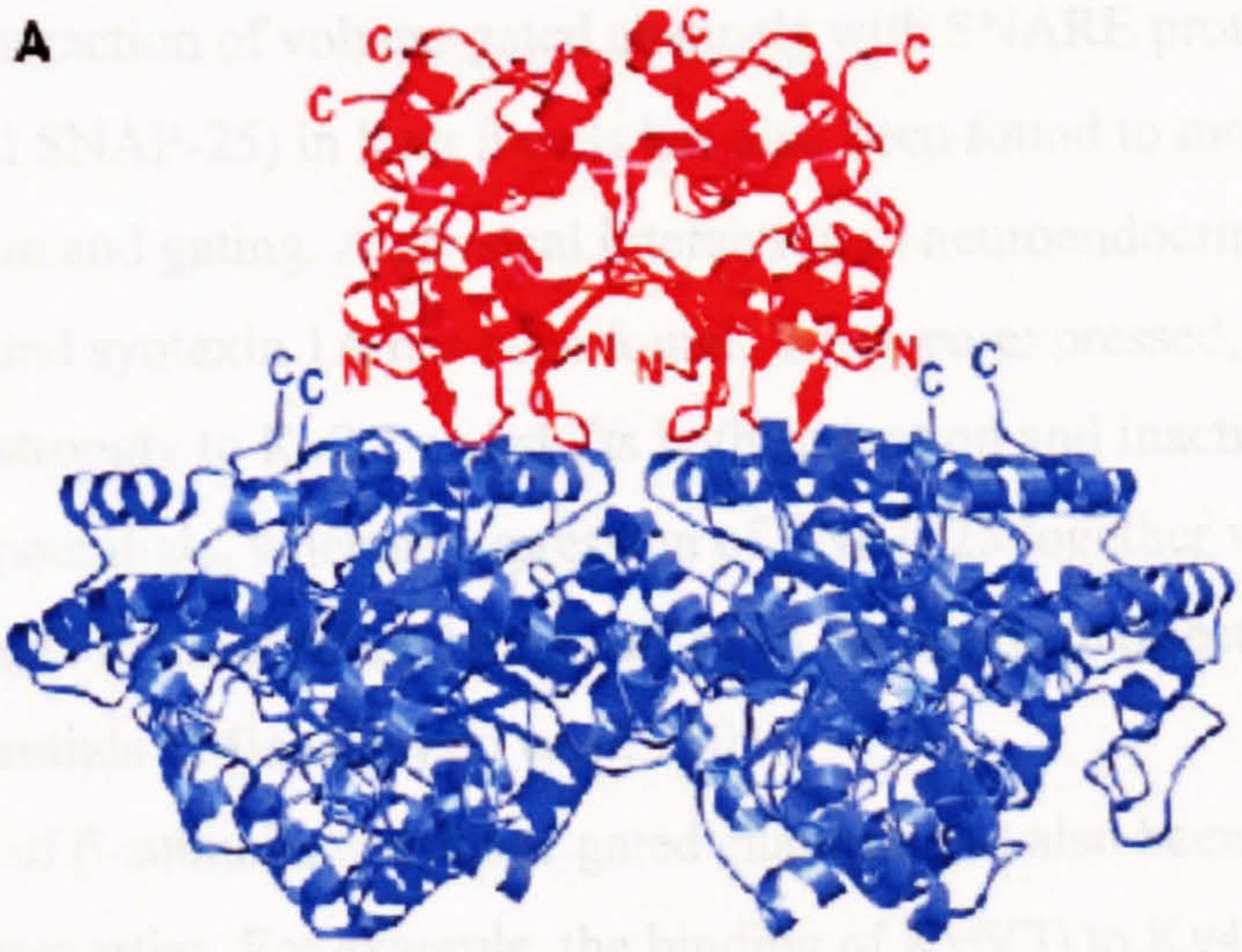

Fig. 1.10 Ribbon representation of the T1 tetramer taken from the side view.
The T1 tetramer is red and the β-tetramer is blue.
(Gulbis *et al*, 200).

Electron microscopy has been used to generate a structure for the *Shaker* channel (as shown in Fig. 1.9) showing a 'hanging gondola' model for this domain, with four strands supporting a hanging basket, and ions reaching the pore of the channel by passing through the four large 'windows' of the basket (Sokolova *et al,* 2001; Sokolova, 2004).

Channels can function when the T1 domain is deleted, so it does not form an essential part of the conducting pore (Kobertz *et al*, 1999). Mutations in the T1 domain lead to a change in voltage sensitivity, suggesting that this domain could participate in conformational changes upon excitation (Choe *et al*, 2002).

1.2.4 Modulation of voltage gated channels

Voltage gated channel current can be modulated in many ways. For example, modulation of Kv2.1 currents is seen when they are co-expressed with Kv10 subunits. When Kv2.1 is expressed in oocytes with Kv10, the Kv2.1 modulated currents are smaller than when expressed alone. Co-expression also causes a slowing of the inactivation rate (deMiera, 2004). Co-assembly of Kv2.1 with Kv9 subunits leads to channels which have sensitivity to intracellular ATP (Patel *et al*, 1997).

Direct interaction of voltage-gated channels with SNARE proteins (syntaxin 1A and SNAP-25) in liver β cells has also been found to modulate channel activation and gating. A physical interaction in neuroendocrine cells between Kv2.1 and syntaxin 1A has been found. When co-expressed, syntaxin 1A alone binds strongly to Kv2.1 and shifts both activation and inactivation to hyperpolarized potentials, whereas expression of SNAP-25 together with syntaxin 1A results in inactivation being shifted to the opposite direction, toward depolarized potentials (Michaelevski *et al*, 2003).

Binding of β-subunits to voltage gated channels has also been shown to affect channel properties. For example, the binding of Kvβ(3) to Kv4.3 increases the current greatly. The β-subunits are hydrophilic and lack any transmembrane domains, and are found on the cytoplasmic side of the cell membrane. Co-localisation *in vivo* has also been demonstrated (Deschenes and Tomaselli, 2002).

Glycosylation of ion channels has been suggested to contribute to efficient cell surface expression (Shi and Trimmer, 1999), with some Kv channels having a single glycosylation site located on the extracellular S1-S2 linker. Glycosylation of voltage gated channels has been demonstrated both *in vivo* and *in vitro* with the extent of processing of N-linked chains on Kv1.1 and Kv1.4, (but not Kv1.2) channels expressed in transfected cells differing from that seen *in vitro*. This may reflect different efficiencies of transport of channels from the endoplasmic reticulum to the golgi apparatus, with glycosylation being important for efficient cell surface expression (Shi and Trimmer, 1999).

Phosphorylation of serine and threonine residues in voltage-gated channels by protein kinases can also alter the function of voltage gated channels. (Murakoshi *et al*, 1997). For instance, this is done by protein kinase A (Wilson *et al*, 1994). Furthermore, both the localization and biophysical properties of Kv2.1 within neurones are affected by phosphorylation, and a link between Kv2.1 phosphorylation and neuronal activity has been shown (Misonou *et al*, 2004).

1.3 Voltage gated potassium channel - Kv2.1

The potassium channel studied in this thesis is Kv2.1. This channel was the first member of the Kv2 family to be cloned, and was first identified through expression cloning from rat brain (Frech *et al*, 1989), with the mouse (Pak *et al*, 1991) and human forms (Albrecht *et al*, 1993) being cloned shortly afterwards. These channels are known to activate slowly and produce outward currents that inactivate slowly.

Kv2.1 is found in a very wide range of excitable tissue. High expression levels have been found in neurons, the heart and lungs, and olfactory, hippocampus and piriform cortex regions of the brain in mammals (Drewe *et al*, 1992; Schultz *et al*, 2001; Coma *et al*, 2002; McCrossan *et al*, 2003; Brunet *et al*, 2004). The human form of the channel is expressed abundantly in the brain, and in pancreatic β- cells.

It has been found that Kv2.1 channel expression can be regulated by nerve growth factor, which has been shown to increase the expression of Kv2.1 channels *in vitro*, and change the distribution *in vivo* (Sharma *et al*, 1993). A

chaperone protein, NFATc3, can regulate Kv2.1 expression in cerebral arterial smooth muscle cells. This is thought to occur through activation of transcription factors, but the exact mechanism is still unclear (Amberg *et al*, 2004).

1.3.1 Kv2.1 structure and function

Like other voltage dependent channels, Kv2.1 has six transmembrane domains and cytoplasmic N- and C- termini, with a T1 domain located within the N- terminus, and a pore region located between transmembrane domains S5 and S6 (Fig. 1.7). It is a delayed rectifier, whose main function is to repolarise the membrane after an action potential.

When an action potential occurs, sodium (and calcium channels if present) are activated, with a subsequent inward flow of their ions. Influx of these ions causes depolarisation of the membrane, which in turn activates potassium channels like Kv2.1. The outward flow of these channels causes repolarisation of the membrane (for review see Hille, 2001).

Kv2.1 is thought to be involved in many important physiological processes. For example, prolongation of the action potential by block of Kv2.1 has been shown to increase intracellular free calcium and to promote insulin release in a glucose-dependent manner in pancreatic β cells (Yan *et al*, 2004). Neuronal apoptosis is mediated by Kv2.1 being the primary exit route for K^+ in neurons undergoing apoptotic cell death (Pal *et al*, 2003).

No human diseases have been associated with Kv2.1, although it is thought that disruption of Kv2.1 channels may cause abnormal action potential firing rates, and durations (Albrecht *et al*, 1993). However, type I diabetic rats show a down-regulation of Kv2.1 expression in the heart, that is thought to cause abnormal heart activity (Qin *et al*, 2001).

1.3.2 Kv2.1 activation

The voltage sensor region S4 has been shown to be important in gating of Kv2.1 (Koopmann *et al*, 1997; Islas and Sigworth, 1999; Scholle *et al*, 2000; Consiglio and Korn, 2004; Scholle *et al*, 2004). Other regions have also been

shown to contribute to Kv2.1 activation; these include the S2 and S3 segments (Milligan and Wray, 2000; Koopmann *et al*, 2001), and the S5 segment (Shieh *et al*, 1997), as well as the N- and C- terminal domains discussed below.

The N- terminal domain has been shown to contribute to channel activation. For instance, native cysteines in this region of Kv2.1 react with cysteine-binding reagents, causing a slowing of activation kinetics. The effect could be prevented by deleting the first 139 amino acids from the N- terminus of the channel (Pascual *et al*, 1997). VanDongen *et al* (1990), also found that the N-terminal domain contributes to activation kinetics, since a deletion of the N-terminal domain caused a slowing of activation kinetics, which was restored when part of the C- terminal domain was deleted also.

Other studies have also shown the C-terminal domain to be involved in channel function. Peptides Synataxin 1A and t-SNARE were found to complex on the C-terminal region of Kv2.1. The effect of these peptides on Kv2.1 was to cause shifts in the steady-state inactivation and activation in the hyperpolarizing direction, and the effects on the inactivation of Kv2.1 were reversed by partial deletions of the C-terminus. These findings suggest that physical interactions of the Syntaxin 1A and t-SNARE complexes with the C-terminus of Kv2.1 are involved in channel regulation (Tsuk *et al*, 2004).

1.3.3 Human and rat forms of Kv2.1

The rat and human forms of Kv2.1 have a high degree of sequence identity, with over 94% of amino acids being identical. All six transmembrane domains are identical and the two forms only differ in their N- and C- terminal domains.

The N-terminal domain is 182 amino acids long in the rat form (four amino acids longer in the human form), and is highly conserved. The additional four residues at the beginning of the sequence in the human form are not thought to contribute to the activation kinetics (Leadbitter, PhD thesis). Major differences occur between the 228 amino acids within the C-terminal domain, with little conservation between the two forms.

Rat Kv2.1 activates around twice as fast as its human counterpart (Ju *et al*, 2003). Because the transmembrane domains have identical amino acids, any differences must be due to the N- and C- terminal domains. It would be interesting to identify key regions within the N- and C- termini that may account for the differing activation kinetics between the two channels.

Physical interactions of the N- and C-terminal regions in an inwardly rectifying potassium channel (Jones *et al*, 2001) have been demonstrated previously. It would therefore also be interesting to determine whether similar interactions occur in rat Kv2.1, and also to solve a structure for this channel.

1.4 Voltage gated calcium channels

Calcium channels are responsible for voltage-gated depolarisations in muscles, and maintain the depolarisation during the plateau of the action potential in heart muscle. Calcium ions also act as intracellular messengers for a wide range of cellular processes, and so calcium channels are involved in many control systems (Hofmann *et al*, 1999).

Calcium channels are found in all excitable cells, and play important roles. They can supply a maintained inward flow of ions, and can serve as a link to transduce membrane depolarisation into all other non-electrical activities controlled by excitation (Hille, 2001).

1.4.1 Classification of voltage gated calcium channels

Voltage gated calcium channels can be split into high and low voltage-activating channels (HVA and LVA respectively). HVA channels require a much larger depolarisation to open, whilst LVA calcium channels open at more negative potentials.

High voltage activating channels can be further classified according to physiological, pharmacological and electrophysiological properties. L- type channels have a large single conductance, and a long lasting current, and are divided into $Ca_v1.1$ to 1.4. Inactivation in L- type channels (high voltage

activating) has been shown to be mediated by the intracellular C- terminal domain, where truncated channels had an increase in expressed current, presumably resulting from removing the inhibitory effect of the C- terminal domain (Wei *et al*, 1994). They are found in cardiac muscle ($Ca_v1.2$, $Ca_v1.3$), skeletal muscle ($Ca_v1.1$), the eyes ($Ca_v1.4$), and smooth muscle ($Ca_v1.2$) to name just a few (Saada *et al*, 2003; Hoda *et al*, 2005; Hulme *et al*, 2005; Qu *et al*, 2005). They have a critical role in the excitation-contraction coupling within these tissues, and are also prominent in many endocrine cells (Mitterdorfer *et al*, 1998). High sensitivity to dihydropyridines such as nifedipine is a defining criterion for L- type classification (Tsien *et al*, 1991; Lipscombe *et al*, 2004). The Ca^{2+} agonist Bay K8644 strongly increases the probability of L-type channel opening (Nowycky *et al*, 1985).

P/Q- type channels comprise $Ca_v2.1$ channels, are sensitive to the toxin ω-AGA IVA and are named P- for Purkinje cells (Llinas *et al*, 1989; Sato *et al*, 2000). They have recently been found to be involved in familial migraine and episodic ataxia type-2 (Guida *et al*, 2001).

N- type channels have an intermediate conductance between T- and L- types, and require strongly negative potentials for complete removal of inactivation (unlike L- type) and strong depolarizations for activation (unlike T- type) (Nowycky *et al*, 1985). They are named N- for neither T or L- type, and are $Ca_v2.2$. These channels have a high sensitivity to, and are irreversibly blocked by, the toxin ω-conotoxin (Sidach and Mintz, 2000).

R- type channels are resistant to ω-conotoxin and ω-AGA IVA, are called R- type for 'resistance' and named $Ca_v2.3$. These types of calcium channels resemble T- type channels, in that both show sensitivity to nickel and voltage dependence of inactivation. However, $Ca_v2.3$ requires stronger depolarisations for channel opening (Perez-Reyes, 2003).

T- type channels have a distinctive rapidly activating low voltage activating current. They also display fast inactivation and have a small conductance and transient current, (being named T for tiny conductance and transient current), and are subdivided into $Ca_v3.1$-3.3 (Klugbauer *et al*, 1999). The S6 transmembrane segment of domain I have previously been shown to be important for the fast inactivation properties of high voltage activated channels (Zhang *et al*, 1994 and Shi *et al*, 2002).

They were first discovered in cardiac myocytes and dorsal root ganglia (Carbone and Lux, 1984; Nilius *et al,* 1985) and have recently been detected in the adrenal and thyroid glands (Monteil *et al*, 2000). T- type channels in the cardiovascular system are thought to mediate a pacemaker action, being found in coronary smooth muscle and atrial pacemaker cells (Cribbs *et al*, 1998). Channels within the T- type sub-family produce firing patterns unique to brain nuclei, suggesting that this sub-family makes contributions to neuronal physiology in the brain (Lee *et al*, 1999; McRory *et al*, 2001).

Table 1.1 shows a summary of the types of calcium channels found in vertebrates.

Table 1.1 Types of calcium channels.

Type	**HVA** L	**HVA** P/Q, N, R	**LVA** T
Structural nomenclature	Ca_v 1.1-1.4	Ca_v 2.1-2.3	Ca_v 3.1-3.3
Dihydopyridine sensitivity	Sensitive	Resistant	Resistant

1.4.2 Structure of voltage gated calcium channels

The main pore forming subunit of calcium channels (α_1) has four homologous domains (I-IV) each consisting of six transmembrane segments (Fig. 1.11).

Fig. 1.11 Schematic diagram of an α_1 subunit of a voltage gated calcium channel.

The α subunit contains binding sites for all of the known blockers, the selectivity filter, the voltage sensor and the ion conducting pore. Other subunits may also associate with the α subunit; intracellular β subunit (which binds to the linker between domains I and II for L- type channels), the $\alpha_2\delta$ dimer (wherein the δ subunit is located with the membrane and the α_2 subunit binds to the extracellular C- terminus of the δ subunit by means of a disulphide bridge; Catterall, 1995; Hofmann *et al*, 1999), and the γ subunit (which binds at the N-terminal end of the α_1 subunit within the membrane) (Fig. 1.12 and 1.13) (Catterall, 1995; Hofmann *et al*, 1999). Co-expression of the β and $\alpha_2\delta$ subunits with the HVA α subunit increases the number of functional channels reaching the plasma membrane, changes the gating rate constants and shifts the midpoints of both activation and inactivation (Hille, 2001). However, for LVA channels, co-expression with the β and $\alpha_2\delta$ subunits do not shift the mid-point of the I/V curves, although they do produce a small increase in current density (Lambert *et al*, 1997; Lacinova *et al*, 1999).

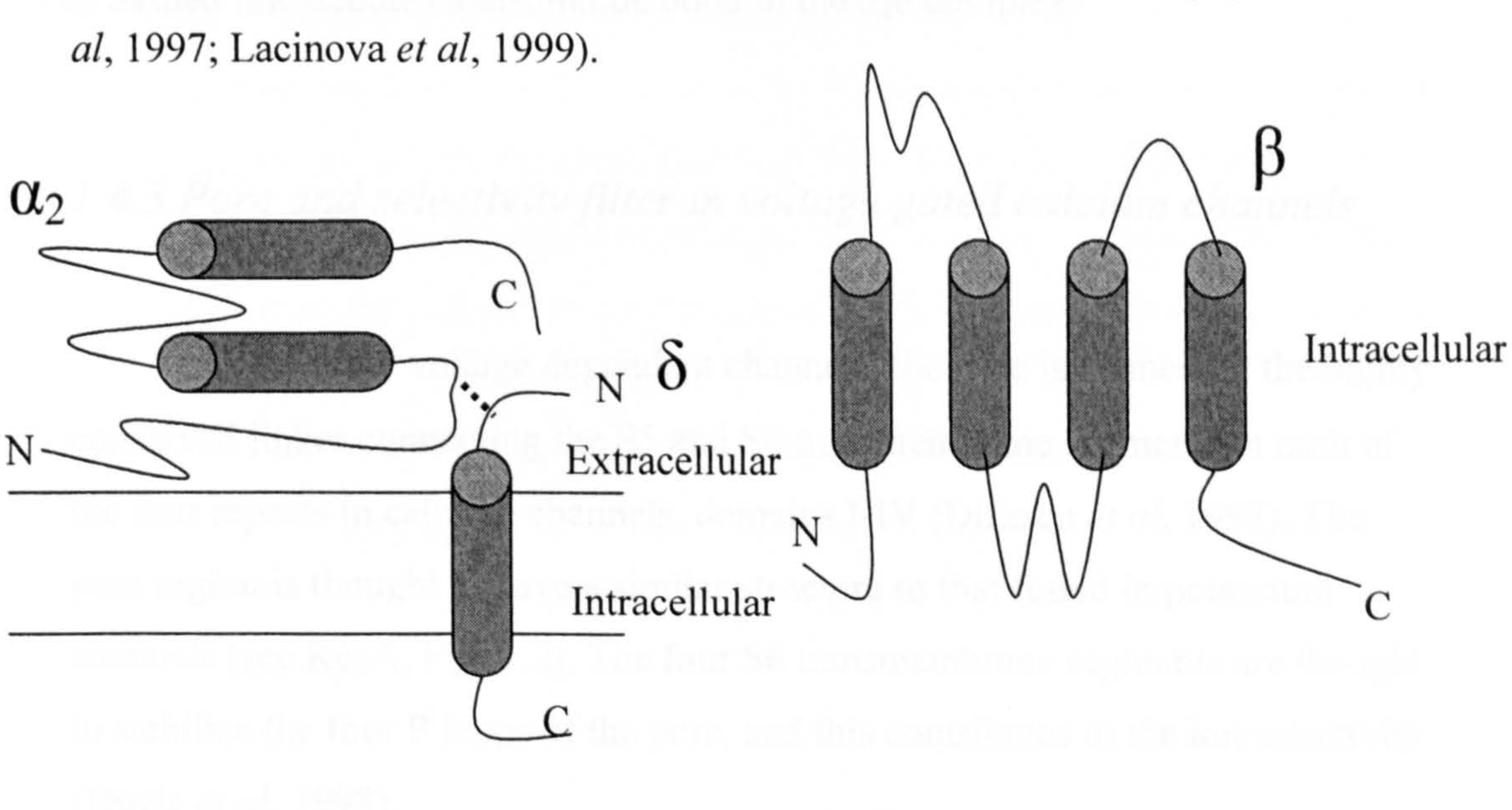

Fig. 1.12 Schematic diagram of $\alpha_2\delta$, β and γ subunits.
$\alpha_2\delta$ family consists of $\alpha_2\delta$1a-e, $\alpha_2\delta$ 2 and $\alpha_2\delta$ 3.
β family consists of β1a-c, β2a-c, β3 and β4.
γ family consists of γ1-4.
The dashed line denotes a disulphide bond in the complex.

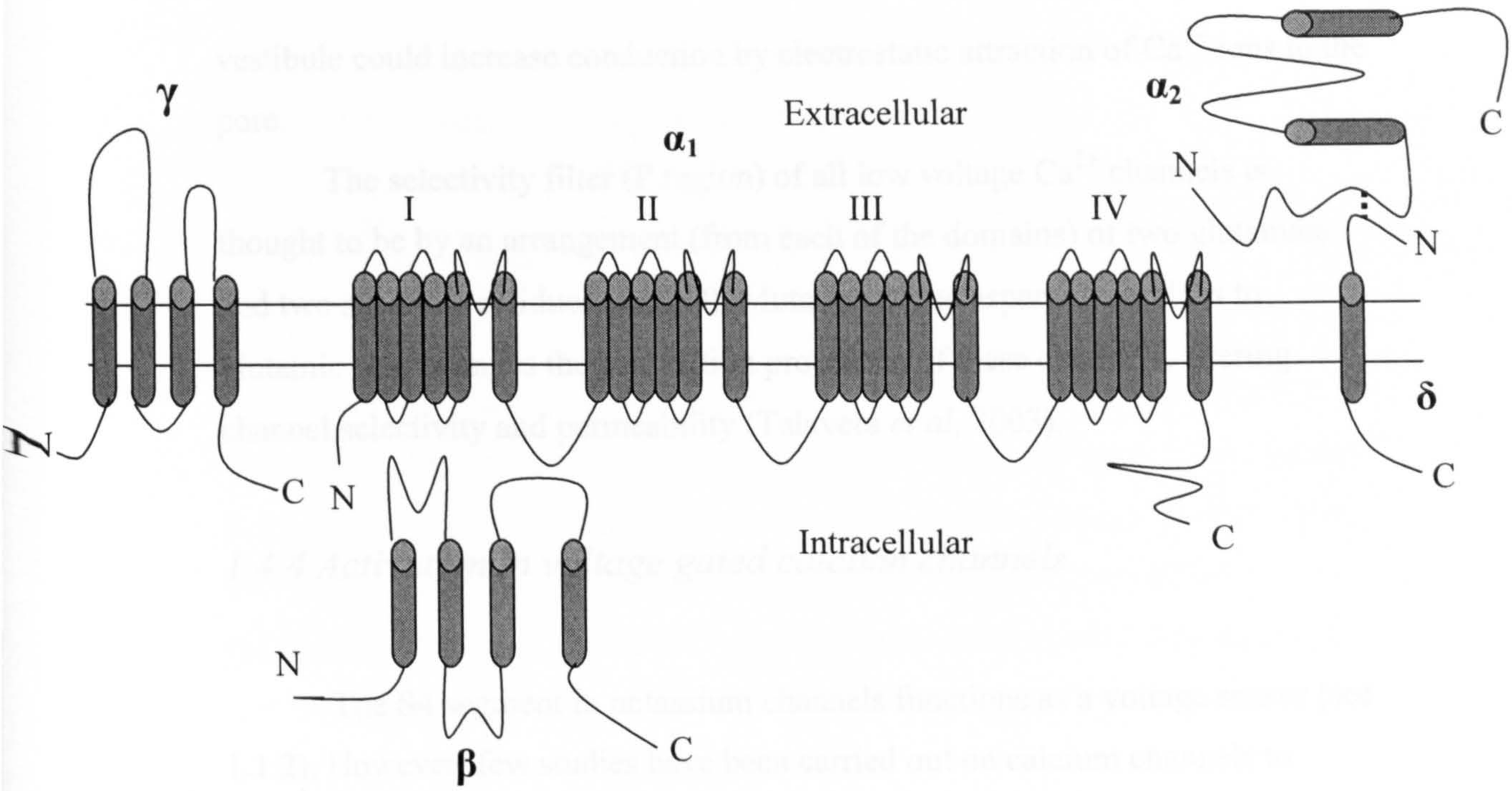

Fig. 1.13 Schematic diagram of an α_1 subunit of a voltage gated calcium channel, with the $\alpha_2\delta$, β and γ subunits.
The dashed line denotes a disulphide bond in the $\alpha_2\delta$ complex.

1.4.3 Pore and selectivity filter in voltage gated calcium channels

As for other voltage dependent channels, the pore is formed by the highly conserved linker connecting the S5 and S6 transmembrane segments in each of the four repeats in calcium channels, domains I-IV (Dirksen *et al*, 1997). The pore region is thought to have a similar structure to that found in potassium channels (see KcsA, Fig. 1.2). The four S6 transmembrane segments are thought to stabilize the four P loops of the pore, and this contributes to the ion selectivity (Doyle *et al*, 1998).

Mutational analysis of a high voltage channel has shown that four glutamate (EEEE) residues in the P regions in each of the domains are important in determining ion selectivity (Yang *et al*, 1993). Equivalent residues are found in all high voltage calcium channels. These glutamate residues are thought to form a single high affinity Ca^{2+} site within the pore, and two Ca^{2+} ions can be accessed at the same time (Ellinor *et al*, 1995). Also, the negative charge in the

vestibule could increase conduction by electrostatic attraction of Ca^{2+} ions to the pore.

The selectivity filter (P region) of all low voltage Ca^{2+} channels is thought to be by an arrangement (from each of the domains) of two glutamate and two aspartate residues (EEDD). Mutation of the aspartate residues to glutamic acid changes the conduction properties of these channels, altering channel selectivity and permeability (Talavera *et al*, 2003).

1.4.4 Activation in voltage gated calcium channels

The S4 segment in potassium channels functions as a voltage sensor (see 1.1.2). However, few studies have been carried out on calcium channels to investigate the role of the S4 region, although mutational studies have supported a role for this region in channel activation. Effects on the mid-point potential and time course of activation have been shown to arise from S4 mutations in domains I and III of a high voltage activated calcium channel, but not from S4 mutations made in domains II and IV (Garcia *et al*, 1997). Leucine or isoleucine mutations in domains I and III had the same effect on the voltage dependence of calcium channel activation as the mutations at equivalent positions in potassium channels, indicating that this region plays a fundamental role in channel activation (Garcia *et al*, 1997).

Recent work on low and high voltage activated calcium channels in this laboratory has suggested that domains I, III, and IV contribute strongly to the differences in voltage dependence of activation between high and low voltage calcium channels (Li *et al*, 2004).

1.5 Voltage gated calcium channels – $Ca_v1.2$ and $Ca_v3.1$

The specific calcium channels investigated within chapter 6 of this thesis are discussed in more detail here. $Ca_v3.1$ is primarily expressed in human brain, but has also been shown to be present in the heart, lung, ovary, testes, intestine and placenta (Monteil *et al*, 2000b; Perez-Reyes *et al* 1998). $Ca_v1.2$ has been found to be expressed in the heart, smooth muscle, kidney and fibroblasts, as

well as in endocrine and neuronal tissue (Hofmann *et al*, 1999). More recently it has also been found in tooth pulp (Westenbroek *et al* 2004).

1.5.1 Function and cloning of $Ca_v1.2$ and $Ca_v3.1$

$Ca_v1.2$ is known to be responsible for initiating excitation-contraction coupling in the heart. Some forms of the channel have been cloned from human heart, rabbit smooth muscle, and rat brain (Schultz *et al*, 1993; Biel *et al*, 1990; Snutch *et al*, 1991). The clone used in the thesis was rabbit cardiac $Ca_v1.2$ (Mikami *et al,* 1989). The channels isolated from rabbit cardiac (Mikami *et al,* 1989) and rabbit smooth muscle (Biel *et al*, 1990) are similar in sequence, but the brain form of the channel differs by containing a small insert in the loop between domains II and III, and a small extension in the C- terminal domain.

$Ca_v3.1$ is known to trigger bursts of action potentials by calcium influx through the channels. Screening of a rat brain cDNA library has facilitated the cloning of $Ca_v3.1$, with human and mouse (used in this thesis) versions following (Perez-Reyes *et al*, 1998; Monteil *et al*, 2000b; Klugbauer *et al*, 1999; Zhang *et al*, 2000). Splice variants of this channel differ in the loop between domains II and III, and in the loop between domains III and IV (Perez-Reyes, 2003).

1.5.2 Differing activation kinetics of $Ca_v1.2$ and $Ca_v3.1$

$Ca_v1.2$ displays L- type currents, is high voltage activating and shows little inactivation. In contrast, $Ca_v3.1$ displays T- type currents, is low voltage activating and has fast inactivation. Replacement of domains I, III, or IV of $Ca_v3.1$ with the corresponding domains of $Ca_v1.2$ leads to high voltage activated channels (Li *et al*, 2004). Therefore, domains I, III, and IV are important in determining differences in voltage dependence of activation between the two channels. Work by Altier *et al*, (2001) has also shown that domains I and III play an important role in voltage dependent activation.

1.6 Summary of aims of this thesis

Firstly, the N- and C- terminal domains of the rat and human Kv2.1 potassium channel were investigated to try and determine which key residues, or molecular regions, responsible for the difference in the rate of activation between the two forms of the channel. For this, a point mutation at residue 75 of the rat channel and rat-human chimeras were characterised using two-electrode voltage clamp.

Secondly, evidence for a direct interaction between the N- and C- terminal domains of rat Kv2.1 was sought. For this, N- and C- terminal protein constructs were used to investigate interactions using GST tags and Biacore surface plasmon resonance. In addition, fluorescent constructs were generated in order to characterize relative movement of the N- and C- terminal domains using FRET.

The structures of some voltage gated potassium channels have been solved by electron microscopy. The generation of such a structure for Kv2.1 would help us to better understand this channel. To this end, initial experiments were undertaken to express and purify rat Kv2.1 channel protein, with and without the N- terminal domain, for single particle electron microscopy analysis.

Finally, no previous studies have systematically studied the movement of the S4 segment in calcium channels in response to depolarisation. Therefore, to establish whether such S4 movement occurs and the extent of this movement has been studied in calcium channels using PCMBS.

Much of the work described in this thesis has already been published.

1.7. Publications

Full papers

Ju*, M., Stevens*, L., Leadbitter, E., and Wray, D. (2003). The roles of N- and C- terminal determinants in the activation of the Kv2.1 potassium channel. *J. Biol. Chem.* **278**, 12769-12778.

Li, J., Stevens, L., and Wray, D. (2004) Roles of molecular regions in determining differences between voltage dependence of activation of $Ca_v3.1$ and $Ca_v1.2$ calcium channels. *J. Biol. Chem.* **279**, 26858-26867.

Li*, J., Stevens*, L., and Wray, D. (2005). Molecular regions underlying the activation of low- and high-voltage activating calcium channels. *Eur. Biophys. J.* online 1432-1017.

Abstracts

Bracey, K. Stevens, L., and Wray, D. (2005). Comparison of the extent of movement of S4 voltage-gated potassium and calcium channels. Biophysical society July 2005 meeting.

Ju, M., Rashleigh, L.R., Ormond, S.J., and Wray, D. (2002). Activation kinetics of rat Kv2.1 potassium channel: and N-terminal determinant. *Brit. J. Pharmacol.* **135**, 343P.

Ju, M., Rashleigh, L., Aslam, M., and Wray, D., (2002). Investigation of the role of a residue in the S4-S5 linker in the activation of heag potassium channels. *J. Physiol.* **544**, 8P.

Li, J., Stevens, L., Klugbauer N., and Wray, D. (2004). Roles of molecular domains in the activation of the calcium channel $Ca_v3.1$. *Biophys. J.* **86**, 271a.

Rashleigh, L., Ju, M., Leadbitter, E., and Wray, D. (2002). Activation kinetics of rat and human Kv2.1 potassium channels: a C terminal determinant. *J. Physiol.* **544**, 25P.

Book chapters

Stevens, L., & Wray, D. (2005). Expression and analysis of recombinant ion channels. *Wiley-VCH.* To be published

CHAPTER 2

MATERIALS AND METHODS

2. Materials and methods

Chemicals and reagents

All of the standard laboratory chemicals were obtained from VWRI (Lutterworth, UK) and Sigma (Poole, UK) through Science Warehouse Ltd. Collagenase Type 1A, ethidium bromide, 3-aminobenzoic acid ethyl ester (tricaine, disodium salt), ampicillin and penicillin-streptomycin solution were obtained from Sigma. Agarose powder was obtained from Helena Biosciences (Sunderland, UK), and PCMBS was obtained from Toronto Research Chemicals (Toronto, Canada). EZ-Glass Milk™ was purchased from Anachem (Luton, UK). *Escherichia coli* JM109 cells (>10^9 cfu/μg) were from Promega.

Enzymes, antibodies and kits

All restriction enzymes were purchased from Helena Biosciences, or Promega (Southampton, UK), unless otherwise stated. The buffers used for each of the digests were supplied with the enzymes. *Pfu* Turbo® DNA polymerase and *Dpn*I were purchased from Stratagene (Amsterdam, Netherlands) as part of the QuikChange™ Site-directed mutagenesis kit. Shrimp Alkaline Phosphatase was obtained from Promega. The QIAquick® Gel Extraction kit was obtained from Qiagen (Crawley, UK). The Wizard® *Plus* SV Miniprep kit was from Promega. The MEGAScript T7 *In Vitro* Transcription kit was obtained from Ambion (Hutingdon, UK). The Clonables™ DNA ligation kit was from Novagen (Lutterworth, UK). All primary and secondary antibodies were purchased from Novagen (Lutterworth, UK), except ID4, which was a kind gift from M. Rigney, USA.

Oligonucleotides and sequencing

All primers were designed using the Primer Premier Program version 4.10 (Premier Biosoft International). Primers were made by Sigma Genosys

(Cambridge, UK). All DNA sequencing was carried out by Lark Technologies (Saffron Walden, UK). Universal primers were provided by Lark. All primer sequences are shown in the 5' to 3' direction.

Xenopus laevis toads

Mature female toads were obtained from Blades (UK).

Potassium and calcium channel cDNA clones

The human Kv2.1 (hKv2.1) clone in pGEM-He-Juel was a kind gift from O. Pongs (Hamburg, Germany), originally cloned as described in Albrecht *et al* (1993). The rat Kv2.1 (rKv2.1) in pBluescript SK$^-$ was a kind gift from J. Drewe (Houston, USA), originally cloned as described in Frech *et al* (1989). The rKv2.1 □7 in Pblu-Sk was provided by K.J. Swartz (National Institute for Health, Maryland), and contained mutations which rendered the rKv2.1 protein susceptible to agitoxin-2 binding. The pEYFP and pECFP fluorescent vectors were donated by N. Soldatov (Baltimore, USA), and the α_{1G} calcium channel clone by F. Hofmann (Munich, Germany). The CGGG and GCGG calcium channel chimeras were made by J. Li.

Growth media, solutions and buffers are as described in table 2.1 a-d.

All solutions were made using double distilled autoclaved water (Millipore system, Watford, UK). The bacterial growth media was sterilized prior to use by autoclaving. RNA solutions were made using RNase free water or 0.05% diethyl pyrocarbonate (DEPC) treated water. All tips used for RNA work were treated with DEPC water and autoclaved.

Table 2.1a: Growth media for *E. coli* competent cells

YT	8g Bacto-Tryptone, 5g Bacto-Yeast extract and 2.5g NaCl in 900ml water. pH 7.0, volume adjusted to 1 litre.
LB	10g Bacto-Tryptone, 5g yeast extract and 10g NaCl in 900ml water. pH7.0, volume adjusted to 1 litre.
LB-Agar Plate	Agar (1%), LB media and ampicillin (100mg/ml, 1µl/ml media).

Table 2.1b: Gel electrophoresis of DNA and RNA

Ethidium Bromide (EtBr) for DNA	10mg/ml in autoclaved water
Tris-EDTA buffer (TE)	Tris HCl pH 8.0 (10mM) and EDTA pH 8.0 (1mM).
10x agarose gel sample buffer 100ml	250mg bromophenol blue in 33ml 150mM Tris pH 7.6, 60ml glycerol and 7ml water.
Tris-acetate 50x (TAE)	242g Tris in 500ml water, 100ml 0.5M Na_2EDTA (pH 8.0) and 57.1ml glacial acetic acid, volume adjusted to 1 litre.

Table 2.1c: RNA Preparation

RNA new wash	50% Ethanol, 10mM Tris HCl (pH 8.0), 100mM NaCl and 2.5mM EDTA (pH 8.0).
Denaturing solution	5mM Guanidine thiocyanate, 0.05% N-lauryl sarcosine, 125mM sodium citrate and 0.007% 2-mercaptoethanol.

Table 2.1d: Oocyte preparation and electrophysiological solutions

Calcium-free Ringer solution	82mM NaCl, 2mM KCl, 5mM HEPES, and 1mM $MgCl_2$. pH was adjusted to 7.2 using 4M NaOH.
Barth's solution	88mM NaCl, 1mM KCl, 2.4mM $NaHCO_3$, 0.82mM $MgSO_4$, 0.4mM $Ca(NO_3)_2$, 7.5mM Tris-HCl pH 7.6, 10,000U/l penicillin, and 100mg/l streptomycin.
Frog Ringer solution	115mM NaCl, 2mM KCl, 1.8mM $CaCl_2$, and 10mM HEPES. pH was adjusted to 7.2 using 4M NaOH.
Barium solution	40mM $Ba(OH)_2$, 50mM NaOH, 2mM KOH, and 5mM HEPES. pH was adjusted to 7.4 with methanesulfonic acid.

2.1 General molecular biology methods

2.1.1 Transformation of plasmid DNA into E. coli competent cells

Plasmid DNA was transformed into *E. coli* JM109 competent cells by a method modified from Sambrook *et al* (1989). A 1.5ml micro-centrifuge tube was pre-chilled and 100µl of competent cells were added. 1µl of plasmid DNA at a concentration of 100ng/µl was added. The mixture was placed on ice for 10 minutes, and then placed in a water bath for 45 seconds at 42°C. The cell mix was then placed on ice for a further 2 minutes. 900µl of pre-warmed LB media was added, and then the tube was placed into an orbital incubator for 1 hour at

37°C and 225rpm. Following this, the cells were spun down in a micro-centrifuge for 3 minutes at 4000rpm. 900µl of supernatant was removed and the pellet re-suspended in the remaining supernatant. This was then spread out on LB agar plates and left to grow overnight in an incubator at 37°C.

2.1.2 Inoculation of LB media with a bacterial colony

Following overnight growth on LB agar plates, individual colonies were randomly selected to inoculate 5ml of LB media containing 1µg/ml ampicillin. One colony was removed from the plate with a 200µl micropipette tip and dipped into the media. The inoculations were placed in an orbital incubator and left to grow overnight at 37°C and 225rpm.

2.1.3 Extraction of plasmid DNA from inoculated cells using the mini-prep method

Overnight inoculations were transferred to 1.5ml micro-centrifuge tubes, and spun in a micro-centrifuge at 10,000rpm for 5 minutes. The supernatant was then removed from the tubes and discarded. Plasmid DNA was extracted from the cells using the Promega Wizard® *Plus* SV Mini-prep kit, according to the manufacturer's recommended protocol.

2.1.4 Agarose gel electrophoresis of DNA and RNA

The yield of DNA was checked using agarose gel electrophoresis. A 0.7% agarose gel was made (0.7g ultra pure agarose in 100ml 1xTAE, table 2.1b), with 6µl 10mg/ml ethidium bromide. The gel was transferred to an electrophoresis tank (Wide Mini Sub Cell, BioRad), containing 1 xTAE buffer. DNA samples were added to 6 x loading buffer (see table 2.1b) and loaded in separate lanes. A DNA marker was also run to allow semi-quantitative analysis of the DNA sample. Gels were run at 80 Volts for approximately 35 minutes, and viewed using Quantity One Imaging Software on a BioRad Gel Doc 2000.

2.1.5 Site-directed mutagenesis

Site-directed mutagenesis is a useful molecular biology tool by which targeted point mutations can be made rapidly and easily using a thermal cycling method. Figure 2.1 shows a diagrammatic representation of the steps involved. The QuikChange™ Mutagenesis Kit (Stratagene) was used according to the manufacturer's recommended thermal cycling protocol, which is derived from the method of Kunkel *et al* (1987). General cycling parameters are shown in table 2.2. Thermal cycling was carried out in a Perkin Elmer GeneAmp 2700 PCR machine.

Table 2.2 General cycling parameters for site-directed mutagenesis.

Segment	No. Cycles	Temperature	Time
1	1	95°C	2 minutes
2	25	95°C	30 seconds
		55°C	1 minute
		72°C	2 minutes/kb
3	1	72°C	10 minutes

Following the completion of the thermal cycling stage, 1µl of *Dpn*I was added to each of the tubes, and left overnight to digest at 37°C. 10µl was transformed into JM109 cells as described in 2.1.1. Colonies were inoculated as described in 2.1.2, and DNA was extracted as described in 2.1.3. Clones were confirmed by automated DNA sequencing (Lark).

2.1.6 Restriction enzyme digest to linearise plasmid DNA

Restriction cuts for sub-cloning and for linearisation of DNA before transcription were carried out in the same way. 15 units of the appropriate enzyme were added to 30µl of plasmid DNA, along with 5µl of the appropriate

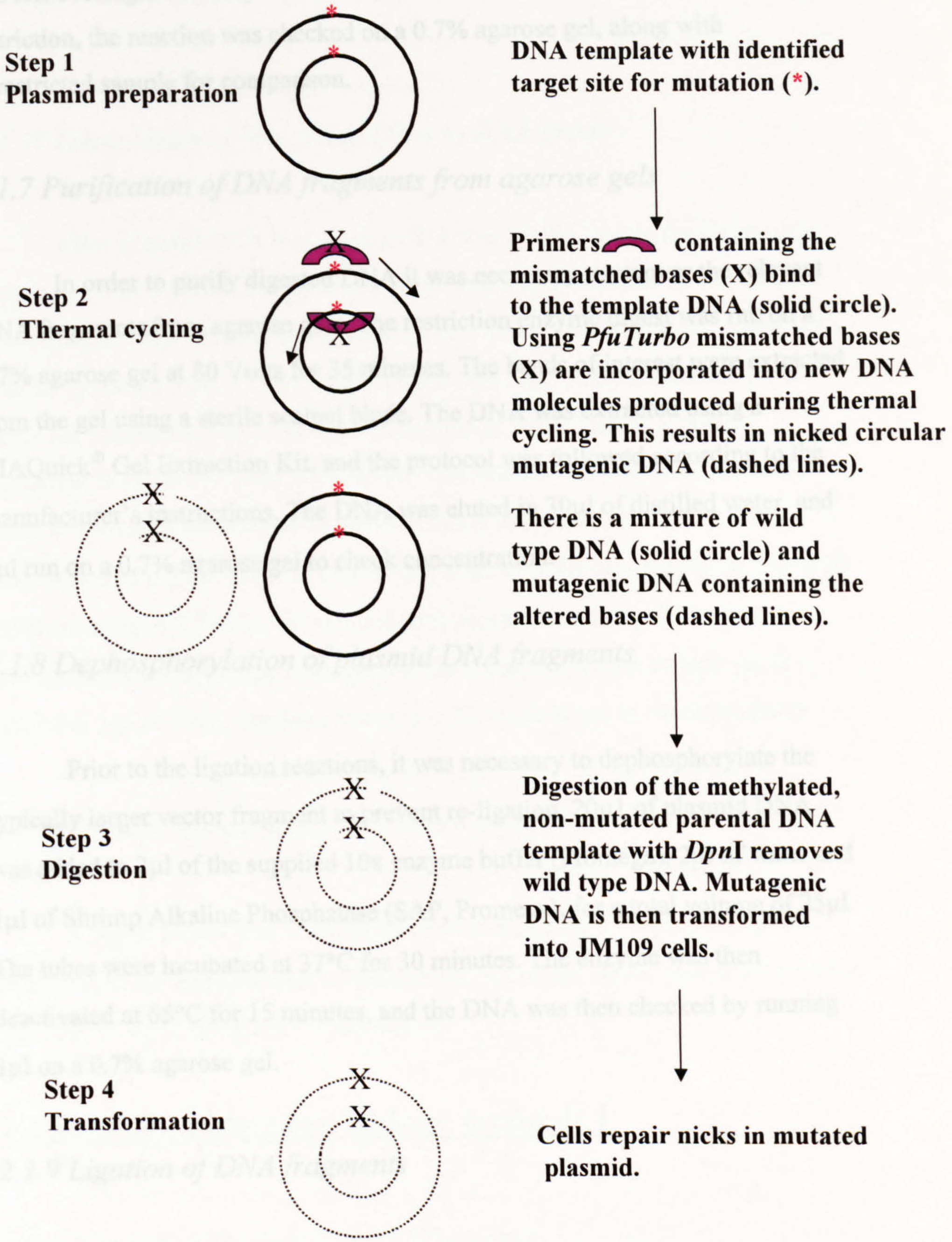

Fig. 2.1 Schematic diagram of the QuickChange™ site-directed mutagenesis method.
Adaptation from the Stratagene protocol.

enzyme buffer, and the volume was made up to 50µl with water. The mixture was left overnight at the optimum temperature for the enzyme. Following restriction, the reaction was checked on a 0.7% agarose gel, along with unrestricted sample for comparison.

2.1.7 Purification of DNA fragments from agarose gels

In order to purify digested DNA it was necessary to recover the relevant DNA fragments from agarose gels. The restriction enzyme digest was run on a 0.7% agarose gel at 80 Volts for 35 minutes. The bands of interest were extracted from the gel using a sterile scalpel blade. The DNA was extracted using a QIAQuick® Gel Extraction Kit, and the protocol was followed according to the manufacturer's instructions. The DNA was eluted in 30µl of distilled water, and 1µl run on a 0.7% agarose gel to check concentration.

2.1.8 Dephosphorylation of plasmid DNA fragments

Prior to the ligation reactions, it was necessary to dephosphorylate the typically larger vector fragment to prevent re-ligation. 20µ1 of plasmid DNA was added to 2µl of the supplied 10x enzyme buffer (Promega), 2µl of water and 1µl of Shrimp Alkaline Phosphatase (SAP, Promega), for a total volume of 25µl. The tubes were incubated at 37°C for 30 minutes. The enzyme was then deactivated at 65°C for 15 minutes, and the DNA was then checked by running 1µl on a 0.7% agarose gel.

2.1.9 Ligation of DNA fragments

After dephosphorylation of the vector fragment, ligation of the relevant insert and vector was carried out. Approximately twice as much insert to vector (concentration) ratios were used in all reactions. The Clonables™ T3 ligase ligation/transformation kit from Novagen was used for all ligations, with the procedure used according to the manufacturer's instructions. The transformed

cells were plated directly onto LB ampicillin agar plates and incubated at 37°C overnight. Inoculation and mini-preps were then carried out as described previously.

2.1.10 Gene-clean of linearised DNA to RNA grade

After plasmid DNA was linearised, it was purified using the Gene-clean protocol so that it would be sufficiently high grade to synthesise RNA. To each DNA sample 200µl of denaturing solution (see table 2.1c) was added, along with 15µl of EZ-Glass Milk™. The samples were then vigorously mixed and placed on ice for 5 minutes. The tubes were then spun at 10,000rpm in a micro-centrifuge to pellet the Glass Milk beads. The supernatant was removed and the pellet was washed three times in 500µl of RNA New Wash (see table 2.1c). The DNA was eluted from the beads by adding 20µl of RNA grade water to the beads and incubating at 55°C for 10 minutes with occasional mixing. The tubes were then spun at 10,000rpm for 1 minute and the supernatant then transferred to a new tube. 1µl of DNA was then run on a 0.7% agarose gel to check recovery.

2.1.11 In vitro transcription to synthesize RNA

Capped cRNA was transcribed *in vitro* using the T7 MEGAScript kit™ according to the manufacturer's instructions. 1µl of the cRNA samples were then checked for yield using a 0.7% agarose gel.

2.2 Specific molecular biology methods I

2.2.1 Construction of rKv2.1 E75D mutant

In order to determine the effect of changing the amino acid at position 75 (rat Kv2.1 numbering) of rKv2.1 wild type, it was necessary to mutate the coding

sequence using the QuikChange™ site-directed mutagenesis method (see section 2.1.5). The mutant generated was rKv2.1 E75D.

Primers were designed with one mismatched base as shown in table 2.3. Mismatched bases are shown in red, and both primers are described in the 5' to 3' direction. The changed amino acid is shown underlined in red.

Table 2.3 PCR primers used for site directed mutagenesis –E75D.

rKv2.1 E75D sense	GCGACGACTACAGCCTTGACGACAACGAGTACTTCTTC
rKv2.1 E75D anti-sense	GAAGAAGTACTCGTTGTCGTCAAGGCTGTAGTCGTCGC

Transformation was as detailed in section 2.1.1, and DNA was extracted as in section 2.1.3. Samples of mini-prepped DNA were sent to Lark Technologies for automated sequencing using a universal T7 primer.

2.2.2 Construction of chimera rKv2.1$_{h108-528}$

The construction of the chimera rKv2.1$_{h108-528}$, which has residues between 108 and 528 of rat replaced by human, was carried out by a restriction enzyme digestion, using *Bsp*1407I and *Bss*HII, followed by ligation of the appropriate fragments (rat wild type digestion was prepared by M. Ju), as shown in figure 2.2.

Briefly, the cDNA of both the channels was digested using the restriction enzymes *Bsp*1407I (15 units, overnight incubation at 37°C) and *Bss*HII (15 units, 5 hour incubation at 50°C). The enzyme *Bsp*1407I cuts both rat and human Kv2.1 cDNA downstream from the S6 domain, and *Bss*HII cuts in the N-terminal domain of both clones. Restriction of cDNA of hKv2.1 yields 2 fragments – a smaller 1264bp fragment, which contains the S1 to S6 domains, and a larger N- and C- terminal vector fragment, which of 4781bp. The fragments were isolated by running on a 0.7% agarose gel and bands excised as described in section 2.1.7. The smaller hKv2.1 fragment was then ligated to the larger rKv2.1 fragment as outlined in section 2.1.9, and mini-prepped according to section 2.1.3.

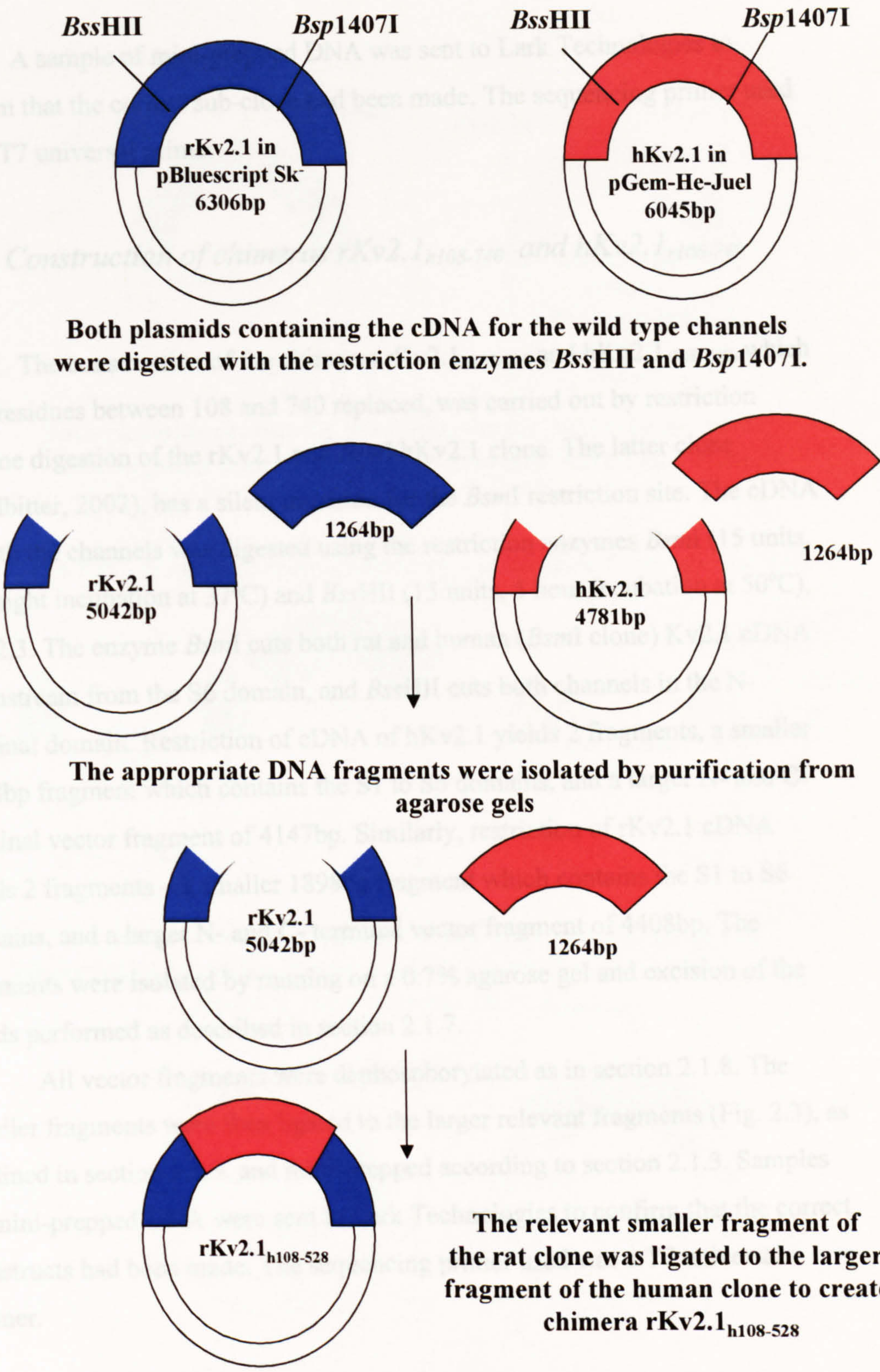

Fig. 2.2 Schematic diagram of the construction of the chimera $rKv2.1_{h108-528}$.

The different parts of the plasmids that were exchanged during construction with the restriction enzymes are shown. The sizes of the fragments are indicated. Diagram not drawn to scale.

A sample of mini-prepped DNA was sent to Lark Technologies to confirm that the correct sub-clone had been made. The sequencing primer used was a T7 universal primer.

2.2.3 Construction of chimeras rKv2.1$_{h108\text{-}740}$ and hKv2.1$_{r108\text{-}740}$

The construction of the chimeras rKv2.1$_{h108\text{-}740}$ and hKv2.1$_{r108\text{-}740}$, which have residues between 108 and 740 replaced, was carried out by restriction enzyme digestion of the rKv2.1 and *Bsm*I hKv2.1 clone. The latter clone (Leadbitter, 2002), has a silent mutation for the *Bsm*I restriction site. The cDNA of both the channels was digested using the restriction enzymes *Bsm*I (15 units, overnight incubation at 37°C) and *Bss*HII (15 units, 5 hour incubation at 50°C), Fig. 2.3. The enzyme *Bsm*I cuts both rat and human (*Bsm*I clone) Kv2.1 cDNA downstream from the S6 domain, and *Bss*HII cuts both channels in the N-terminal domain. Restriction of cDNA of hKv2.1 yields 2 fragments, a smaller 1898bp fragment which contains the S1 to S6 domains, and a larger N- and C-terminal vector fragment of 4147bp. Similarly, restriction of rKv2.1 cDNA yields 2 fragments – a smaller 1898bp fragment which contains the S1 to S6 domains, and a larger N- and C- terminal vector fragment of 4408bp. The fragments were isolated by running on a 0.7% agarose gel and excision of the bands performed as described in section 2.1.7.

All vector fragments were dephosphorylated as in section 2.1.8. The smaller fragments were then ligated to the larger relevant fragments (Fig. 2.3), as outlined in section 2.1.9, and mini-prepped according to section 2.1.3. Samples of mini-prepped DNA were sent to Lark Technologies to confirm that the correct constructs had been made. The sequencing primer used was a T7 universal primer.

2.2.4 Construction of chimera rKv2.1$_{h741\text{-}795}$

In the absence of any convenient restriction sites, the rKv2.1$_{h741\text{-}795}$ chimera, which has residues between 741 and 795 of the rat channel replaced by

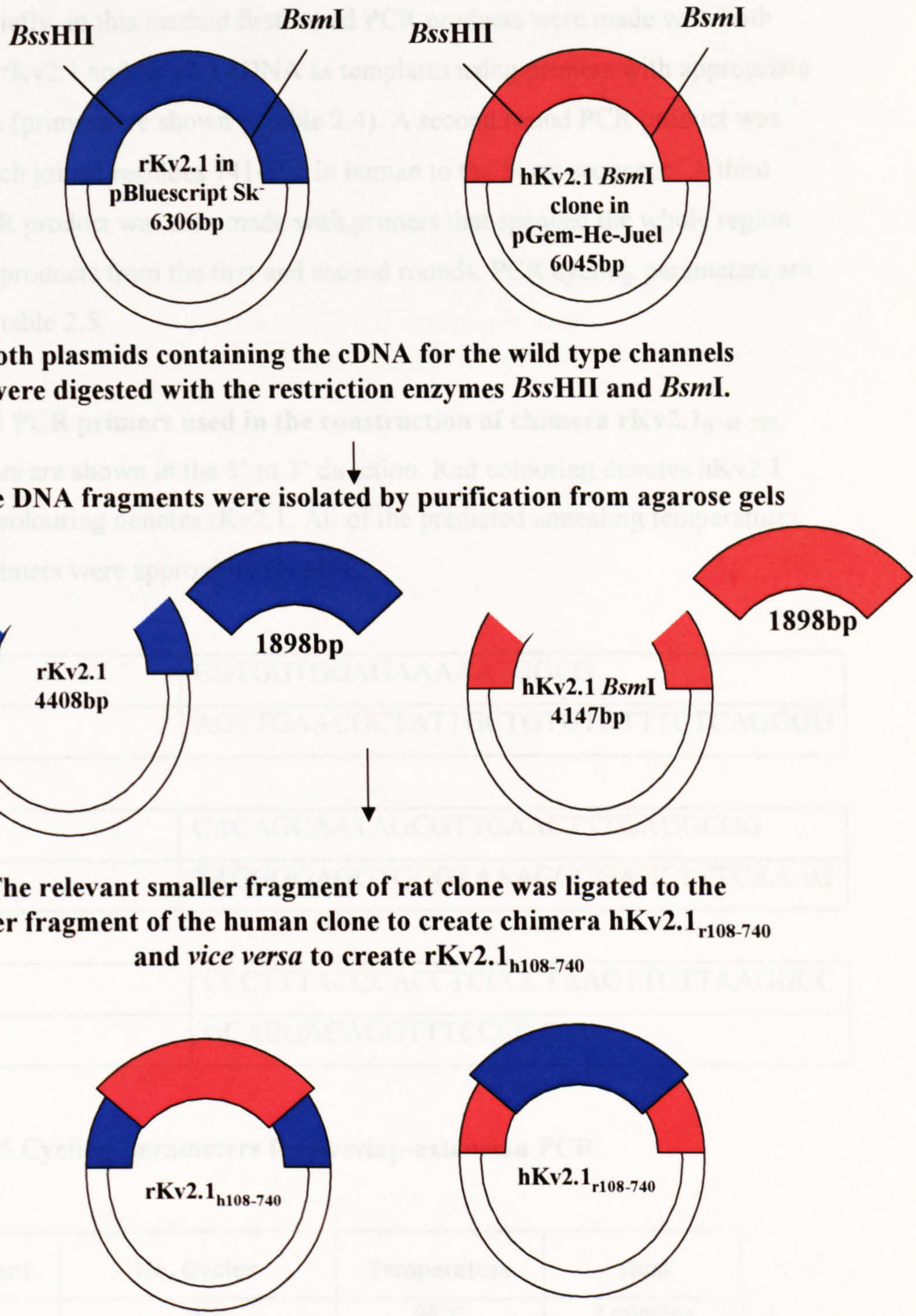

Fig. 2.3 Schematic diagram of the construction of the chimeras $hKv2.1_{r108-740}$ and $rKv2.1_{h108-740}$.
The different parts of the plasmids that were exchanged during construction with the restriction enzymes are shown schematically. The sizes of the fragments are indicated. Diagram not drawn to scale.

human, was generated using the PCR overlap extension protocol described by Horton *et al* (1989), as illustrated schematically in Fig. 2.4.

Briefly, in this method first round PCR products were made with both wild type rKv2.1 and hKv2.1 cDNA as templates using primers with appropriate overhangs (primers are shown in table 2.4). A second round PCR product was made which joined residues 741-795 in human to the 5' rat sequence. A third round PCR product was then made with primers that spanned the whole region using the products from the first and second rounds. PCR cycling parameters are shown in table 2.5.

Table 2.4 PCR primers used in the construction of chimera rKv2.1$_{h741-795}$. All primers are shown in the 5' to 3' direction. Red colouring denotes hKv2.1 and blue colouring denotes rKv2.1. All of the predicted annealing temperatures for the primers were approximately 60°C.

1R	CGTGGTGGAGAAAAATGGCG
2R	AGTTGAACGCTATTGCTGTGTGTTTCTCAGGGG
3H	CACAGCAATAGCGTTCAACTTTGAGGCGG
4H	TAGGGGAGGTGGGTAAAGGGGAGCTTTCAAAG
5R	CCCTTTACCCACCTCCCCTAAGTTCTTAAGGCC
6R	GCACGACAGGTTTCCCGACT

Table 2.5 Cycling parameters for overlap-extension PCR.

Segment	No. Cycles	Temperature	Time
1	1	95°C	2 minutes
2	25	95°C 55°C 72°C	30 seconds 30 seconds 2 minutes/kb
3	1	72°C	10 minutes

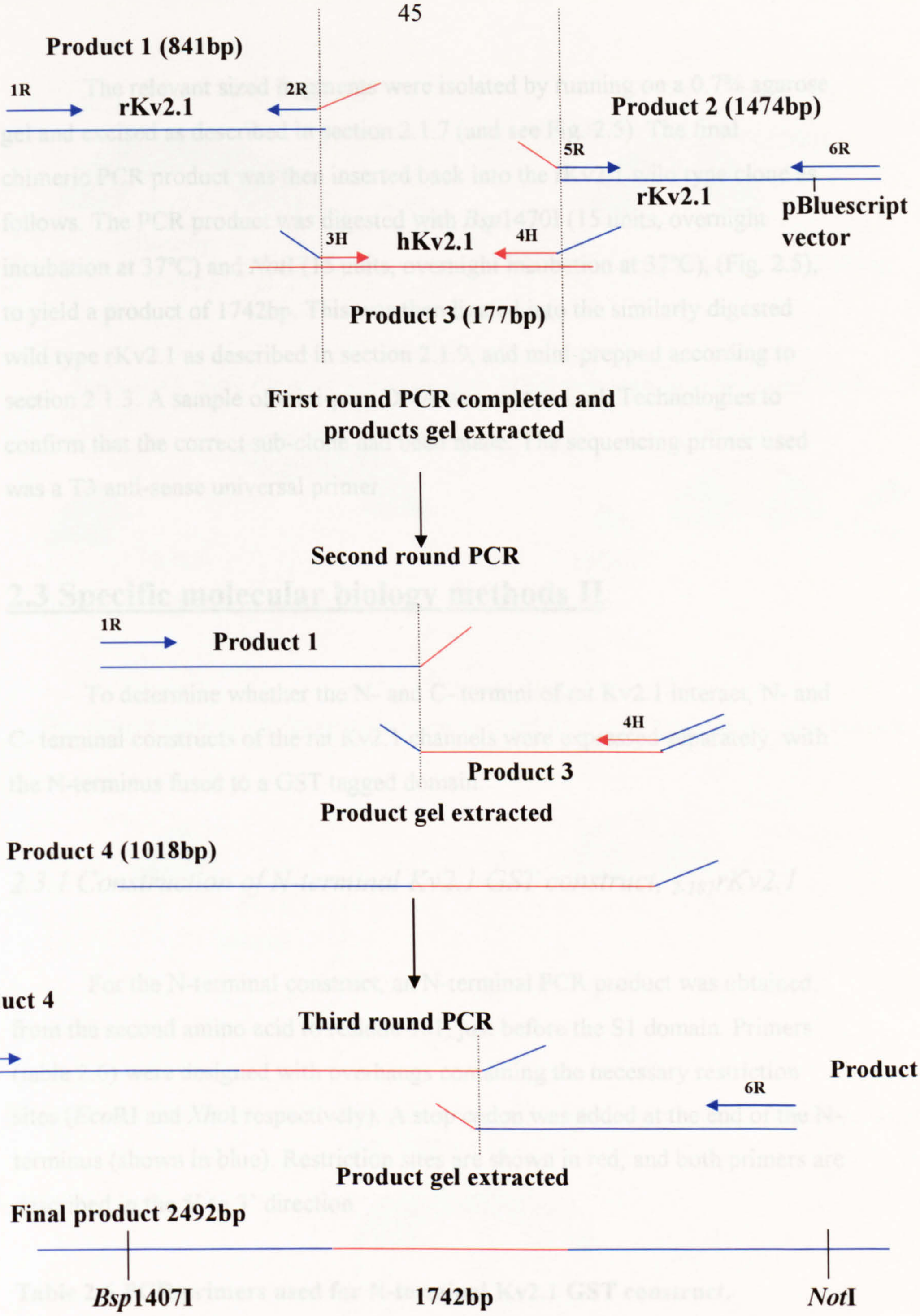

Fig. 2.4 PCR protocol for the construction of chimera rKv2.1$_{h741-795.}$
PCR was carried out using the cycling parameters shown in table 2.5. The relevant sized fragments were gel extracted and used as templates in the next round as shown. The red colouration denotes human Kv2.1 sequence and the blue denotes rat Kv2.1 sequence. The dotted lines show the fragment join.

The relevant sized fragments were isolated by running on a 0.7% agarose gel and excised as described in section 2.1.7 (and see Fig. 2.5). The final chimeric PCR product was then inserted back into the rKv2.1 wild type clone as follows. The PCR product was digested with *Bsp*1470I (15 units, overnight incubation at 37°C) and *Not*I (15 units, overnight incubation at 37°C), (Fig. 2.5), to yield a product of 1742bp. This was then ligated into the similarly digested wild type rKv2.1 as described in section 2.1.9, and mini-prepped according to section 2.1.3. A sample of mini-prep DNA was sent to Lark Technologies to confirm that the correct sub-clone had been made. The sequencing primer used was a T3 anti-sense universal primer.

2.3 Specific molecular biology methods II

To determine whether the N- and C- termini of rat Kv2.1 interact, N- and C- terminal constructs of the rat Kv2.1 channels were expressed separately, with the N-terminus fused to a GST tagged domain.

2.3.1 Construction of N-terminal Kv2.1 GST construct, $_{2\text{-}181}$rKv2.1

For the N-terminal construct, an N-terminal PCR product was obtained, from the second amino acid to residue 181, just before the S1 domain. Primers (table 2.6) were designed with overhangs containing the necessary restriction sites (*Eco*RI and *Xho*I respectively). A stop codon was added at the end of the N-terminus (shown in blue). Restriction sites are shown in red, and both primers are described in the 5' to 3' direction.

Table 2.6 PCR primers used for N-terminal Kv2.1 GST construct.
Both primers had an estimated annealing temperature of 60°C.

Kv2.1 *Eco*RI N-S	GGCGGAATTCCACGAAGCATGGCTCGCGCTC
Kv2.1 *Xho*I N-AS	GCCGCTCGAGTCACGACGAGTTGGGCTTCTCCA

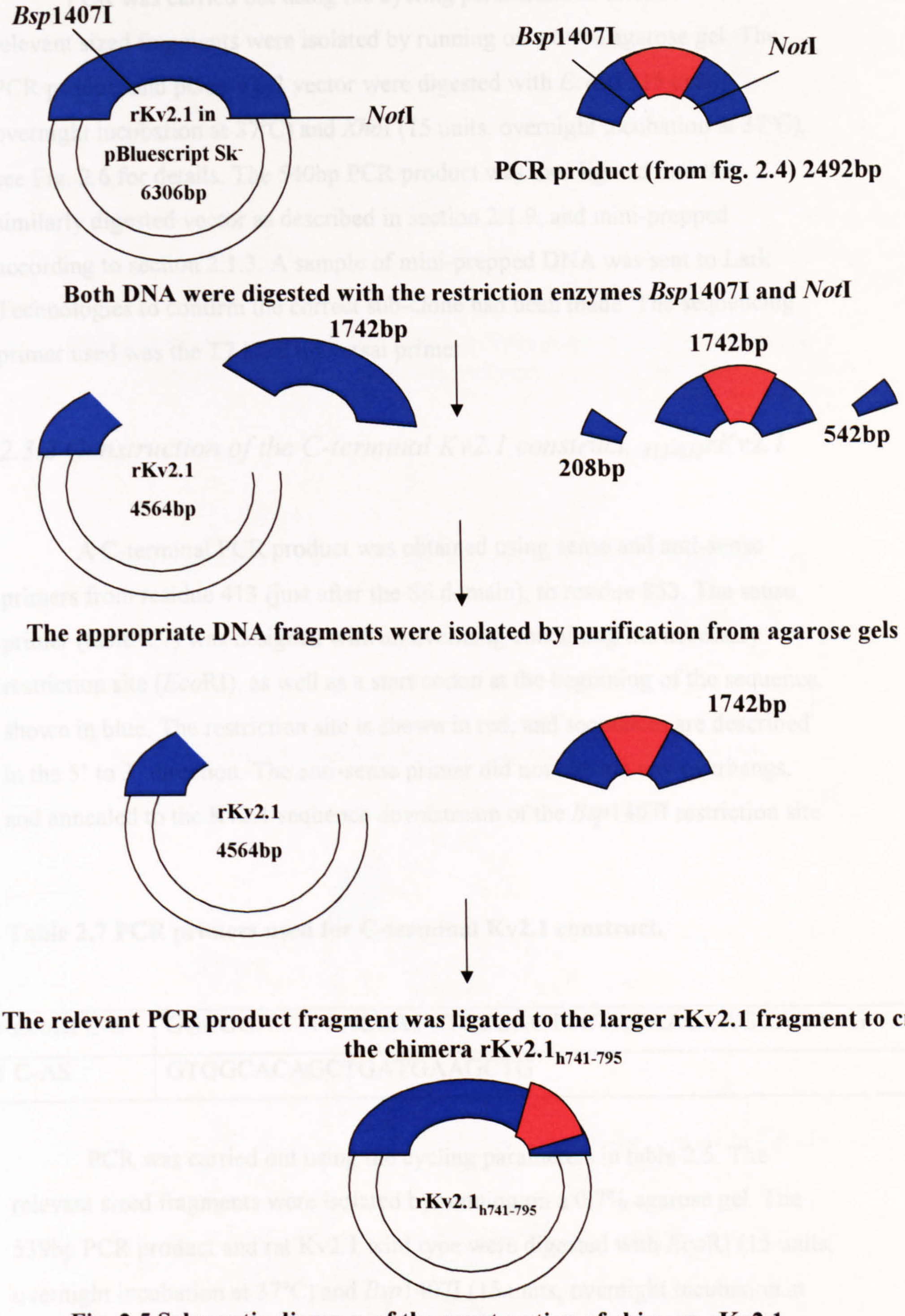

Fig. 2.5 Schematic diagram of the construction of chimera rKv2.1$_{h741-795}$. Only the restriction sites involved are labelled, and the sizes of fragments are indicated. Diagram not drawn to scale.

PCR was carried out using the cycling parameters in table 2.5. The relevant sized fragments were isolated by running on a 0.7% agarose gel. The PCR product and pGex-4T-3 vector were digested with *Eco*RI (15 units, overnight incubation at 37°C) and *Xho*I (15 units, overnight incubation at 37°C), see Fig. 2.6 for details. The 540bp PCR product was then ligated into the similarly digested vector as described in section 2.1.9, and mini-prepped according to section 2.1.3. A sample of mini-prepped DNA was sent to Lark Technologies to confirm the correct sub-clone had been made. The sequencing primer used was the T7 Lark universal primer.

2.3.2 Construction of the C-terminal Kv2.1 construct, $_{413\text{-}853}$rKv2.1

A C-terminal PCR product was obtained using sense and anti-sense primers from residue 413 (just after the S6 domain), to residue 853. The sense primer (table 2.7) was designed with an overhang containing the necessary restriction site (*Eco*RI), as well as a start codon at the beginning of the sequence, shown in blue. The restriction site is shown in red, and sequences are described in the 5' to 3' direction. The anti-sense primer did not contain any overhangs, and annealed to the Kv2.1 sequence downstream of the *Bsp*1407I restriction site.

Table 2.7 PCR primers used for C-terminal Kv2.1 construct.

Kv2.1 *Eco*RI C-S	GGCGGAATTCACCATGTCCGAGTTCTACAAGGAGCAGAAG
Kv2.1 C-AS	GTGGCACAGCTGATGAAGCTG

PCR was carried out using the cycling parameters in table 2.5. The relevant sized fragments were isolated by running on a 0.7% agarose gel. The 539bp PCR product and rat Kv2.1 wild type were digested with *Eco*RI (15 units, overnight incubation at 37°C) and *Bsp*1407I (15 units, overnight incubation at 37°C), Fig. 2.7. The 346bp digested product was ligated into the similarly digested vector (4703bp) as described in section 2.1.9, and mini-prepped as

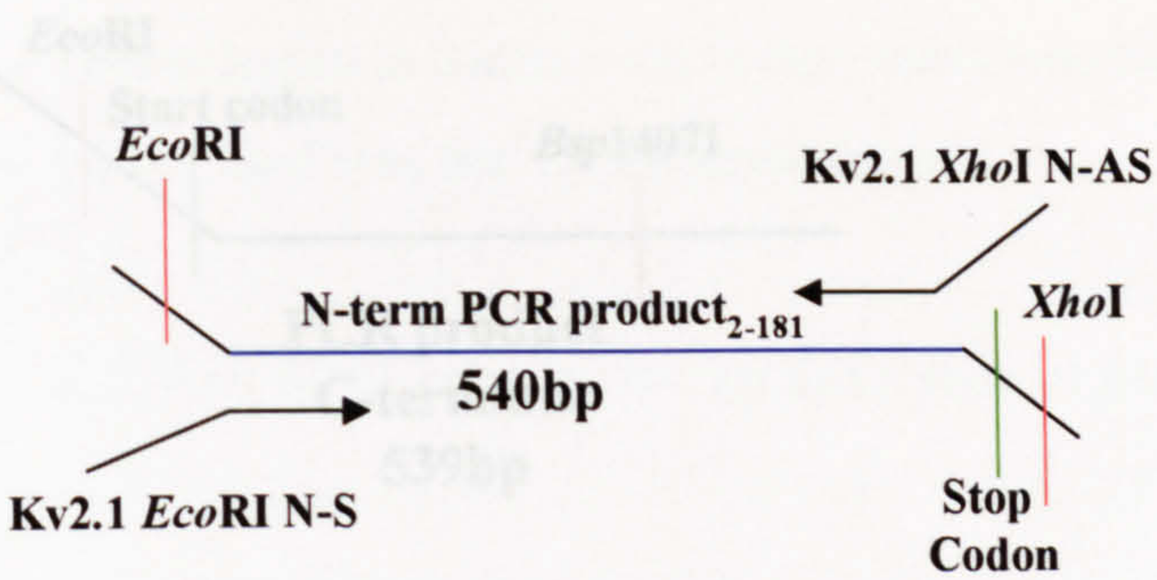

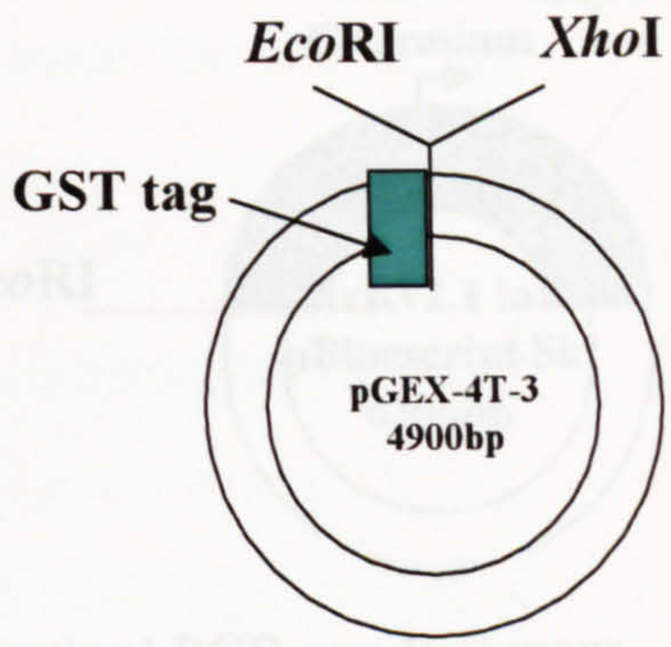

Both the pGEX-4T-3 plasmid and the N-terminal PCR product were digested with the restriction enzymes *Eco*RI and *Xho*I

The DNA fragments were isolated by purification from agarose gels

The PCR fragment was ligated into the pGEX-4T-3 vector

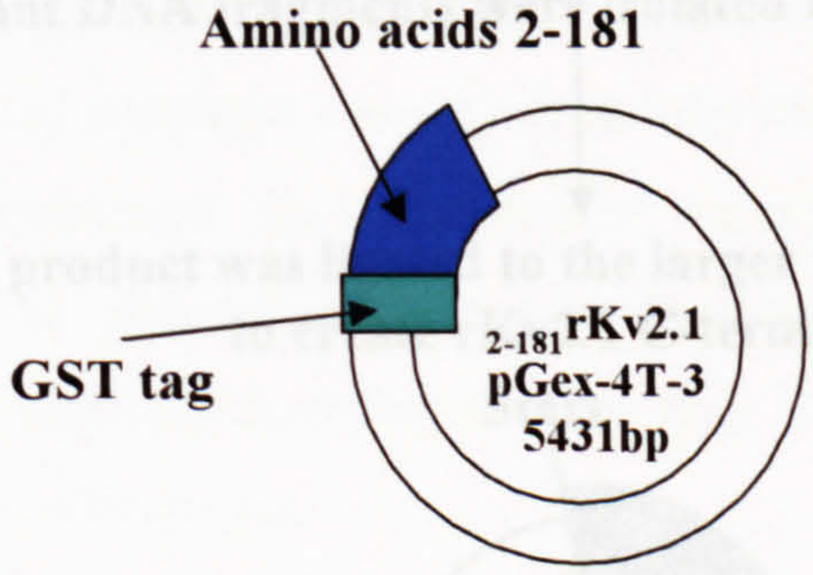

N-terminal GST fusion construct

Fig. 2.6 Schematic diagram of the construction of N-terminal GST fusion construct.
The PCR product and the wild type vector were ligated after digestion with restriction enzymes as shown. The sizes of the fragments are indicated. Red lines denote restriction sites and the green line denotes the stop codon in the PCR product. Diagram not drawn to scale.

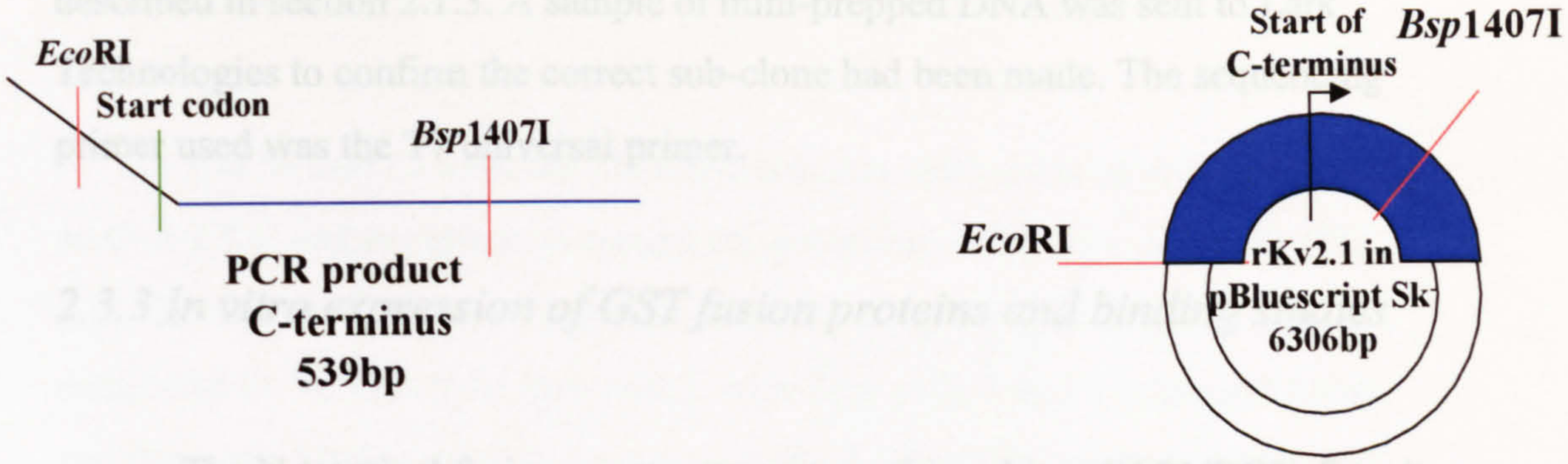

Fig. 2.7 Schematic diagram of the construction of $_{413\text{-}853}$rKv2.1.
The PCR product and the larger rKv2.1 fragment were ligated after digestion with the relevant enzymes. The sizes of the PCR fragments and rKv2.1 in pBluescript are shown. Red lines denotes restriction enzyme sites and the green line denotes the start codon. Diagram not drawn to scale.

described in section 2.1.3. A sample of mini-prepped DNA was sent to Lark Technologies to confirm the correct sub-clone had been made. The sequencing primer used was the T7 universal primer.

2.3.3 In vitro expression of GST fusion proteins and binding studies

The N-terminal fusion construct was transformed into BL21(DE3) *E. coli* cells (Promega), using the method in 2.1.1. Large scale cultures were grown in YT media (table 2.1a) for 5 hours at 37°C, and protein expression induced with 0.25mM isopropyl-1-thio-β-D-galactopyranoside (IPTG), and grown for a further 90 minutes. Cells were lysed by multiple freeze/thaw cycles, and insoluble material removed by centrifugation for 5 minutes at 10,000rpm.

The C-terminal construct was synthesised using the reticulocyte lysate TNT T7 coupled transcription/translation system (Promega), according to the manufacturer's protocol, in the presence of ^{35}S-labelled methionine.

In vitro binding studies were carried out using the protocol as described by Jones *et al* (2001). Briefly, 20µl of 50% slurry glutathione–agarose beads (Amersham Biosciences) was added to 1ml of N-terminal fusion construct cell lysate. Tubes were incubated for 1 hour at room temperature and washed three times with 100µl of sterile 1xphosphate buffered saline (PBS). 20µl of the labelled C-terminal construct was added, and the samples incubated for a further hour at room temperature. The samples were washed again with 100µl 1xPBS, and eluted from the glutathione-agarose beads using 10µl of elution buffer (Amersham Biosciences). Samples were run on a 12% SDS-PAGE gel, and subjected to autoradiography.

A Western blot was also performed to check the presence of the GST tag. Protein was transferred onto nitrocellulose membrane from the SDS-PAGE gel using a BioRad semi-dry transfer system, for 15 minutes at 15 Volts. The Western blot protocol was performed with the mouse anti-GST antibody and goat anti-mouse alkaline phosphatase conjugated secondary antibody. Chemiluminescence detection was performed using CSPD as a substrate, according to the manufacturer's recommended protocol (Amersham Biosciences).

2.3.4 Biacore surface plasma resonance experiments

The N- and C- terminal protein constructs were made as described in section 2.3.3, and experiments carried out according to Biacore protocols (Fig. 2.8). Briefly, the C-terminal protein was amide coupled (this step only was completed by A. Baron) to flow cell 2, with flow cells 1 and 3 being left blank, and flow cell 3 being used as a negative control. The GST coupled N-terminal construct was then washed over flow cells 2 and 3, and a relative response recorded where one response unit corresponds to 0.0001° change in the angle of the reflected light. After intensive washing, the GST vector alone control was washed over flow cells 2 and 3, and again a relative response recorded. Relative interactions of all proteins were then analysed by plotting the response against time.

2.3.5 Construction of N-terminal CFP and YFP fluorescent clones

The construction of four fluorescent N-terminal tagged rat Kv2.1 channel clones (as shown in table 2.8) was carried out using the standard PCR overlap extension method, as described in Horton *et al* (1989), and illustrated schematically in Fig. 2.9. It is worth noting that both tags are very similar with only a few amino acids differences within the centre of the tag, and hence the same primers were suitable for both pEYFP or pECFP DNA (see figure 4.1). Briefly, PCR products were made from rKv2.1-pcDNA$_3$ and either pEYFP or pECFP (Clontech) as a template, using primers with appropriate overhangs in the regions to be replaced (primers shown in table 2.9). A second round product was made which joined either CFP or YFP to the vector pcDNA$_3$. A third round product was made with primers which spanned the whole region. PCR cycling parameters were as shown in table 2.5. The relevant sized fragments were isolated by running on a 0.7% agarose gel, and excision of the bands performed as described in 2.1.7.

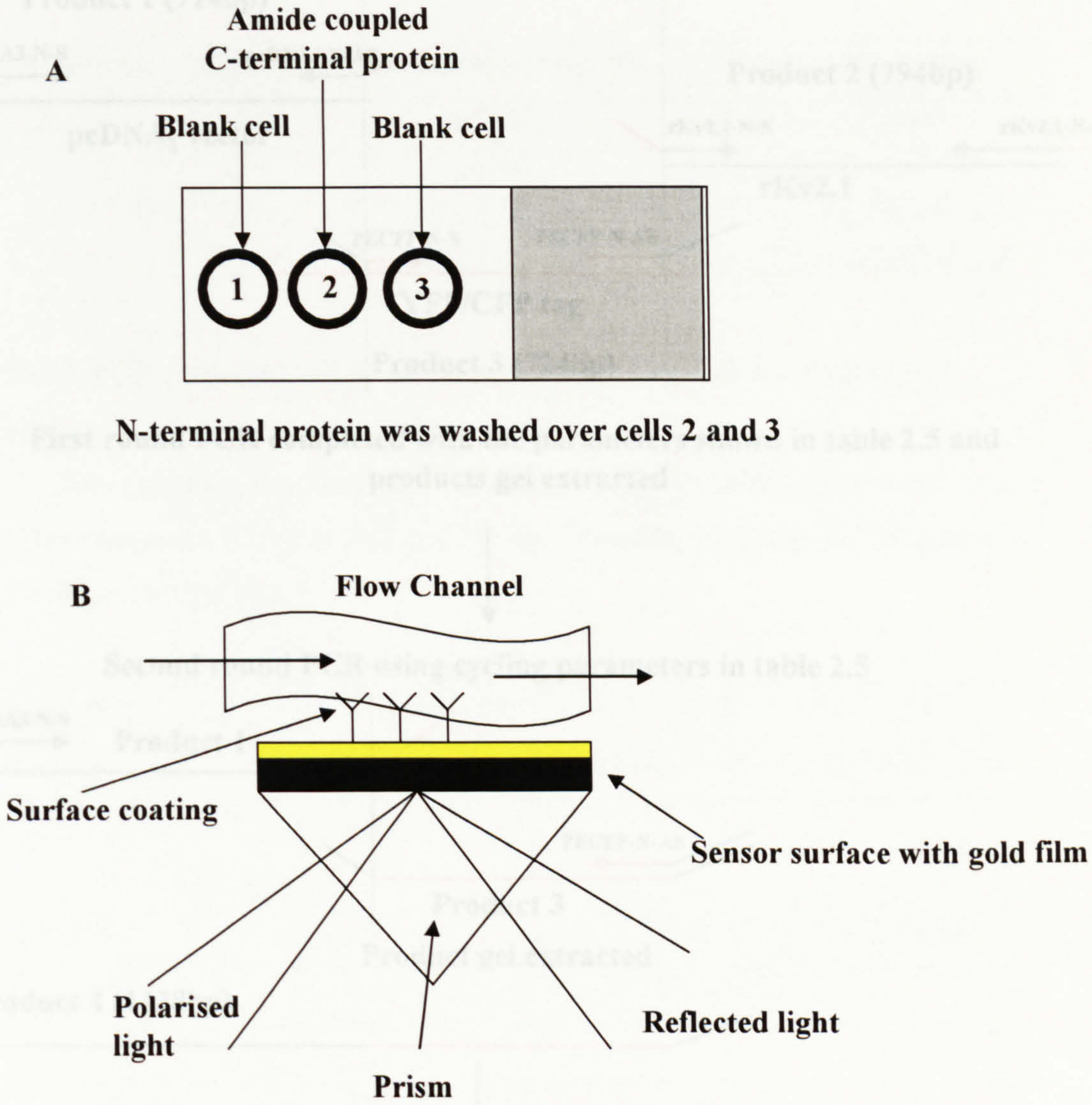

Fig. 2.8 Schematic diagram of the Biacore surface plasmon resonance system.

A) Diagram to show the contents of each cell on the Biacore chip. The C-terminal protein was attached to cell 2, with cells 1 and 3 being left blank. The N-terminal protein was then washed over cells 2 and 3. Cell 1 remained blank to check background levels of the Biacore system.

B) Polarised light is focused onto the sensor continuously. An increased sample concentration in the surface coating of the sensor (i.e an interaction with a molecule in the flow channel) causes a corresponding increase in the refractive index. This alters the angle of incidence altering the surface plasmon resonance (SPR) angle. By monitoring the SPR-angle as a function of time, the kinetic events at the surface are displayed in a sensorgram.
Taken from Technology Note 1, Biacore.

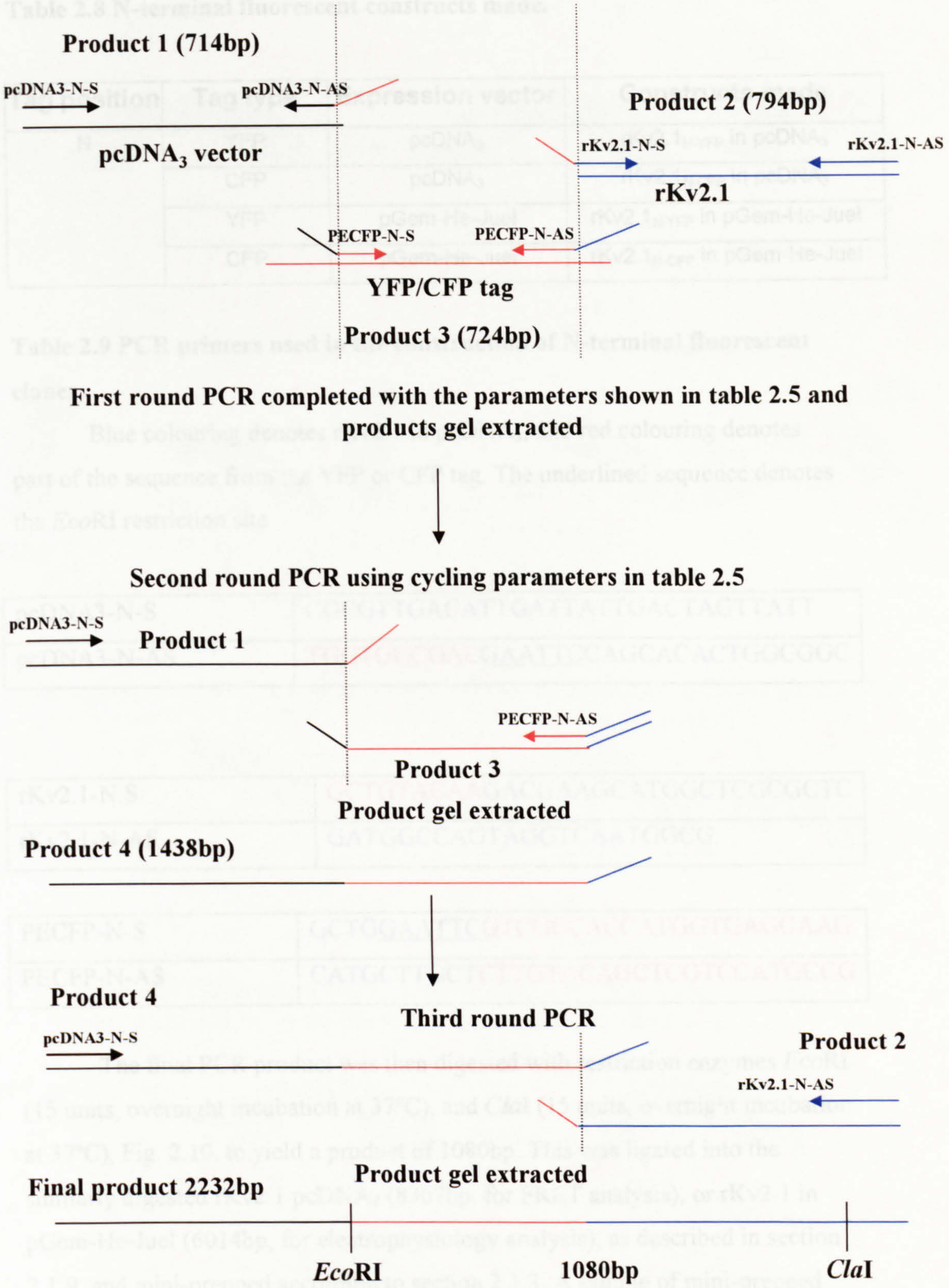

Fig. 2.9 PCR protocol of clone rKv2.1$_{N\text{-}YFP/CFP}$
PCR was carried out using the cycling parameters shown in table 2.5.
The relevant sized fragments were gel extracted and used in the next round as shown. The red colouration denotes YFP or CFP tag, black denotes pcDNA$_3$ vector and the blue denotes rat Kv2.1. The dotted lines show the fragment joins.

Table 2.8 N-terminal fluorescent constructs made.

Tag position	Tag type	Expression vector	Constructs made
N	YFP	$pcDNA_3$	$rKv2.1_{N\text{-}YFP}$ in $pcDNA_3$
	CFP	$pcDNA_3$	$rKv2.1_{N\text{-}CFP}$ in $pcDNA_3$
	YFP	pGem-He-Juel	$rKv2.1_{N\text{-}YFP}$ in pGem-He-Juel
	CFP	pGem-He-Juel	$rKv2.1_{N\text{-}CFP}$ in pGem-He-Juel

Table 2.9 PCR primers used in the construction of N-terminal fluorescent clones.

Blue colouring denotes rKv2.1 in $pcDNA_3$, and red colouring denotes part of the sequence from the YFP or CFP tag. The underlined sequence denotes the *Eco*RI restriction site.

pcDNA3-N-S	CGCGTTGACATTGATTATTGACTAGTTATT
pcDNA3-N-AS	TGGTGGCGACGAATTCCAGCACACTGGCGGC

rKv2.1-N.S	GCTGTACAAGACGAAGCATGGCTCGCGCTC
rKv2.1-N-AS	GATGGCCAGTAGGTCAATGGCG

PECFP-N-S	GCTGGAATTCGTCGCCACCATGGTGAGCAAG
PECFP-N-AS	CATGCTTGCTCTTGTACAGCTCGTCCATGCCG

The final PCR product was then digested with restriction enzymes *Eco*RI (15 units, overnight incubation at 37°C), and *Cla*I (15 units, overnight incubation at 37°C), Fig. 2.10, to yield a product of 1080bp. This was ligated into the similarly digested rKv2.1 $pcDNA_3$ (8367bp, for FRET analysis), or rKv2.1 in pGem-He-Juel (6014bp, for electrophysiology analysis), as described in section 2.1.9, and mini-prepped according to section 2.1.3. A sample of mini-prepped DNA was sent to Lark Technologies to confirm that the correct clone had been made. The universal sequencing primer T7 was used. The $pcDNA_3$ clone was used for tissue culture expression for FRET analysis, and the pGem-He-Juel clone was used for two voltage clamp experiments.

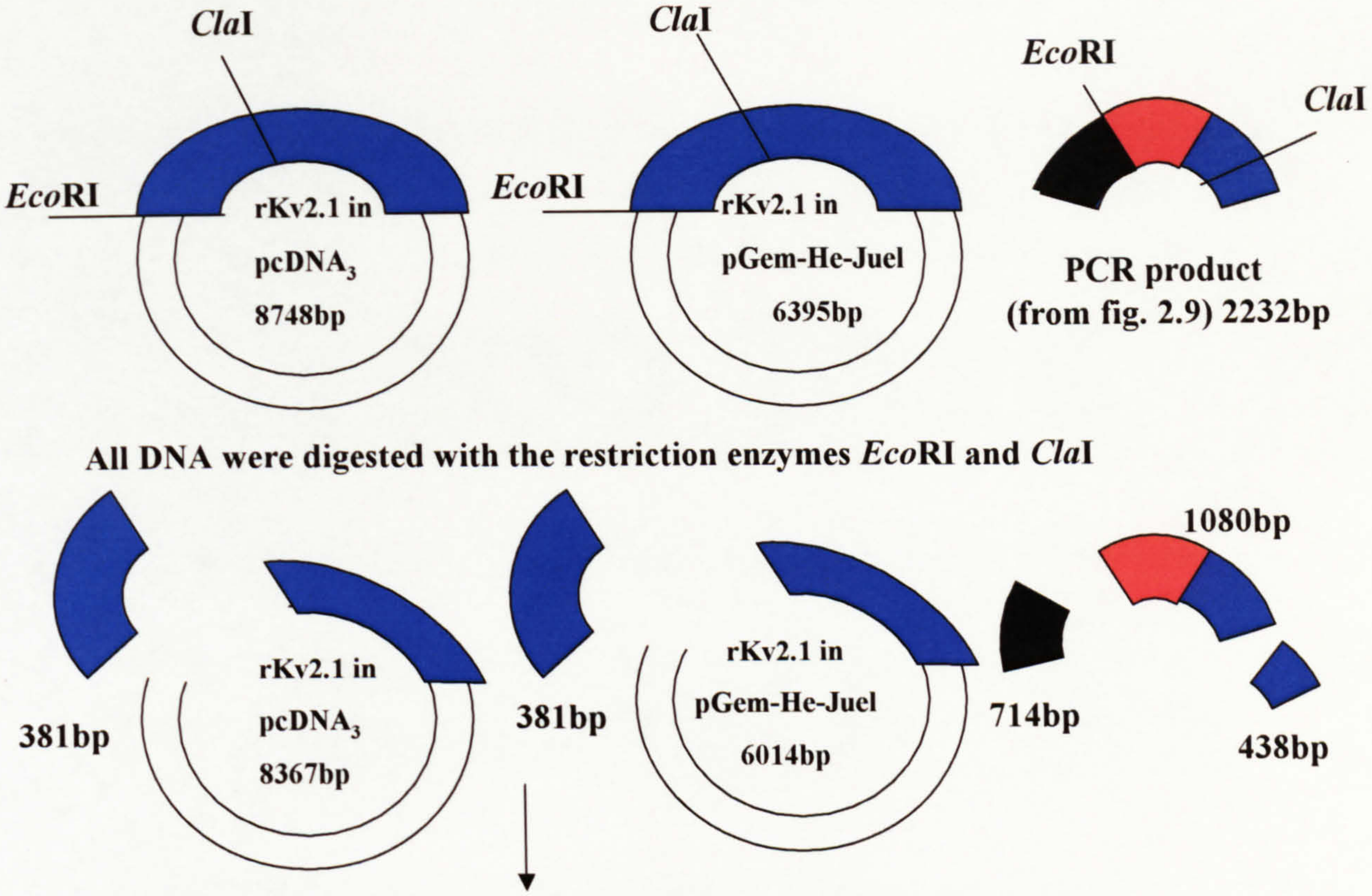

Fig. 2.10 Schematic diagram of the construction of clone rKv2.1$_{N\text{-}YFP/CFP}$. Only the restriction sites involved are labelled, and the sizes of fragments are indicated. Red colouration denotes YFP/CFP tag, blue denotes rKv2.1 and black (in PCR fragment) denotes pcDNA$_3$. Diagram not drawn to scale.

2.3.6 Construction of C-terminal CFP and YFP fluorescent clones

The construction of four fluorescent C-terminal tagged rat Kv2.1 channel clones was also carried out using the standard PCR overlap extension (Horton *et al,* 1989), and is illustrated schematically in Fig. 2.11. Constructs made are shown in table 2.10.

Table 2.10 C-terminal fluorescent constructs made.

Tag position	Tag type	Expression vector	Constructs made
C	YFP	$pcDNA_3$	$rKv2.1_{C\text{-}YFP}$ in $pcDNA_3$
	CFP	$pcDNA_3$	$rKv2.1_{C\text{-}CFP}$ in $pcDNA_3$
	YFP	pGem-He-Juel	$rKv2.1_{C\text{-}YFP}$ in pGem-He-Juel
	CFP	pGem-He-Juel	$rKv2.1_{C\text{-}CFP}$ in pGem-He-Juel

Briefly, PCR products were made from rKv2.1-$pcDNA_3$ and either pEYFP or pECFP (Clontech) as a template, using primers with appropriate overhangs in the regions to be replaced (primers shown in table 2.11). A second round product was made which joined the CFP or YFP at the C-terminal position in rKv2.1. A third round product was made with primers which spanned the whole region. PCR cycling parameters were as shown in table 2.5. The relevant sized fragments were isolated by running on a 0.7% agarose gel, and excision of the bands performed as described in 2.1.7. The C-terminal YFP clone in pcDNA3 was made by J. Li.

Table 2.11 PCR primers used in the construction of C-terminal fluorescent clones.

Blue colouring denotes rKv2.1 in $pcDNA_3$, and red colouring denotes YFP or CFP tag.

rKv2.1-C-S	CCCCTTGAAGCTGCGAGCG
rKv2.1-C-AS	TGCTCACCATGATACTCTGATCCCTAGTGCTCCC

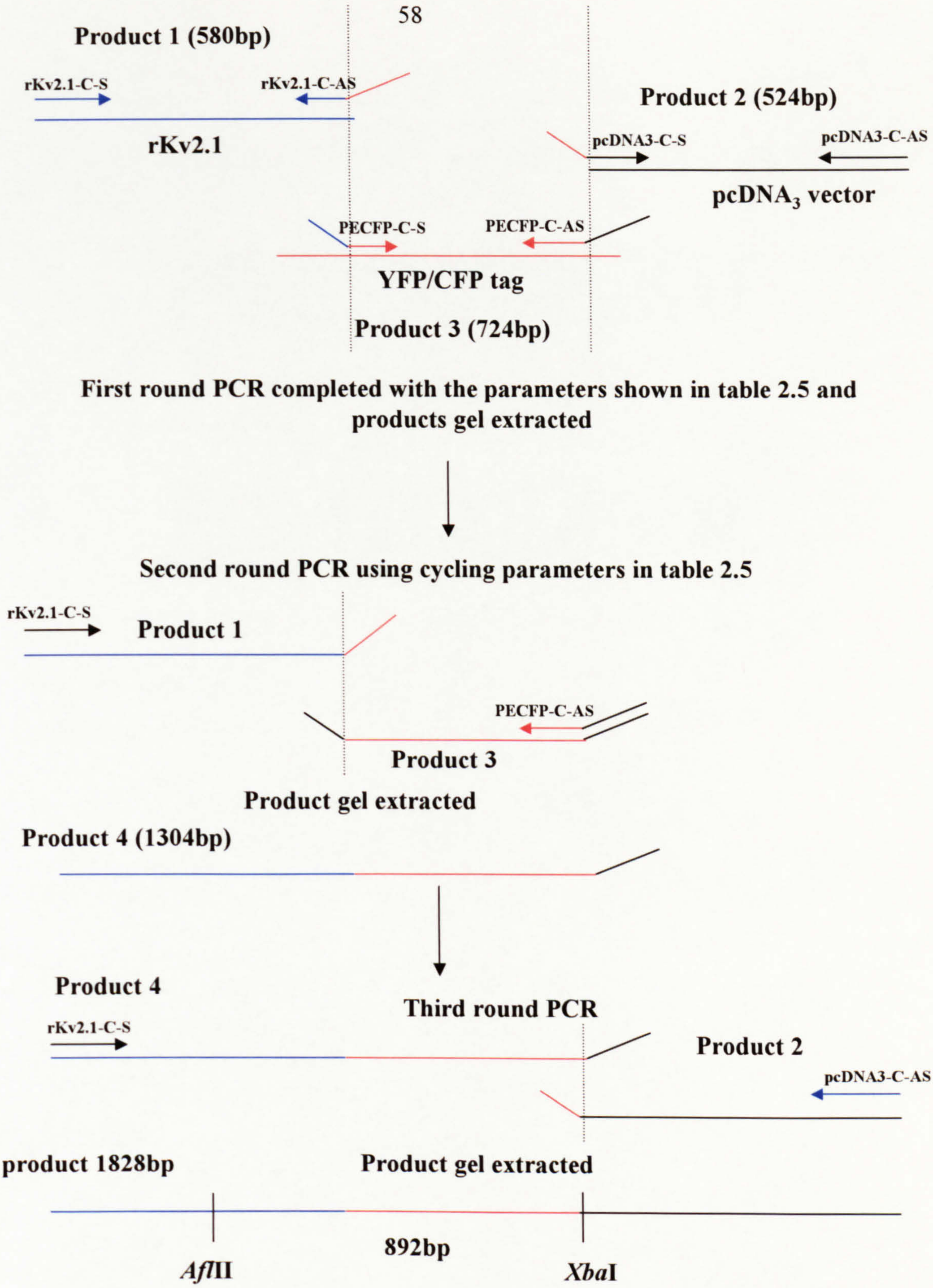

Fig. 2.11 PCR protocol of clone rKv2.1$_{C\text{-}YFP/CFP}$
PCR was carried out using the cycling parameters shown in table 2.5. The relevant sized fragments were gel extracted and used in the next round as shown. The red colouration denotes YFP or CFP tag, black denotes pcDNA$_3$ vector and the blue denotes rat Kv2.1. The dotted lines show the fragment joins.

pcDNA3-C-S	CGACTCTAGAGGGCCCTATTCTATAGTGTCACCTAAATG
pcDNA3-C-AS	GGGTCGAGGTGCCGTAAAGCACT

PECFP-C-S	TCAGAGTATCATGGTGAGCAAGGGCGAGGAG
PECFP-C-AS	AATAGGGCCCTCTAGAGTCGCGGCCGCTTTAC

The PCR product was digested with restriction enzymes *Afl*II (15 units, overnight incubation at 37°C), and *Xba*I (15 units, overnight incubation at 37°C), Fig. 2.12, to yield a product of 892bp. This was ligated into the similarly digested rKv2.1 pcDNA$_3$ (8098bp digested vector size, for FRET analysis) or rKv2.1 in pGem-He-Juel (5745bp digested vector size, for electrophysiology analysis), as described in section 2.1.9, and mini-prepped as described in section 2.1.3. Samples of mini-prepped DNA were sent to Lark Technologies to confirm that the correct clones had been made. The universal sequencing primer M13 was used.

2.3.7 Construction of double tagged fluorescent clone rKv2.1$_{N\text{-}YFP/C\text{-}CFP}$

Constructs were made with an N-terminal YFP and a C-terminal CFP tag in pcDNA$_3$ and pGem-He-Juel (as shown in table 2.12). For this the starting point was the N-terminal PCR product (as described in section 2.3.6) and rKv2.1$_{C\text{-}CFP}$ in either pcDNA$_3$ or PGem-He-Juel. These were digested using the restriction enzymes *Eco*RI (15 units, overnight incubation at 37°C), and *Cla*I (15 units, overnight incubation at 37°C), see Fig. 2.13 for details. The fragments were isolated by running on a 0.7% agarose gel and excision of the bands performed as described in section 2.1.7. The larger PCR fragment (1080bp) was ligated to the larger (rKv2.1$_{C\text{-}CFP}$) vector fragment (8323bp for the pcDNA$_3$ construct and 5970bp for the pGem-He-Juel construct (sizes of fragments before ligation), as outlined in section 2.1.9, and mini-prepped according to section 2.1.3. A sample

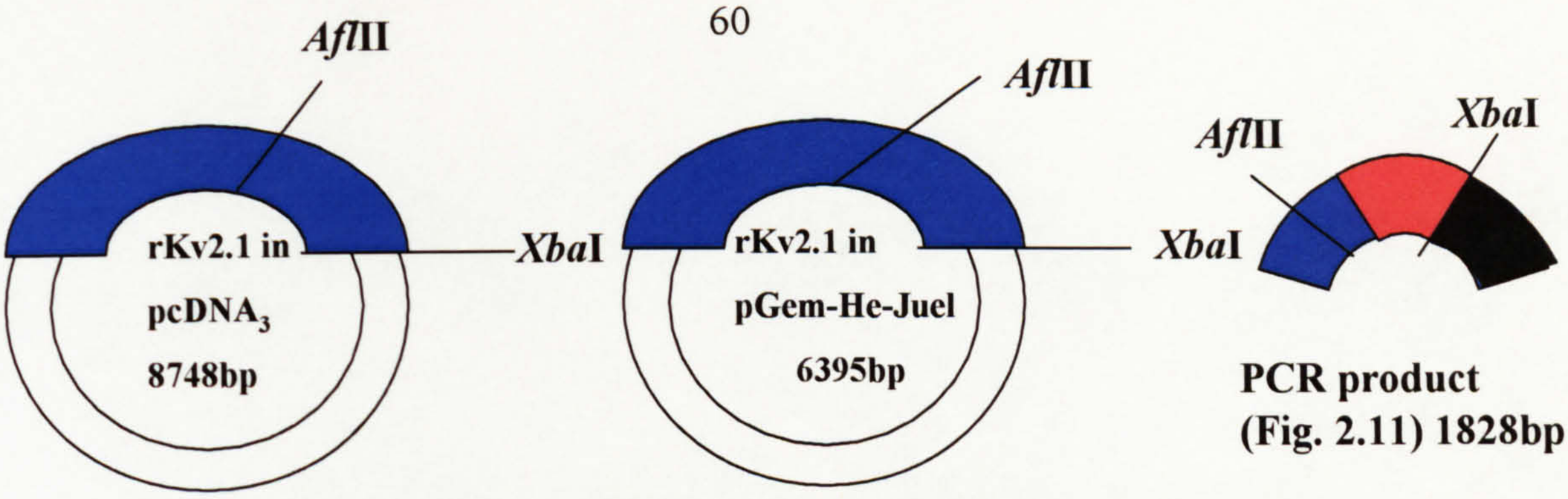

Fig. 2.12 Schematic diagram of the construction of clone rKv2.1$_{C\text{-}CFP/YFP}$.

Only the restriction sites involved are labelled, and the sizes of fragments are indicated. Red colouration denotes the YFP/CFP tag, blue denotes rKv2.1, and black (in PCR fragment) denotes pcDNA$_3$ vector. Diagram not drawn to scale.

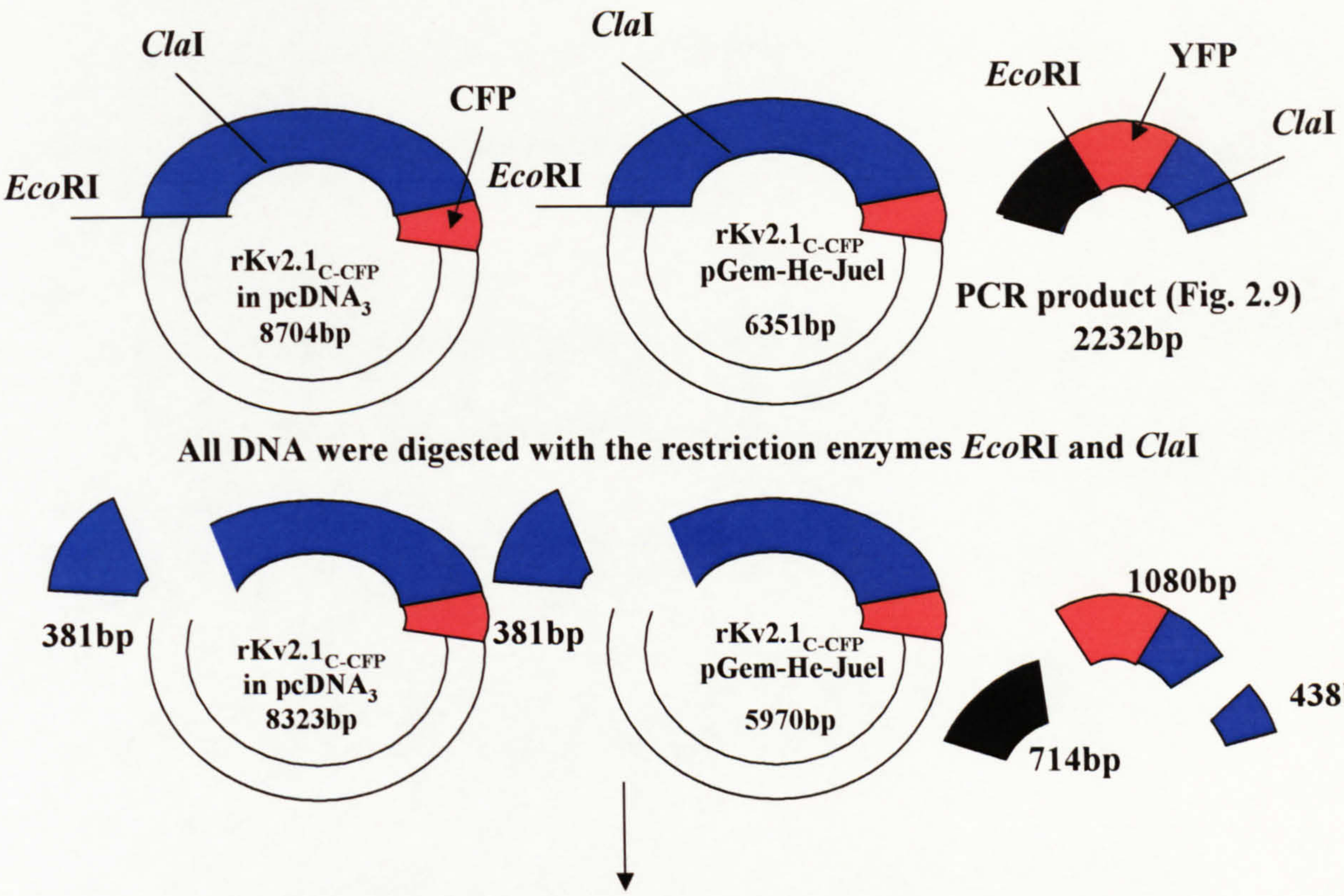

Fig. 2.13 Schematic diagram of the construction of the double tagged rKv2.1$_{N\text{-}YFP/C\text{-}CFP}$.
Only the restriction sites involved are labelled, and the sizes of the fragments are indicated. Red colouration denotes the YFP/CFP tags, blue denotes rKv2.1, and black (in the PCR fragment) denotes pcDNA$_3$. Diagram not drawn to scale.

of mini-prepped DNA was sent to Lark Technologies to confirm that the correct sub-clone had been made. The universal sequencing primer T7 was used.

Table 2.12 Double tagged fluorescent constructs made.

Tag position/Type	Tag position/Type	Expression vector	Constructs made
N/YFP	C/CFP	$pcDNA_3$	$rKv2.1_{N\text{-}YFP\text{-}C\text{-}CFP}$ in $pcDNA_3$
N/YFP	C/CFP	pGem-He-Juel	$rKv2.1_{N\text{-}YFP\text{-}C\text{-}CFP}$ in pGem-He-Juel

2.4 Specific molecular biology methods III

2.4.1 Construction of rKv2.1 pMT3 clone

rKv2.1 was sub-cloned into the pMT3 vector already containing the ID4 tag, to enable purification for electron microscopy (the sequence of the tag is shown in Fig. 5.1c). The construction of this clone was also performed using standard overlap extension PCR (Horton *et al,* 1989) and is illustrated schematically in Fig. 2.14.

Briefly, first round PCR products were made using rKv2.1 in pBluescript and *Shaker* in pMT3 as template (clone donated by N. Grigorieff, Brandeis University, MA) using appropriate overhangs at the regions to be replaced in the clone (primers are shown in table 2.13). A second round product was made which joined the pMT3 vector to rKv2.1, using primers that span the whole region. PCR cycling parameters are shown in table 2.5.

Table 2.13 PCR primers used in the construction of rKv2.1 pMT3.

All primers are shown 5' to 3'. Red colouring denotes pMT3 vector and blue denotes rKv2.1 in pBluescript. The pBluescript sense primer runs from the pBluescript vector through into the N-terminal end of rKv2.1. The annealing temperature of all primers was approximately 60°C.

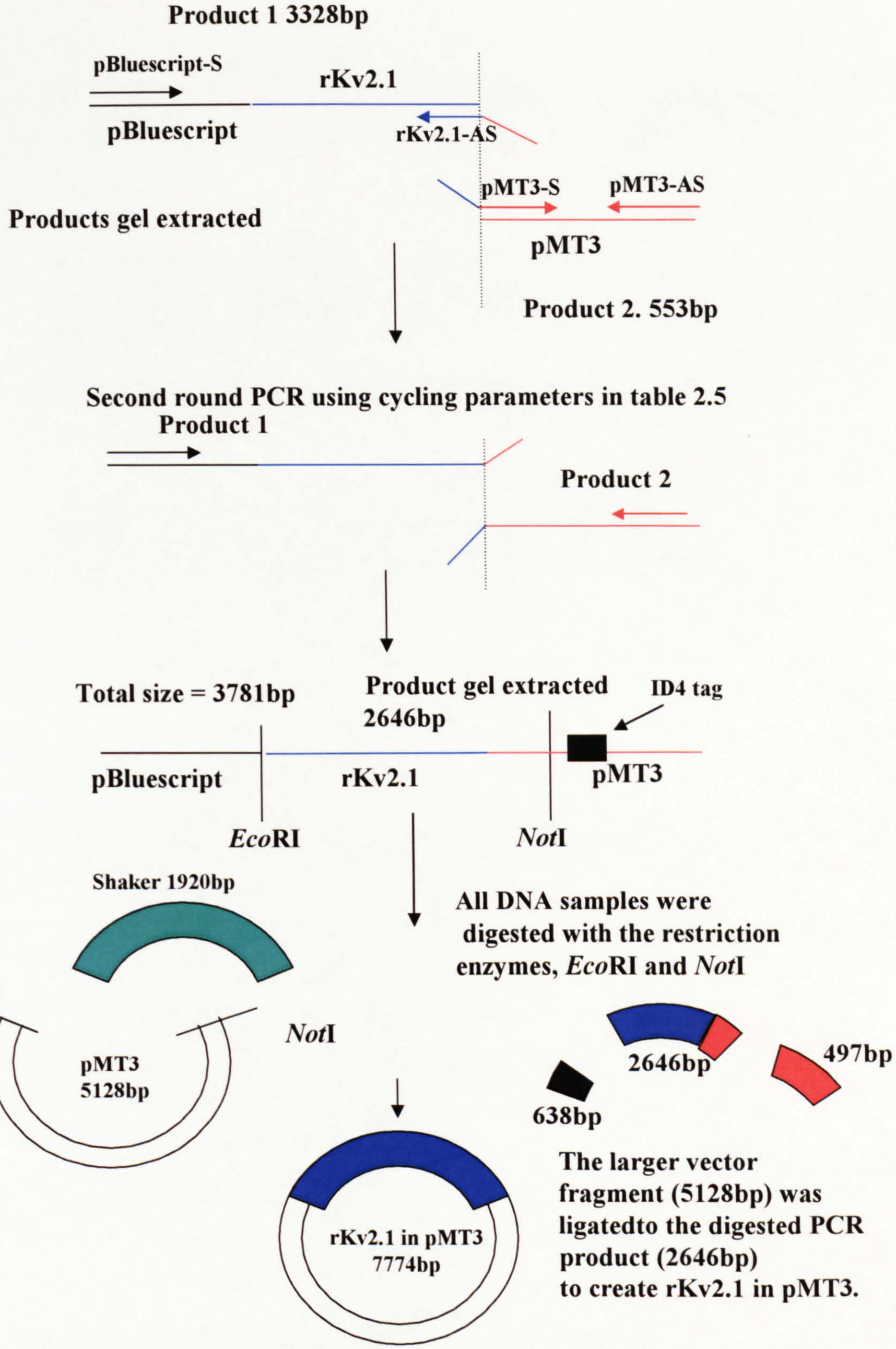

Fig. 2.14 PCR protocol and schematic diagram of the construction of rKv2.1-pMT3. Restriction sites involved are labelled, and sizes of the fragments indicated. The red colouration denotes the pMT3 vector, the blue denotes rKv2.1, and the black in the PCR product denotes the pcDNA$_3$ vector. The dotted lines show the joins of the two PCR overhangs. Diagram not drawn to scale.

pBluescript-S	CCGCTACACTTGCCAGCGCC
rKv2.1-AS	CGTCGGGCTGGATACTCTGATCCCTAGTGCTCCCG
pMT3-S	TCAGAGTATCCAGCCCGACGGTGACCCG
pMT3-AS	CAAAGTACCGTAATCTCCGAGCTG

The relevant sized fragments were excised by running on a 0.7% agarose gel and excision of the bands performed as described in 2.1.7. The final PCR fragment was digested with *Eco*RI (15 units, overnight incubation at 37°C) and *Not*I (15 units, overnight incubation at 37°C), see Fig. 2.14 for details. The digested PCR product (2646bp) was then ligated into the similarly digested pMT3 vector (5128bp), as described in section 2.1.9, and mini-prepped according to section 2.1.3. A sample of mini-prepped DNA was sent to Lark Technologies to confirm that the correct sub-clone had been made, using the pMT3 sequencing primer (5'-CCCTTGCCCACC-3').

2.4.2 Insertion of Δ7 agitoxin site

In order to render the rKv2.1 protein susceptible to binding of agitoxin-2 (Lee *et al,* 2004) a Δ7 site was sub-cloned into the rKv2.1 pMT3 clone. This contained seven mutations in the S5-S6 linker between residues 361 and 390. The relevant part of the sequence was sub-cloned from a construct containing these mutations, rKv2.1 Δ7 in Pblu-Sk provided by K.J. Swartz, National Institute for Health, Maryland, constructed as described in Lee *et al* (2004). Firstly, both plasmids were digested with *Nru*I (15 units, overnight incubation at 37°C), and *Bsp*1407I (15 units, overnight incubation at 37°C), see Fig. 2.15. Fragments were isolated by running on a 0.7% agarose gel, and excision of the bands was performed as described in section 2.1.7. The smaller, Δ7 site (579bp) fragment was ligated into the larger rKv2.1 pMT3 (7195bp) as outlined in section 2.1.9, and mini-prepped according to section 2.1.3. A sample of mini-prepped DNA was sent to Lark Technologies to confirm that the rKv2.1 Δ7 in pMT3 clone had been made, by sequencing using the pMT3 Δ7 sequencing primer (5'-GATCTTTCGCATCATGCGC-3').

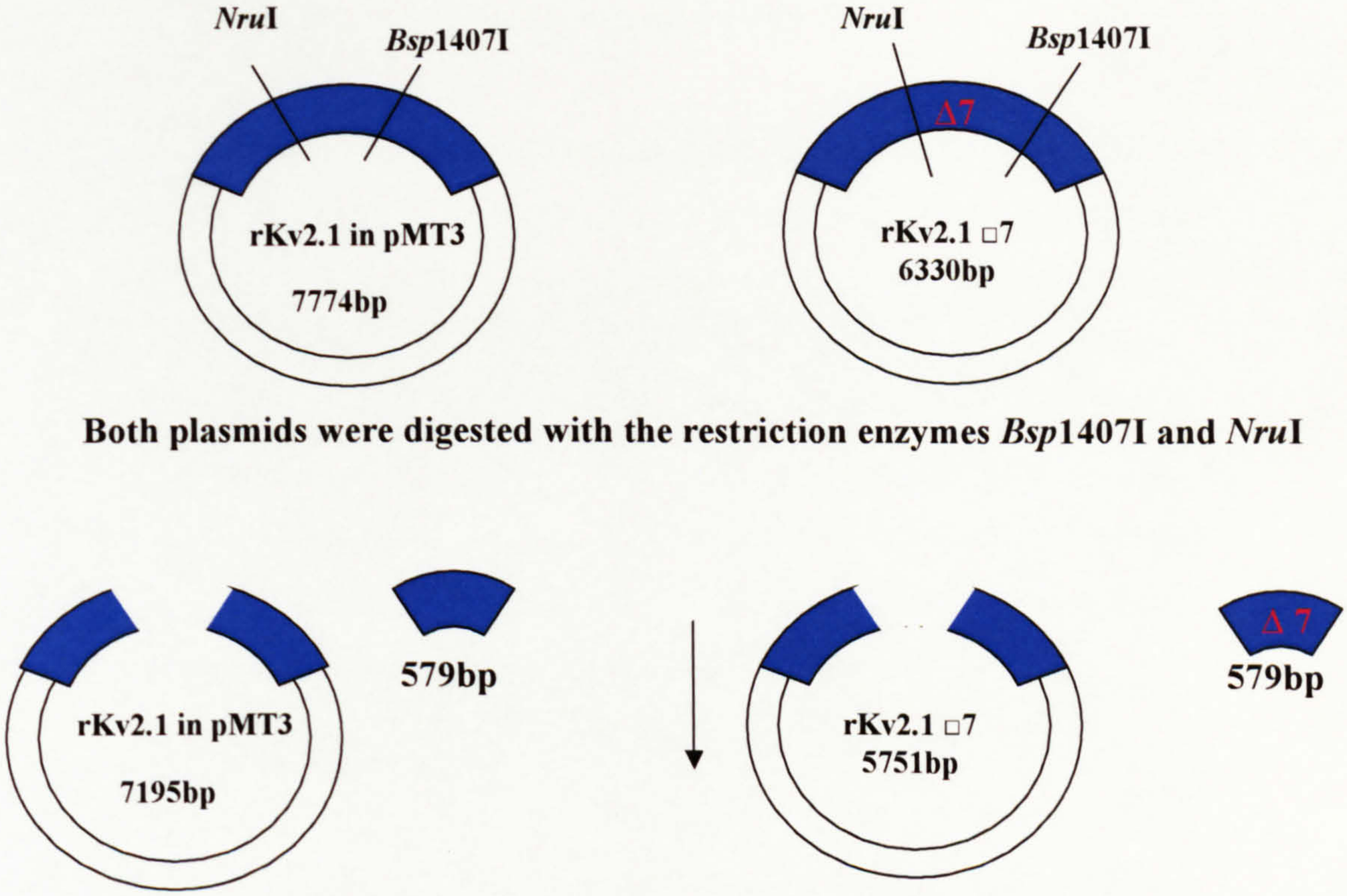

Fig. 2.15 Schematic diagram of the construction of the rKv2.1 Δ7 in pMT3 clone. The different parts of the plasmids that were exchanged following restriction enzyme digestion are shown. Diagram not drawn to scale.

2.4.3 Construction of the C-terminal deletion clone

In order to investigate the structural importance of the C-terminus of Kv2.1, a deletion of the whole C-terminal domain was made. The construction of this clone was again carried out using standard overlap extension PCR, (Horton *et al*, 1989) see Fig. 2.16 for protocol. Briefly, first round PCR products were made using rKv2.1 Δ7 in pMT3 as template, using appropriate overhangs at the regions to be replaced in the clone; primers are shown in table 2.14. A second round PCR product was made which joined the pMT3 vector to rKv2.1 after the S6 domain, using primers that span the whole region. PCR cycling parameters are shown in table 2.5.

Table 2.14 PCR primers used in the construction of rKv2.1($\Delta 7$)$_{\text{-no C}}$ pMT3.

All primers are shown 5' to 3'. Red colouring denotes pMT3 vector, and blue denotes Kv2.1.

rKv2.1-no C-S	GATGAGATCTACCTGGAGTCCTGC
rKv2.1-no C-AS	CGTCGGGCTGGTTATTGACGATGATGGGGATG
pMT3-no C-S	CGTCAATAACCAGCCCGACGGTGACCC
pMT3-no C-AS	CTAAAGCCAGCAAAAGTCCCATG

The relevant sized fragments were excised by running on a 0.7% agarose gel and excision of the bands performed as described in 2.1.7. The PCR fragment was digested with *Apa*I (15 units, overnight incubation at 37°C) and *Not*I (15 units, overnight incubation at 37°C), Fig. 2.16. The digested PCR product (532bp) was then ligated into the similarly digested rKv2.1 Δ7 pMT3 vector (5919bp) as described in section 2.1.9, and mini-prepped according to section 2.1.3. A sample of mini-prepped DNA was sent to Lark Technologies to confirm that the rKv2.1 $\Delta 7_{\text{-no C}}$ in pMT3 clone had been made, using the pMT3 Δ7 sequencing primer (section 2.4.2).

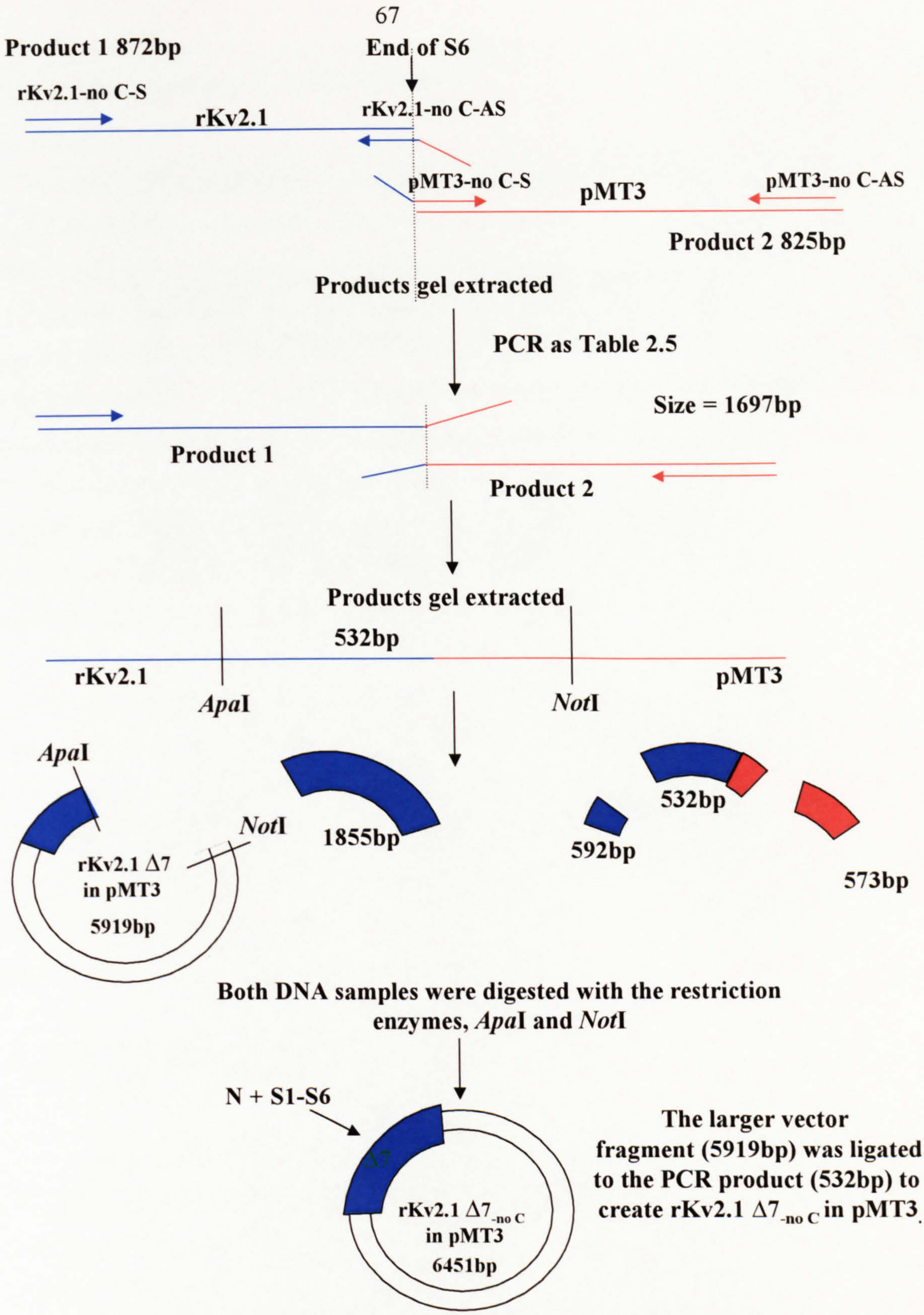

Fig. 2.16 PCR protocol and schematic diagram of the construction of rKv2.1 $\Delta 7_{-no\ C}$ in pMT3.

Restriction sites involved are labelled, and sizes of the fragments indicated. Red colouration denotes pMT3 vector and blue denotes Kv2.1. The dotted lines show the joins of the PCR products. Diagram not drawn to scale.

2.4.4 Protein expression and purification

rKv2.1 Δ7 in pMT3 wild type and rKv2.1 $\Delta 7_{\text{-no C}}$ pMT3 channels were expressed in COS-7 cells at 37°C under 5% CO_2 atmosphere, in a high-glucose DMEM with 10% FBS. GeneJuice (Novagen) transfection was performed when the cells were at 70% confluence, according to the manufacturer's recommended protocol. Cells were harvested with a cell scraper after 72 hours, and washed twice using 1xPBS. Whole cells were solublized using the protocol described by Sokolova *et al* (2003). Purification was carried out on a ID4 affinity column (antibody-coupled sepharose beads). The channel was eluted by using a ID4 peptide solution (0.2mg/ml) in an elution buffer containg 80mM KCl, 2mM NaEDTA, 40mM HEPES-KOH, 300mM NaCl, 0.5% CHAPS, and protease inhibitors (Roche complete protease tablet). Protein samples were run on an SDS-PAGE protein gel to confirm the purity of the protein. A Western blot was carried out to confirm the presence of the ID4 tag. Protein was transferred onto nitrocellulose membrane from the SDS-PAGE gel using a BioRad semi-dry transfer system, for 15 minutes at 15 Volts. The Western blot protocol was performed with the anti-ID4 antibody and goat anti-mouse HRP conjugated secondary antibody., chemiluminescence detection was performed using horseradish peroxidase, according to the manufacturer's recommended protocol (Novagen).

2.4.5 [I^{125}]-agitoxin binding assay

Assay was carried out according to Sokolova *et al* (2003). Firstly, [I^{125}]-labelled agitoxin-2 was added to the elution fractions (from section 2.4.4) to a final concentration of 12.5nM. After 30 minutes incubation on ice, unbound toxin (which is smaller in size) was removed from the Kv2.1-toxin complexes using a Microcon filter device (pore size 100μM, Millipore). The filter was transferred to a scintillation vial, and scintillation counted.

2.5 Specific molecular biology methods IV

2.5.1 Construction of CGGG calcium channel cysteine mutants

In order to determine the effects of PCMBS on cysteine residues substituted into the domain I S4 region of the CGGG calcium channel chimera (Li *et al*, 2004), it was necessary to mutate wild type amino acids in the S4 segment of domain I (this chimera contained $Ca_v1.2$ in domain I and $Ca_v3.1$ in domains II-IV). This was done using the QuikChange™ site-directed mutagenesis method, as explained in 2.1.5. The mutants to be generated were V263C, A265C, L266C, A268C, F269C, and V271C.

In order to limit the size of the fragments amplified by PCR, and hence reduce the probability of errors, the thermal cycling was performed in a section of the chimera in pUC18 vector, as shown in Figure 2.17. Pairs of primers were used as shown in table 2.15.

Table 2.15 PCR primers used in the construction of CGGG cysteine mutants.

Sequences are shown in the 5' to 3' direction. Mismatched bases are shown in red, and the changed amino acid is underlined.

V263C sense	GCTGGATTCGAC**TGC**AAGGCGCTGAGG
V263C anti-sense	CCTCAGCGCCTT**GCA**GTCGAATCCAGC

A265C sense	CGACGTGAAG**TGC**CTGAGGGCTTTCCG
A265C anti-sense	CGGAAAGCCCTCAG**GCA**CTTCACGTCG

L266C sense	GACGTGAAGGCG**TGC**AGGGCTTTCCGC
L266C anti-sense	GCGGAAAGCCCT**GCA**CGCCTTCACGTC

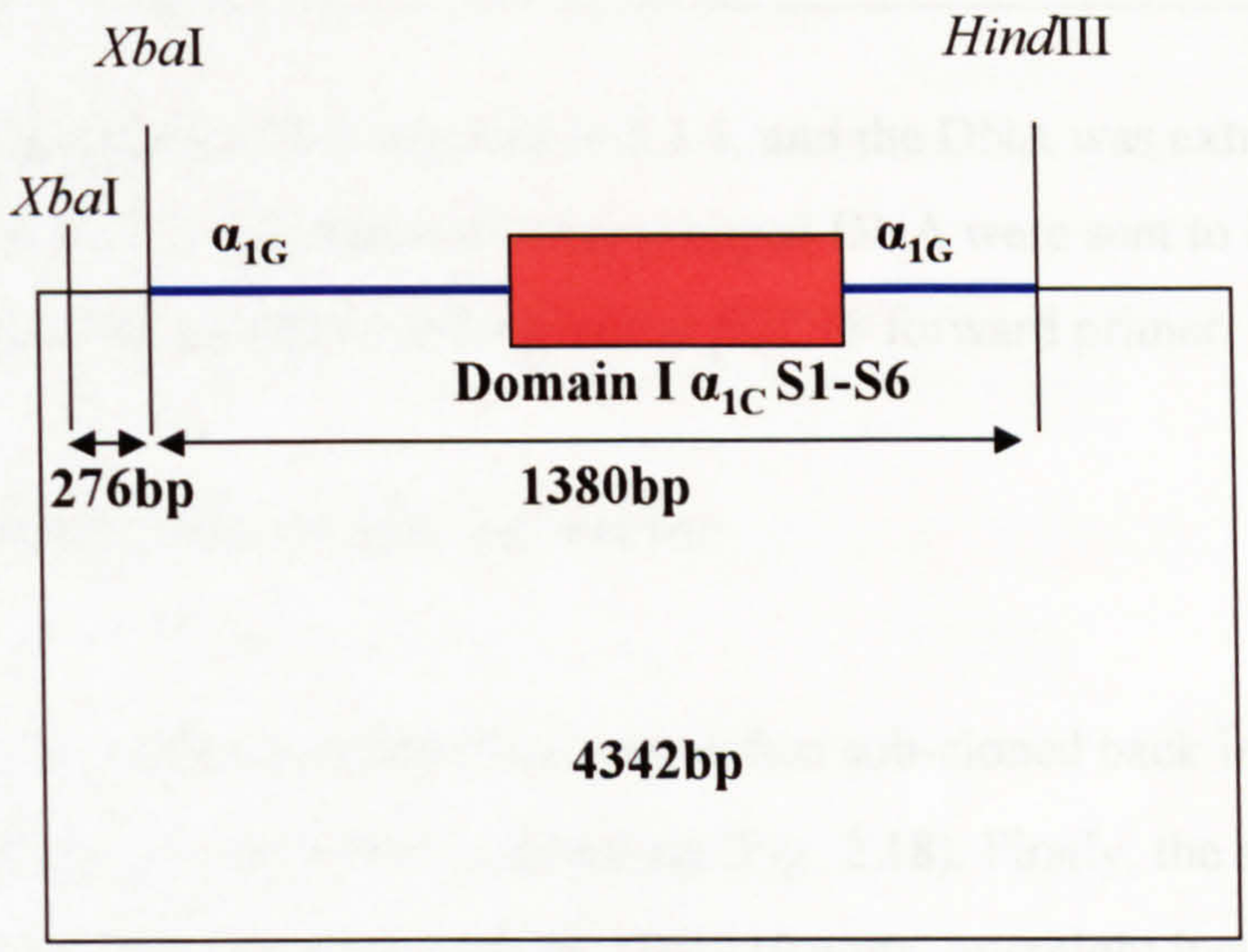

Fig. 2.17 Schematic diagram of CGGG in the pUC18 vector
The restriction sites for *Xba*I and *Hind*III are shown, along with the fragment sizes.

A268C sense	GAAGGCGCTGAGGTGTTTCCGCGTGC
A268C anti-sense	GCACGCGGAAACACCTCAGCGCCTTC

F269C sense	GCGCTGAGGGCTTGCCGCGTGCTG
F269C anti-sense	CAGCACGCGGCAAGCCCTCAGCGC

V271C sense	GGGCTTTCCGCTGCCTGCGCCCCC
V271C anti-sense	GGGGGCGCAGGCAGCGGAAAGCCC

Transformation was as detailed in 2.1.1, and the DNA was extracted as outlined in section 2.1.3. Samples of mini-prepped DNA were sent to Lark for automated sequencing using a Lark universal pUC18 forward primer.

2.5.2 Sub-cloning into pGem-hel vector

All of the mutant cysteine clones were then sub-cloned back into wild type α_{1G} in pGem-hel vector after sequencing (Fig. 2.18). Firstly, the site-directed clones were restricted using the enzyme *Xba*I (10 units, overnight incubation at 37°C), which cuts the cysteine mutant clones twice giving bands of 276bp and 4066bp (see Fig. 2.18). The wild type α_{1G} clone was also linearised with *Xba*I giving a fragment of 9989bp. After checking the digest was successful, the reaction product was gel extracted as described in section 2.1.7.

The larger 4066bp fragment of the *Xba*I- restricted DNA was then cut using *Hind*III (10 units, overnight incubation at 37°C). This second restriction digest produced two fragments. For the cysteine mutants the larger vector fragment was 2686bp (which was discarded), and the smaller, 1380bp fragment (which contained the cysteine mutation) was gel extracted as described in section 2.1.7. For the $\alpha_{1G,}$ the larger vector fragment was 8609bp, and the smaller domain I fragment was 1380bp. The larger fragment was gel extracted, and dephosphorylated as in section 2.1.8 to prevent self-ligation.

Ligation of the dephosphorylated vector and the cysteine fragment was performed for each of the six cysteine mutations, as outlined in section 2.1.9, and

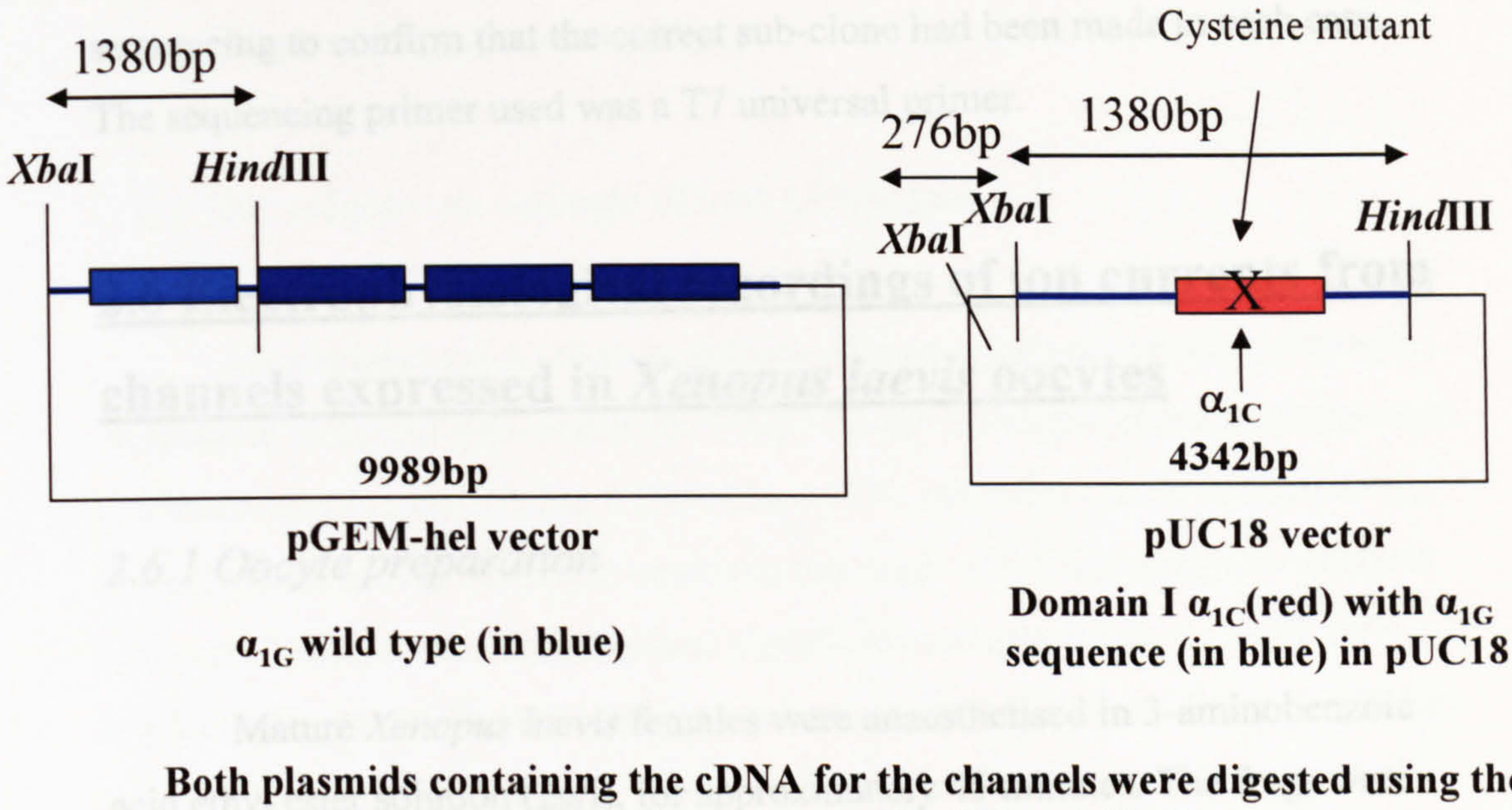

Fig. 2.18 Schematic diagram of the sub-cloning of the cysteine mutants.

following transformation and selection, DNA were mini-prepped as described in section 2.1.3. Samples of mini-prepped DNA was sent to Lark Technologies for sequencing to confirm that the correct sub-clone had been made in each case. The sequencing primer used was a T7 universal primer.

2.6 Electrophysiological recordings of ion currents from channels expressed in *Xenopus laevis* oocytes

2.6.1 Oocyte preparation

Mature *Xenopus laevis* females were anaesthetised in 3-aminobenzoic acid ethyl ester solution (2g/l), for approximately 45 minutes. The frogs were then killed using a standard schedule 1 method of severing the spinal cord, and pithing the brain. The ovarian lobes were dissected out and placed in calcium-free Ringer solution (table 2.1d). Oocytes were isolated by placing a lobe in a collagenase 1A solution (2mg/ml) with gentle agitation for 40 minutes. The cells were then washed three times in calcium free Ringer solution to remove any remaining collagenase. The follicular layer was removed using ultra fine watchmaker's forceps (Dumont, size 5, Agar Scientific). Stage V and VI ooctyes (Dumont, 1972) were selected and stored in calcium free Ringer solution prior to injection of cRNA.

2.6.2 Microinjection of oocytes with cRNA

Oocytes were injected using a micropipette made from borosilicate glass tubing (Drummond Scientific Company), by pulling using a Sutter Instrument Model P-87 Flaming/Brown horizontal pipette puller. The tip of the micropipette was manually broken to a diameter of approximately 15μm using forceps. The micropipette was then backfilled with mineral oil, and loaded onto a 10μl Drummond microinjection syringe mounted on a Micro-instruments manipulator. A microscope slide was then covered with Nescofilm (VWRI), onto which 1μl of cRNA was deposited, and drawn up into the micropipette. Each individual

oocyte was injected with 50nl of cRNA within the vegetal pole of the cell. After injection, oocytes were stored in 96 well plates at 19.6°C for 1 day (potassium channels) or 4 days (calcium channels).

2.6.3 Two-electrode voltage clamp technique

All electrophysiological recordings of potassium and calcium channels were made using the two-electrode voltage clamp technique at room temperature. Currents were recorded using a GeneClamp 500 amplifier (Axon Instruments), controlled via a CED 1401plus analogue interface with CED computer analysis software. Voltage and current output signals were displayed on a Gould 4064 digital oscilloscope. Current signals were sampled at 4kHz, and filtered at 2kHz.

Oocytes were held in a 50µl recording chamber (as shown in Fig. 2.19) and perfused with either frog Ringer (table 2.1d) for potassium channels, or calcium free barium solution (table 2.1d) for calcium channels. Perfusion was at a rate of 2ml/min in all recordings. Microelectrodes were pulled from borosilicate glass (Harvard), using a two-stage vertical puller, and filled with 3M KCl. The microelectrodes were then inserted into the holders (Harvard), which contained a chlorided silver wire, and attached to the headstages (Axon Instruments). Headstages and holders were mounted onto micro-manipulators (Micro-instruments). The bath electrode was made from a Ag/AgCl pellet for potassium channels, and was a chloride silver wire in 3M KCl agar for calcium channel recording. Tip resistances were measured, and were typically between 1.0 and 2.5MΩ for the voltage electrode, and 0.5-1.0MΩ for the current electrode.

The oocyte was impaled by the voltage and current electrodes, and the resting membrane potential was measured after being allowed to stabilise for 5 minutes. The internal voltage clamp offset was set to the resting membrane potential, and the GeneClamp was switched to voltage clamp. The gain and stability were increased while the GeneClamp repetitively depolarised the oocyte by 10mV (0.1Hz) until a square voltage trace was visible on the oscilloscope. The membrane was then clamped to -80mV, and the input resistance noted.

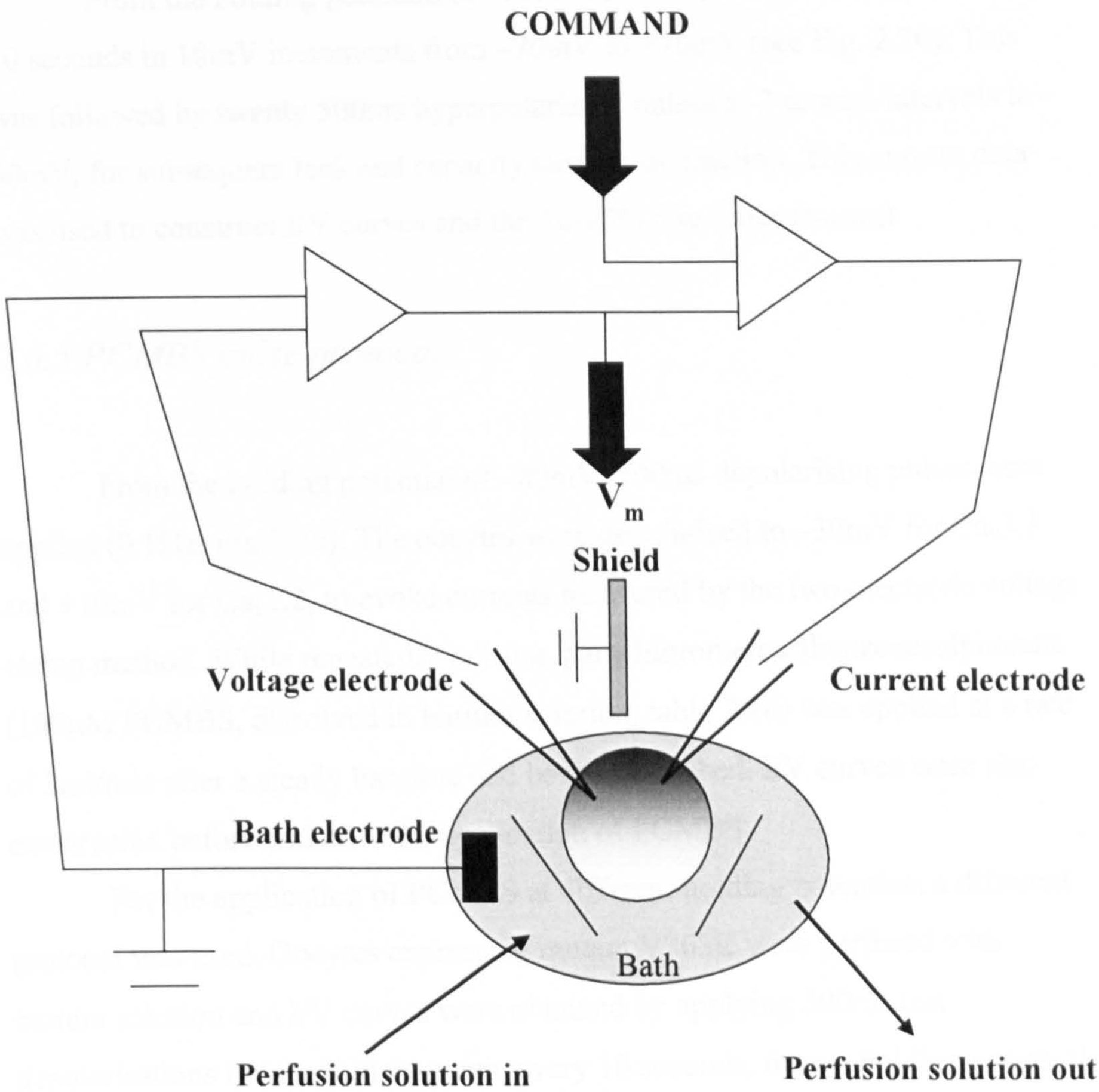

Fig. 2.19 Schematic diagram of the two-electrode voltage clamp chamber.
The oocyte is held within a cradle made from wire and is impaled by the voltage and current electrodes. The vegetal pole is shown in dark grey, and the animal pole is shown in yellow.

2.6.4 Current-voltage protocol

From the holding potential of –80mV, 500ms pulses were applied every 10 seconds in 10mV increments from –70mV to +70mV (see Fig. 2.20). This was followed by twenty 500ms hyperpolarizing pulses at 2 second intervals to -90mV, for subsequent leak and capacity current subtraction. This current data was used to construct I/V curves and the 10-90% rise times ($t_{10\text{-}90\%}$).

2.6.5 PCMBS pulse protocol

From the holding potential of –80mV, 500ms depolarising pulses were applied (0.1Hz, Fig 2.20). The oocytes were depolarised to –30mV for $Ca_v3.1$, and +10mV for $Ca_v1.2$, to evoke currents measured by the two-electrode voltage clamp method. While repeatedly pulsing, parachloromercuribenzenesulphonate (100μM PCMBS, dissolved in barium solution, table 2.1d) was applied at a rate of 2ml/min after a steady baseline had been established. I/V curves were also constructed before and after the application of PCMBS.

For the application of PCMBS at different holding potentials a different protocol was used. Oocytes expressing mutant V263C were perfused with barium solution and I/V curves were obtained by applying 500ms test depolarisations in 10mV increments, every 10 seconds, from a holding potential of -80mV. Pulsing was then stopped, and the cells were then held at the indicated holding potentials (either -140, -110, -80, -40 or 0mV) initially for 2 min in the absence of PCMBS, and then in the presence of PCMBS (100μM) for a further 4 min. Unreacted PCMBS was removed by washing the cells with barium solution for 2 min at the same holding potential. No test pulses were applied during PCMBS application. Finally the holding potential was returned to -80mV and I/V curves obtained. All I/V curves were normalised to the value of +10mV before the application of PCMBS. For the experiments applying dithiothreitol (DTT), oocytes expressing the mutant V263C were held at -80mV and stepped to +10mV repeatedly every 10s. Oocytes were then superfused with PCMBS (100μM), washed for 2 minutes, and then DTT (1mM) was applied for 5

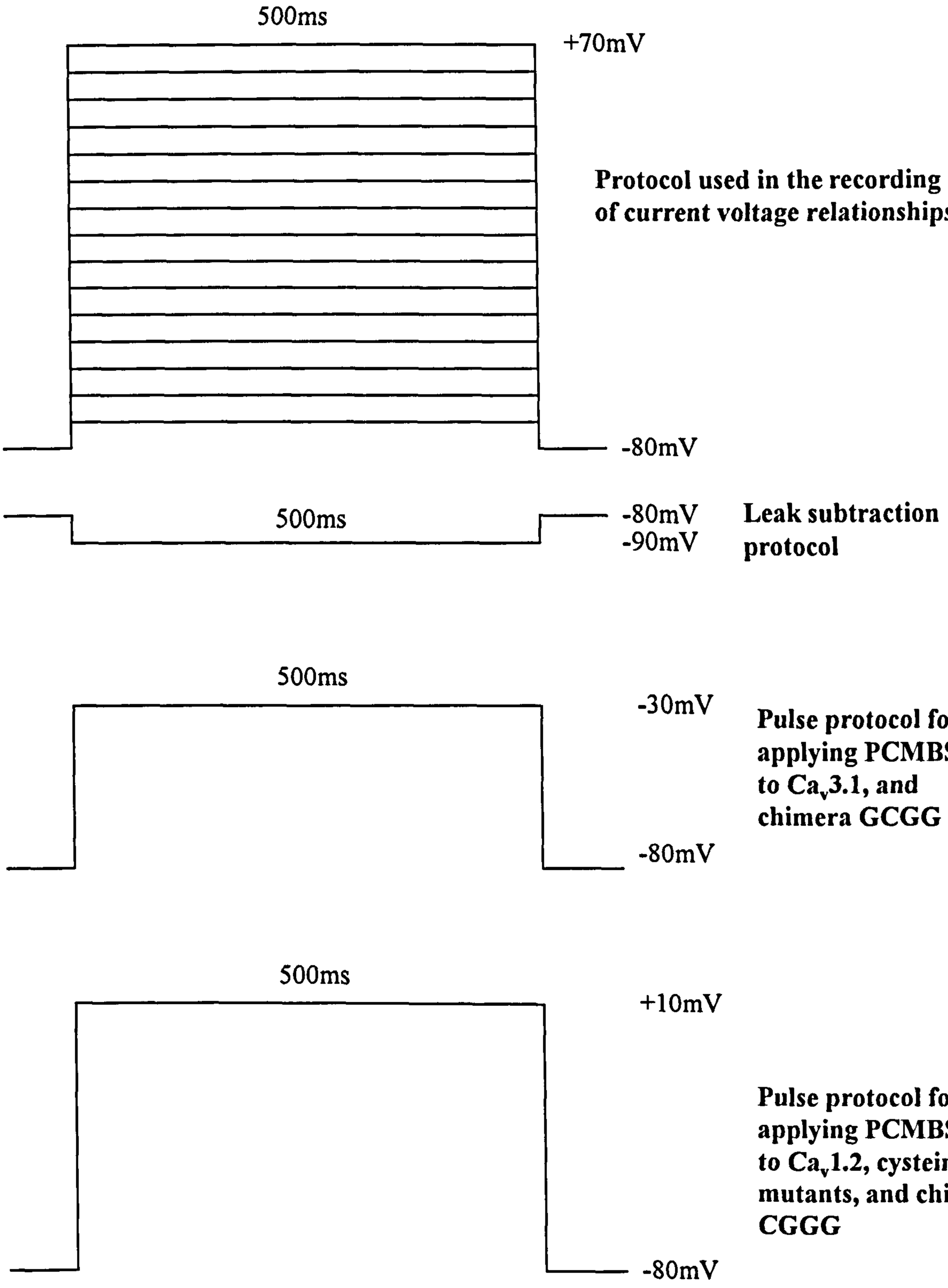

Fig. 2.20 Diagrammatic representations of pulse protocols used.

minutes. All currents were normalised with respect to the first 5 minutes of recording.

2.6.6 Analysis of current data

Construction of the current-voltage relationships and subtraction of leak current was carried out using CED software. 10-90% rise times were calculated from the leak subtracted current traces.

Current data were converted to conductance data using the following equation: $G=I/(V-V_{Rev})$, where G is the conductance, I is the current, V is the membrane potential, and V_{rev} is the reverse potential (assumed to be -98.5mV).

Conductance-voltage data was fitted with the Boltzmann equation: $G= G_{Max}/(1+exp((V_{0.5}-V_{test})/k))$, where $V_{0.5}$ is the potential for half maximal current, V_{test} is the test potential, and k is the slope factor (=RT/ZF, where R is the gas constant, T is the absolute temperature, Z is the effective charge valency and F is the Faraday constant).

The time course of the block of currents by PCMBS was fitted using a single exponential. The single exponential decay equation used was as follows: $I=I_L+I_0e^{(t0-t)/\tau}$, where I is the current, I_L and I_0 are constants (whereby, I_L+I_0 is the initial current), t is the time, and τ is the time constant of decay.

Analysis of the current data was performed using Microcal Origin 6.0 and statistical analysis was performed using Microsoft Excel 2000. Significance testing was carried out using the paired Student's t-test where $p < 0.05$ was considered to be statistically significant.

CHAPTER 3

N- AND C-TERMINAL DETERMINANTS IN THE ACTIVATION OF THE POTASSIUM CHANNEL Kv2.1

3.1 Introduction

The rat and human forms of the Kv2.1 channel have very similar protein sequences (Fig. 3.1 and Chapter 1). They have identical amino acids over the membrane spanning regions (S1-S6), and only differ in their N- and C- termini. Despite the sequence similarity, the two forms of these channels have very different activation kinetics; rat Kv2.1 is much faster activating than the human Kv2.1. This suggests that the N- and C- termini play a role in determining these differences in activation kinetics.

In this chapter, the molecular regions that are responsible for these differences in activation times between the two forms of Kv2.1 have been systematically investigated. This was carried out by constructing both point mutants and chimeras, and expressing these in oocytes. Electrophysiological measurements using the two-electrode voltage clamp method were used to determine the effects of the changes introduced, and thus which regions are responsible for these differences in activation kinetics.

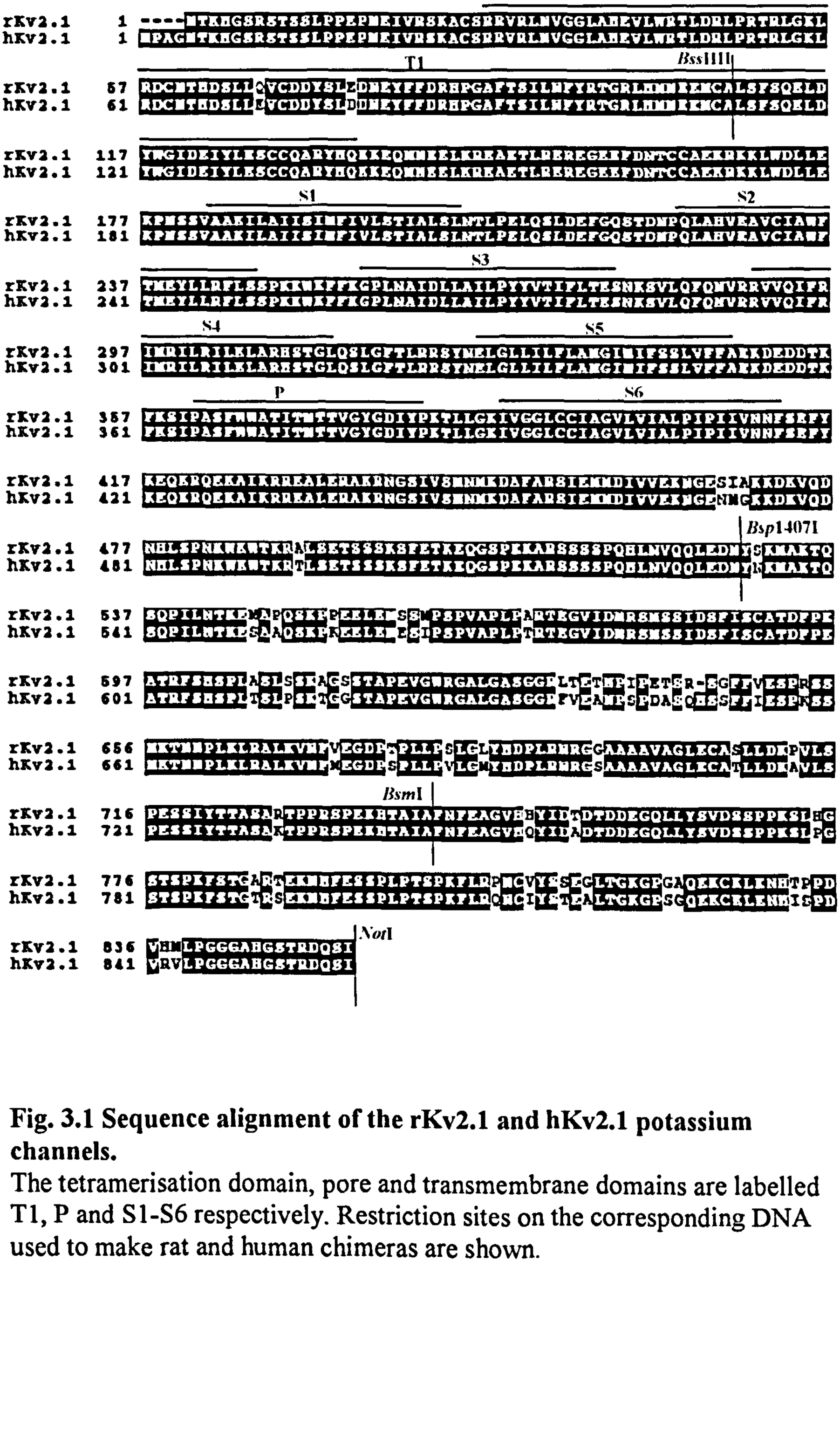

Fig. 3.1 Sequence alignment of the rKv2.1 and hKv2.1 potassium channels.

The tetramerisation domain, pore and transmembrane domains are labelled T1, P and S1-S6 respectively. Restriction sites on the corresponding DNA used to make rat and human chimeras are shown.

3.2 Results

3.2.1 Construction of rKv2.1 E75D point mutation

To investigate the role of one of the two N-terminal amino acids that differ between the rat and human channels, a point mutation was made to change the glutamate at position 75 in rat Kv2.1 into aspartate (the residue found at the equivalent position in human Kv2.1). Sense and anti-sense primers were designed that contained the mismatched base at the desired point, and were used in the mutagenesis cycling stage (see section 2.2.1). Following thermal cycling a *Dpn*I digest was performed and the restricted template DNA transformed into *E. coli*. Plasmid DNA was extracted (2.1.3), and samples of mini-prepped DNA were sequenced. Figure 3.2 shows the results of the automated sequencing using the T7 universal primer, confirming the presence of the correct point mutation in three of the four samples tested. cRNA was transcribed *in vitro* from sample 1 and injected into *Xenopus* oocytes for two-electrode voltage clamp recording.

3.2.2 Construction of chimera rKv2.1$_{h108\text{-}528}$

There are 51 amino acid differences between rat and human Kv2.1 channels, with 49 of these differences located in the C-terminal region (residues 413 to 853). In order to investigate whether some of these amino acids had any effect on activation kinetics, a chimera was generated where bases corresponding to residues between 108 and 528 from rat were replaced with human. Because of the sequence identity between the channels, no residues at the N- terminal side of position 467 were changed by this manipulation. In fact, because of the sequence identity between the two channels (Fig 3.1) just corresponds to just swapping four residues in the C-terminus, S467, I468, A469, and A490.

The DNA for the human Kv2.1 was digested with the restriction enzymes *Bss*HII and *Bsp*1407I (Fig. 3.1). This produced two fragments corresponding to the predicted sizes - a smaller 1264bp fragment which included domains S1 to S6, and a larger N- and C-terminal vector fragment which was 4781bp. The

a

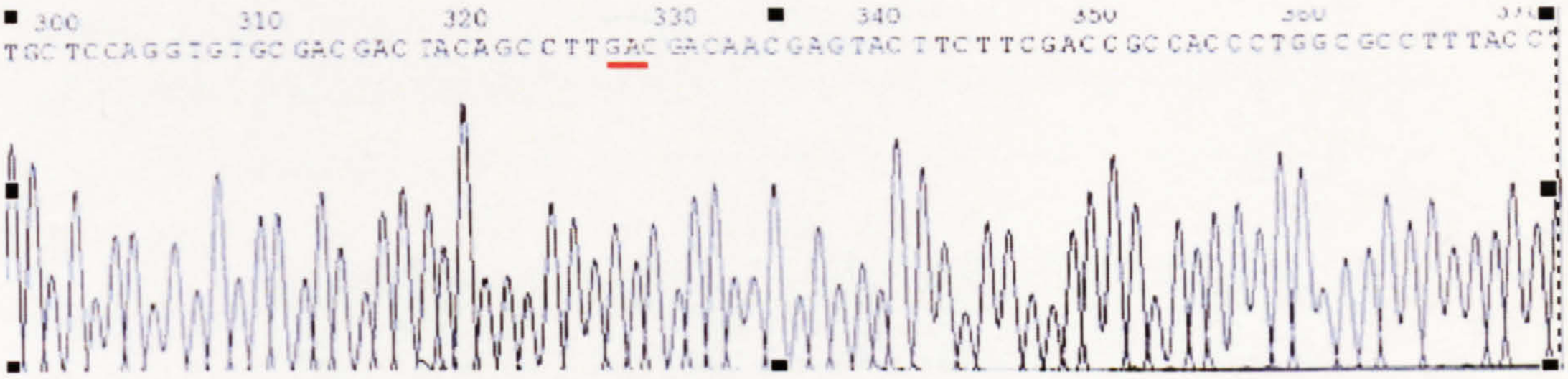

b

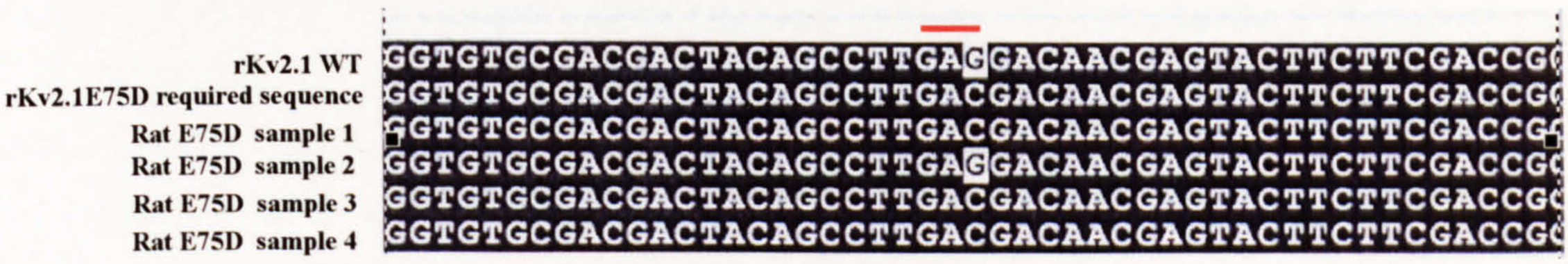

Fig. 3.2 Sequencing of mutant rKv2.1 E75D.

a, Electrophoretogram for clone rKv2.1 E75D (rat E75D sample 1). Red line denotes the amino acid changed.

b, Sequence alignment. Sequences were aligned using ClustalW, and visualised using Boxshade. In this and all subsequent sequence alignment, black shading denotes identical bases, and white areas denote differences between the sequences. It can be seen that wild type rKv2.1 GAG has been changed to GAC in rat E75D samples 1, 3 and 4.

appropriate fragments were isolated and gel extracted as described in section 2.1.7. Figure 3.3a shows a 0.7% agarose gel with the fragments after isolation. For the rKv2.1, the digest was carried out with the same enzymes by M. Ju. The relevant fragments were ligated, transformed and mini-prepped as described in section 2.1.3. A sample of the nucleotide sequencing generated for this chimera (from sample 1) is shown in Fig. 3.3b, including the *Bss*HII join. All of the samples gave the correct mutant sequence (Fig. 3.3c). cRNA from sample 1 was transcribed *in vitro* and injected into *Xenopus* oocytes for two-electrode voltage clamp recording.

3.2.3 Construction of chimeras rKv2.1$_{h108\text{-}740}$, and hKv2.1$_{r108\text{-}740}$

The construction of the two chimeras rKv2.1$_{h108\text{-}740}$ and hKv2.1$_{r108\text{-}740}$ was carried out by digestion with restriction enzymes *Bss*HII and *Bsm*I (Fig 3.1). This corresponds to a substitution of 34 C-terminal amino acids that are different between rat and human Kv2.1, including the 4 substituted in chimera 108-528. Restriction of rKv2.1 yielded two fragments corresponding to the predicted sizes (1898bp and 4408bp, Fig. 3.4a). Similarly digestion of hKv2.1-*Bsm*I clone (see section 2.2.3) also yielded two fragments corresponding to the predicted sizes (1898bp and 4147bp, Fig. 3.4b). Following excision the relevant fragments were ligated, and the DNA transformed.

A section of the electrophoretograms for the sequences for the two chimeric channels at the *Bss*HII join is shown in Figs. 3.5a and b. Alignment of the sequenced DNA shows the correct construction of the two chimeras more clearly (Fig. 3.5c). cRNA was transcribed *in vitro* using sample 1 for each chimera and injected into *Xenopus* oocytes for two-electrode voltage clamp recording.

3.2.4 Construction of chimera rKv2.1$_{h741\text{-}795}$

Construction of this chimera was carried out by the overlap-extension PCR method, as described in section 2.2.4. This corresponds to a change of only 5 amino acids, H749, T750, H774, A785, and T787. The PCR product and

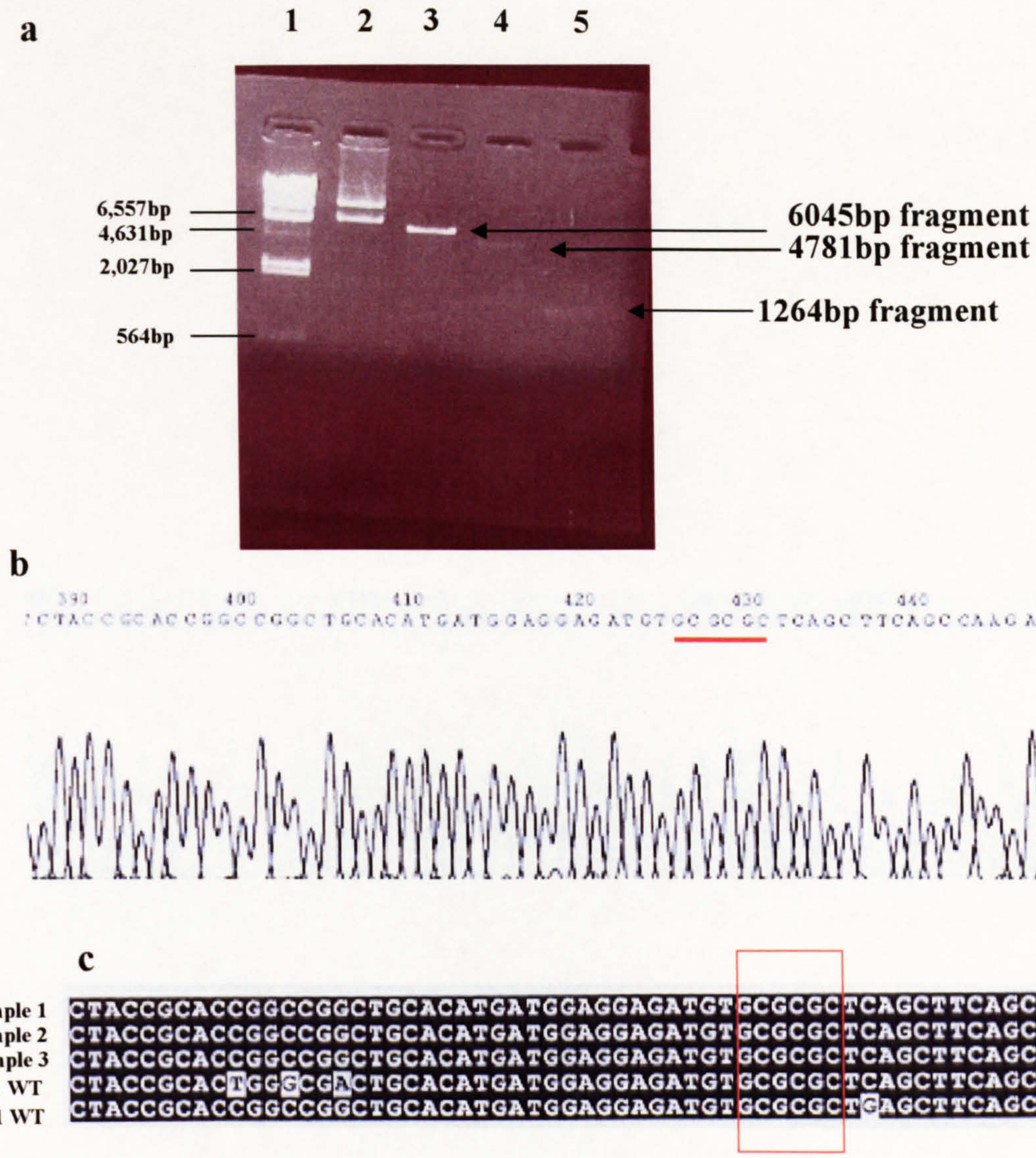

Fig. 3.3 Digestion of hKv2.1 and sequencing of chimera rKv2.1$_{h108-528}$.
a, Agarose gel showing the gel extracted fragments produced by the restriction digest of hKv2.1 wild type with *Bss*HII and *Bsp*1407I. Lane 1 contains the λ-*Hind*III marker, lane 2 contains the hKv2.1 wild type DNA, lane 3 contains the hKv2.1 wild type linearised by *Bsp*1407I (6045bp), lane 4 contains the hKv2.1 double digest by *Bsp*1407I and *Bss*HII (4781bp fragment) and lane 5 contains the hKv2.1 double digest by *Bsp*1407I and *Bss*HII (1264bp fragment). In all gel pictures, only the relevant sizes on the markers are shown
b, Electrophoretogram for clone rKv2.1$_{h108-528,}$ sample 1. Red line denotes the *Bss*HII restriction site.
c, Sequence alignment for chimera rKv2.1$_{h108-528}$. Sequences were aligned using ClustalW and visualised using BoxShade. It can be seen that the sequences of the chimera samples 1-3 are identical to rKv2.1 until the *Bss*HII restriction site (red box), and thereafter is identical to hKv2.1. Sample 1 was used to make cRNA for injection into oocytes.

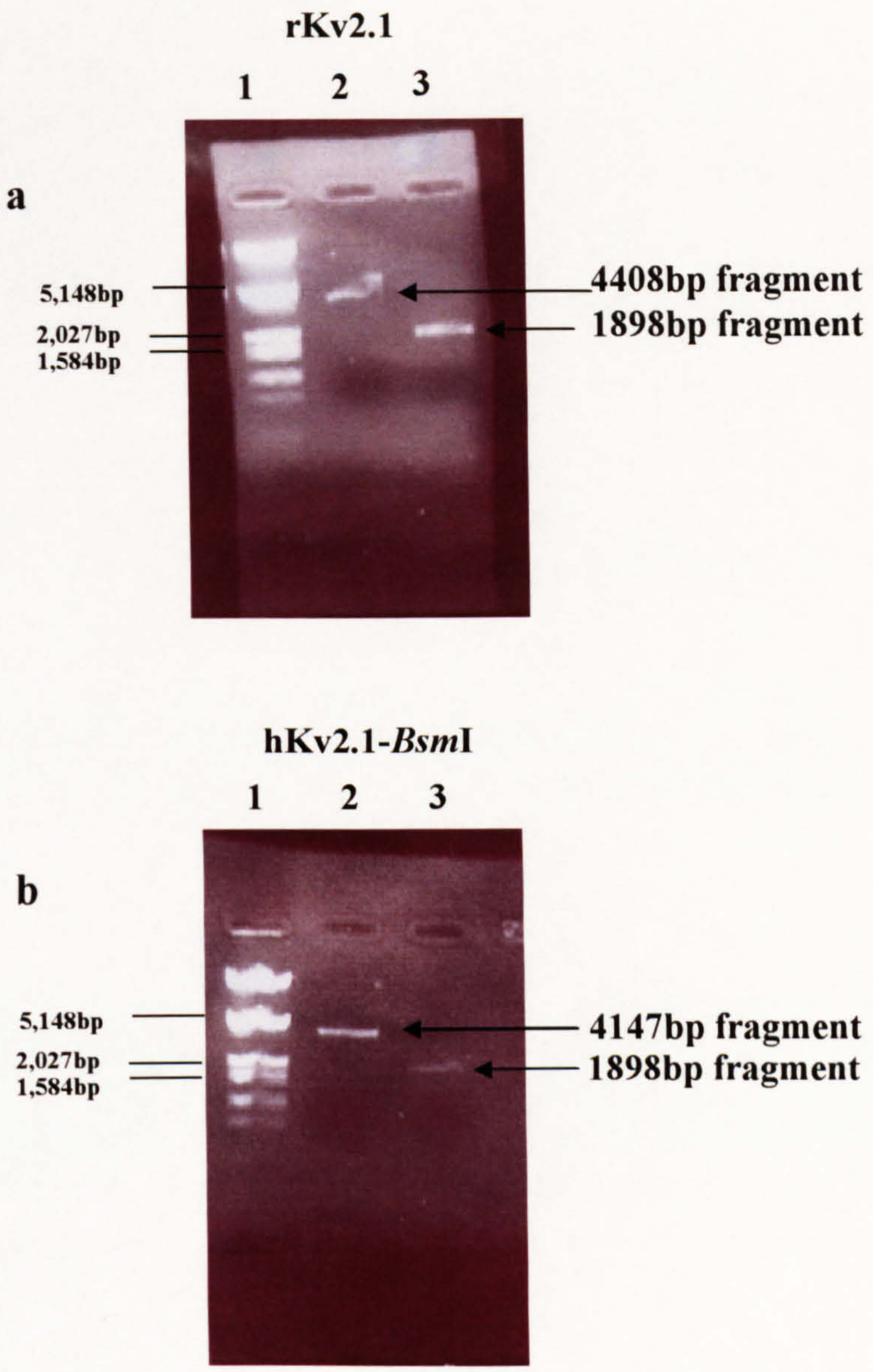

Fig. 3.4 Digestion of the wild type channel rKv2.1 and hKv2.1 -*Bsm*I clones.

a, Fragments were produced by digestion of rKv2.1 with restriction enzymes *Bss*HII, and *Bsm*I. Gel shows extracted bands. Lane 1 contains the λ DNA/*Eco*RI + *Hind*II marker, lane 2 contains the larger (vector) fragment rKv2.1, lane 3 contains the smaller fragment rKv2.1.
b, Fragments were produced by digestion of hKv2.1-*Bsm*I with restriction enzymes *Bss*HII, and *Bsm*I. Gel shows relevant gel extracted bands. Lane 1 contains the λ DNA/*Eco*RI + *Hind*II marker, lane 2 contains the larger (vector) fragment hKv2.1 and lane 3 contains the smaller hKv2.1 fragment.

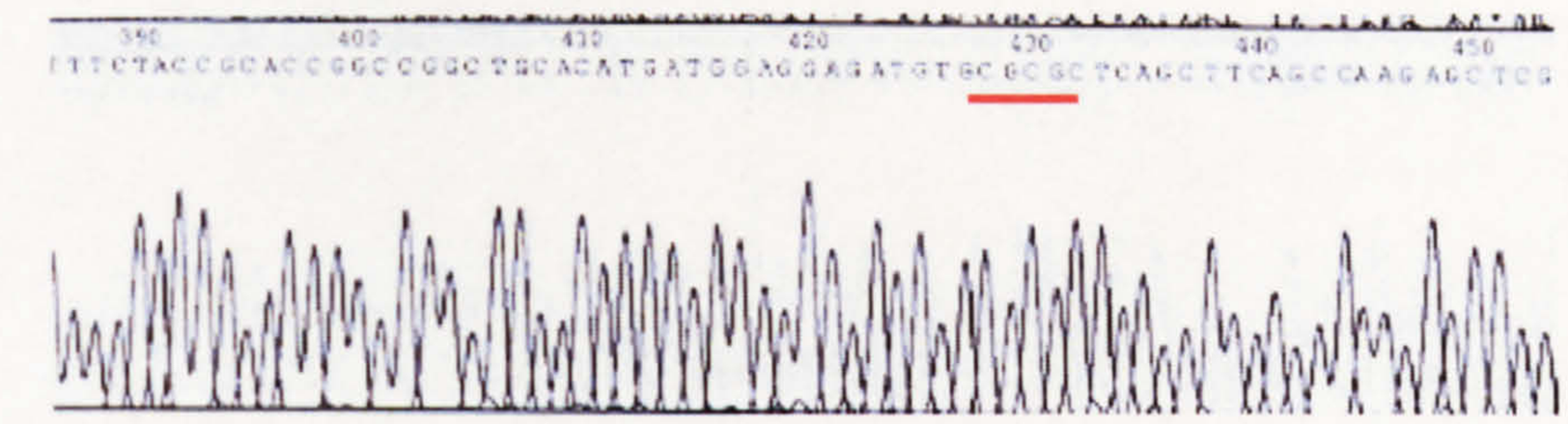

Fig. 3.5 Sequencing for the chimeric channels rKv2.1$_{h108-740}$ and hKv2.1$_{r108-740}$.

a, Electrophoretogram for chimera rKv2.1$_{h108-740}$ sample 1. The red line indicates the *Bss*HII site.

b, Electrophoretogram for chimera hKv2.1$_{r108-740}$ sample 1. The red line indicates the *Bss*HII site.

c, Alignment of the wild type channels hKv2.1, rKv2.1, and the chimeras rKv2.1$_{h108-740}$ and hKv2.1$_{r108-740}$. DNA sequences were aligned using ClustalW and visualised using Boxshade. The restriction site for *Bss*HII is indicated by the red box.

rKv2.1 wild type were digested with restriction enzymes *Bsp*1407I and *Not*I (Fig. 3.6a and b). This yielded fragments corresponding to the predicted 1742bp for the PCR insert and 4564bp for the digest of the rKv2.1, which were gel extracted as described in section 2.1.7 (smaller fragments were discarded). These fragments were then ligated as described in section 2.1.3, and then mini-prepped. The sequence for the rat and human join was then confirmed by sequencing (Fig. 3.6c and d).. cRNA was transcribed *in vitro* for the sample shown and injected into *Xenopus* oocytes for two-electrode voltage clamp recording.

3.2.5 Characterisation of rKv2.1 and hKv2.1 channels

Xenopus laevis oocytes were micro-injected with cRNA for wild type hKv2.1 (0.5ng in 50nl) or rKv2.1 (5.0ng in 50nl). Potassium channel recordings were made using the two-electrode voltage clamp technique and the cells perfused with frog Ringer's solution (table 2.1d) at room temperature.

Outward potassium currents were evoked by pulsing from a holding potential of –80mV for 500ms in 10mV increments to +70mV at 0.1Hz. Fig. 3.7 shows sample rat and human currents after stepping to 0mV. When the rat and human currents are normalised, the time course for activation can be seen to be clearly different between the two channels, with rKv2.1 having a faster activation rate.

Normalised current-voltage (I/V) relationships (Fig. 3.8b) show that the two channels have identical voltage-dependence. In contrast, the activation times were significantly faster for rKv2.1 than hKv2.1 at all test potentials (Fig. 3.8c shows the mean 10-90% rise times).

It is clear that some of the 51 differences in the amino acids between the two channels must contribute to the difference in activation rates.

3.2.6 Characterisation of mutant clone rKv2.1 E75D

There are two residues that are different between rat and human forms of Kv2.1 in the N-terminus; the importance of one of these (residue 75) was studied by mutating a glutamate to aspartic acid in rat Kv2.1. Mutant rKv2.1 E75D and

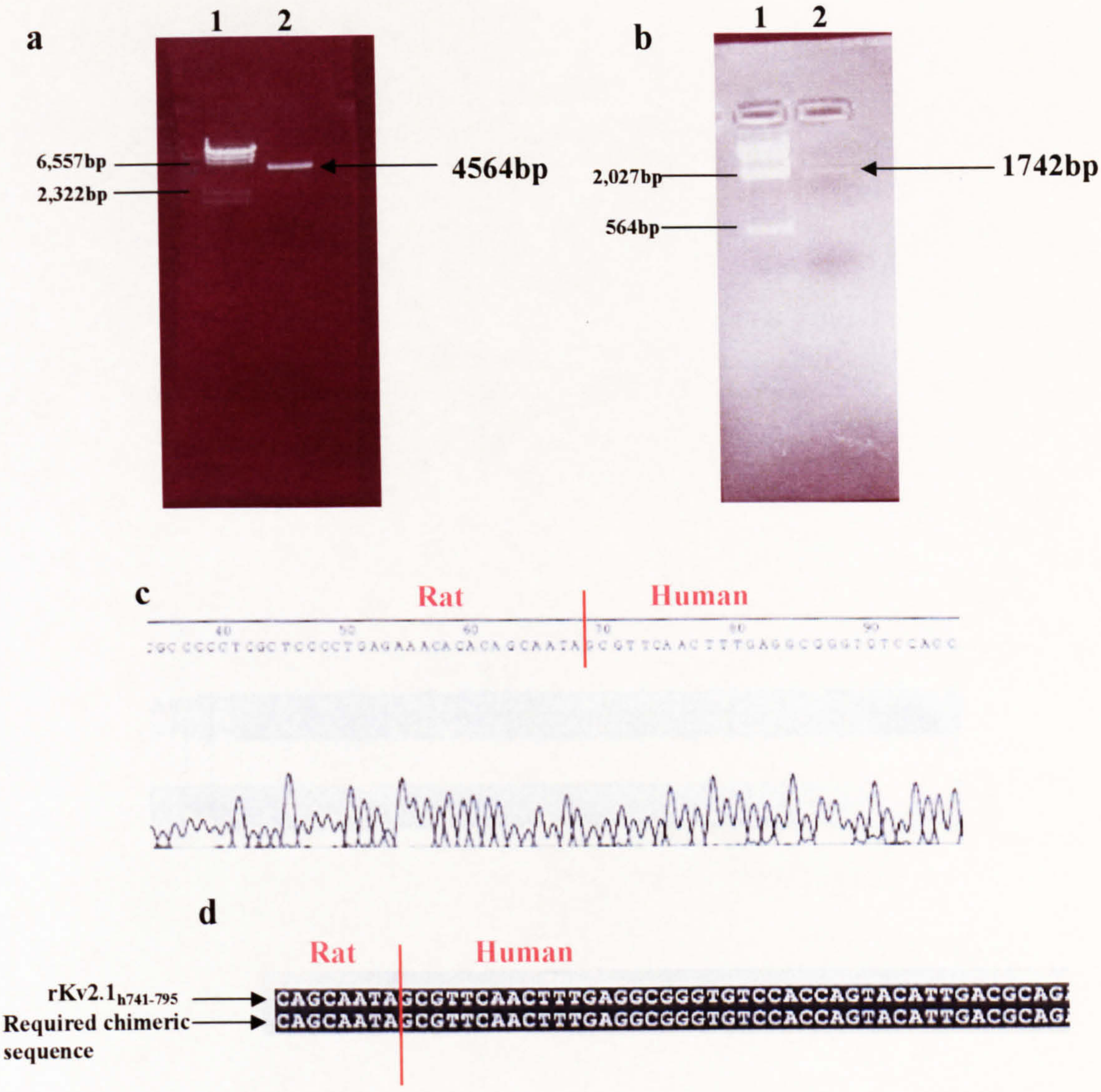

Fig. 3.6 Digestion and sequencing for chimera rKv2.1$_{h741-795}$.
a, Restriction digest of wild type rKv2.1. DNA was digested with *Bsp*1407I and *Not*I, and the relevant sized fragment gel extracted. Lane 1 contains the λ-*Hind*III marker and lane 2 contains the gel extracted rKv2.1 digested with *Bsp*1407I and *Not*I (4564bp fragment).
b, Restriction digest of the PCR product produced by overlap extension PCR. DNA was digested with *Bsp*1407I and *Not*I. Lane 1 contains the λ-*Hind*III marker and lane 2 contains the digested PCR fragment after gel extraction (1742bp fragment).
c, Sequence electrophoretogram of chimera rKv2.1$_{h741-795}$. Red line denotes the join from rat to human DNA.
d, The sequence was aligned against the desired chimeric predicted DNA sequence, using ClustalW and BoxShade software.

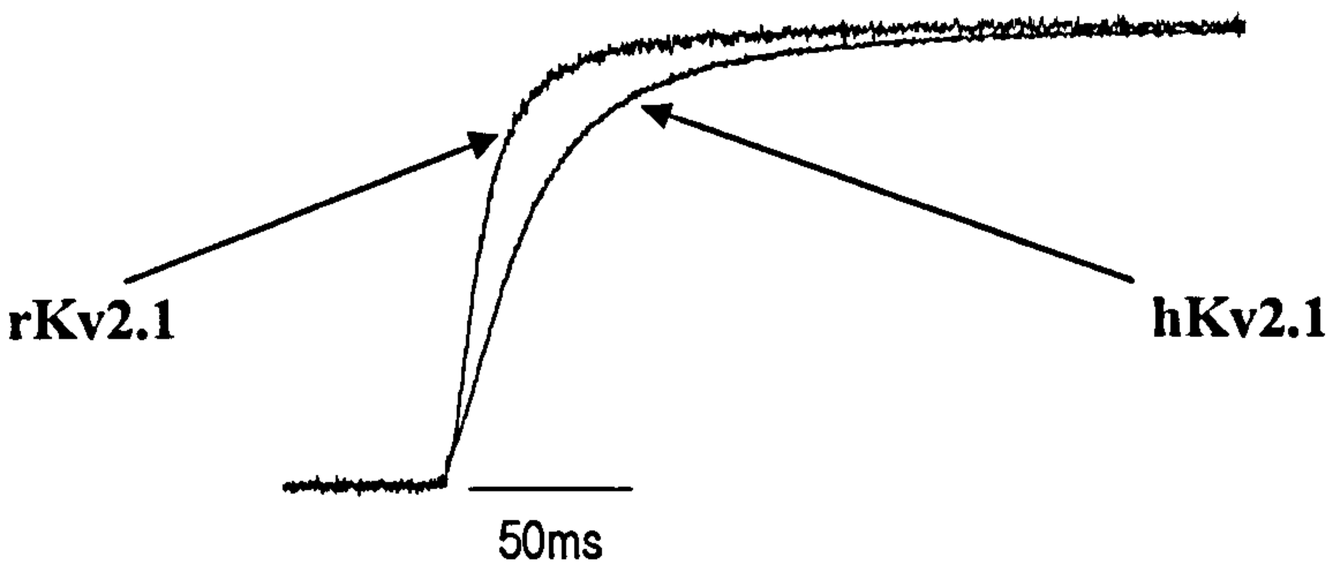

Fig. 3.7 Current traces recorded from *Xenopus laevis* oocytes injected with wild type rKv2.1 and hKv2.1.
Currents were recorded using two-electrode voltage clamp in frog Ringer's solution. A 500ms pulse was applied from a holding current of –80mV to 0mV. Currents were normalised to the maximum current value.

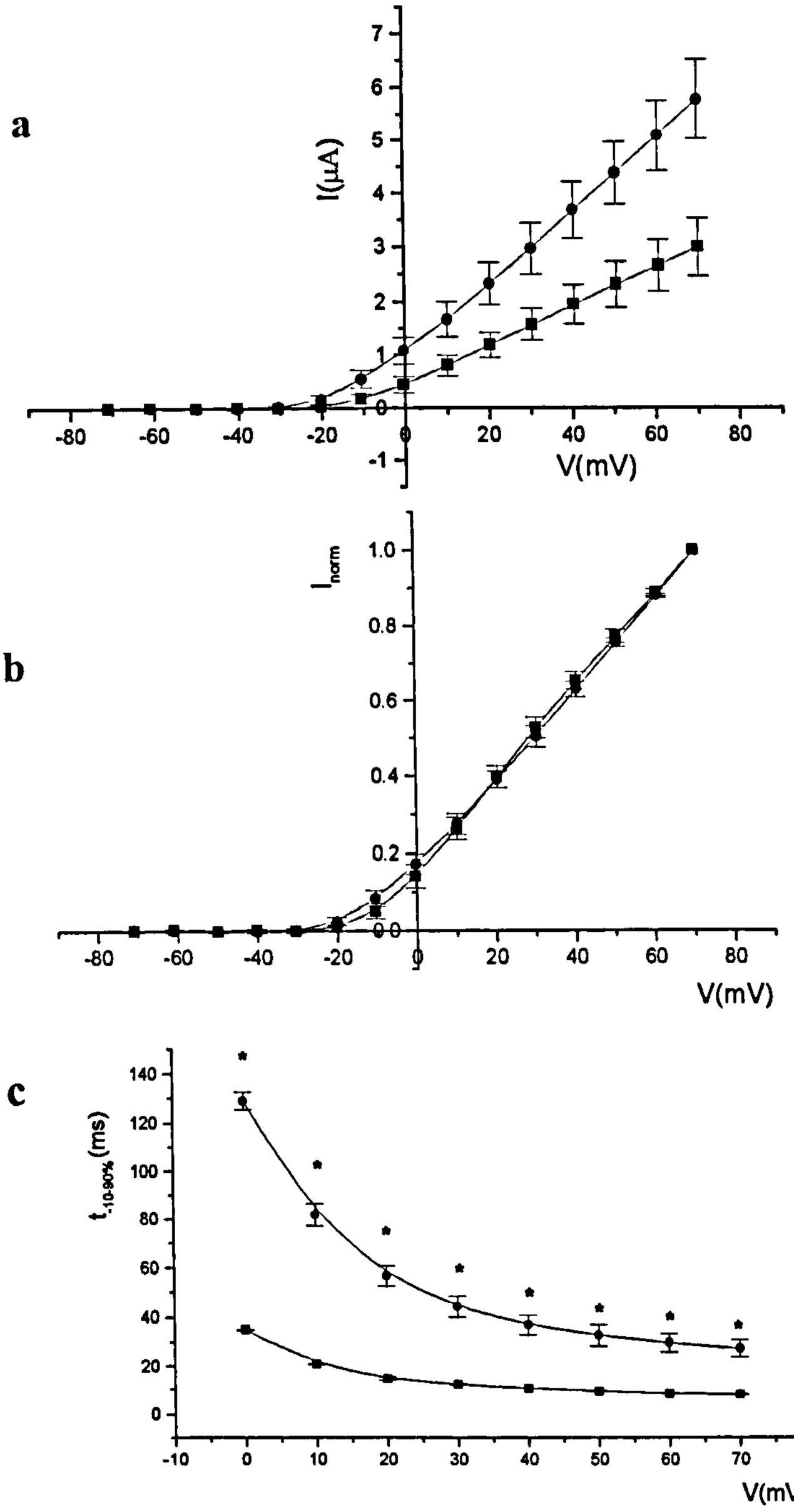

Fig. 3.8 Characteristics of wild type rat and human Kv2.1 channels.

a, The figure shows I/V curves for rat (■, *n*=24) and human (●, *n*=29) wild type channels.

b, Currents were normalised to the current value at +70mV (2.98±0.74 μA for rat and 5.76±0.74 μA for human).

c, The figure shows the 10-90% rise times for rat and human wild type channels (the same data was used as for A). (*) Significant differences ($p<0.05$).

wild type cRNA were injected into *Xenopus* oocytes and the two-electrode voltage clamp technique used a day later. Outward potassium currents were evoked by stepping from a holding potential of –80mV to +70mV in 10mV increments (see section 2.6.4).

Currents were recorded and current-voltage relationships constructed. A typical current trace for mutant clone rKv2.1 E75D is shown in Fig. 3.9. Fig. 3.10 shows the current-voltage relationship of both the wild type and mutated channels before (Fig. 3.10a) and after normalisation (Fig. 3.10b). No significant differences between rKv2.1 wild type and rKv2.1 E75D currents were found for the normalised I/V curves.

Fig. 3.11 shows mean 10-90% rise times plotted against voltage for rKv2.1 and rKv2.1 E75D. The mutant E75D showed fast activation similar to rat Kv2.1 wild type (although there were some slight differences at some voltages). However, the values were significantly different than for the human wild type channel (Fig. 3.8c). This result shows that this change at residue 75 (i.e. changing the residue from E to D) did not alter the characteristics of the channel from rat to human; therefore this residue does not by itself account for the differences in activation kinetics between the two channels. However, the importance of this residue will be discussed later (see section 3.3) in the context of other results.

3.2.7 Characterisation of chimera rKv2.1$_{h108\text{-}528}$

In order to determine whether residues between 108 and 528 (which have four amino acids different between rat and human Kv2.1) contribute to differences in activation kinetics between rat and human forms of Kv2.1, chimera rKv2.1$_{h108\text{-}528}$ was studied. Mutant and wild type cRNA were injected into *Xenopus* oocytes and the two-electrode voltage clamp technique used a day later. Outward potassium currents were evoked by stepping from a holding potential of –80mV to +70mV in 10mV increments.

Currents were recorded for the construction of current-voltage relationships. Typical current traces for the mutant clone rKv2.1$_{h108\text{-}528}$ are shown in Fig. 3.12. Fig. 3.13 shows the current-voltage relationships (mean currents are shown in Fig. 3.13a, and normalised currents in Fig. 3.13b). For normalised

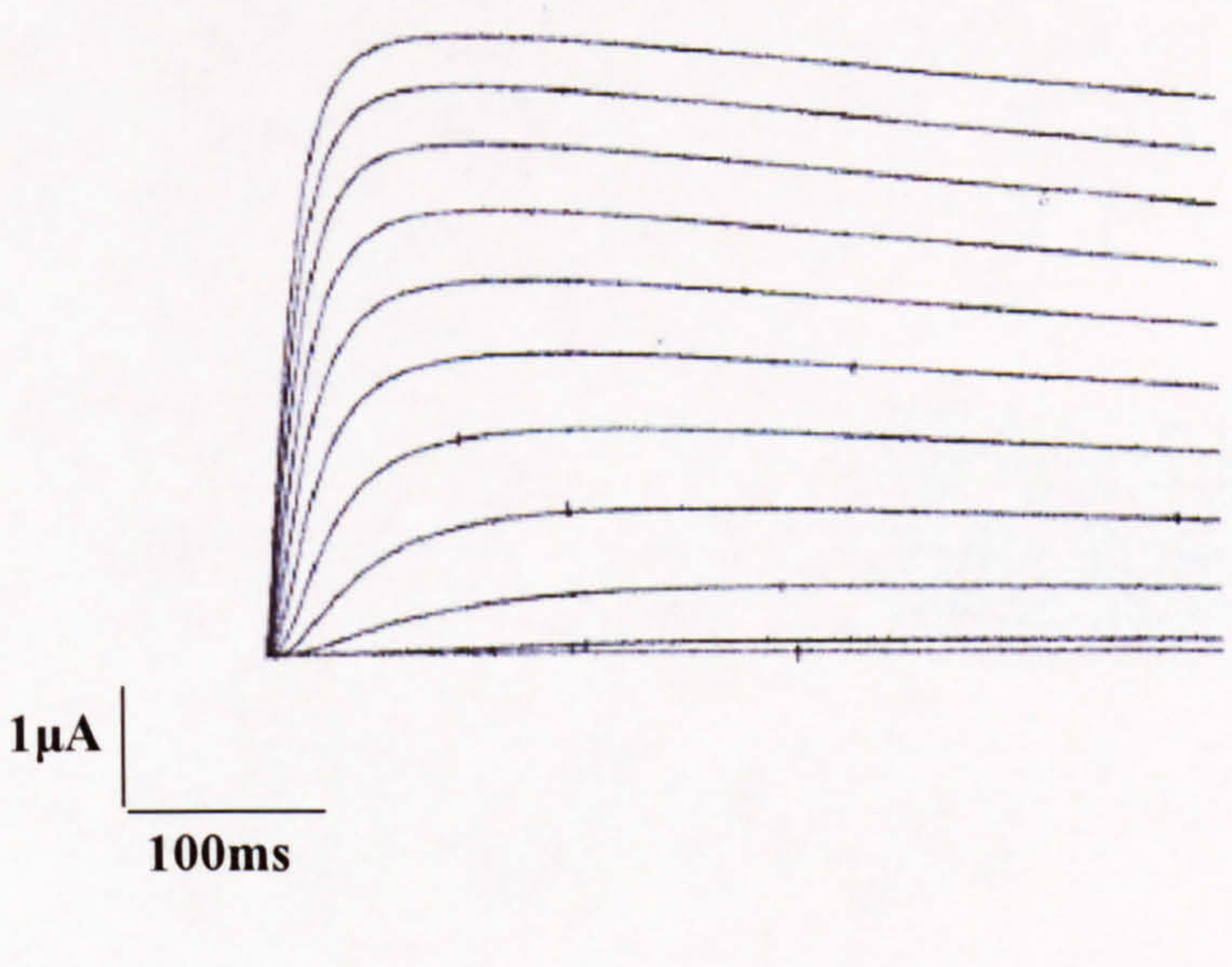

Fig. 3.9 Current families for mutant clone rKv2.1 E75D.
A family of currents (leak subtracted) is shown for a single oocyte during the construction of the I/V curve. Bars indicate the current and time calibration.

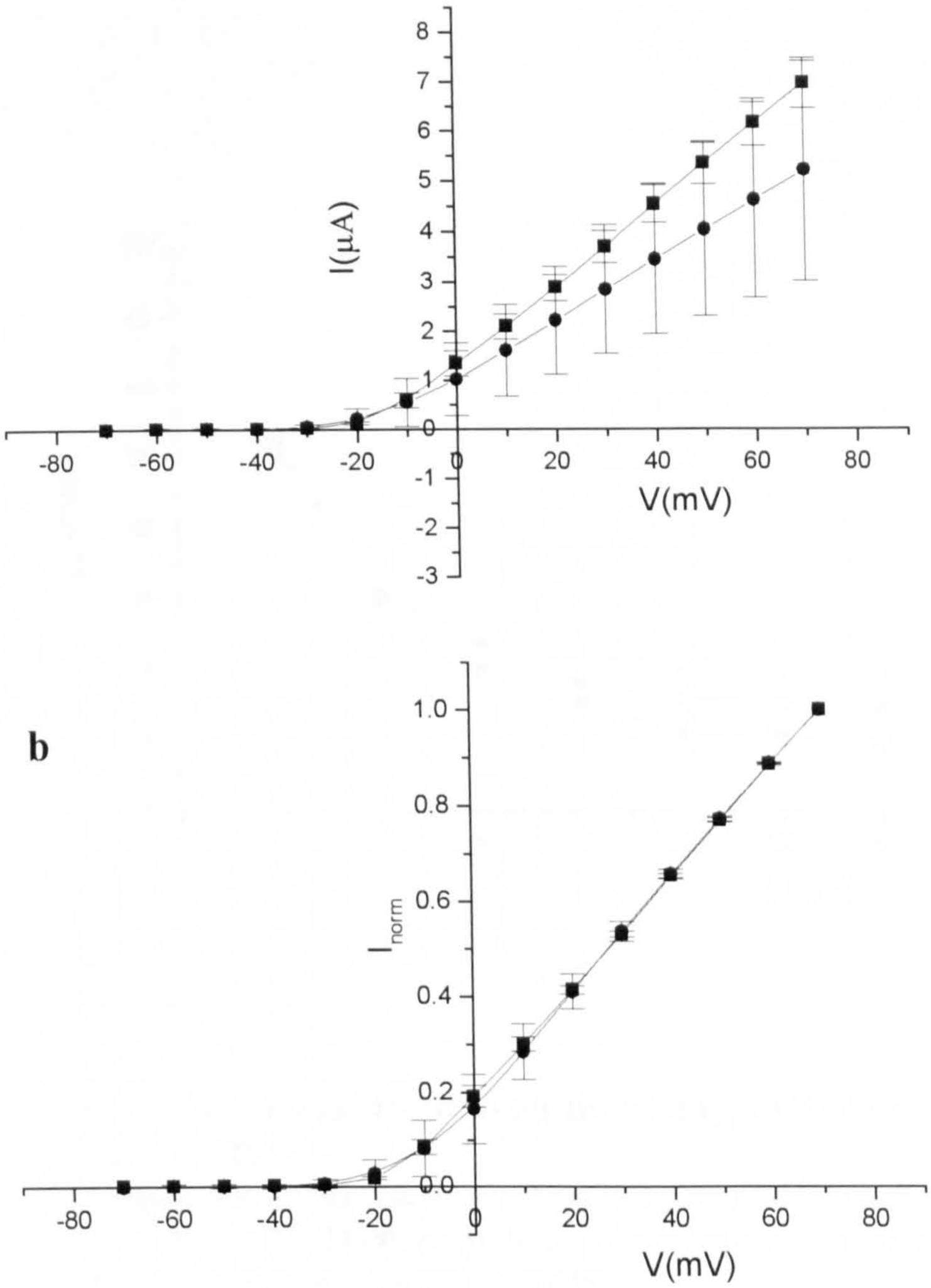

Fig. 3.10 Characteristics of wild type rat and rKv2.1 E75D mutant I/V curves.

a, The figure shows I/V curves for rat (■, *n*=5) and rKv2.1 E75D (●, *n*=6) channels.

b, Currents were normalised to the current value at +70mV (6.9±0.5 μA for rat and 5.2±2.2 μA for rKv2.1 E75D). There were no significant differences between the two normalised sets of data ($p<0.05$).

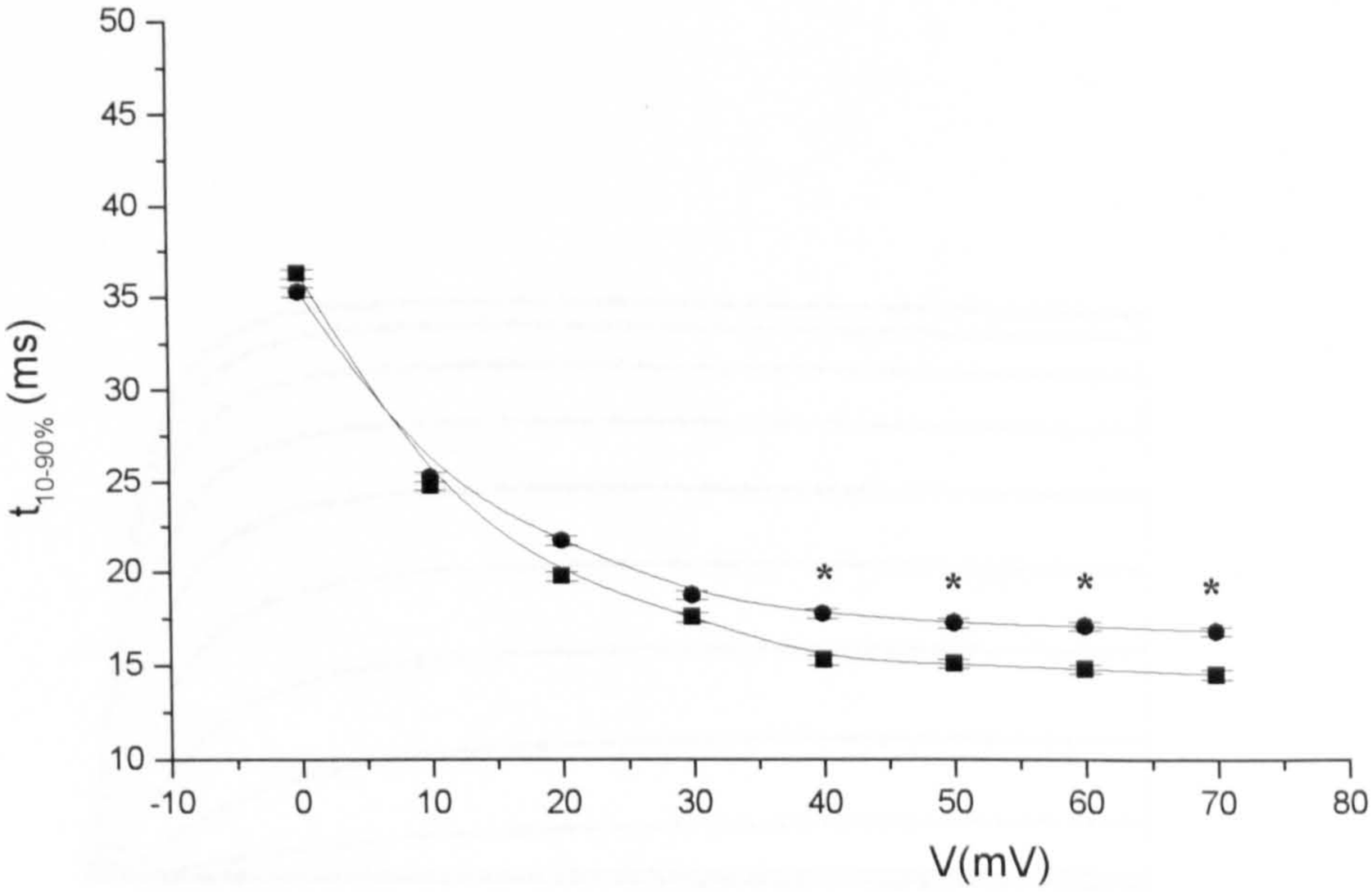

Fig. 3.11 Rise times (10-90%) for the wild type rKv2.1 and mutant rKv2.1 E75D.

The figure shows the rise time versus test potential for rat Kv2.1 (■, n=5), and rat Kv2.1 E75D (●, n=6). Some of the data points were significantly different from each other (*), ($p<0.05$).

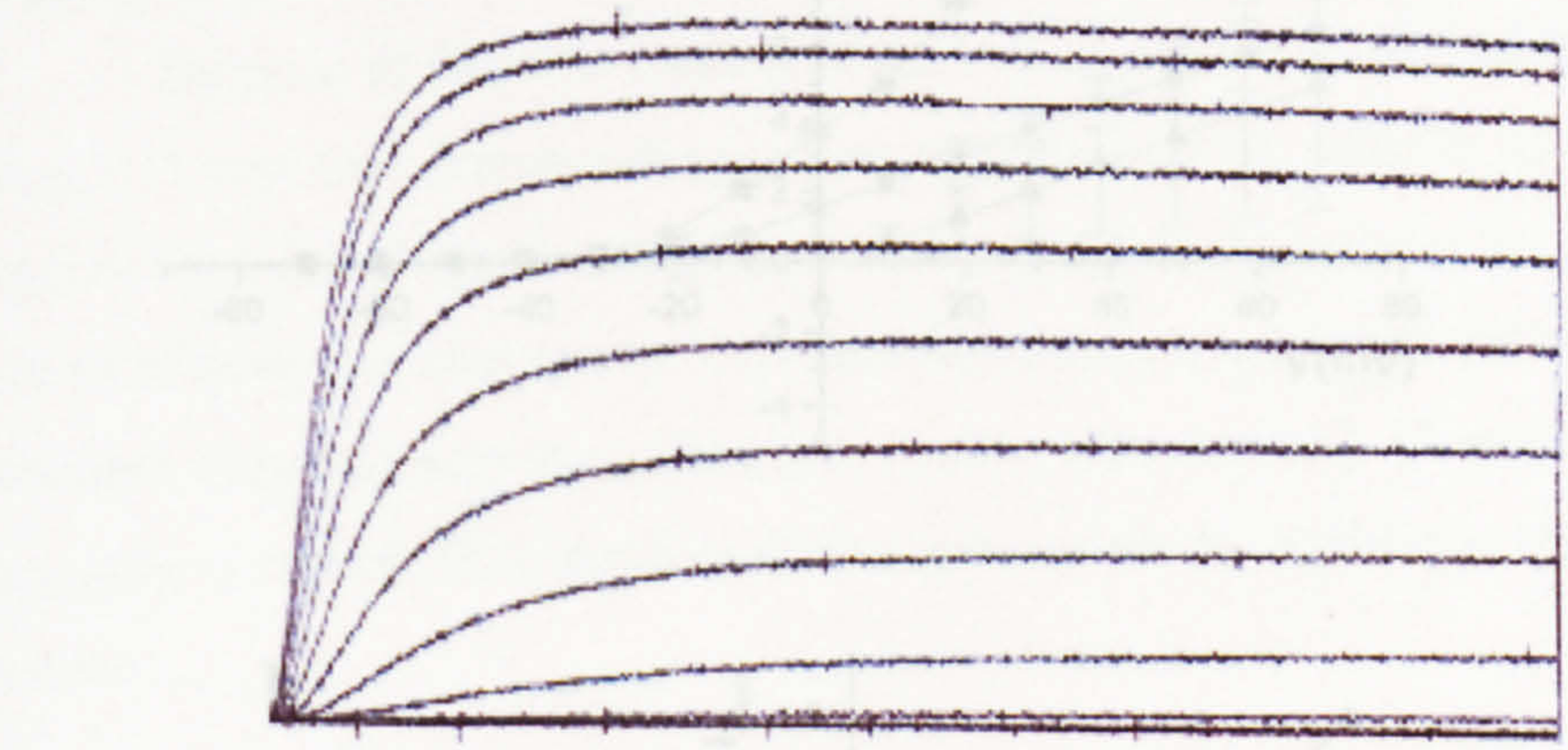

Fig. 3.12 Current families for chimera rKv2.1$_{h108-528}$.
A family of currents (leak subtracted) is shown for a single oocyte for the construction of the I/V curve. Bars indicate the current and time calibration.

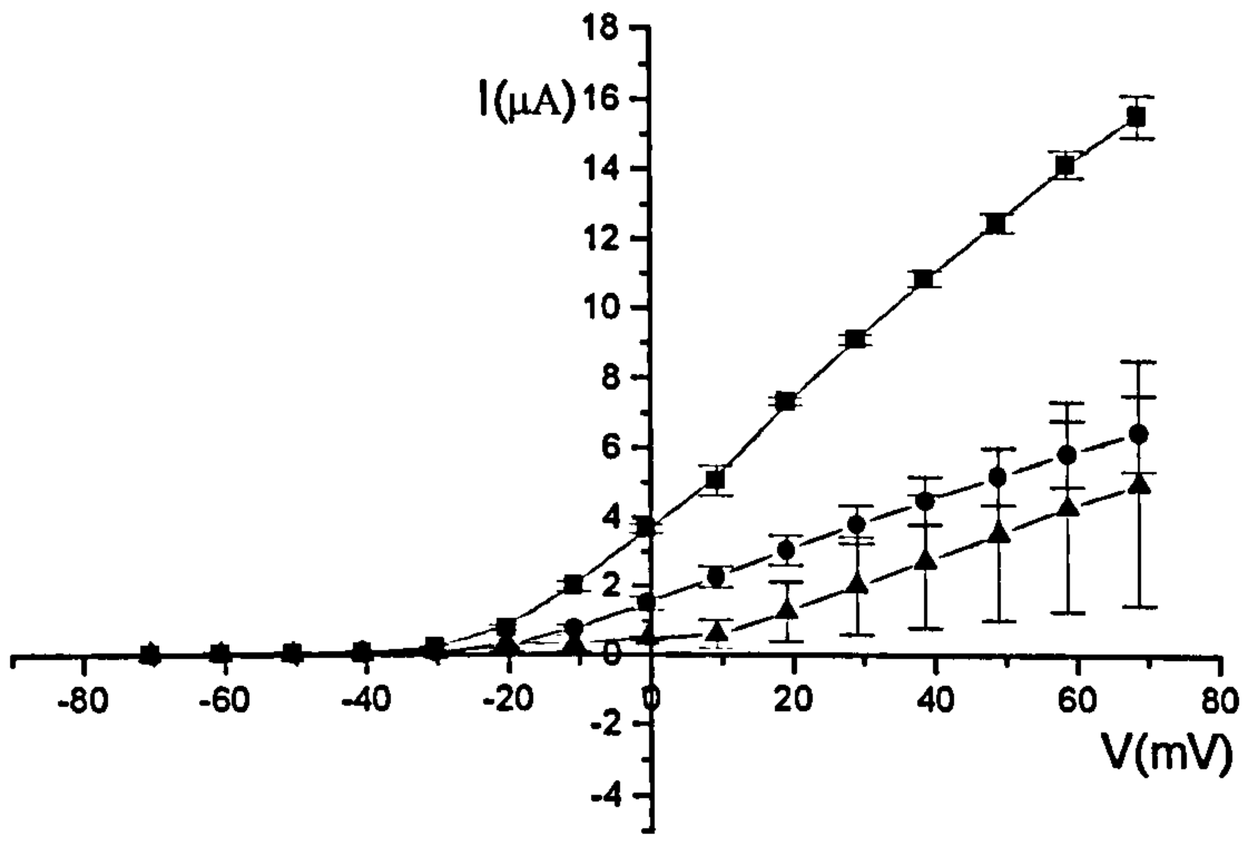

Fig. 3.13 Characteristics of I/V curves for wild type rat and human Kv2.1 and the chimera rKv2.1$_{h108-528}$.

a, The figure shows I/V curves for wild type rKv2.1 (●, *n*=10), wild type hKv2.1, (■, *n*=7), and chimera rKv2.1$_{h108-528}$ (▲, *n*=7).
b, Currents were normalised to the current value at +70mV (6.4±1 μA for rat, 15.5±0.6 μA for human and 5.0±3.5 μA for rKv2.1$_{h108-528}$). There were no significant differences between the three sets of normalised data ($p<0.05$).

curves, no significant differences between rKv2.1 wild type, hKv2.1 wild type and $rKv2.1_{h108\text{-}528}$ current-voltage relationships were found. The differences seen in Fig. 3.13a for un-normalised data may reflect differing levels of protein expression.

Fig. 3.14 shows mean 10-90% rise times versus test potential for rKv2.1, hKv2.1 and $rKv2.1_{h108\text{-}528}$. Both rKv2.1 wild type and $rKv2.1_{h108\text{-}528}$ showed fast activation kinetics and there were no significant differences between rat wild type and mutant rise times. The hKv2.1 rise times on the other hand were significantly slower at all data points tested.

Because of the near identity of the two channels (human and rat Kv2.1, Fig. 3.1) over the corresponding region, only four amino acids in the C-terminal region have actually been swapped between the two channels in the chimera. The data indicates that changes to these residues from rat to human did not change the channel from fast activation (like rat), to slow (like human). Therefore the data suggests that these four residues do not account for the differing activation kinetics.

3.2.8 Characterisation of chimeras $rKv2.1_{h108\text{-}740}$, and $hKv2.1_{r108\text{-}740}$

In order to determine whether residues between 108 and 740 (a region in which 34 amino acids differ between rat and human Kv2.1) contribute to differences in activation kinetics between the channels, chimeras $rKv2.1_{h108\text{-}740}$ and $hKv2.1_{r108\text{-}740}$ were studied. N.B because the protein sequences are identical between 108 and 466, only residues in the C- terminus are changed in this chimera. Mutant and wild type cRNA were injected into *Xenopus* oocytes and two-electrode voltage clamp technique used a day later. Outward potassium currents were evoked by stepping from a holding potential of –80mV to +70mV in 10mV increments.

Sample current trace families for chimeric clones, $rKv2.1_{h108\text{-}740}$ and $hKv2.1_{r108\text{-}740}$ are shown in Fig. 3.15. Fig. 3.16 shows the current-voltage relationships (mean I/V curves are shown in Fig. 3.16a, and normalised curves in Fig. 3.16b). There were no significant differences between rKv2.1 wild type, hKv2.1 wild type, $rKv2.1_{h108\text{-}740}$ and $hKv2.1_{r108\text{-}740}$ normalised currents at any test

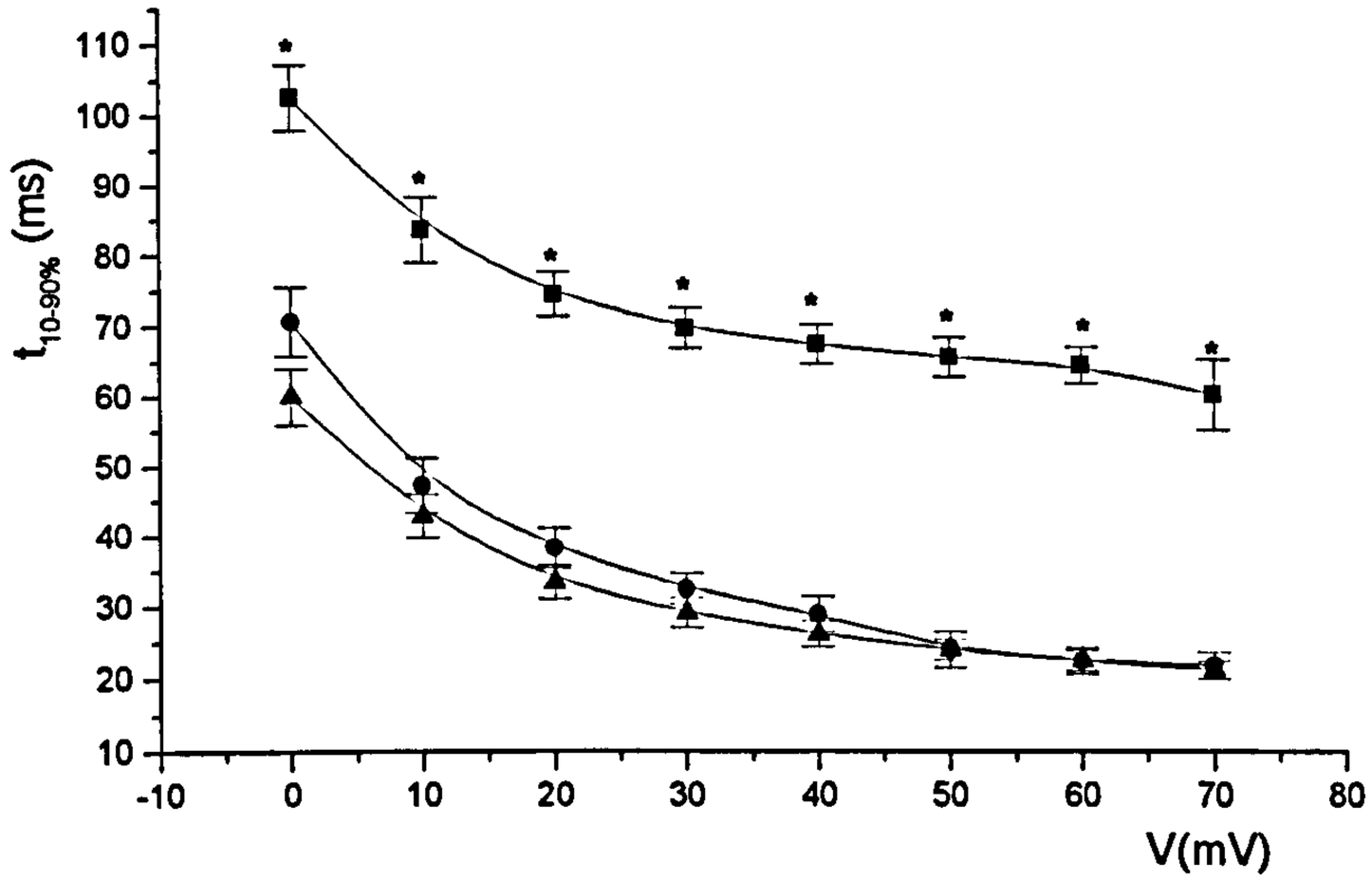

Fig. 3.14 Rise times (10-90%) for the wild types rKv2.1 and hKv2.1 and the chimera rKv2.1$_{h108-528}$.
The figure shows the rise time versus test potential for hKv2.1 (■, *n*=7), rat Kv2.1 (●, *n*=10), and the chimera rKv2.1$_{h108-528}$ (▲, *n*=7). Significance differences (*), are shown ($p<0.05$).

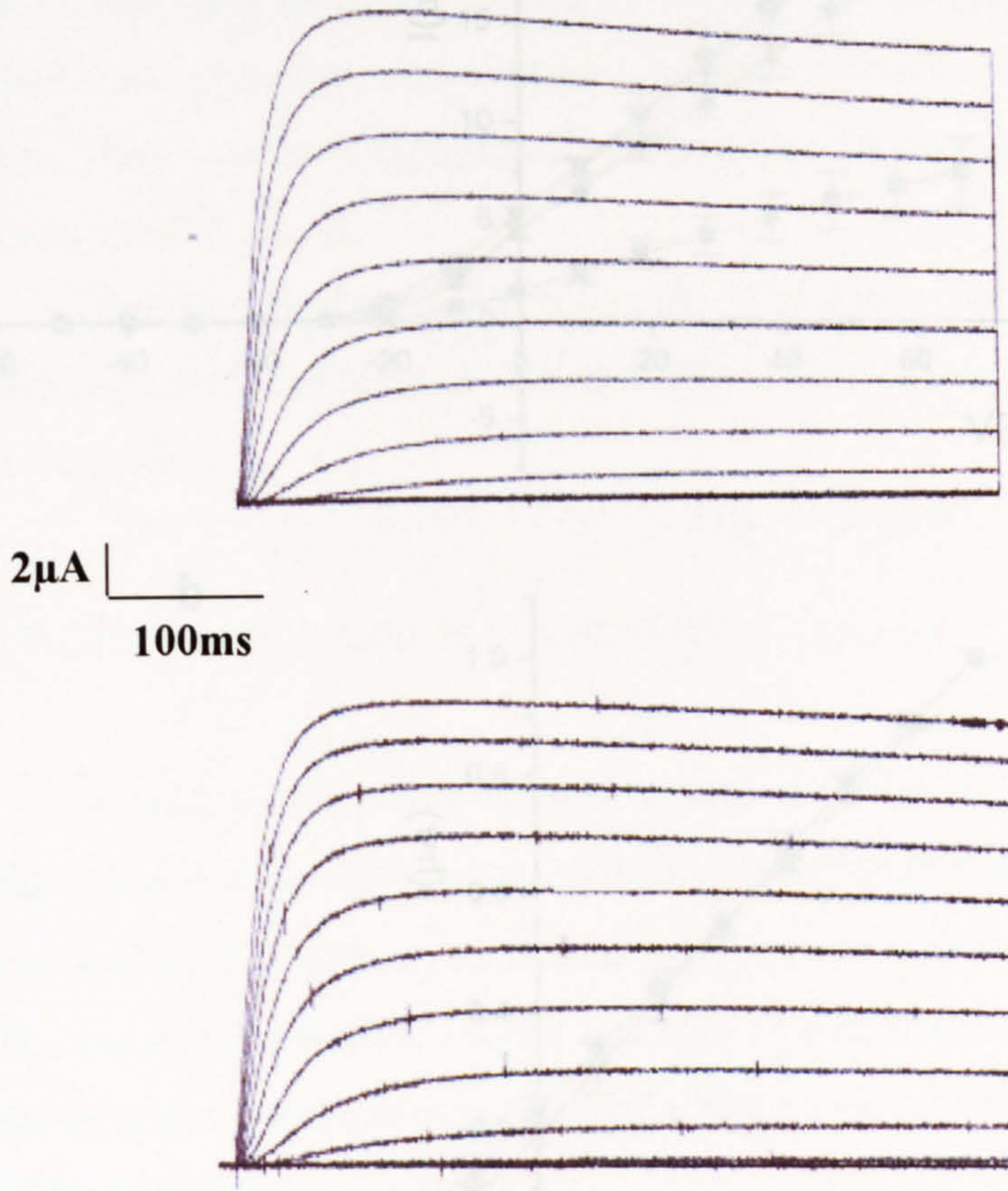

Fig. 3.15 Current families for chimeras $rKv2.1_{h108-740}$, and $hKv2.1_{r108-740}$.
Families of currents (leak subtracted) are shown, created for the construction of the I/V curves. Bars indicate the current and time calibration.

a

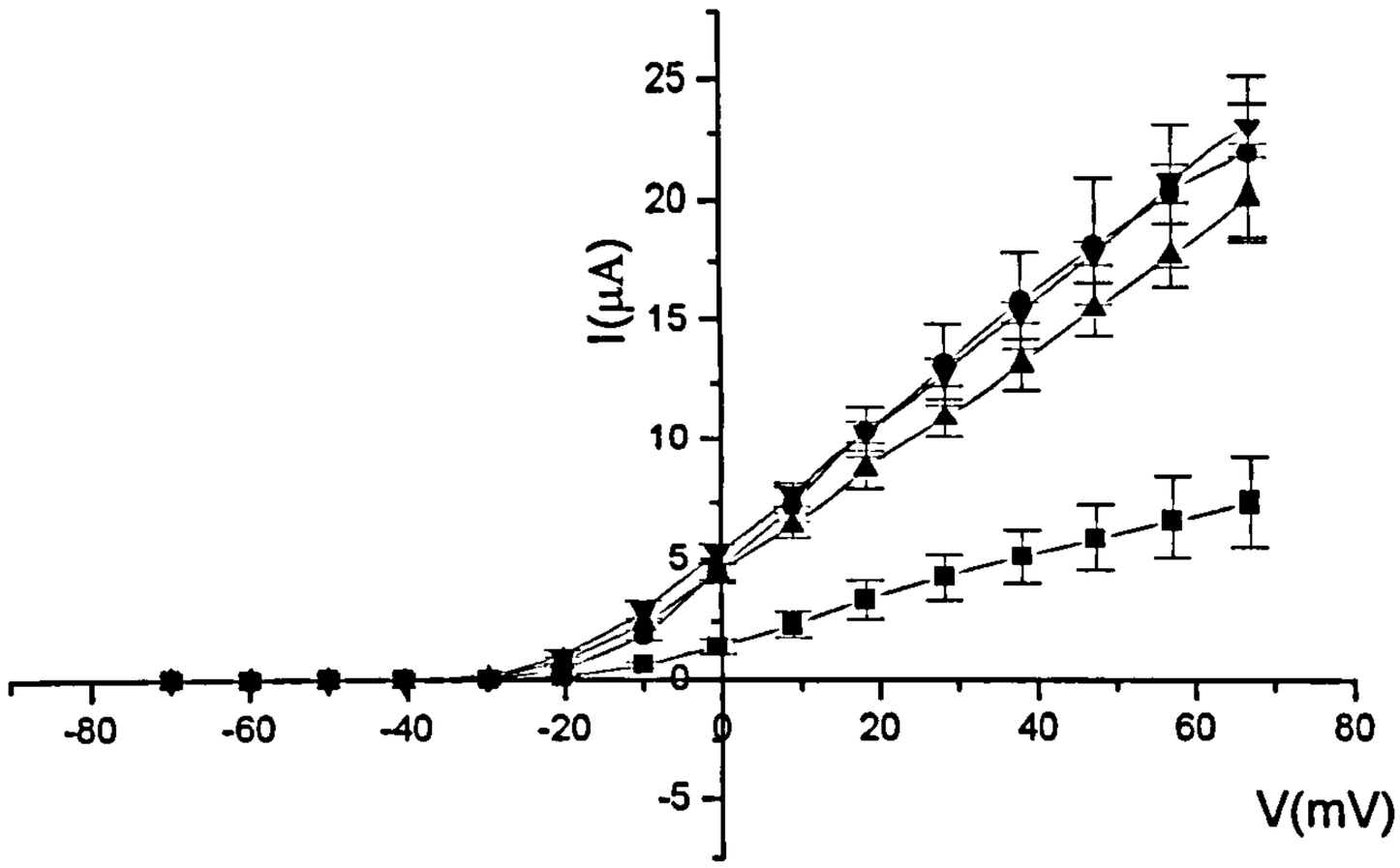

b

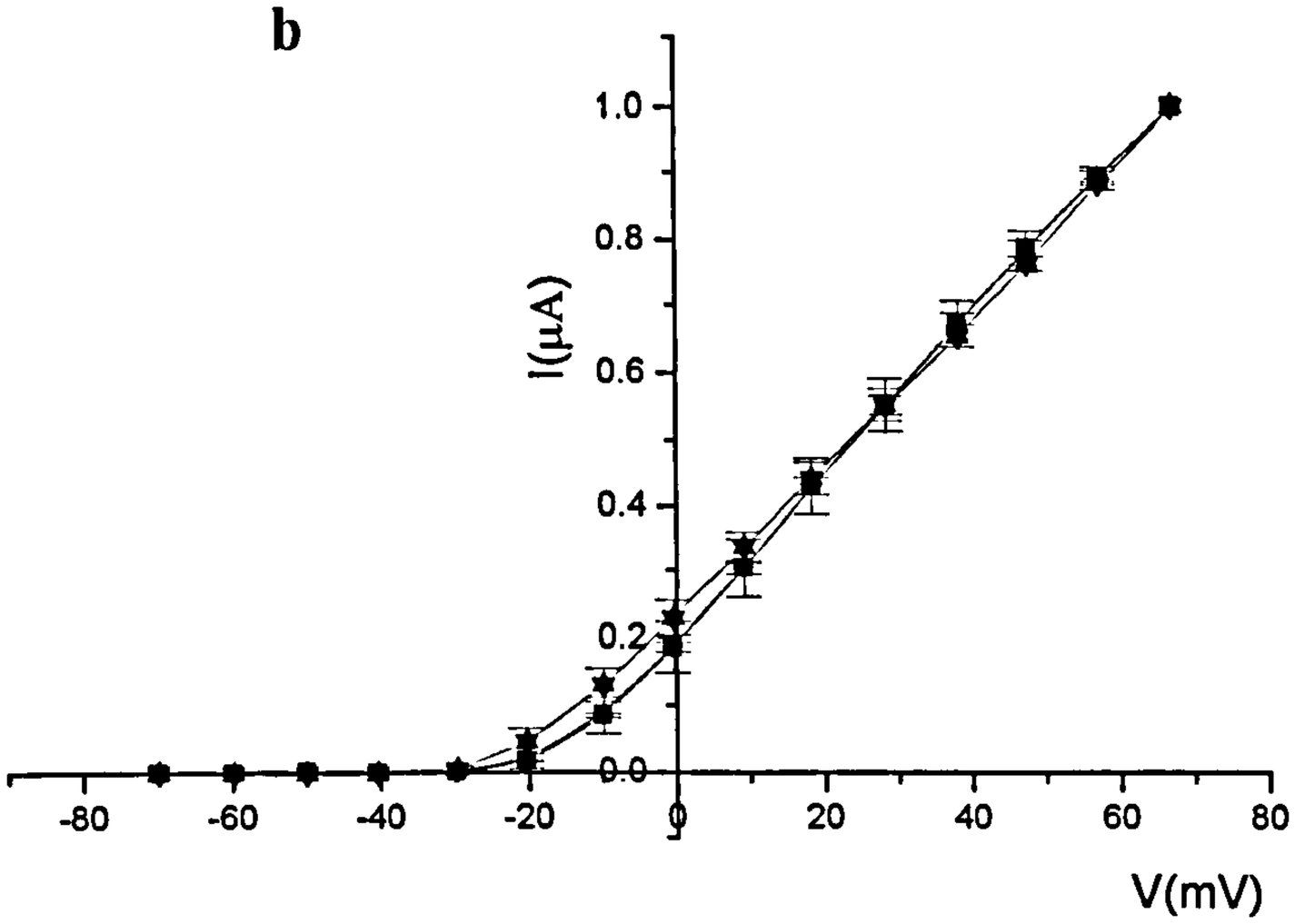

Fig. 3.16 I/V curves for wild type rat and human Kv2.1 and the chimeras rKv2.1$_{h108-740}$ and hKv2.1$_{r108-740}$.
a, The figure shows I/V curves for wild type rKv2.1 (■, *n*=5), wild type hKv2.1, (●, *n*=5), chimera rKv2.1$_{h108-740}$ (▲, *n*=6) and chimera hKv2.1$_{r108-740}$ (▼, *n*=9).
b, Currents were normalised to the current value at +70mV (7.4±1.8 μA for rat, 21.7±3.3 μA for human, 20.0±1.5 μA for rKv2.1$_{h108-740}$ and 23.0±0.9 μA for hKv2.1$_{r108-740}$).
No significant differences were found ($p<0.05$) between the normalised data.

potentials studied. The differences seen for un-normalised data again may simply reflect differing levels of protein expression.

Fig. 3.17 shows mean 10-90% rise times versus test potential for rKv2.1, hKv2.1, rKv2.1$_{h108-740}$ and hKv2.1$_{r108-740}$. Both rKv2.1 wild type and rKv2.1$_{h108-740}$ clones had fast activation and there were no significant differences between them. On the other hand hKv2.1 and the human chimera, hKv2.1$_{r108-740}$ both showed slow activation, also with no significant differences between the two sets of data. They were both significantly slower than for rat wild type and rat chimera, rKv2.1$_{h108-740}$.

Therefore the data suggests that the 34 residues that are different between the chimeras between residues 108 and 740 do not account for the differing activation kinetics.

3.2.9 Characterisation of chimera rKv2.1$_{h741-795}$

In order to determine whether residues between 741 and 795 (a region which 5 amino acids differ between the channels) contribute to differences in activation kinetics between rat and human forms of Kv2.1 the chimera rKv2.1$_{h741-795}$ was studied. Mutant and wild type cRNA were injected into *Xenopus* oocytes and currents recorded using two-electrode voltage clamp as described above.

Typical current traces for the mutant clone rKv2.1$_{h741-795}$ are shown in Fig. 3.18. Fig. 3.19 shows the current-voltage relationships (the mean is shown in Fig. 3.19a, and normalised curves in Fig. 3.19b). No significant differences between normalised rKv2.1 wild type, hKv2.1 wild type and rKv2.1$_{h741-795}$ current-voltage relationships were found. Fig. 3.20 shows mean 10-90% rise times versus test potential for rKv2.1, hKv2.1 and rKv2.1$_{h741-795}$. Both rKv2.1 wild type and rKv2.1$_{h741-795}$ chimera showed fast activation kinetics and there were no significant differences between rat wild type and mutant rise times. The hKv2.1 on the other hand was slower at least for test potential up to +20mV.

Therefore, replacing residues 741-795 in the rat channel with the human sequence did not alter the activation kinetics. Hence, the five amino acids that are

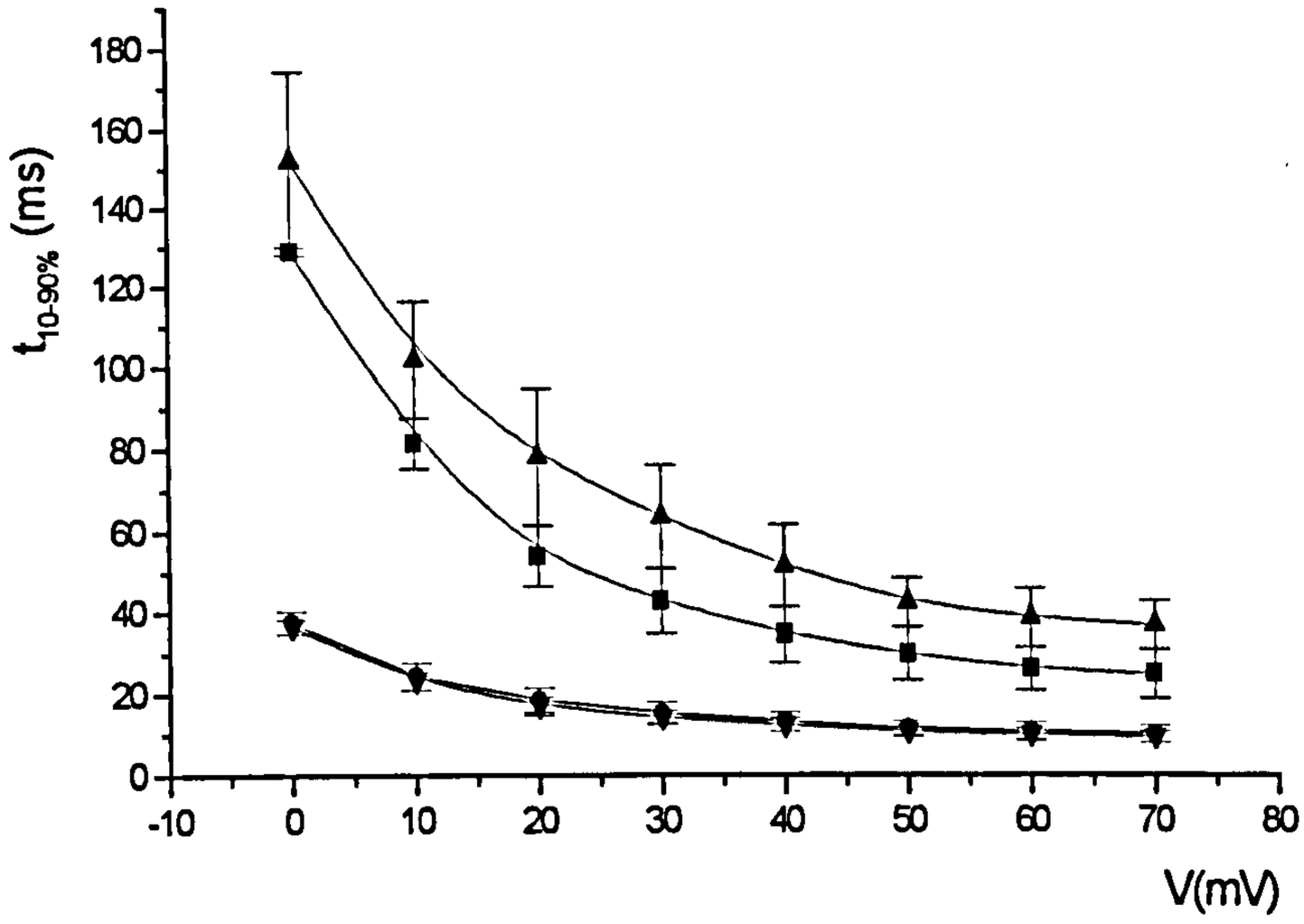

Fig. 3.17 Rise times (10-90%) for the wild types rKv2.1 and hKv2.1 and for chimeras rKv2.1$_{h108-740}$, and hKv2.1$_{r108-740}$.
The figure shows the rise time versus test potential for human Kv2.1 (■, *n*=5), rat Kv2.1 (●, *n*=5), and the chimeras hKv2.1$_{r108-740}$ (▲, *n*=9) and rKv2.1$_{h108-740}$ (▼, *n*=6).
Human wild type and hKv2.1$_{r108-740}$ rise times were not significantly different at any data point. Rat wild type and rKv2.1$_{h108-740}$ rise times were also not significantly different at any data points ($p<0.05$).

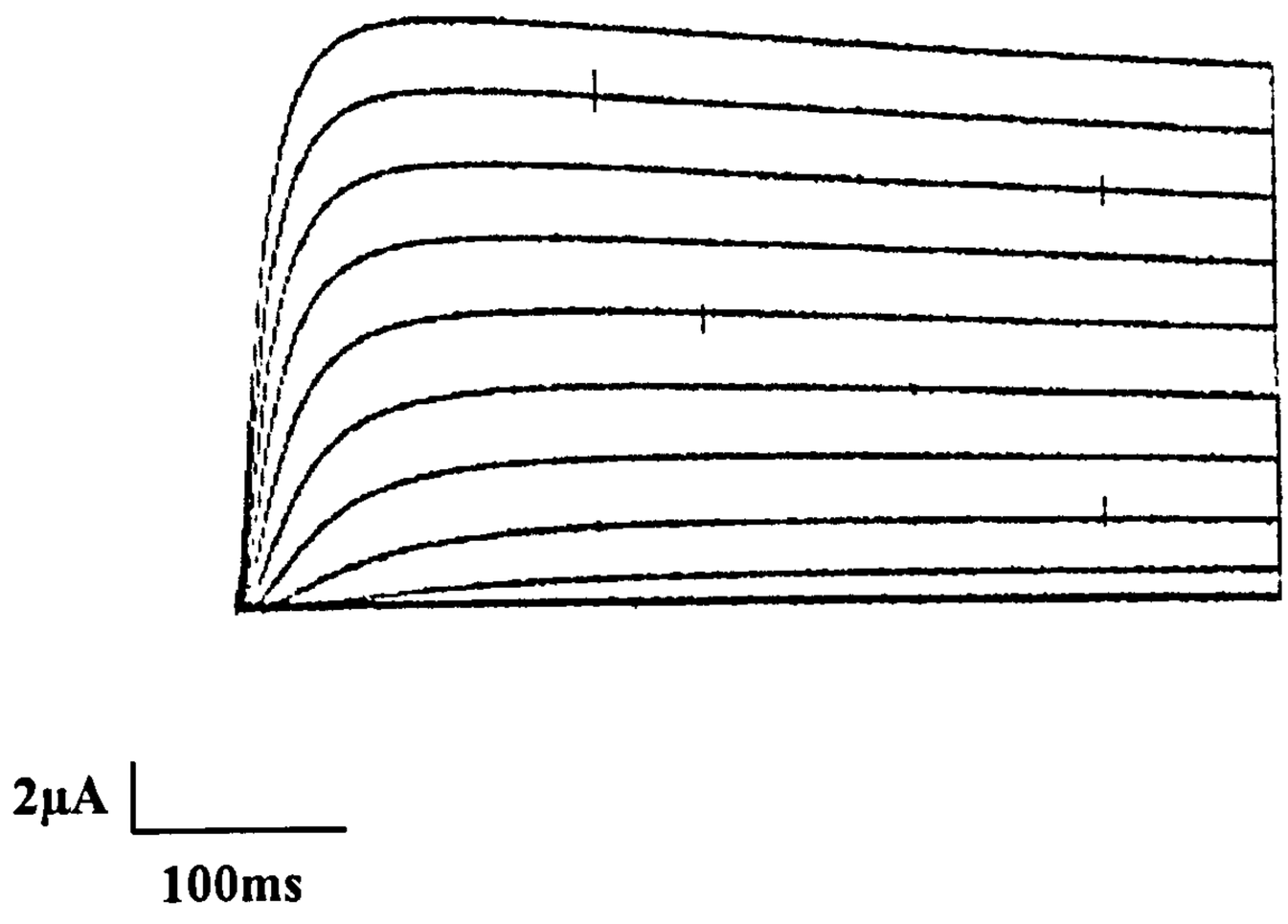

Fig. 3.18 Current families for chimera rKv2.1$_{h741-795}$.
A family of currents (leak subtracted) for a single oocyte are shown for the construction of the I/V curve. Bars indicate the current and time calibration.

a

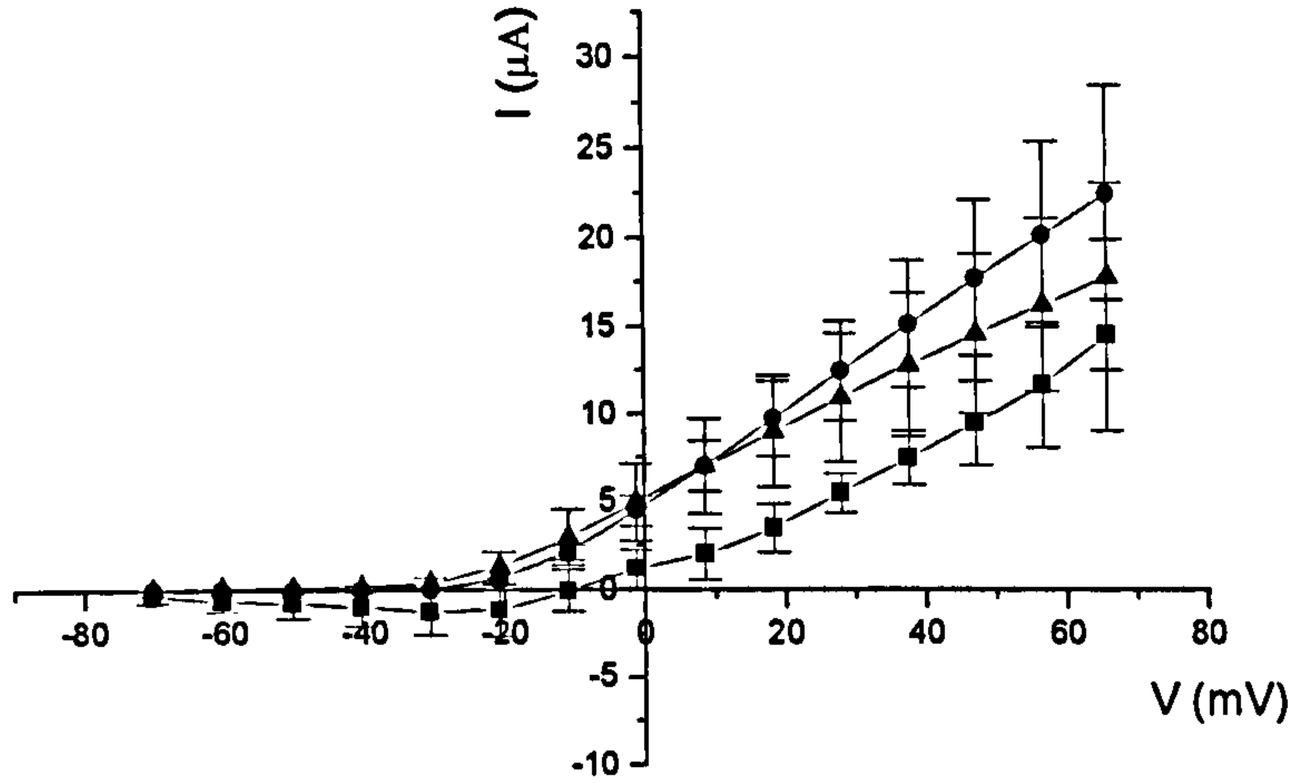

b

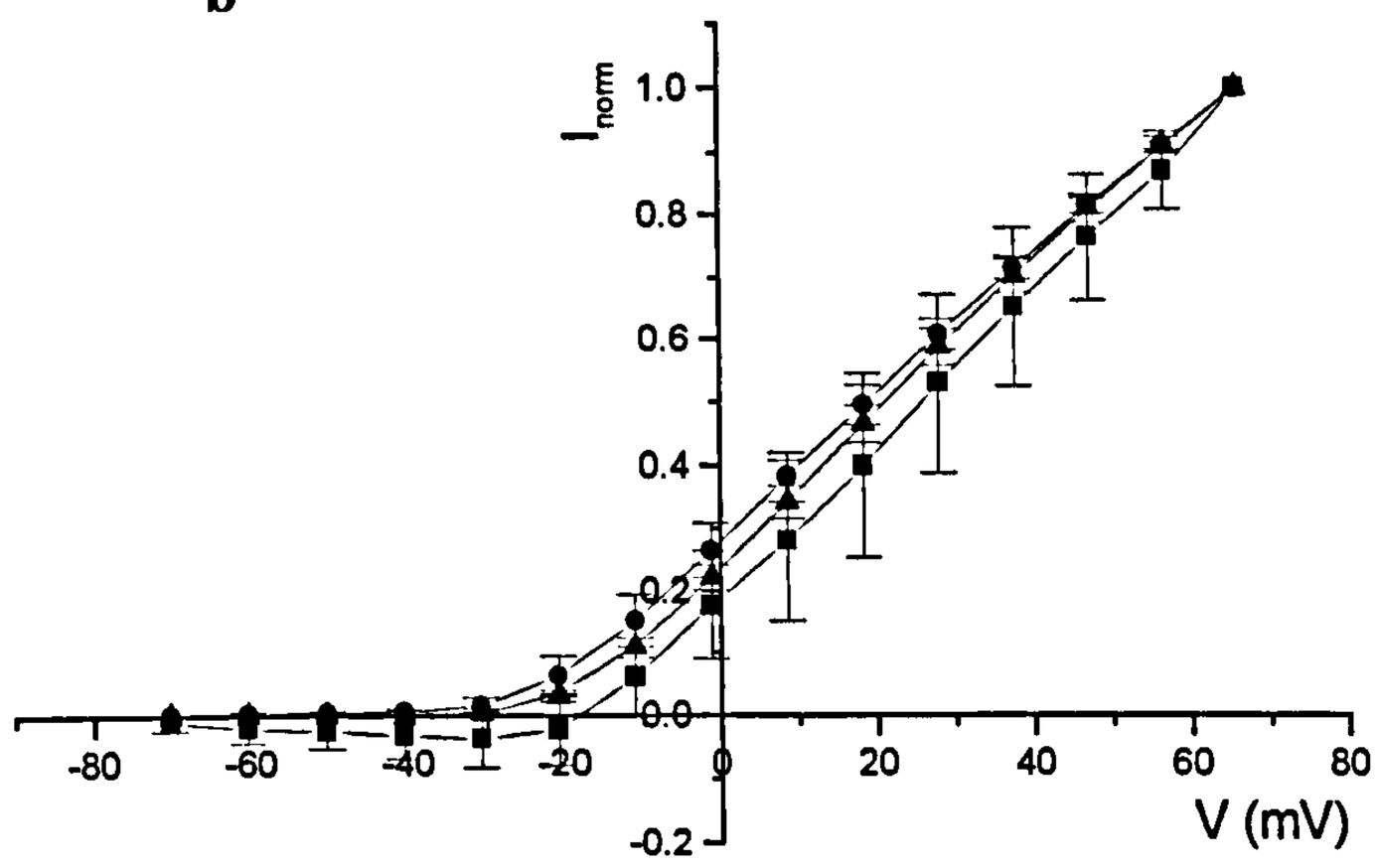

Fig. 3.19 I/V curves for wild type rat and human Kv2.1 and the chimera rKv2.1$_{h741-795}$.

a, The figure shows I/V curves for wild type rKv2.1 (●, *n*=4), wild type hKv2.1, (■, *n*=5), and chimera rKv2.1$_{h741-795}$ (▲, *n*=6).

b, Currents were normalised to the current value at +70mV (22.5±6 μA for rat, 14.5±5.4 μA for human and 17.8±6 μA for rKv2.1$_{h741-795}$). There were no significant differences between the three sets of normalised data ($p<0.05$).

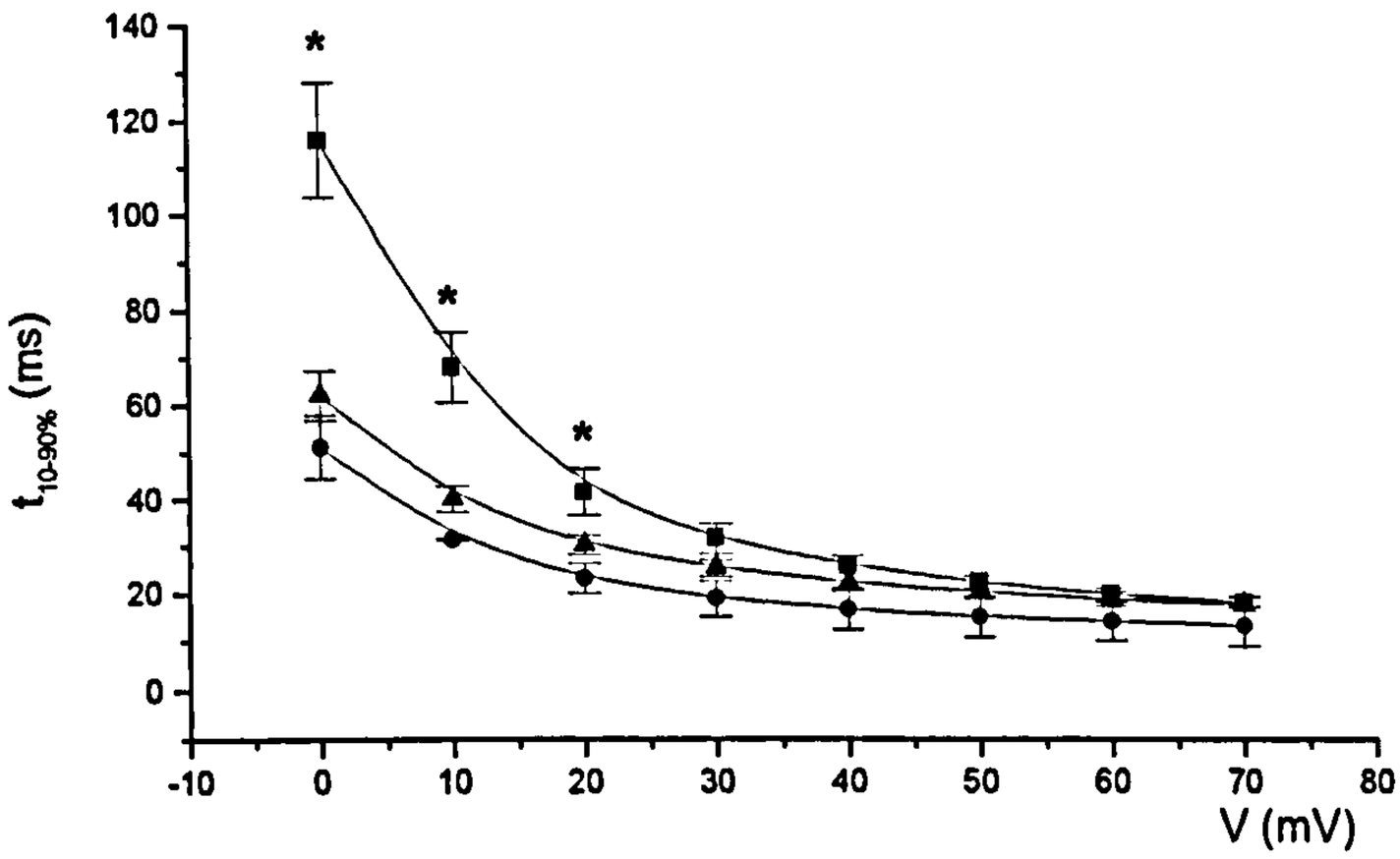

Fig. 3.20 Rise times (10-90%) for the wild types rKv2.1 and hKv2.1 and the chimera rKv2.1$_{h741-795}$.
The figure shows the rise time versus test potential for human Kv2.1 (■, *n*=5), rat Kv2.1 (●, *n*=4), and the chimera rKv2.1$_{h741-795}$ (▲, *n*=6). Significant differences between the human wild type and the chimera are shown (*), ($p<0.05$).

different within this region do not determine the differences in activation kinetics between the wild type rat and human Kv2.1 channels.

3.3 Discussion

In this study, molecular regions in the N- and C- terminal domains that are responsible for the differences in the activation kinetics between rat and human Kv2.1 were investigated. Results are summarised in Fig. 3.21.

Regarding rise times, rKv2.1 E75D, rKv2.1$_{h108-528}$, rKv2.1$_{h108-740}$ and rKv2.1$_{h741-795}$ were like rat Kv2.1, while hKv2.1$_{r108-740}$ was like human Kv2.1. For the chimeras, these data, when considered in isolation, suggest that residues between 108 and 795 in the C- terminus do not determine activation times. However, taking into account that the membrane spanning regions between the two channels are identical (Fig. 3.1), the data indicates that residues, that are different between the rat and human forms of Kv2.1, (between 467 and 787) do not seem to contribute. Residue 75 in the N-terminus also does not appear to contribute to the differences in the activation kinetics between rat and human. Since it is clear that some parts of the N and C-terminus do determine these differences in activation times, the data suggests that the remaining sequences that are different may be important, i.e. residue 67 in the N-terminus, and/or residues within the 796-843 region. However, as will shortly be explained, the conclusions will need to be modified in the light of further experiments.

Figure 3.22 shows a summary of other site-directed mutants made for the rat and human forms of the channel (constructed within this laboratory, Ju *et al*, 2003). Mutation Q67E in the rat channel caused a slowing in the activation kinetics at all test potentials indicating the involvement of residue 67. Similarly, the double mutant, rKv2.1 Q67E/E75D also had slowed activation. Thus the data shows that residue 67 is involved in determining activation kinetics in the rat channel.

Interestingly, a single point mutation in the human channel at residue 67 (E67Q), had no effect on the activation kinetics, with the mutant still showing slow activation. However, changing residue 75 (D75E) in the human channel did have an effect and resulted in fast activation kinetics similar to rat, indicating the importance of residue 75. Surprisingly, the double mutant (E67Q/D756E) retained slow activation kinetics similar to the human wild type. Taken together, these residues suggest, that residues at positions 67 and 75 are involved in

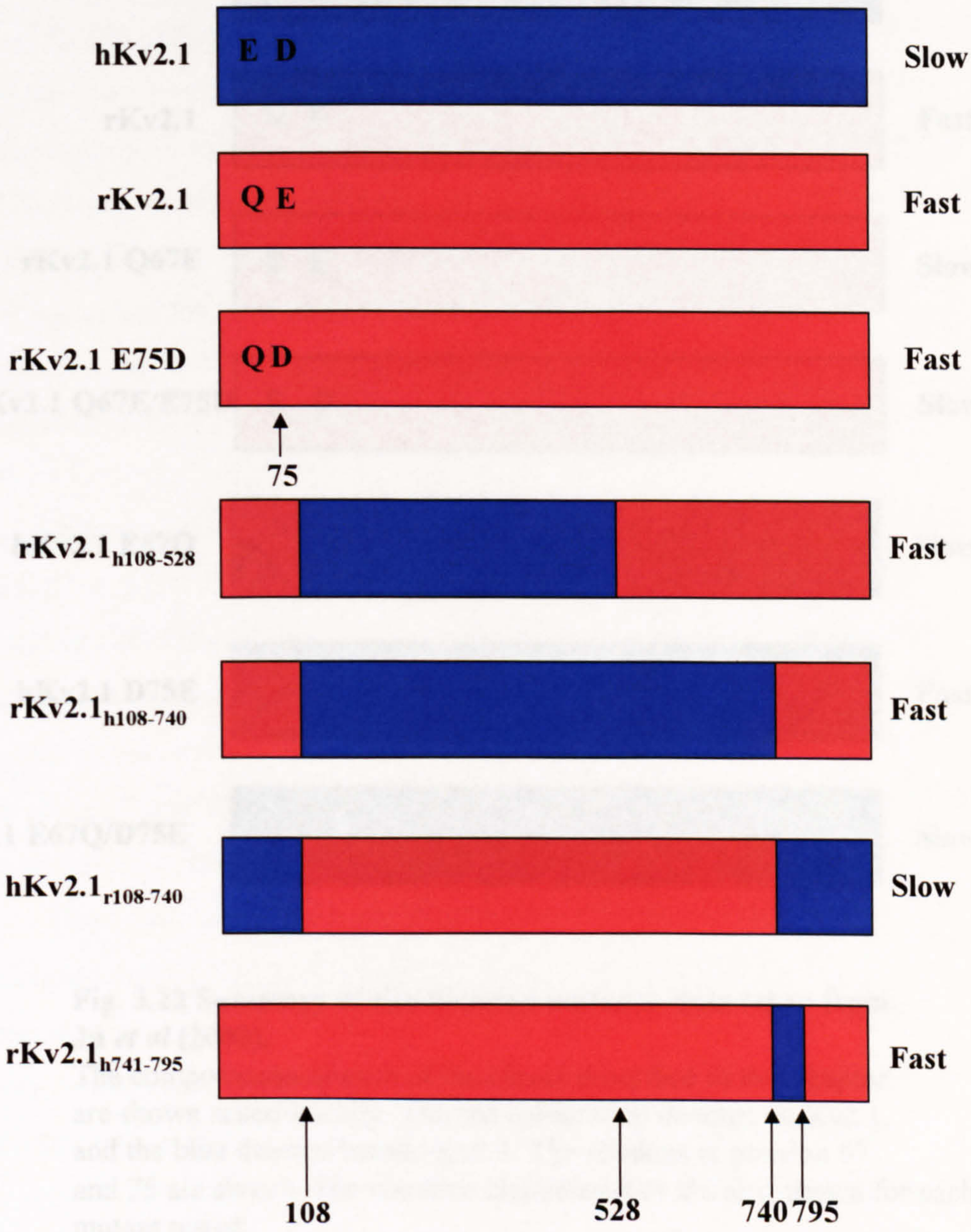

Fig. 3.21 Summary of the 10-90% rise times of the point mutants and all chimeras tested in this thesis.

The compositions of each of the clones described in this chapter are shown schematically. The red colouration denotes rat Kv2.1, and the blue denotes human Kv2.1. Residue 75 is marked in human, rat and mutant E75D (D in human wild type, E in rat wild type and D in rKv2.1 E75D mutant). Also, the domains of the chimeras are shown. The rise time characteristics are also shown for each mutant tested.

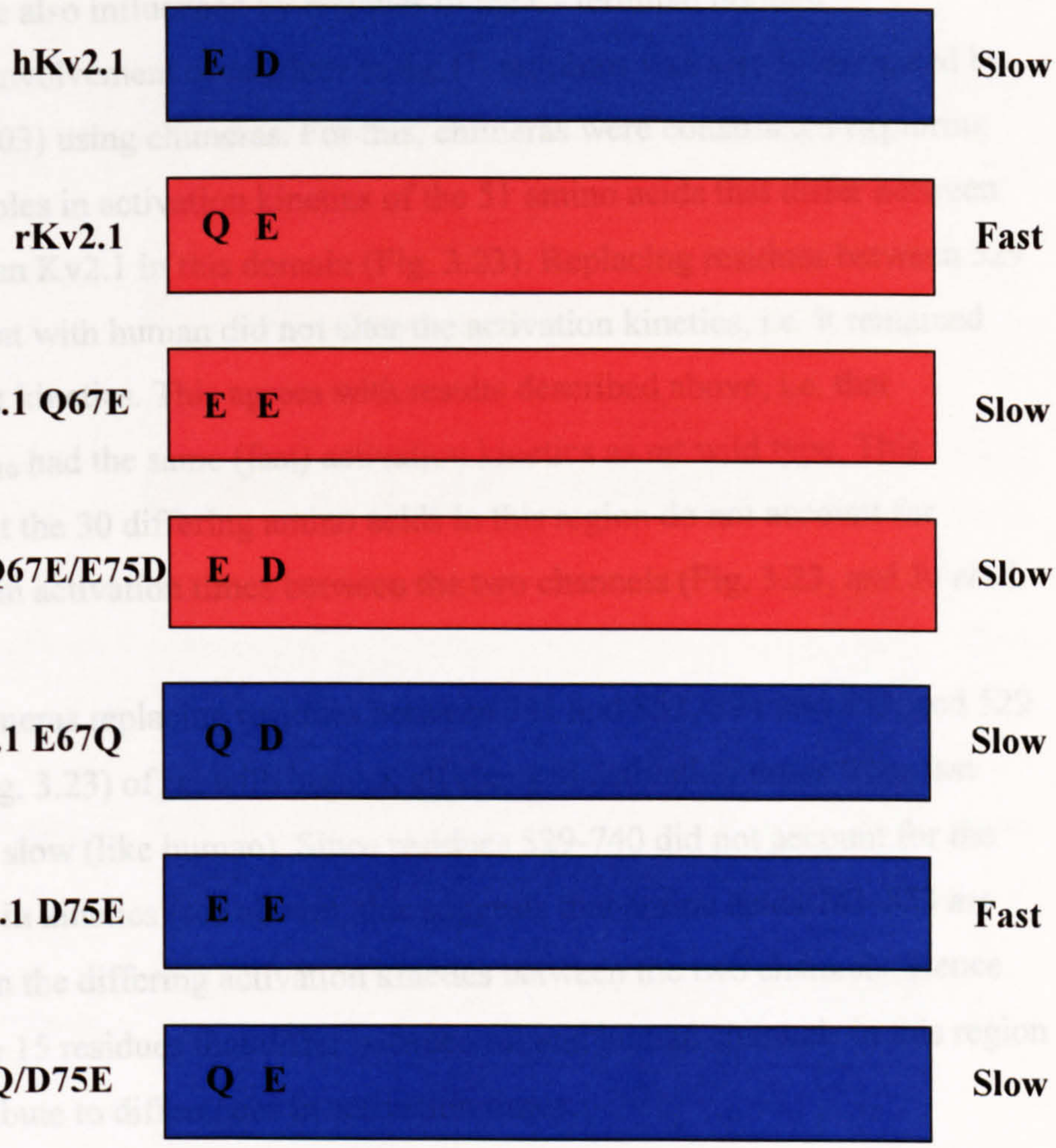

Fig. 3.22 Summary of site-directed mutants, data taken from Ju *et al* (2003).
The compositions of each of the clones described in this chapter are shown schematically. The red colouration denotes rat Kv2.1, and the blue denotes human Kv2.1. The residues at position 67 and 75 are shown. The rise time characteristics are also shown for each mutant tested.

determining the activation kinetics of Kv2.1, but the precise characteristics of activation are also influenced by residues in the C- terminal domain.

The involvement of residues in the C- terminus was also investigated by Ju. *et al,* (2003) using chimeras. For this, chimeras were constructed exploring further the roles in activation kinetics of the 51 amino acids that differ between rat and human Kv2.1 in this domain (Fig. 3.23). Replacing residues between 529 and 740 of rat with human did not alter the activation kinetics, i.e. it remained similar to rat kinetics. This agrees with results described above, i.e. that $rKv2.1_{h108\text{-}740}$ had the same (fast) activation kinetics as rat wild type. This suggests that the 30 differing amino acids in this region do not account for differences in activation times between the two channels (Fig. 3.23, and Ju *et al*, 2003).

Chimeras replacing residues between 741 and 853, 594 and 853, and 529 and 853 (Fig. 3.23) of rat with human, all changed activation times from fast (like rat) to slow (like human). Since residues 529-740 did not account for the differences in kinetics (see above), this suggests that amino acids 741-853 are important in the differing activation kinetics between the two channels. Hence some of the 15 residues that differ between rat and human channels in this region must contribute to differences in activation times.

There may appear to be an apparent contradiction between the involvement of 741-853 residues described above and the kinetics of the chimeras swapping residues between 741-795, and 796-853, as these smaller domain swaps each singly appeared to have no effect. The likely explanation is that both these regions 741-795, and 796-853 are co-operatively involved.

In conclusion, the results in this chapter show that neither residue 75, nor regions 108-528, 108-740, or 741-795 alone solely determine activation kinetics in the potassium channel Kv2.1. However, considering these results alongside other results described in Ju *et al* it appears that residues 67 and 75 in the T1 domain and residues from 741-795 and 796-853 affect the activation kinetics of this channel. It therefore appears that residues 67 and 75 in the N- terminus, and residues between 741-795 and 796-853 in the C- terminus are important in determining activation rate. We have named the region 741-853 the CTA domain (C-terminal activation domain). It is interesting to note that the residues of importance within the N-terminus are located within the T1 or tetramerisation

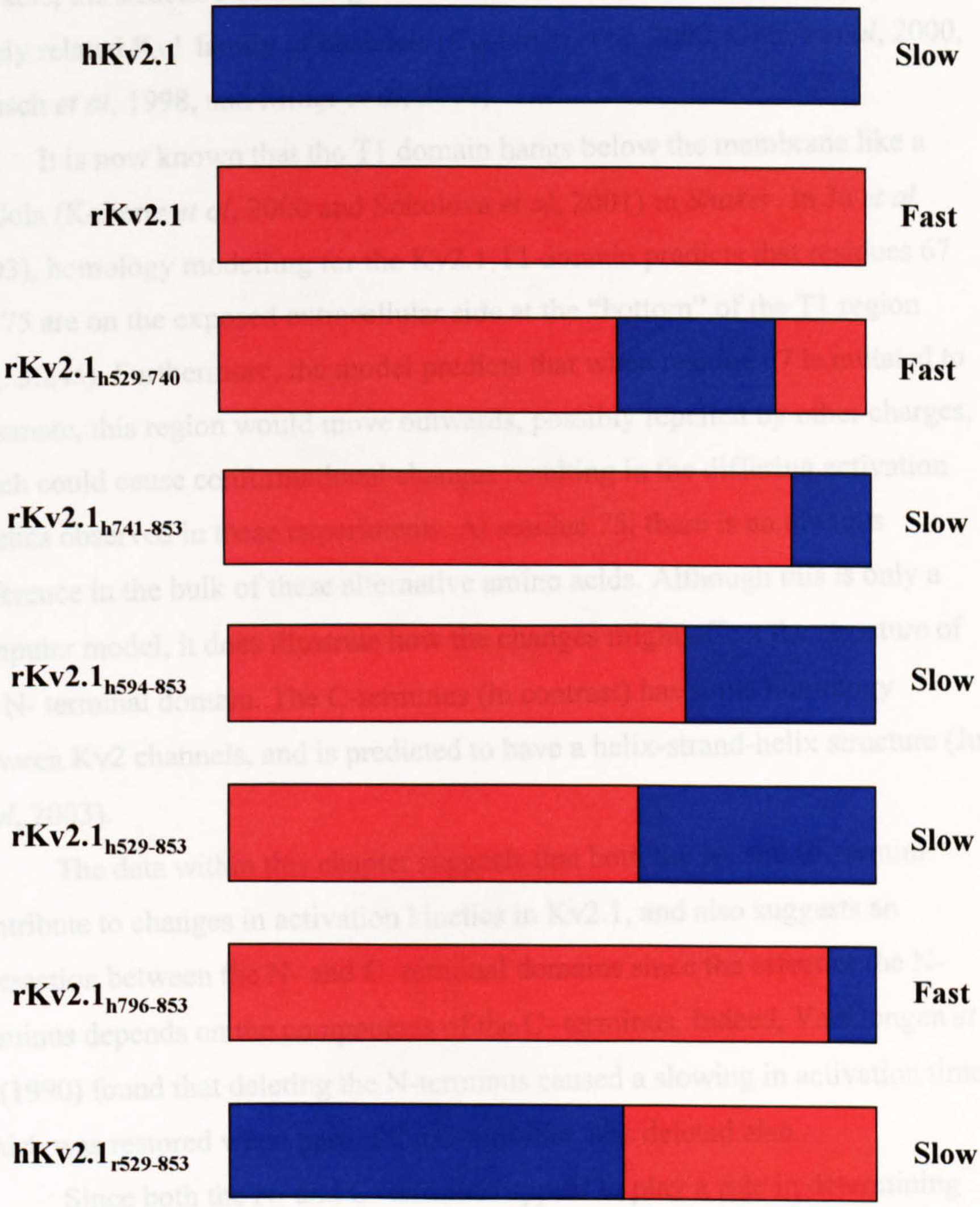

Fig. 3.23 Summary of chimera results, data taken from Ju *et al* (2003).
The compositions of each of the clones described in this chapter are shown schematically.
The red colouration denotes rat Kv2.1, and the blue denotes human Kv2.1. The rise time characteristics are also shown for each chimera tested.

domain. Although a three-dimensional structure for Kv2.1 T1 domain is not available, the structure of this region has been investigated and determined in the closely related Kv1 family of channels (Cushman *et al*, 2000, Gulbis *et al*, 2000, Kreusch *et al*, 1998, and Minor *et al*, 2000).

It is now known that the T1 domain hangs below the membrane like a gondola (Kobertz *et al*, 2000 and Sokolova *et al*, 2001) in *Shaker*. In Ju *et al* (2003), homology modelling for the Kv2.1 T1 domain predicts that residues 67 and 75 are on the exposed extracellular side at the "bottom" of the T1 region (Fig. 3.24a). Furthermore, the model predicts that when residue 67 is mutated to glutamate, this region would move outwards, possibly repelled by other charges, which could cause conformational changes resulting in the differing activation kinetics observed in these experiments. At residue 75, there is an obvious difference in the bulk of these alternative amino acids. Although this is only a computer model, it does illustrate how the changes might affect the structure of the N- terminal domain. The C-terminus (in contrast) has some homology between Kv2 channels, and is predicted to have a helix-strand-helix structure (Ju *et al*, 2003).

The data within this chapter suggests that both the N- and C- termini contribute to changes in activation kinetics in Kv2.1, and also suggests an interaction between the N- and C- terminal domains since the effect of the N-terminus depends on the components of the C- terminus. Indeed, VanDongen *et al* (1990) found that deleting the N-terminus caused a slowing in activation time, which was restored when part of the C-terminus was deleted also.

Since both the N- and C- terminus appear to play a role in determining the activation kinetics of the Kv2.1 channel, it would be plausible to suggest that these termini might physically interact. Such a prediction is supported by electron microscope pictures of the T1 domain of Kv1.1, which shows that the bulk of the hanging gondola is too big for the T1 structure alone (Sokolova *et al*, 2001), i.e. it probably includes the C-terminal region.

A schematic model of the Kv2.1 channel (Fig. 3.24b), showing the membrane spanning part and the intracellular domains T1, Kv2, and CTA has been made guided by the electron microscope pictures for the Shaker channels (Sokolova *et al*, 2001). The linkers comprise both N-terminal (T1-S1) and C-terminal (S6-Kv2) parts. The CTA domains are shown overlapping the T1

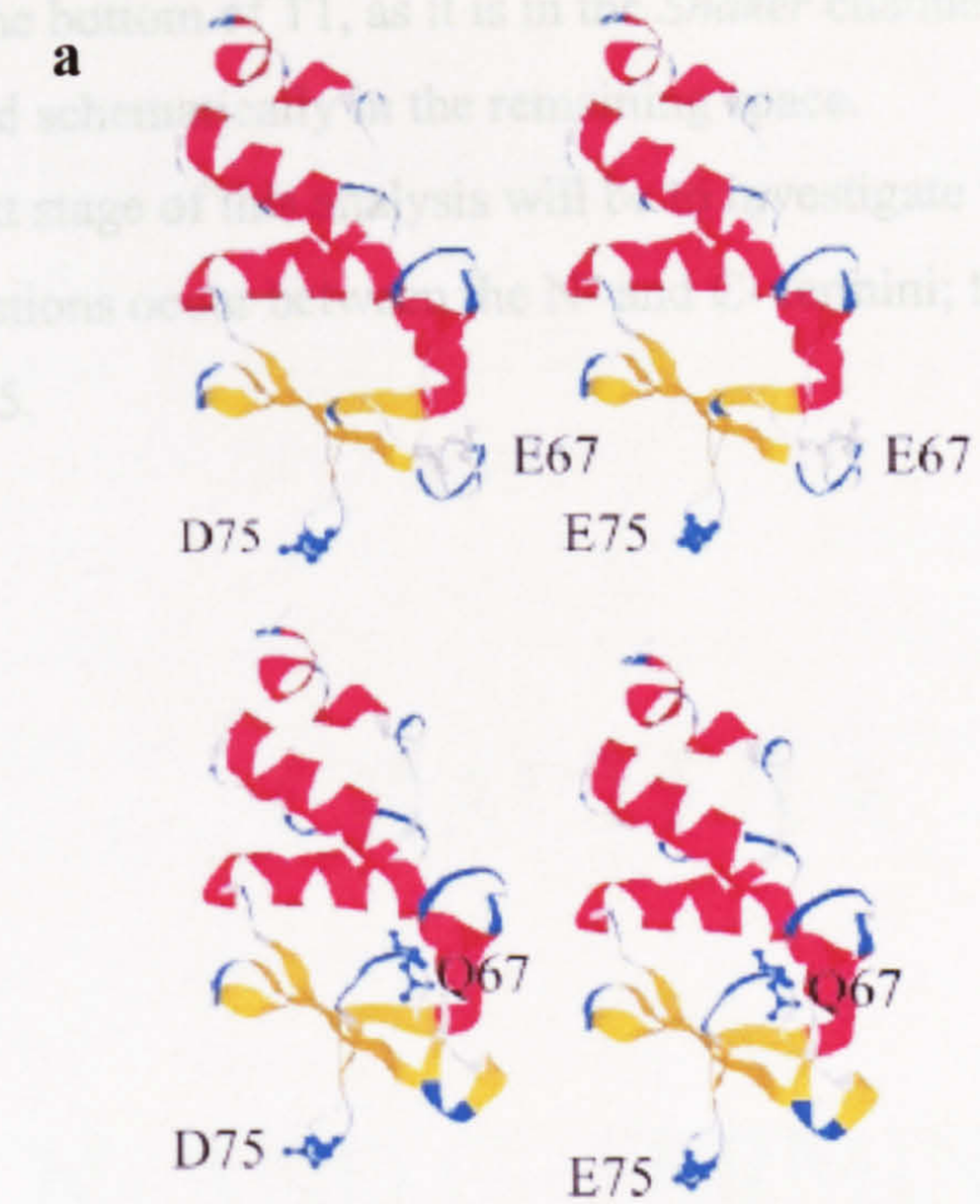

Fig. 3.24 N- terminal and C- terminal models of Kv2.1.
a, Computer homology-based models for the T1 domains of the Kv2.1 point mutants (Ju *et al* (2003)). Amino acids 27-137 are shown and each of the mutated N- terminal residues are labelled.
b, Schematic model of Kv2.1 showing the membrane spanning domains and the intracellular T1 domains, Kv2 domain and CTA domain. The linkers comprise both the N- terminal (T1-S1) and C-terminal (S6-Kv2) regions. Model taken from Ju *et al* (2003).

residues 67 and 75, and the C linker (S6-Kv2) has been drawn as directly connecting to the bottom of T1, as it is in the *Shaker* channel. The Kv2 domain has been located schematically in the remaining space.

The next stage of this analysis will be to investigate whether direct physical interactions occur between the N- and C- termini; this is described in chapters 4 and 5.

CHAPTER 4

N- AND C- TERMINAL INTERACTION STUDIES OF THE RAT POTASSIUM CHANNEL, $K_V2.1$

4.1 Introduction

In the previous chapter it was shown that some residues in the N-terminal region, namely residues 67 and 75, and residues between positions 740 and 853 within the C-terminal region, are involved in determining the difference in activation kinetics between rat and human forms of the Kv2.1 channel. This data suggested that a direct interaction may occur between the N and C termini.

In this chapter, this possible interaction was investigated directly using glutathione S-transferase (GST) binding studies, Biacore surface plasma resonance studies, and fluorescence resonance energy transfer (FRET) experiments.

4.2 Results

4.2.1 Construction of the N-terminal GST construct

To investigate whether the N- and C- termini of rat Kv2.1 interact, an N-terminal GST clone was first made. An N-terminal PCR product consisting of codons 2 to 181 was obtained using the method described in section 2.3.1. The product was then digested with enzymes *Eco*RI and *Xho*I producing a correctly sized fragment (540bp, Fig. 4.1a), and ligated into the similarly digested pGEX-4T-3 vector (4894bp, Fig. 4.1b) (as described in section 2.3.1) to create the construct, rKv2.1$_{N2\text{-}181}$ GST. The DNA was transformed into *E. coli*, and samples sent for sequencing using a universal GST primer. Figures 4.1c and d show the results of the automated sequencing, and subsequent sequence alignment, indicating the correct construction of the clone at one of the joins. The sequence at the other join was also verified by DNA sequencing (data not shown).

4.2.2 Construction of the C-terminal construct

A C-terminal PCR product consisting of codons 413 to the end of the rat sequence, codon 853, was obtained using the method described in section 2.3.2. The product was then digested with enzymes *Eco*RI and *Bsp*I407I producing a correctly sized fragment of 346bp (Fig. 4.2a, with the fragments of 8bp and 185bp being discarded), and ligated into similarly digested rKv2.1 in pBluescript vector (4703bp, Fig. 4.2b) (as described in section 2.3.2) to create the C- terminal construct, rKv2.1$_{C413\text{-}853}$ clone. The DNA was transformed into *E. coli*, and samples sent for sequencing using the universal T7 primer. Figures 4.2c and d show the results of the automated sequencing, and subsequent sequence alignment, indicating that the correct clone had been made.

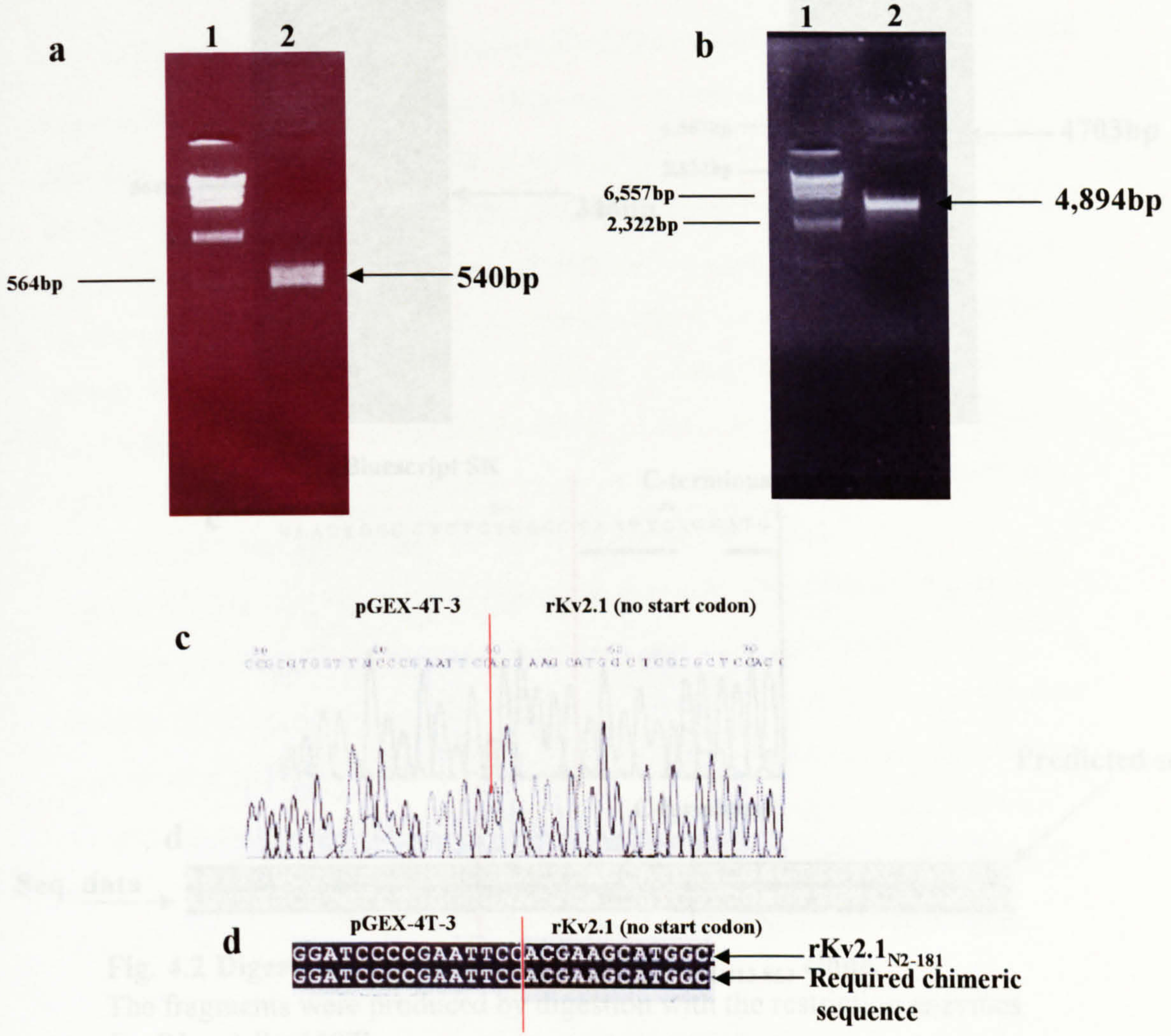

Fig. 4.1 Digestion and sequencing for rKv2.1$_{N2-181}$ GST clone.
The fragments were produced by digestion with restriction enzymes *Eco*RI and *Xho*I.
a, The PCR product was digested with *Eco*RI and *Xho*I, and the relevant sized fragment gel extracted. Lane 1 contains λ-*Hind*III marker and lane 2 contains the gel extracted PCR product (540bp).
b, Wild type rKv2.1 in pBluescript was digested with *Eco*RI and *Xho*I, and the relevant sized fragment gel extracted. Lane 1 contains the λ-*Hind*III marker and lane 2 contains the gel extracted Kv2.1 product digested by the enzymes (4894bp).
c, Sequence electrophoretogram of the rKv2.1$_{N2-181}$ GST clone. The red line denotes the join from pGEX-4T-3 vector to rKv2.1.
d, The DNA sequence was aligned against the desired predicted sequence using ClustalW and Boxshade on-line software (a small sample is shown). The red line denotes the join from vector to rat.

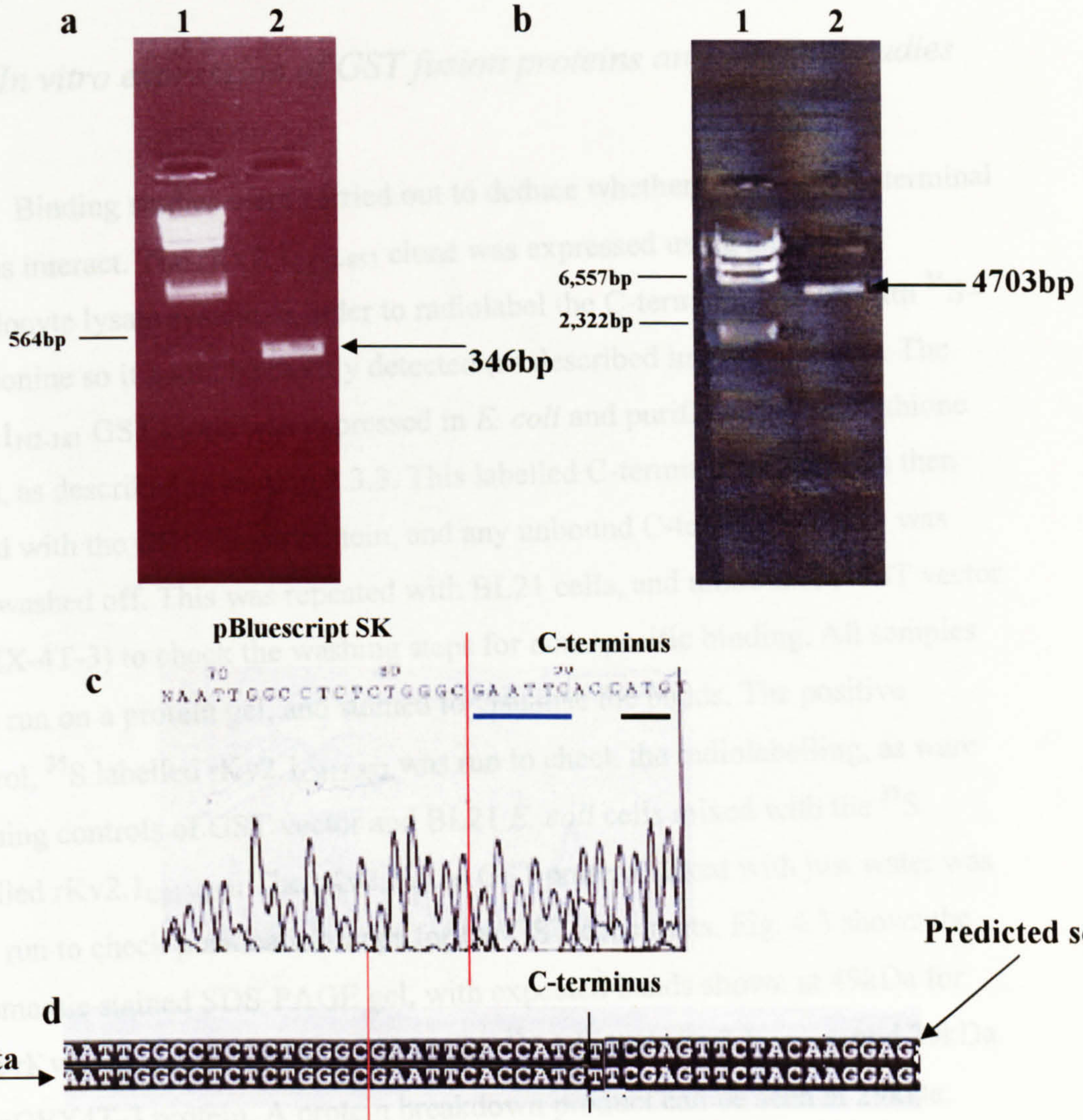

Fig. 4.2 Digestion and sequencing for rKv2.1$_{C413-853}$ clone.
The fragments were produced by digestion with the restriction enzymes *Eco*RI and *Bsp*1407I.
a, The PCR product was digested with the enzymes *Eco*RI and *Bsp*1407I , and the relevant sized fragment gel extracted (346bp). Lane 1 contains λ-*Hind*III marker and Lane 2 contains the gel extracted PCR product.
b, Rat wild type Kv2.1 DNA was digested by enzymes *Eco*RI and *Bsp*1407I, and the relevant fragment gel extracted (4703bp).Lane 1 contains λ-*Hind*III marker and Lane 2 contains the gel extracted rKv2.1 product.
c, Sequence electrophoretogram of the rKv2.1$_{C413-853}$ clone. The red line denotes the join from the pBluescript vector to the rat sequence, the blue line shows the *Eco*RI restriction site join, and the black line shows the start codon of Kv2.1. A Kozac sequence ACC linker was also added between the restriction site and the start codon to facilitate efficient expression.
d, The sequence was aligned against the desired chimeric DNA sequence, using ClustalW and Boxshade on-line software. The red line denotes the join from the pBluescript vector to the rat sequence, and the black line shows the start of the C- terminal domain.

4.2.3 In vitro expression of GST fusion proteins and binding studies

Binding studies were carried out to deduce whether the N- and C-terminal regions interact. The rKv2.1$_{C413-853}$ clone was expressed using an *in vitro* reticulocyte lysate system in order to radiolabel the C-terminal protein with ^{35}S–Methionine so it could be readily detected (as described in section 2.3.3). The rKv2.1$_{N2-181}$ GST clone was expressed in *E. coli* and purified using glutathione beads, as described in section 2.3.3. This labelled C-terminal protein was then mixed with the GST fusion protein, and any unbound C-terminal protein was then washed off. This was repeated with BL21 cells, and unmodified GST vector (pGEX-4T-3) to check the washing steps for non-specific binding. All samples were run on a protein gel, and stained to visualise the bands. The positive control, ^{35}S labelled rKv2.1$_{C413-853}$ was run to check the radiolabelling, as were washing controls of GST vector and BL21 *E. coli* cells mixed with the ^{35}S labelled rKv2.1$_{C413-853}$. The rKv2.1$_{N2-181}$ GST protein mixed with just water was also run to check purification steps for the GST constructs. Fig. 4.3 shows the Coomassie stained SDS-PAGE gel, with expected bands shown at 49kDa for pure rKv2.1$_{N2-181}$ GST protein, 48kDa for ^{35}S labelled rKv2.1$_{C413-853}$ and 29kDa for pGEX4T-3 protein. A protein breakdown product can be seen at 29kDa, representing just the GST tag.

Another gel was also run to confirm the presence of the GST tag, as described in section 2.3.3. After detection using a GST primary antibody, an alkaline phosphatase-conjugated secondary antibody and CSPD substrate, bands could be seen at 29kDa for the GST vector and at 49kDa for the GST tagged rKv2.1$_{N2-181}$ GST protein (Fig. 4.4a). The GST tag was therefore shown to be present.

An SDS-PAGE gel was examined by autoradiography for any ^{35}S labelled product from rKv2.1$_{C413-853}$ (Fig. 4.4b). Lane 1 shows the ^{35}S labelled rKv2.1$_{C413-853}$ alone which indicates the presence of radiolabelled product. The middle lane shows a weaker but still clearly discernable ^{35}S-labelled band, indicating that binding did occur between the N- and C-terminal proteins. No band was seen in lane 3, GST alone (control lane), indicating that the C-terminal

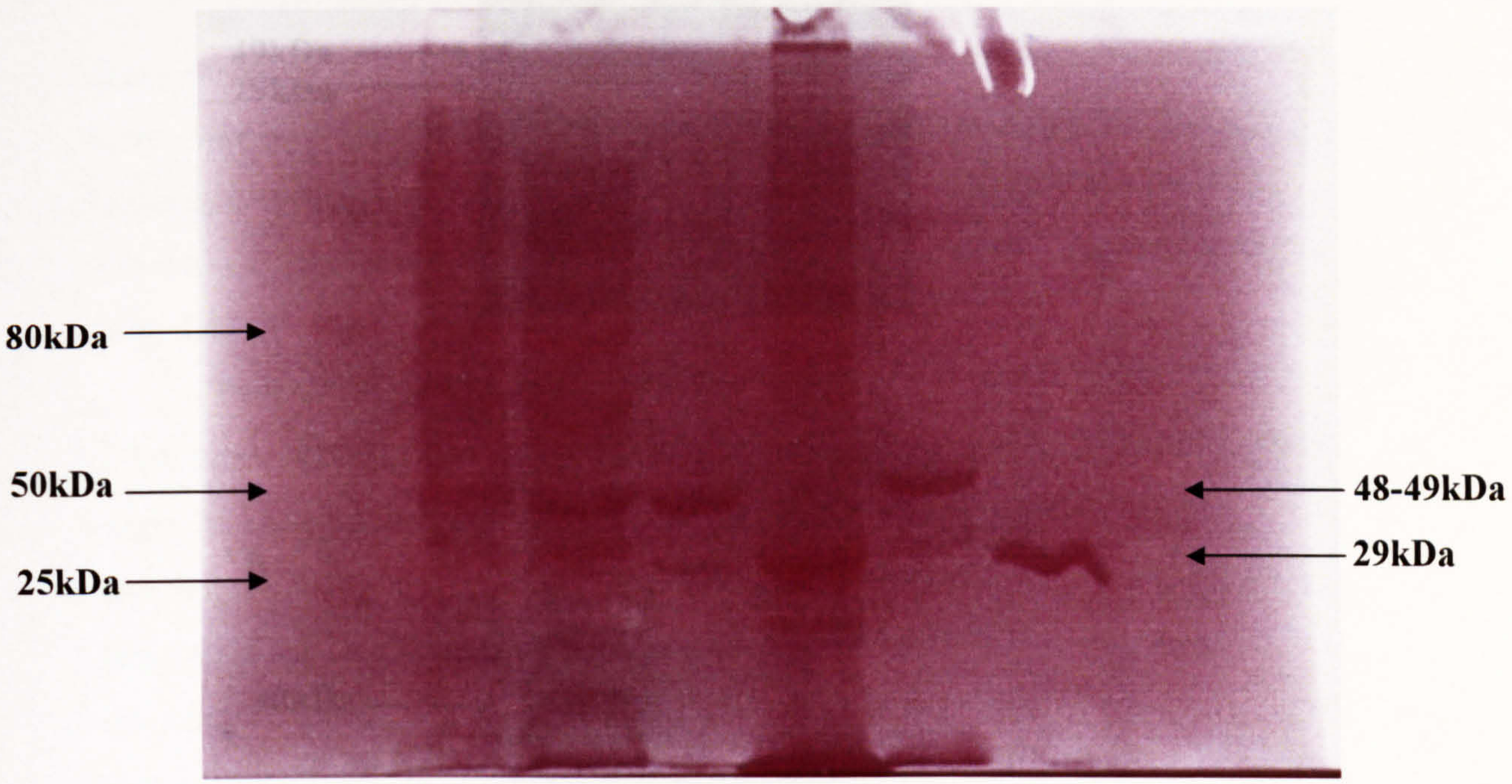

Fig. 4.3 Rat Kv2.1 N- and C- terminal domain interaction assay.
Interaction assay protein samples were run on a 12% SDS-denaturing gel, and stained with Coomassie. The radiolabelled C- terminal domain was mixed with the GST vector and BL21 cells to ensure that the binding found with the N- terminal domain was specific, as explained in 4.2.3. **Lane 1** contains the $rKv2.1_{N2\text{-}181}$ insoluble non-purified protein. **Lane 2** contains the $rKv2.1_{N2\text{-}181}$ GST soluble non-purified protein, a strong band can be seen at the correct size of 49kDa. **Lane 3** contains the $rKv2.1_{N2\text{-}181}$ GST purified protein, a band can be seen at the correct size of 49kDa. **Lane 4** contains the ^{35}S-labelled $rKv2.1_{C413\text{-}853}$ alone, a faint band can be seen at the correct size of 48kDa. **Lane 5** contains the purified $rKv2.1_{N2\text{-}181}$GST + ^{35}S-labelled $rKv2.1_{C413\text{-}853}$; the N- and C- constructs were mixed and purified. As the constructs are of similar size a single band can be seen at 48-49kDa. **Lane 6** contains the pGEX4T-3 vector + ^{35}S-labelled $rKv2.1_{C413\text{-}853}$; the vector was mixed with the labelled C- terminal domain as a negative control. **Lane 7** BL21(DE3) cells + ^{35}S-labelled $rKv2.1_{C413\text{-}853}$, also as a negative control.

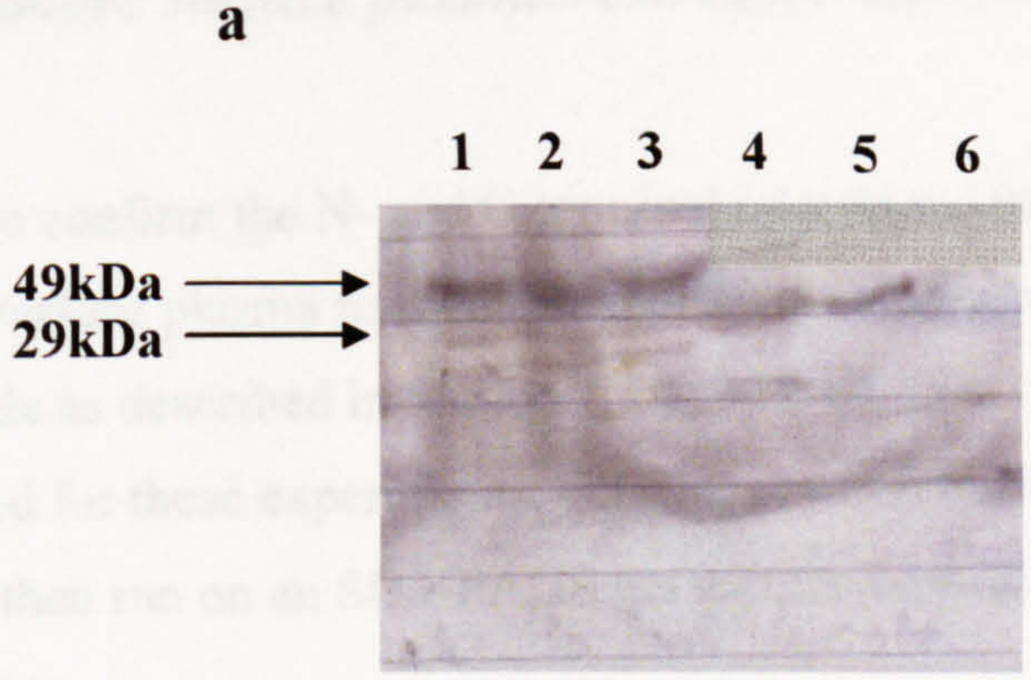

Fig. 4.4 Western blot of GST tagged protein, and corresponding autoradiograph.

a, Western blot of the interaction assay protein run on an SDS-PAGE gel, transferred to nitrocellulose membrane, and detected via an anti-GST antibody, an alkaline phosphatase conjugated secondary antibody, and a CSPD substrate. **Lane 1** contains the rKv2.1$_{N2-181}$ GST soluble fraction, a band of the correct size band can be seen at 49kDa. **Lane 2** contains the rKv2.1$_{N2-181}$ GST after purification. Again a correctly sized band can be seen at 49kDa. **Lane 3** contains the purified rKv2.1$_{N2-181}$ GST mixed with the ^{35}S-labelled rKv2.1$_{C413-853.}$ A correctly size band can be seen at 49kDa. **Lane 4** contains the correctly sized pGEX4T-3 vector alone (29kDa). **Lane 5** contains the pGEX4T-3 vector (alone) + ^{35}S-labelled rKv2.1$_{C413-853}$. A correctly sized band can be seen at 29kDa. **Lane 6** BL21(DE3) cells + ^{35}S-labelled rKv2.1$_{C413-853}$, showing no bands, indicating the efficiency of the washing steps.

b, An autoradiograph detecting radioactivity with lanes as follows: **Lane 1** ^{35}S-labelled rKv2.1$_{C413-853}$, a correctly sized band is seen at 48kDa. **Lane 2** contains the purified rKv2.1$_{N2-181}$ GST mixed with the ^{35}S-labelled rKv2.1$_{C413-853}$, a weak band is also seen at 48kDa. **Lane 3** contains the pGEX4T-3 vector mixed with the ^{35}S-labelled rKv2.1$_{C413-853}$. No band can be seen.

protein did not bind to GST itself. This confirms that the N- and C-termini indeed bind to each other, albeit weakly.

4.2.4 Biacore surface plasma resonance experiments

To confirm the N- and C-terminal interaction found in section 4.2.3, Biacore surface plasma resonance experiments were also carried out. Constructs were made as described in section 2.3.3, with the rKv2.1$_{C413-853}$ protein being unlabelled for these experiments. GST tagged N-terminal protein was purified and was then run on an SDS-PAGE gel and the correctly sized band can be seen (Fig. 4.5).

Plasma resonance experiments were carried out as described in section 2.3.4. Here, one response unit is equal to a 0.0001-degree change in the reflected angle. The results in Fig. 4.6 show that when the rKv2.1$_{C413-853}$ was amide coupled to the Biacore cell and then washed with the rKv2.1 $_{N2-181}$GST protein, a large response was seen, showing binding between the N- and C-terminal domains. However, when a blank cell was washed with the rKv2.1$_{N2-181}$ GST protein, a medium response was seen. This indicates that this protein is quite 'sticky' and does produce a reaction on its own, although not as large a reaction as with the C-terminal protein. The controls of the rKv2.1$_{C413-853}$ washed with the GST vector alone and a blank cell washed with just GST both showed similar and small responses. However, the N- and C- terminal regions together gave by far the largest response, which indicates that these two regions do interact – confirming the results found in section 4.2.3.

4.2.5 Preparation of N-terminal constructs for FRET

An N-terminal PCR product containing either a CFP or YFP fluorescent tag was generated using the method described in section 2.3.5. The PCR product was then digested with enzymes *Eco*RI and *Cla*I, producing a correctly sized fragment of 1080bp (Fig. 4.7a) with the smaller sized fragments discarded, and ligated into a similarly digested rKv2.1 in pGem-He-Juel clone (6014bp, Fig. 4.7b) (as described in section 2.3.5) to create the rKv2.1$_{N-CFP}$ or rKv2.1$_{N-YFP}$ in

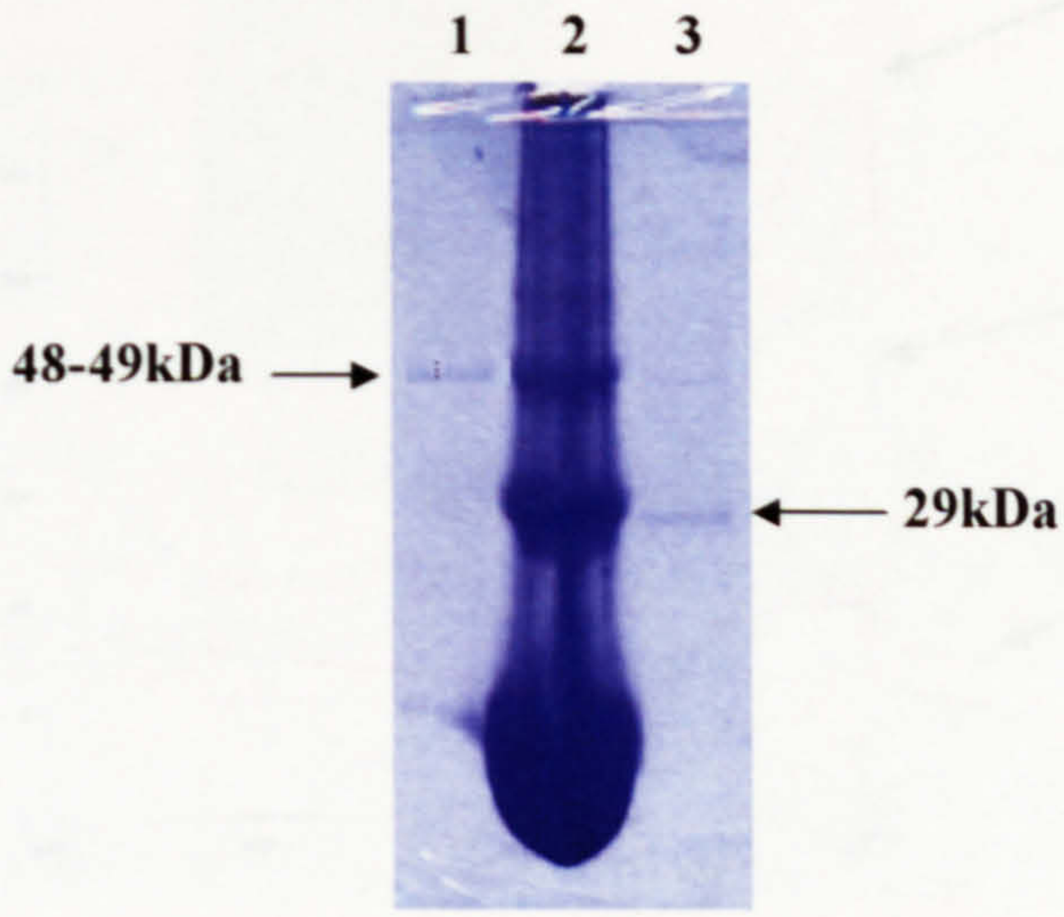

Fig. 4.5 Protein samples for Biacore analysis.
Coomassie blue stained 12% SDS-PAGE gel of proteins used for Biacore analysis. **Lane 1** contains the rKv2.1$_{N2-181}$ GST purified protein; a band can be seen at 49kDa. **Lane 2** contains the non-labelled rKv2.1$_{C413-853}$, a correctly sized band can be seen at 48kDa. **Lane 3** contains the GST vector protein purified, at the correct size (29kDa). The gel confirms the correct size of all proteins, and the purity of the rKv2.1$_{N2-181}$GST and GST vector.

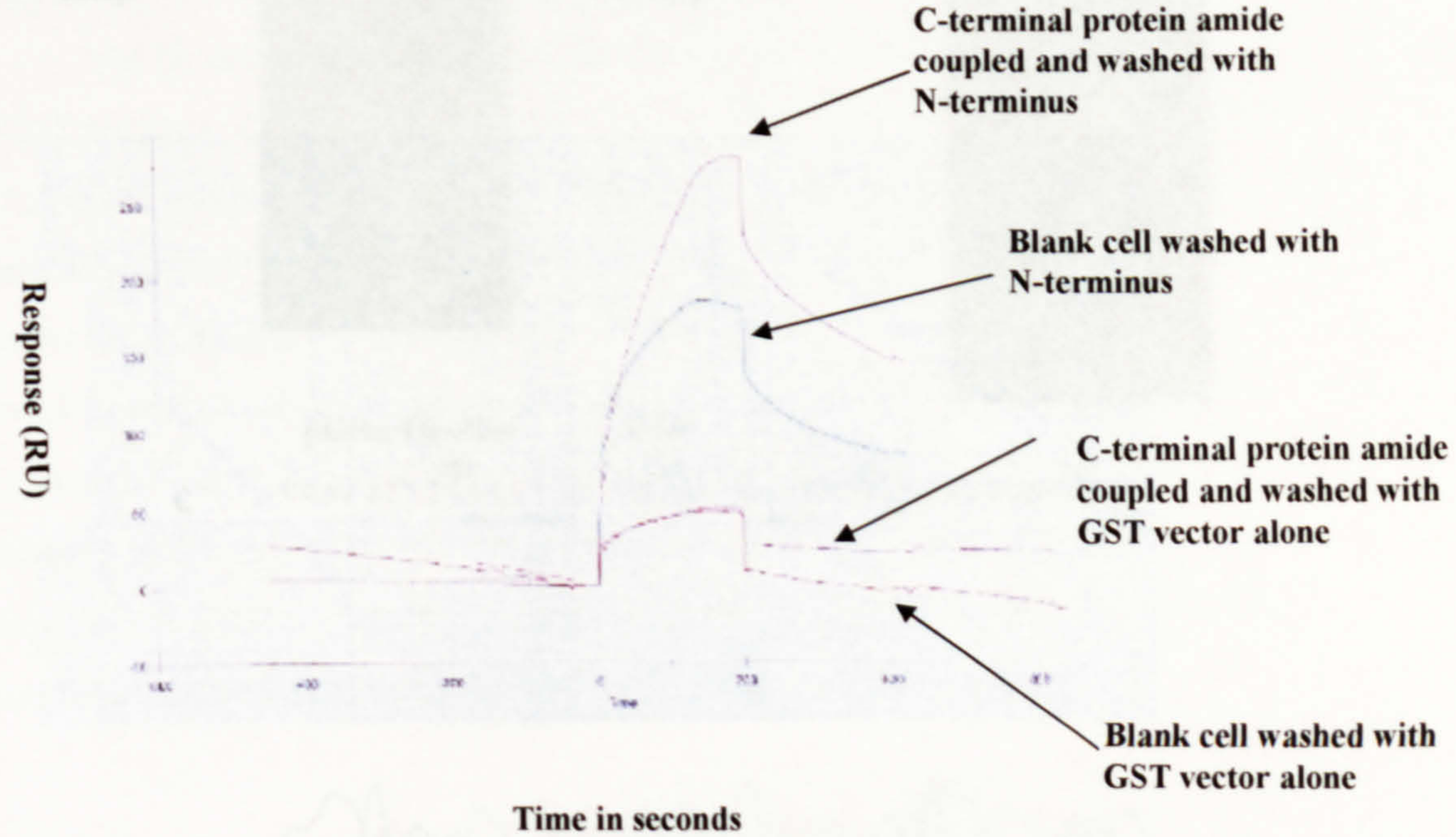

Fig. 4.6 Binding of the N- terminal domain to the C- terminal domain using Biacore.

This figure shows the Biacore SPR trace response from the Biacore during the application of the N-terminal domain GST-fusion protein or the GST alone. Cells contained either the C-terminal protein or were blank as labelled.

One response unit is equal to a 0.0001 degree change in the reflected angle.

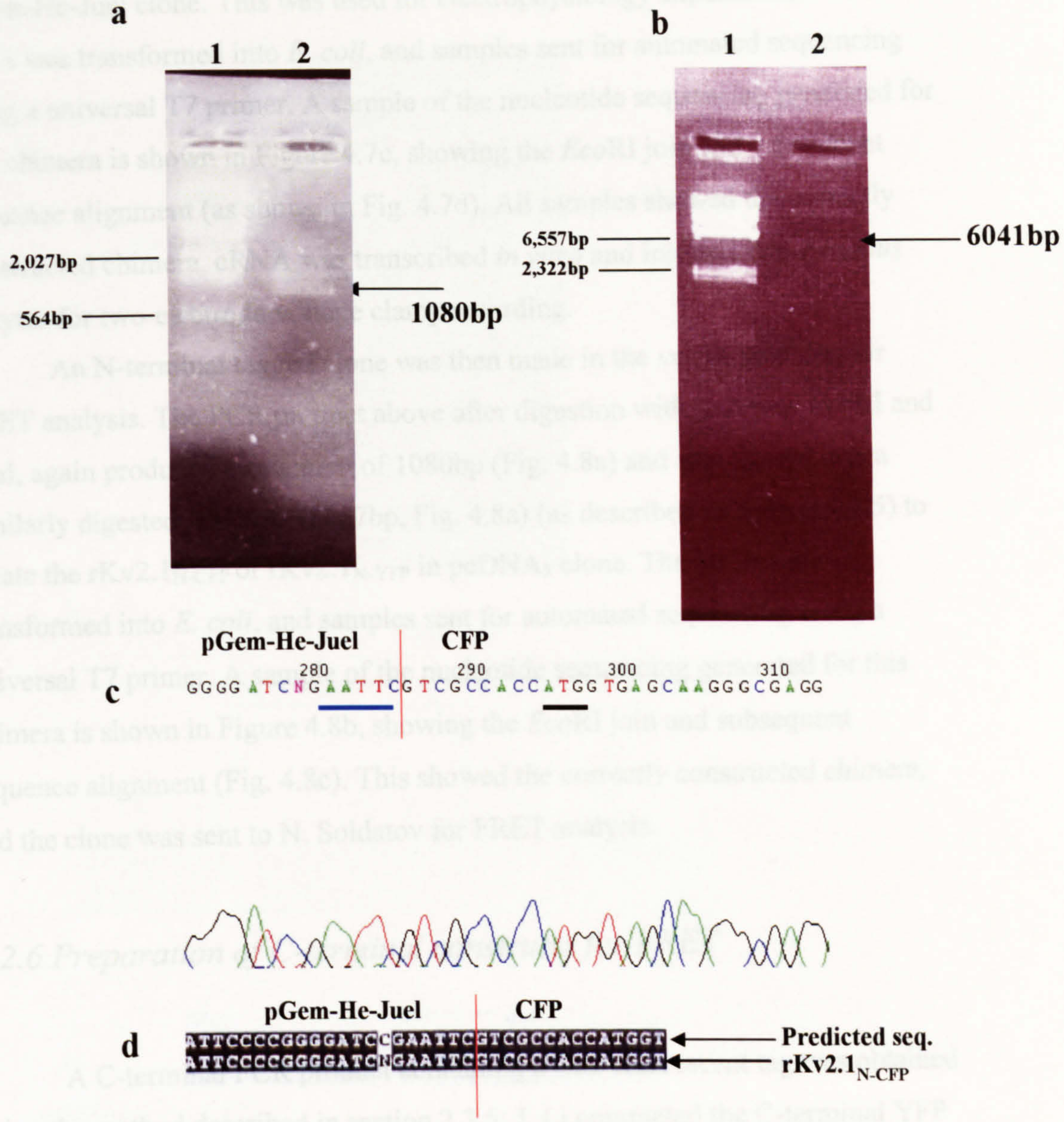

Fig. 4.7 Digestion and sequencing for the rKv2.1$_{N\text{-}CFP}$ in pGem-He-Juel clone.
The fragments were produced by digestion with the restriction enzymes *Eco*RI and *Cla*I.
a, Restriction digest of the CFP PCR product. DNA was digested with *Eco*RI and *Cla*I, and the relevant sized fragment gel extracted (1080bp). Lane 1 contains λ-*Hind*III marker and Lane 2 contains the gel extracted CFP PCR product digested by enzymes *Eco*RI and *Cla*I.
b, Restriction digest of wild type rKv2.1 in pGem-He-Juel. DNA was digested with *Eco*RI and *Cla*I, and the relevant sized fragment gel extracted (6041bp). Lane 1 contains λ-*Hind*III marker and Lane 2 contains the gel extracted rKv2.1 digested by enzymes *Eco*RI and *Cla*I.
c, Sequence electrophoretogram of the rKv2.1$_{N\text{-}CFP}$ in pGem-He-Juel clone. The red line denotes the join from rat to the pGem-He-Juel vector, the blue line shows the *Eco*RI restriction site, and the black line shows the start codon.
d, The sequence was aligned against the desired chimeric predicted DNA sequence, using ClustalW and Boxshade on-line software. The N in the sequence alignment denotes a mis-read, and the correct base was detected in a subsequent read.

pGem-He-Juel clone. This was used for electrophysiology experiments. The DNA was transformed into *E. coli*, and samples sent for automated sequencing using a universal T7 primer. A sample of the nucleotide sequencing generated for this chimera is shown in Figure 4.7c, showing the *Eco*RI join and subsequent sequence alignment (as shown in Fig. 4.7d). All samples showed the correctly constructed chimera. cRNA was transcribed *in vitro* and injected into *Xenopus* oocytes for two-electrode voltage clamp recording.

An N-terminal tagged clone was then made in the vector pcDNA$_3$ for FRET analysis. The PCR product above after digestion with enzymes *Eco*RI and *Cla*I, again produced a fragment of 1080bp (Fig. 4.8a) and was ligated into a similarly digested pcDNA$_3$ (8367bp, Fig. 4.8a) (as described in section 2.3.5) to create the rKv2.1$_{N\text{-}CFP}$ or rKv2.1$_{N\text{-}YFP}$ in pcDNA$_3$ clone. The DNA was transformed into *E. coli*, and samples sent for automated sequencing using a universal T7 primer. A sample of the nucleotide sequencing generated for this chimera is shown in Figure 4.8b, showing the *Eco*RI join and subsequent sequence alignment (Fig. 4.8c). This showed the correctly constructed chimera, and the clone was sent to N. Soldatov for FRET analysis.

4.2.6 Preparation of C-terminal constructs for FRET

A C-terminal PCR product containing a CFP fluorescent tag was obtained using the method described in section 2.3.5; J. Li completed the C-terminal YFP PCR. The PCR product was digested with the enzymes *Afl*II and *Xba*I producing the correctly sized fragment of 892bp (Fig. 4.9a). This fragment was then ligated into a similarly digested rKv2.1 in pGem-He-Juel clone (5745bp, Fig. 4.9b) (as described in section 2.3.6) to create the rKv2.1$_{C\text{-}CFP}$ in pGem-He-Juel clone, used for electrophysiology. The DNA was transformed into *E. coli*, and samples sent for automated sequencing using the universal SP6 primer. A sample of the nucleotide sequencing generated for this chimera is shown in Figure 4.9c, showing the *Xba*I join and subsequent sequence alignment (Fig. 4.9d). The correctly made clone was transcribed *in vitro* and injected into *Xenopus* oocytes for two-electrode voltage clamp recording.

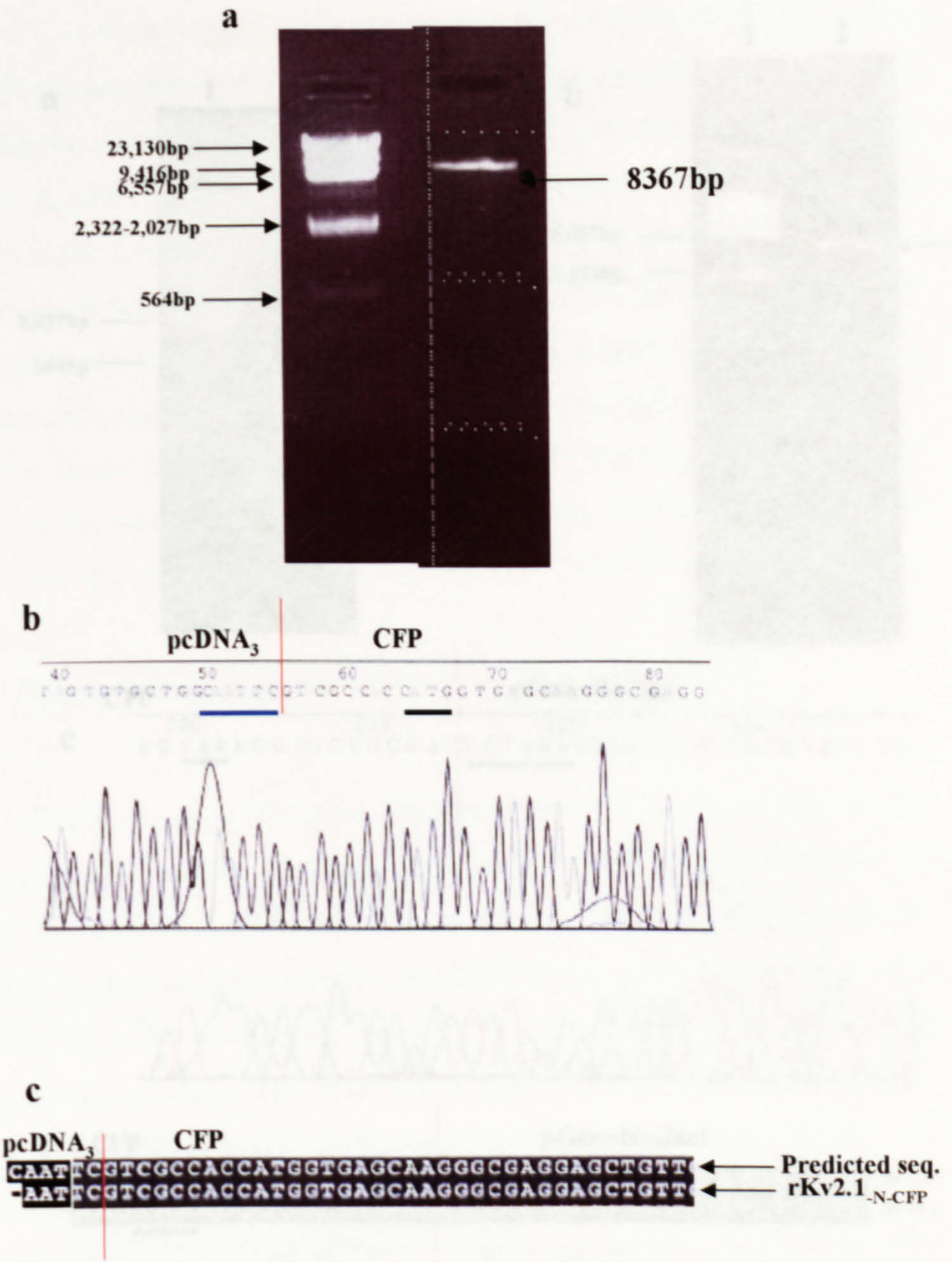

Fig. 4.8 Digestion and sequencing for the rKv2.1$_{\text{-N-CFP}}$ in pcDNA$_3$ clone.
The fragments were produced by digestion with the restriction enzymes *Eco*RI and *Cla*I.
a, Restriction digest of wild type rKv2.1 in pcDNA$_3$. DNA was digested with *Eco*RI and *Cla*I, and the relevant size fragment gel extracted (8367bp). Lane 1 contains λ-*Hind*III marker and Lane 2 contains the gel extracted rKv2.1 in pcDNA$_3$ product digested by enzymes *Eco*RI and *Cla*I.
b, Sequence electrophoretogram of the rKv2.1$_{\text{-N-CFP}}$ in pcDNA$_3$ clone. The red line denotes the join from rat to the pcDNA$_3$ vector, the blue line shows the *Eco*RI restriction site, and the black line shows the start codon.
c, The sequence was aligned against the desired chimeric predicted DNA sequence, using ClustalWand Boxshade on-line software.

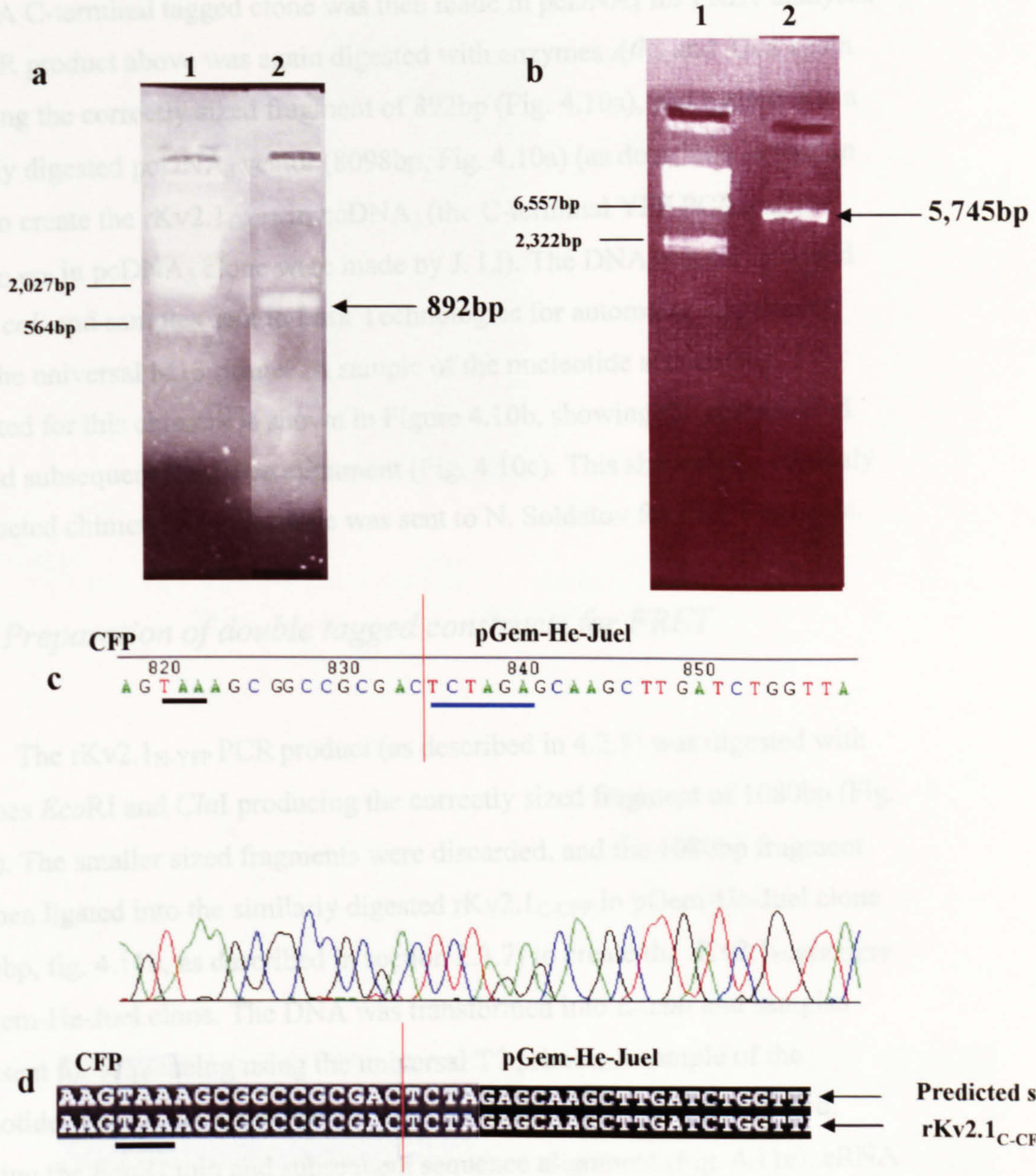

Fig. 4.9 Digestion and sequencing for the rKv2.1$_{C\text{-}CFP}$ in pGem-He-Juel clone.
a, Restriction digest of the CFP PCR product. DNA was digested with *Afl*II and *Xba*I, and the relevant sized fragment gel extracted (892bp). Lane 1 contains λ-*Hind*III marker and Lane 2 contains the gel extracted CFP PCR product digested by enzymes *Afl*II and *Xba*I.
b, Restriction digest of wild type rKv2.1 in pGem-He-Juel. DNA was digested with *Afl*II and *Xba*I, and the relevant sized fragment gel extracted (5745bp). Lane 1 contains λ-*Hind*III marker and Lane 2 contains the gel extracted rKv2.1 digested by enzymes *Afl*II and *Xba*I.
c, Sequence electrophoretogram of the rKv2.1$_{C\text{-}CFP}$ in pGem-He-Juel clone. The red line denotes the join from CFP to the pGem-He-Juel vector, the blue line shows the *Xba*I restriction site, and the black line shows the stop codon.
d, The sequence was aligned against the desired chimeric predicted DNA sequence, using ClustalW and Boxshade on-line software. The red line denotes the join from CFP to the pGem-He-Juel vector.

A C-terminal tagged clone was then made in pcDNA$_3$ for FRET analysis. The PCR product above was again digested with enzymes *Afl*II and *Xba*I again producing the correctly sized fragment of 892bp (Fig. 4.10a), and ligated into a similarly digested pcDNA$_3$ vector (8098bp, Fig. 4.10a) (as described in section 2.3.6) to create the rKv2.1$_{C\text{-}CFP}$ in pcDNA$_3$ (the C-terminal YFP PCR and the rKv2.1$_{C\text{-}YFP}$ in pcDNA$_3$ clone were made by J. Li). The DNA was transformed into *E. coli* and samples sent to Lark Technologies for automated sequencing using the universal M13 primer. A sample of the nucleotide sequencing generated for this chimera is shown in Figure 4.10b, showing the correct *Xba*I join and subsequent sequence alignment (Fig. 4.10c). This showed the correctly constructed chimera, and the clone was sent to N. Soldatov for FRET analysis.

4.2.7 Preparation of double tagged constructs for FRET

The rKv2.1$_{N\text{-}YFP}$ PCR product (as described in 4.2.5) was digested with enzymes *Eco*RI and *Cla*I producing the correctly sized fragment of 1080bp (Fig. 4.11a). The smaller sized fragments were discarded, and the 1080bp fragment was then ligated into the similarly digested rKv2.1$_{C\text{-}CFP}$ in pGem-He-Juel clone (5970bp, fig. 4.11b, as described in section 2.3.7) to create the rKv2.1$_{N\text{-}YFP\text{-}C\text{-}CFP}$ in pGem-He-Juel clone. The DNA was transformed into *E. coli* and samples were sent for sequencing using the universal T7 primer. A sample of the nucleotide sequencing generated for this chimera is shown in Figure 4.11d, showing the *Eco*RI join and subsequent sequence alignment (Fig. 4.11e). cRNA was transcribed *in vitro* and injected into *Xenopus* oocytes for two-electrode voltage clamp recording.

A double tagged clone was then made in pcDNA$_3$ for FRET analysis. The PCR product above was again digested with the enzymes *Eco*RI and *Cla*I (1080bp, fig. 4.11a), and the smaller sized fragments discarded. This fragment was then ligated into the similarly digested rKv2.1$_{C\text{-}CFP}$ in pcDNA$_3$ clone (8323bp, Fig. 4.11c) (as described in section 2.3.7) to create the rKv2.1$_{N\text{-}YFP\text{-}C\text{-}CFP}$ in pcDNA$_3$ clone. The DNA was transformed into *E. coli* and samples sent for sequencing using a universal T7 primer. A sample of the nucleotide sequencing

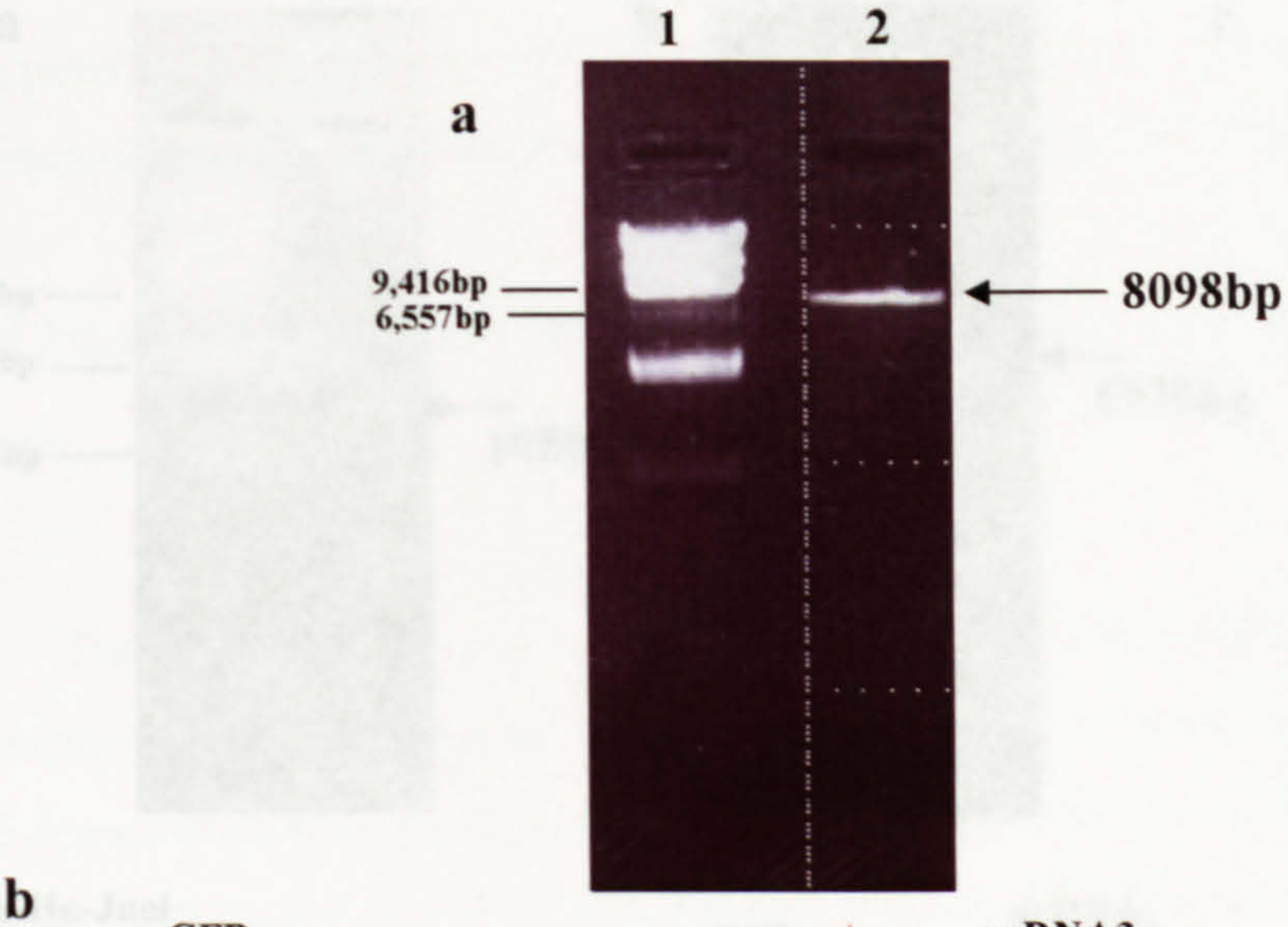

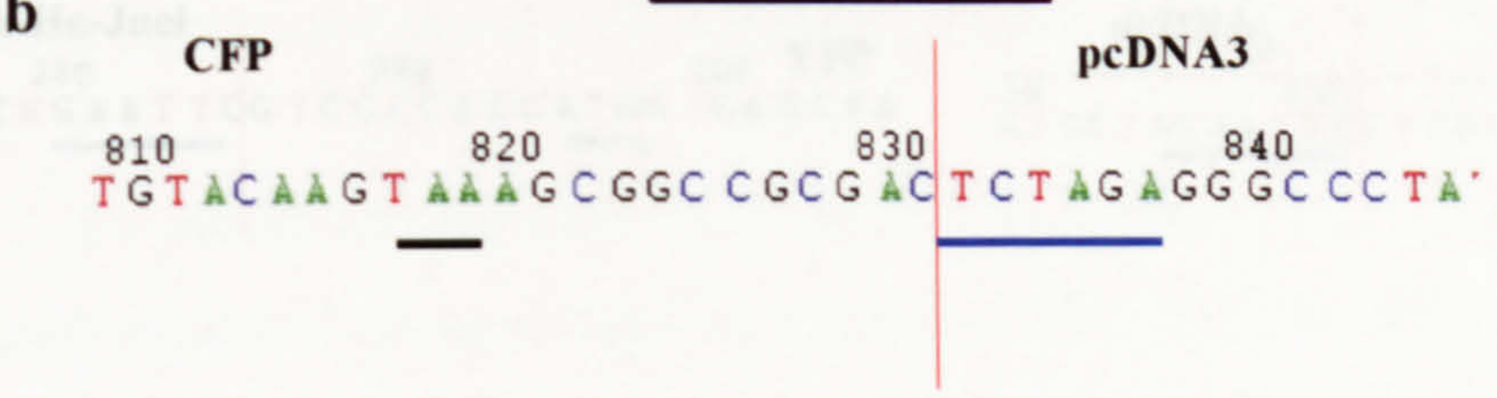

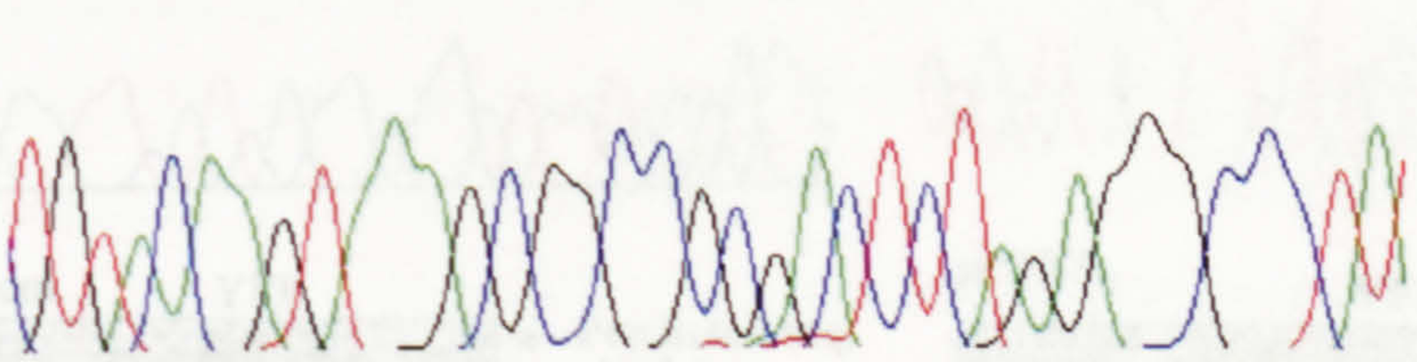

Fig. 4.10 Digestion and sequencing for the rKv2.1$_{C\text{-}CFP}$ in pcDNA$_3$ clone.
a, Restriction digest of wild type rKv2.1 in pcDNA$_3$. DNA was digested with *Afl*II and *Xba*I, and the relevant sized fragment gel extracted (8098bp). Lane 1 contains λ-*Hind*III marker and Lane 2 contains the gel extracted rKv2.1 in pcDNA$_3$ product digested by enzymes *Afl*II and *Xba*I.
b, Sequence electrophoretogram of the rKv2.1$_{C\text{-}CFP}$ in pcDNA$_3$ clone. The red line denotes the join from CFP to the pcDNA$_3$ vector, the blue line shows the *Xba*I restriction site, and the black line shows the stop codon.
c, The sequence was aligned against the desired chimeric predicted DNA sequence, using ClustalW and Boxshade on-line software. The red line denotes the join from CFP to the pcDNA$_3$ vector.

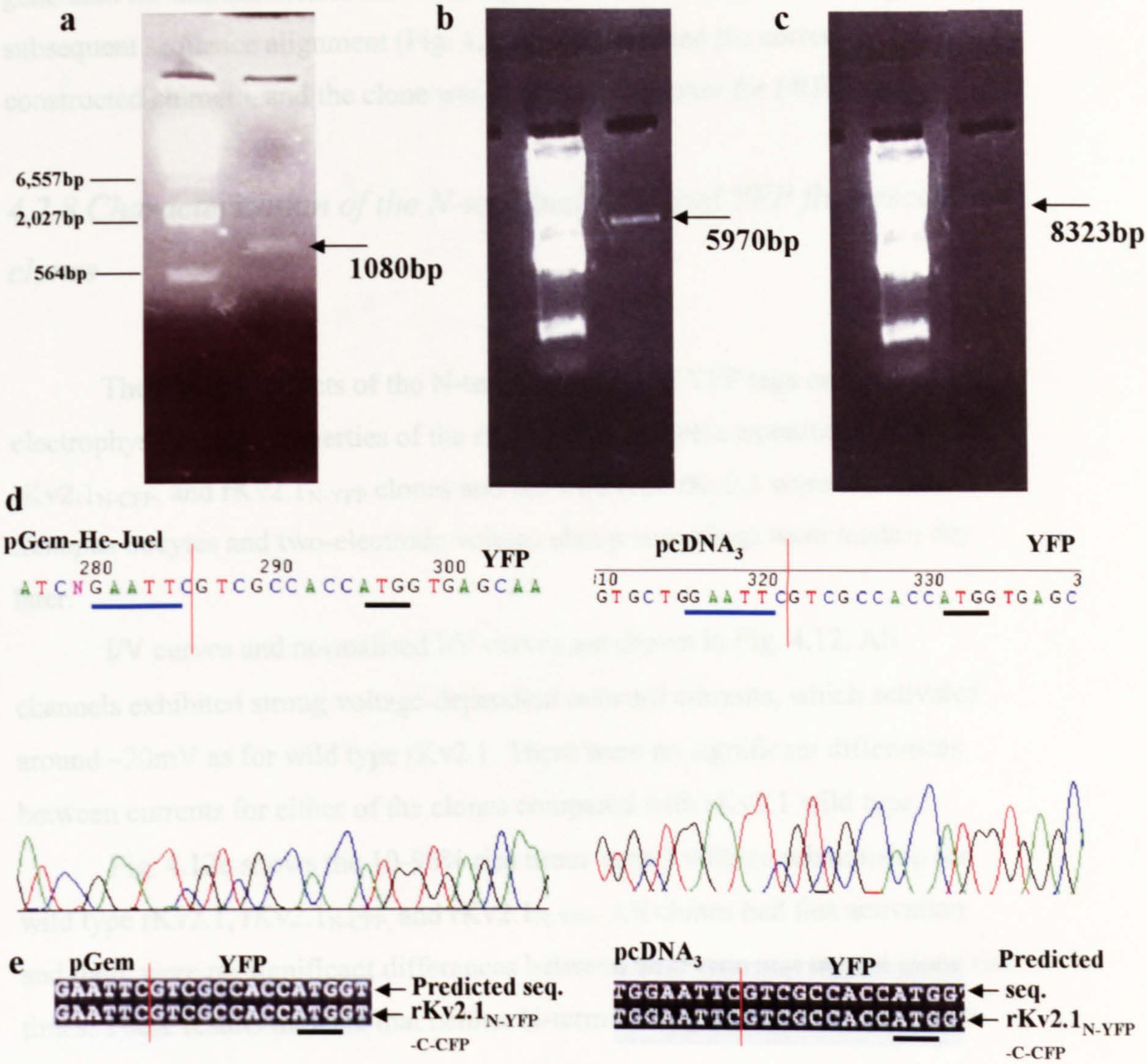

Fig. 4.11 Digestion and sequencing for the rKv2.1$_{N\text{-}YFP\text{-}C\text{-}CFP}$ in pGem-He-Juel and rKv2.1$_{N\text{-}YFP\text{-}C\text{-}CFP}$ in pcDNA$_3$ clones.

Lane 1 contains λ-*Hind*III marker and lane 2 contains the gel extracted relevant product digested by enzymes *Eco*RI and *Cla*I in a, b and c. The marker sizes are shown next to figure a.

a, Restriction digest of rKv2.1 N terminal YFP PCR product. DNA was digested with *Eco*I and *Cla*I, and the relevant sized fragment gel extracted (1080bp).

b, Restriction digest of rKv2.1$_{C\text{-}CFP}$ in pGem-He-Juel. DNA was digested with *Eco*I and *Cla*I, and the relevant sized fragment gel extracted (5970bp).

c, Restriction digest of rKv2.1$_{C\text{-}CFP}$ in pcDNA$_3$. DNA was digested with *Eco*I and *Cla*I, and the relevant sized fragment gel extracted (8323bp).

d, Sequence electrophoretograms of the rKv2.1$_{N\text{-}YFP\text{-}C\text{-}CFP}$ in pGem-He-Juel and pcDNA$_3$ clones. The red lines denote the join from the vectors to the YFP tags, the blue lines show the *Eco*RI restriction sites, and the black lines show the start codons.

e, The sequences were aligned against the desired chimeric predicted DNA sequences, using ClustalW and Boxshade on-line software.

generated for this chimera is shown in Figure 4.11d, showing the *Eco*RI join and subsequent sequence alignment (Fig. 4.11e). This showed the correctly constructed chimera, and the clone was sent to N. Soldatov for FRET analysis.

4.2.8 Characterisation of the N-terminal CFP and YFP fluorescent clones

The possible effects of the N-terminal CFP and YFP tags on the electrophysiological properties of the rKv2.1 channel were examined. cRNA for $rKv2.1_{N\text{-}CFP}$, and $rKv2.1_{N\text{-}YFP}$ clones and the wild type rKv2.1 were injected into *Xenopus* oocytes and two-electrode voltage clamp recordings were made a day later.

I/V curves and normalised I/V curves are shown in Fig. 4.12. All channels exhibited strong voltage-dependent outward currents, which activated around –20mV as for wild type rKv2.1. There were no significant differences between currents for either of the clones compared with rKv2.1 wild type.

Fig. 4.12c shows the 10-90% rise times versus voltage relationship for wild type rKv2.1, $rKv2.1_{N\text{-}CFP}$, and $rKv2.1_{N\text{-}YFP}$. All clones had fast activation and there were no significant differences between wild type and tagged clone rise times. These results indicate that neither N-terminal tag affected the activation properties of rKv2.1.

4.2.9 Characterisation of the C-terminal CFP and YFP fluorescent clones

The possible effects of the C-terminal CFP and YFP tags on the electrophysiological properties of the rKv2.1 channel were examined. Rat $Kv2.1_{C\text{-}CFP}$ and $rKv2.1_{C\text{-}YFP}$ clone and wild type rKv2.1 cRNA were injected into *Xenopus* oocytes and two-electrode voltage clamp recordings made a day later.

Figure 4.13a shows the mean I/V curve, and the normalised I/V curve is shown in Fig. 4.13b. All channels exhibited strong voltage-dependent outward currents, which activated around –20mV as for wild type Kv2.1. There were no

a

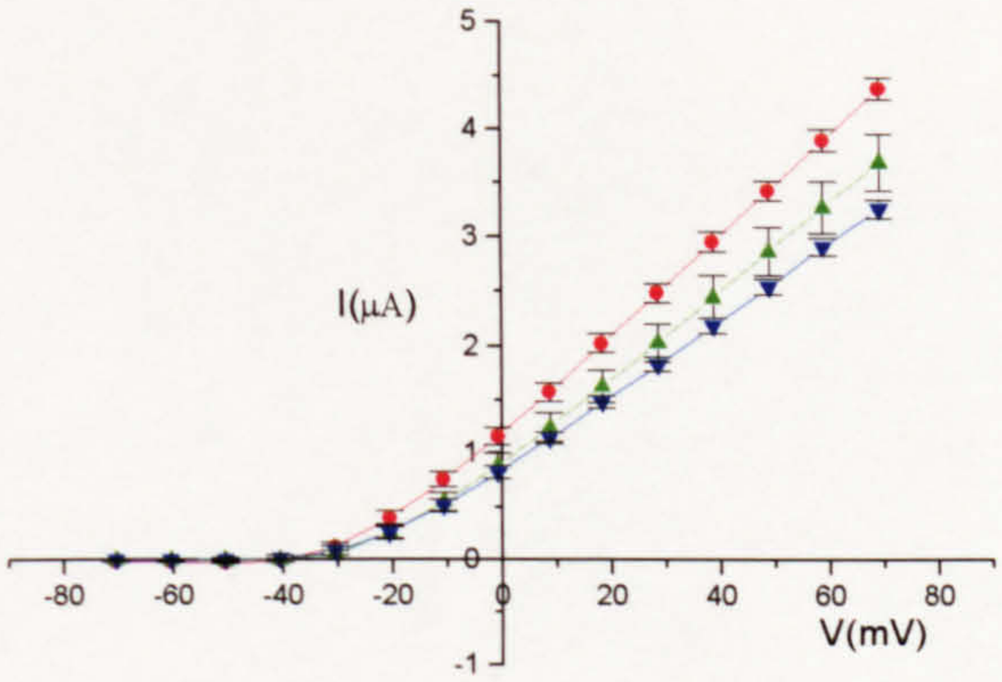

b

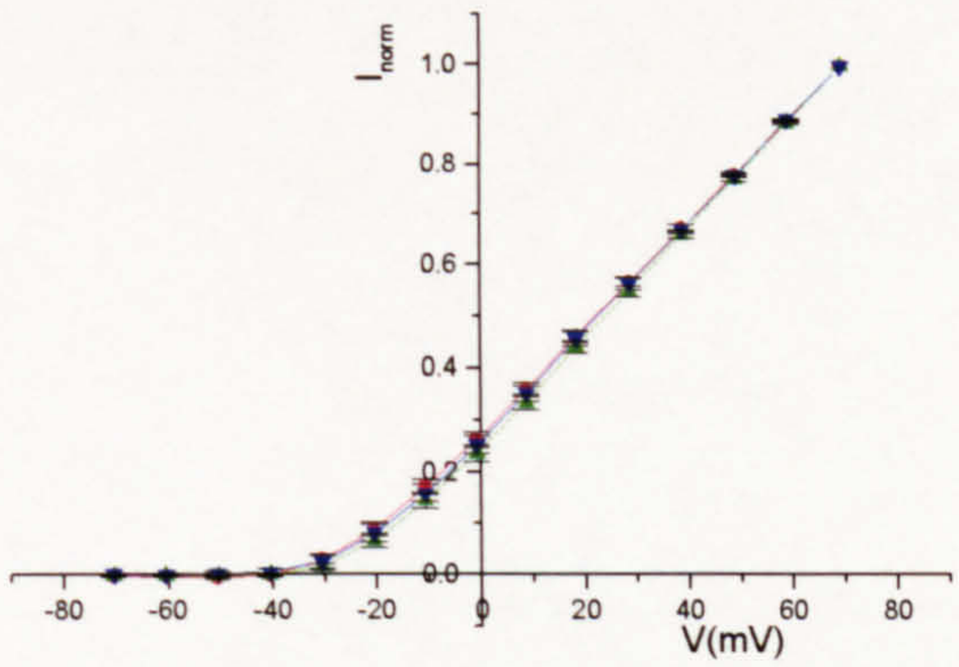

c

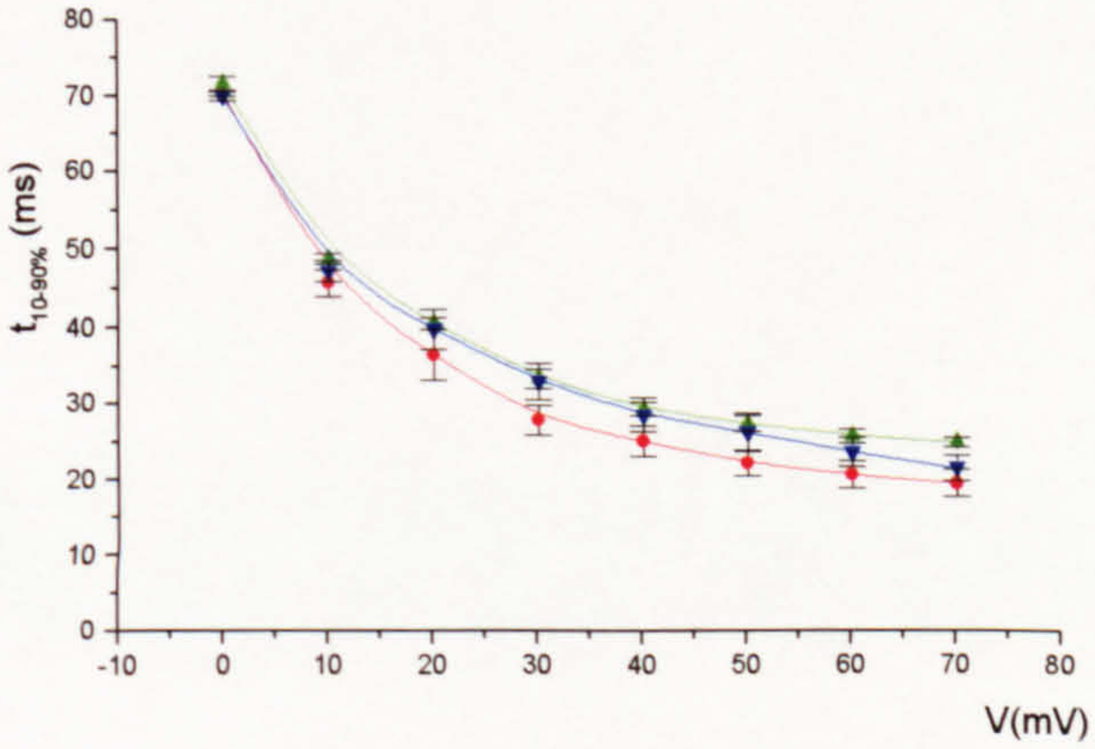

Fig. 4.12 Characteristics of wild type rKv2.1, rKv2.1$_{N\text{-}CFP}$ and rKv2.1$_{N\text{-}YFP}$ clones.

a, The figure shows I/V curves for wild type rKv2.1(▼, n=5), rKv2$_{N\text{-}CFP}$ (●, n=6) and rKv2.1$_{N\text{-}YFP}$ (▲, n=5) channels.
b, Currents were normalised to the current value at +70mV (3.25μA ±0.09 for rat Kv2.1 wild type (▼, n=5), 4.38±0.11 μA for rKv2.1$_{N\text{-}CFP}$ (●, n=6) and 3.69±0.27 μA for rKv2.1$_{N\text{-}YFP}$ (▲, n=5)).
c, The figure shows the rise time versus test potential for rKv2.1(▼, n=5), rKv2.1$_{N\text{-}CFP}$ (●, n=6) and rKv2.1$_{N\text{-}YFP}$ (▲, n=5) channels.
There were no significant differences between the sets of data (student's t-test ($p<0.05$)).

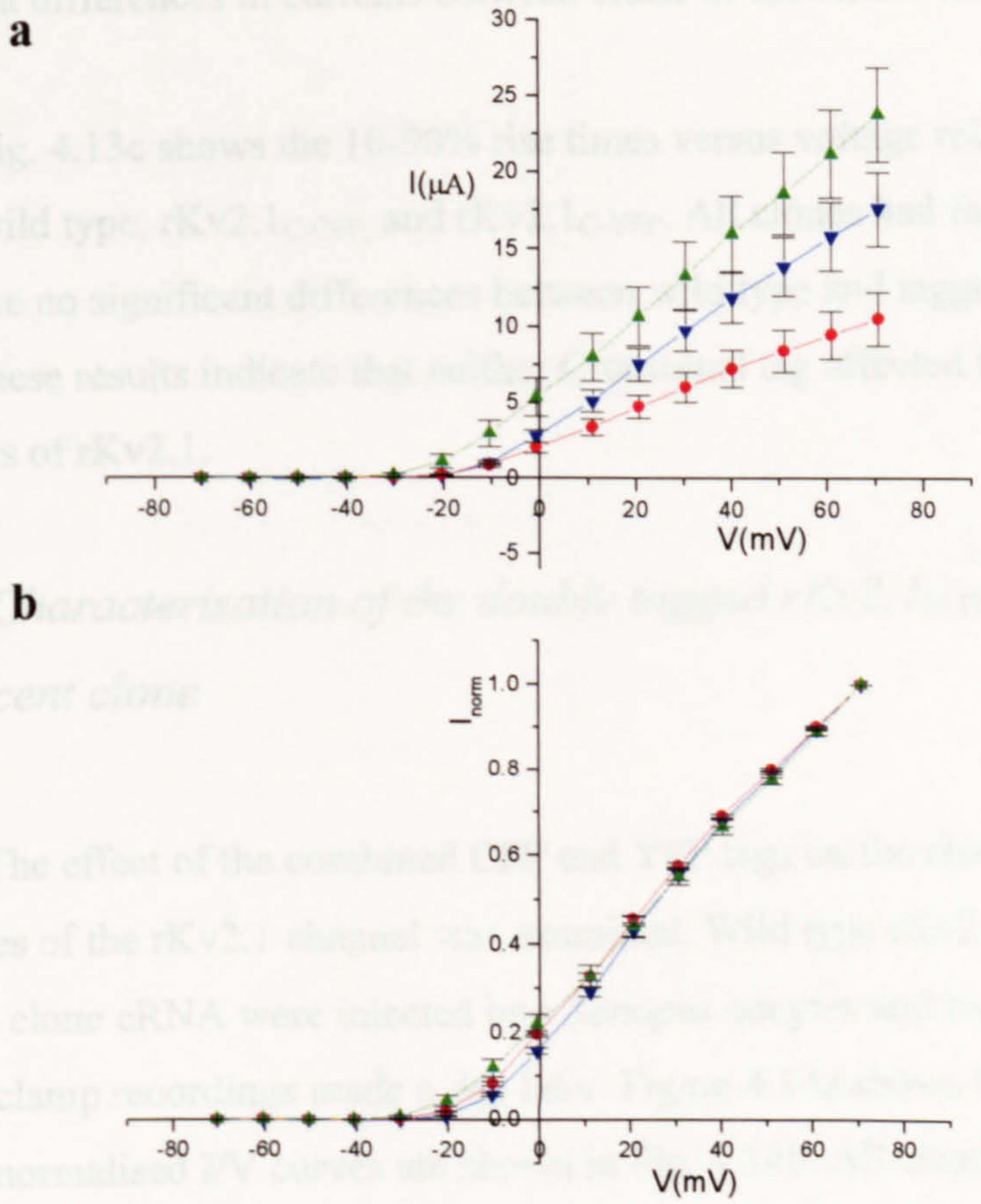

Fig. 4.13 Characteristics of wild type rKv2.1, rKv2.1$_{C\text{-}CFP}$ and rKv2.1$_{C\text{-}YFP}$ clones.

A, The figure shows I/V curves for wild type rKv2.1(▼, *n*=8), rKv2.1$_{C\text{-}CFP}$ (●, *n*=4) and rKv2.1$_{N\text{-}YFP}$ (▲, *n*=6) channels.

B, Currents were normalised to the current value at +70mV (17.6±2.4 μA for rKv2.1 (▼, *n*=8), 10.5±1.7 μA for rKv2.1$_{C\text{-}CFP}$ (●, *n*=4) and 23.8±3.1 μA for rKv2.1$_{C\text{-}YFP}$ (▲, *n*=6)).

C, The figure shows the rise time versus test potential for rKv2.1(▼, *n*=8), rKv2.1$_{C\text{-}CFP}$ (●, *n*=4) and rKv2.1$_{C\text{-}YFP}$ (▲, *n*=6) channels.

There were no significant differences between the sets of data (student's t-test ($p<0.05$)).

significant differences in currents between either of the clones and rKv2.1 wild type.

Fig. 4.13c shows the 10-90% rise times versus voltage relationship for rKv2.1 wild type, rKv2.1$_{C\text{-}CFP,}$ and rKv2.1$_{C\text{-}YFP}$. All clones had fast activation and there were no significant differences between wild type and tagged clones rise times. These results indicate that neither C-terminal tag affected the activation properties of rKv2.1.

4.2.10 Characterisation of the double tagged rKv2.1$_{N\text{-}YFP\text{-}C\text{-}CFP}$ fluorescent clone

The effect of the combined CFP and YFP tags on the electrophysiological properties of the rKv2.1 channel was examined. Wild type rKv2.1 and rKv2.1$_{N\text{-}YFP\text{-}C\text{-}CFP}$ clone cRNA were injected into *Xenopus* oocytes and two-electrode voltage clamp recordings made a day later. Figure 4.14a shows the I/V curves, and the normalised I/V curves are shown in Fig. 4.14b. All channels exhibited strong voltage-dependent outward currents, which activated around –20mV as for wild type rKv2.1. There was no significant difference between the double tagged clone and wild type Kv2.1.

Fig. 4.14c shows the 10-90% rise times versus voltage relationship for wild type rKv2.1 and rKv2.1$_{N\text{-}YFP\text{-}C\text{-}CFP}$. Both clones had fast activation and there were no significant differences between wild type and tagged clone rise times. These results indicate that the double tag did not affect the activation properties of rKv2.1.

4.2.11 Characterisation of the rKv2.1 fluorescent clones using FRET, completed by N. Soldatov & E. Kobrinsky (NIH, Baltimore, USA)

FRET experiments depend on a distance-dependant interaction between the electronic states of two dyes. Excitation is transferred from a donor to an acceptor molecule, and the efficiency of transfer is a function of the proximity of the two dye molecules. The two dye molecules used in these experiments are pCFP (cyan fluorescent protein, the donor molecule), and pYFP (yellow

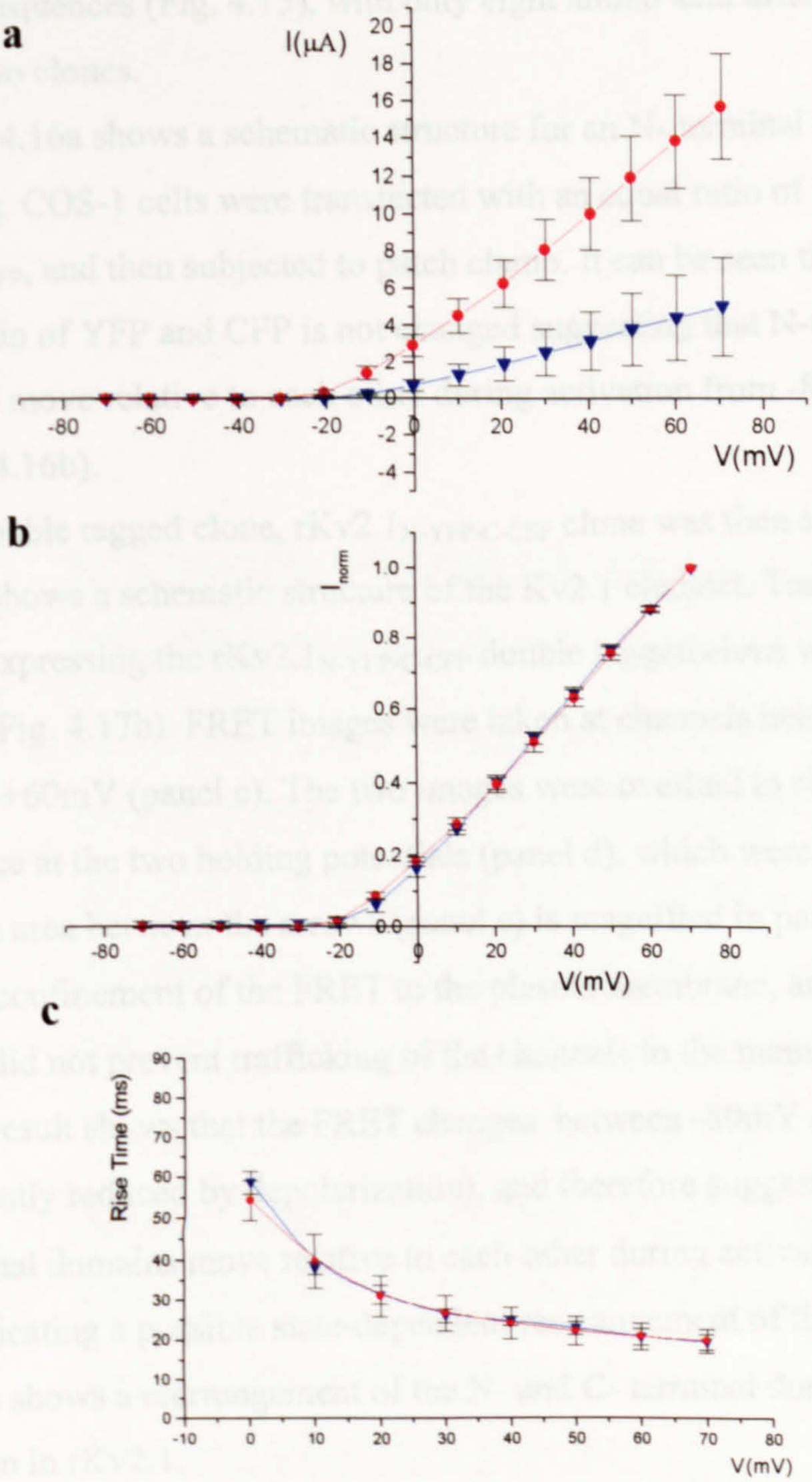

Fig. 4.14 Characteristics of wild type rKv2.1, and rKv2.1$_{N\text{-}YFP\text{-}C\text{-}CFP}$ clone.

a, The figure shows I/V curves for wild type rKv2.1(▼, n=4), and rKv2.1$_{N\text{-}YFP\text{-}C\text{-}CFP}$ (●, n=5)

b, Currents were normalised to the current value at +70mV (5.02±2.66 μA for rKv2.1 (▼, n=4), and 15.69±2.82 μA for rKv2.1$_{N\text{-}YFP\text{-}C\text{-}CFP}$ (●, n=5)).

c, The figure shows the rise time versus test potential for rKv2.1(▼, n=4), and rKv2.1$_{N\text{-}YFP\text{-}C\text{-}CFP}$ (●, n=5) channels.

There were no significant differences between the sets of data (student's t-test ($p<0.05$)).

fluorescent protein, the acceptor molecule), with the two dye molecules having similar DNA sequences (Fig. 4.15), with only eight amino acid differences between the two clones.

Figure 4.16a shows a schematic structure for an N- terminal Kv2.1 fluorescent tag. COS-1 cells were transfected with an equal ratio of $rKv2.1_{N\text{-}CFP}$ and $rKv2.1_{N\text{-}YFP}$, and then subjected to patch clamp. It can be seen that the fluorescent ratio of YFP and CFP is not changed suggesting that N-terminal regions do not move relative to each other during activation from -80mV to +60mV (Fig. 4.16b).

The double tagged clone, $rKv2.1_{N\text{-}YFP\text{-}C\text{-}CFP}$ clone was then analysed. Figure 4.17a shows a schematic structure of the Kv2.1 channel. Transfected COS-1 cells expressing the $rKv2.1_{N\text{-}YFP\text{-}C\text{-}CFP}$ double tagged clone were analysed using FRET (Fig. 4.17b). FRET images were taken at channels held at –80mV (panel b) and +60mV (panel c). The two images were overlaid to show the ratio of fluorescence at the two holding potentials (panel d), which were found to be different. The area between the arrows (panel c) is magnified in panel d, suggesting a confinement of the FRET to the plasma membrane, and showing that the tags did not prevent trafficking of the channels to the membrane.

This result shows that the FRET changes between -80mV and +60mV (it was significantly reduced by depolarization), and therefore suggests that the N- and C- terminal domains move relative to each other during activation, (at +60mV), indicating a possible state-dependent rearrangement of these two regions. This shows a rearrangement of the N- and C- terminal domains upon depolarisation in rKv2.1.

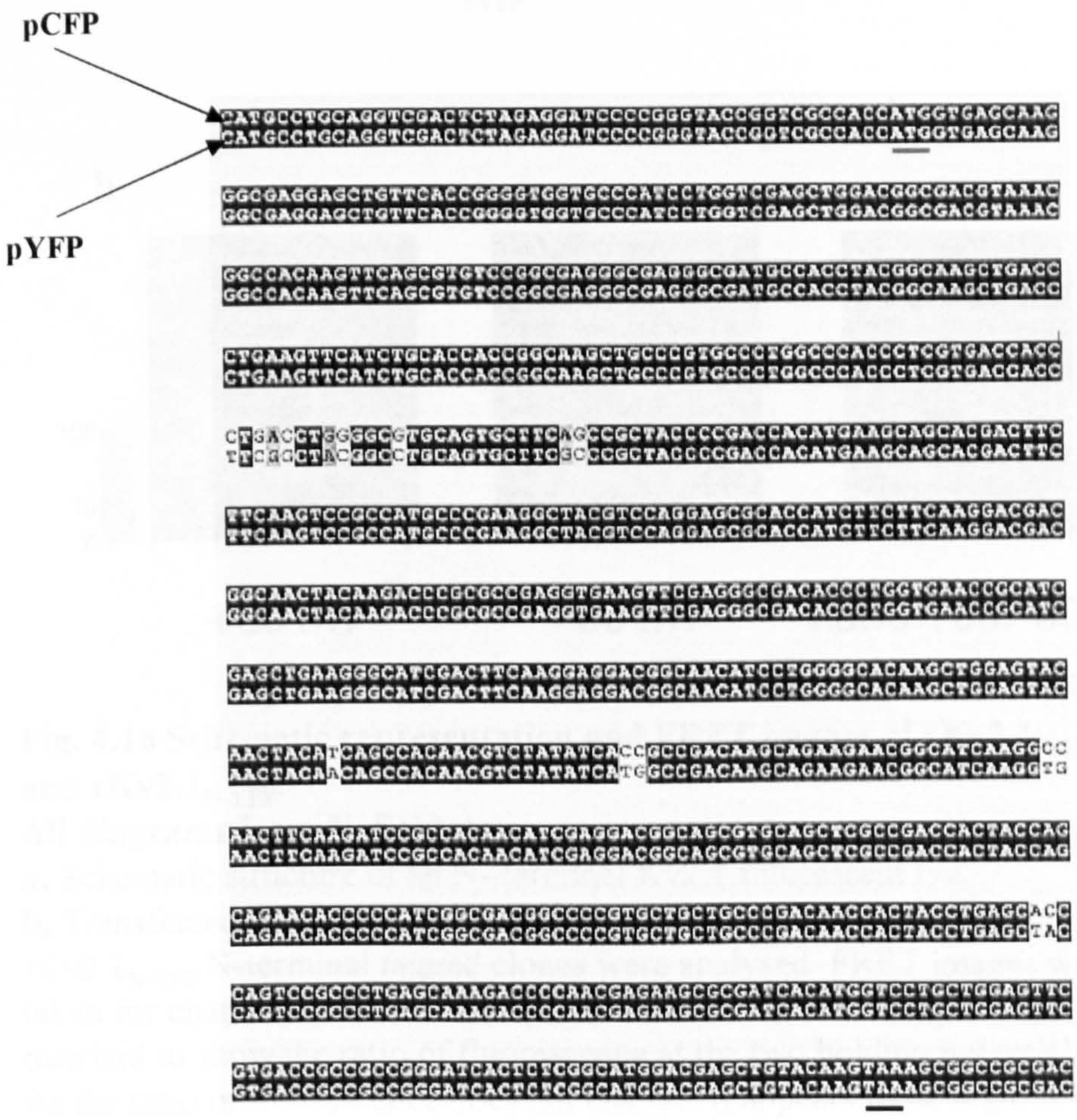

Fig. 4.15 DNA sequences from pCFP and pYFP plasmids

The figure shows the alignment of the sequences for pCFP and pYFP using ClustalW and Boxshade on-line software.

The red line denotes the start codon and the black line denotes the stop codon.

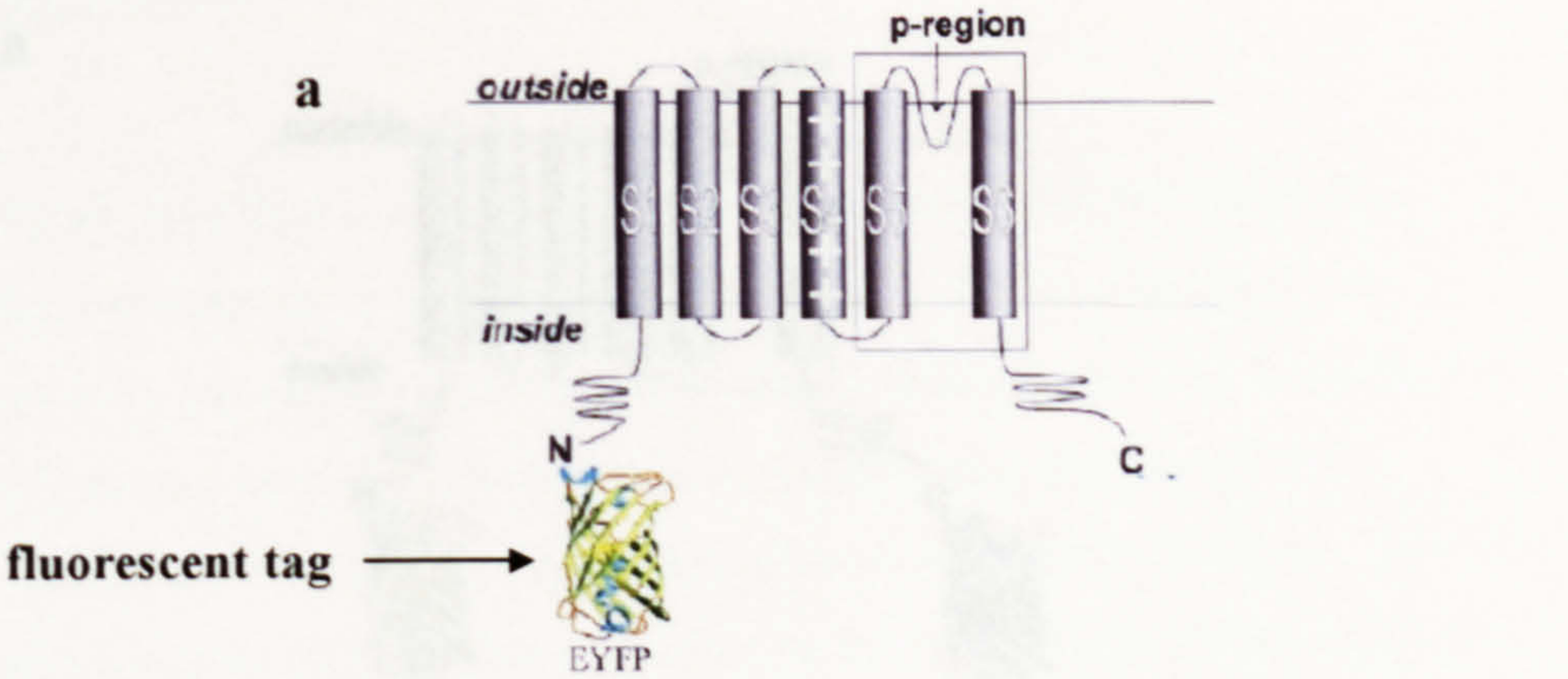

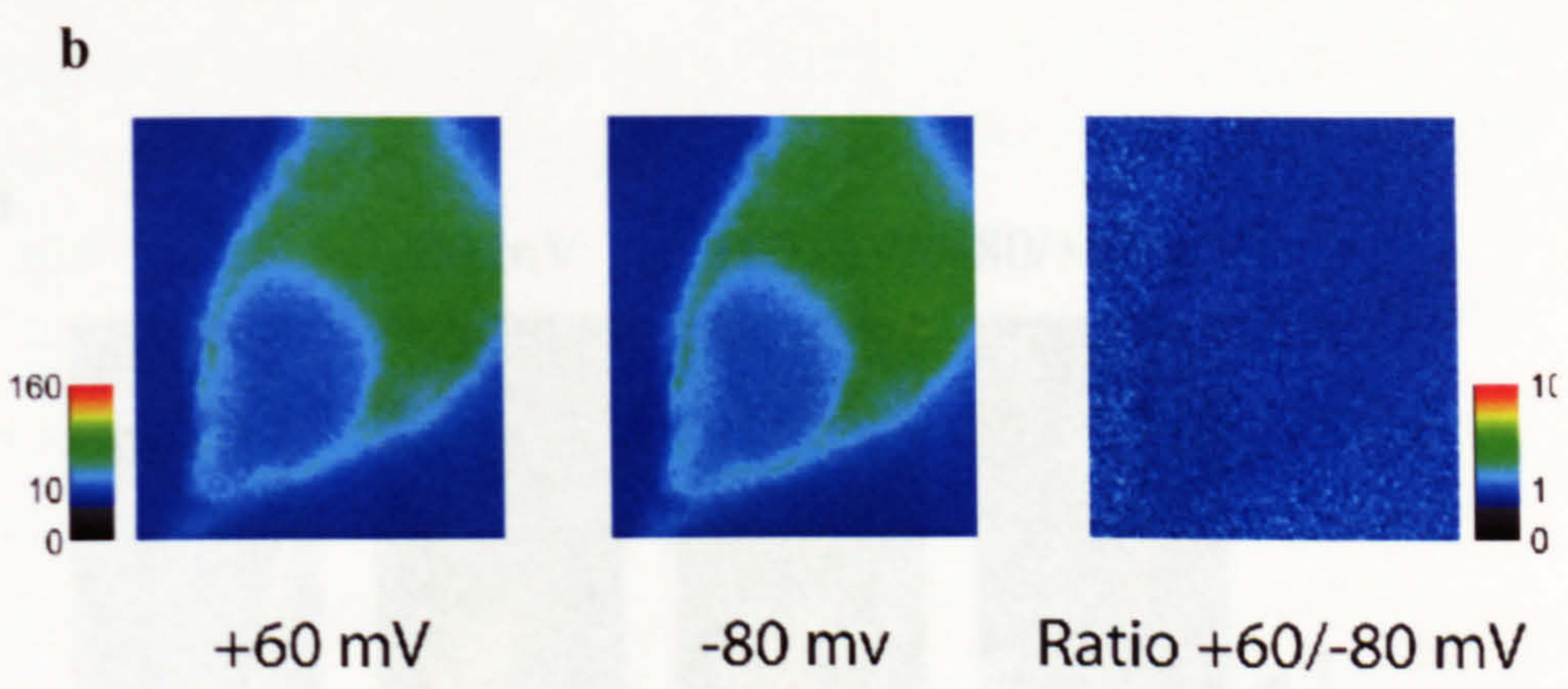

Fig. 4.16 Schematic representation and FRET images of rKv2.1$_{N\text{-}CFP}$ and rKv2.1$_{N\text{-}YFP}$.
All diagrams from N. Soldatov.
a, Schematic structure of an N- terminal Kv2.1 fluorescent tag.
b, Transfected COS-1 cells expressing a 1:1 mixture of rKv2.1$_{N\text{-}CFP}$ and rKv2.1$_{N\text{-}YFP}$ N-terminal tagged clones were analysed. FRET images were taken for channels held at –80mV and +60mV. The two images were overlaid to show the ratio of fluorescence at the two holding potentials. As the ratio of fluorescence does not change, it appears these regions do not more relative to each other under these conditions.

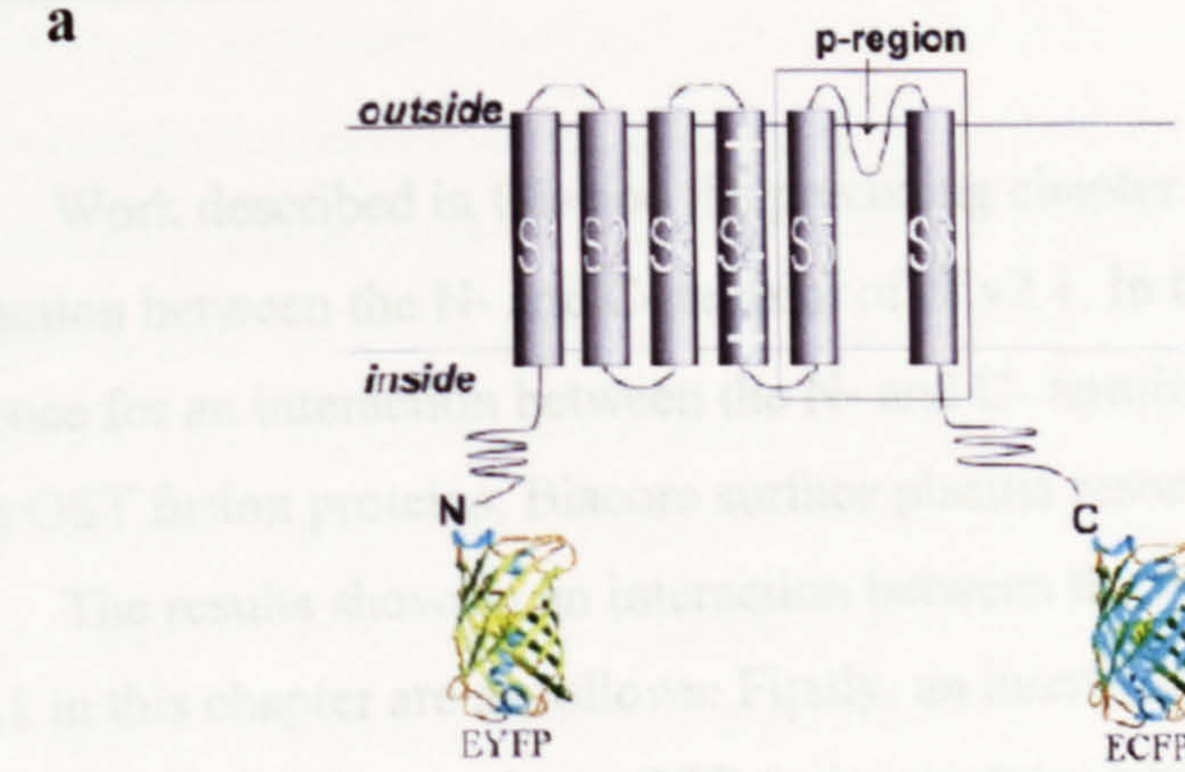

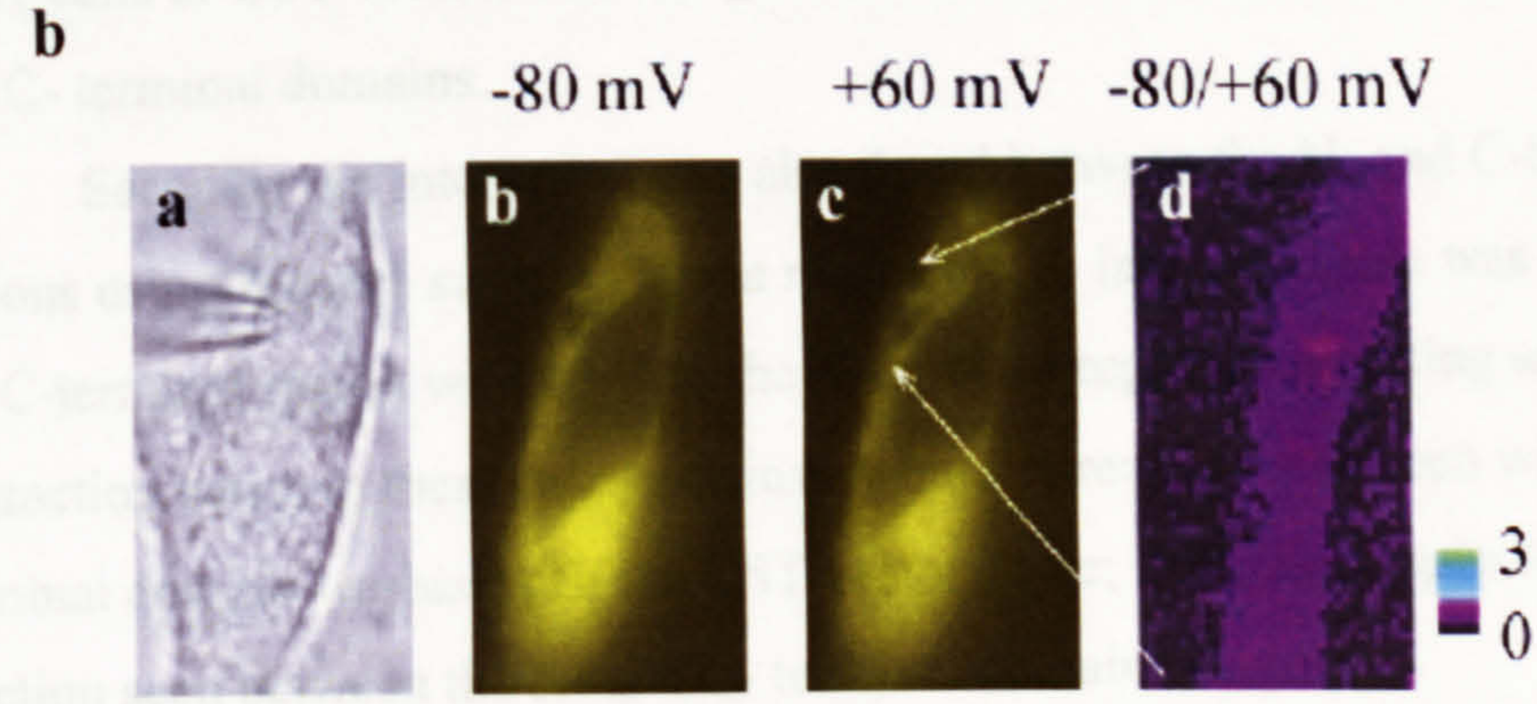

Fig. 4.17 Schematic representation and FRET image of rKv2.1$_{N\text{-}YFP\text{-}C\text{-}CFP}$.
All diagrams from N. Soldatov.
a, Schematic structure of an N- and C- terminal Kv2.1 fluorescent tag.
b, Transfected COS-1 cells expressing rKv2.1$_{\text{-}N\text{-}YFP\text{-}C\text{-}CFP}$ tagged clone were analysed. Panel **a** shows a phase-contrast image of a cell with a patch pipette. FRET images were taken at channels held at –80mV (panel **b**) and +60mV (panel **c**). The two images were overlaid to show the ratio of fluorescence at the two holding potentials (panel **d**). The area between the arrows shown in panel **c** is magnified in panel **d**.
The fluorescence changes between the two holding potentials, which indicates a rearrangement of these two regions upon depolarisation.

4.3 Discussion

Work described in this and the preceding chapter has supported an interaction between the N- and C- termini of rKv2.1. In this chapter, direct evidence for an interaction between the N- and C- termini has been investigated using GST fusion proteins, Biacore surface plasma resonance and FRET.

The results showing an interaction between the N- and C- termini of rat Kv2.1 in this chapter are as follows: Firstly, an interaction was found for the N- and C- terminal regions using a GST-fusion protein; a band of radiolabelled C-terminal protein was retained after mixing with the N-terminal GST protein. No bands were seen when the radiolabelled C- terminal protein was mixed with the BL21 cells or GST vector, indicating that this binding is specific between the N- and C- terminal domains.

Secondly, an interaction was also found between the N- and C-terminal regions using Biacore surface plasma resonance. A large response was seen for the C-terminal region washed with the N-terminal region, suggesting an interaction between these two domains. A smaller reaction was seen with C-terminal domain washed with the GST vector alone; indicating again that the reaction seen between the N- and C- terminal domains is specific.

Thirdly, to investigate the extent of this interaction, fluorescent tags were cloned in frame to the N- and C- terminal regions of rKv2.1 to enable FRET analysis. Electrophysiological analysis completed using two-electrode voltage clamp showed that these tags do not affect the activation kinetics (i.e. the I/V curves and the 10-90% rise times), when compared to wild type rKv2.1 recordings. These clones were then used for FRET-microscopy combined with patch clamp experiments. This was completed by N Soldatov. The fluorescent ratio of YFP and CFP in the N- labelled single tagged experiments did not change suggesting that N-terminal regions do not move relative to each other during activation from -80mV to +60mV (Fig. 4.16b), but are in close proximity as FRET could be recorded. However, analysis of the double tagged rKv2.1 clone (Fig. 4.17b) shows that FRET between the N- and C- terminal tags was significantly reduced upon depolarisation, indicating a state-dependent rearrangement of these two regions. This result shows that the N- and C-terminal

domains are in close proximity to each other (again by the presence of fluorescence), and move upon activation. This shows a rearrangement of the N- and C- terminal domains upon depolarisation in rKv2.1. This movement of the N- terminus relative to the C- terminus probably occurs in such a way that the C- terminus moves relative to the N-terminus, as the N- terminal tag alone did not show FRET movement upon depolarisation (Fig. 4.16b).

Further support for an interaction is found in the electron microscope derived structure of the Kv1.1 channel (Sokolova *et al*, 2001). In this paper single particle electron microscopy shows that the space filled by the intracellular region seems to be too large for the T1 domain alone. It has been suggested that the C- terminus, which seems to envelop the T1 domain, occupies the remaining space. This contact between the T1 region and the C- terminus has been hypothesised to result from the the hydrophobicity of the outer surface of the T1 region (Minor *et al*, 2001).

It is also known that the N- terminal region contributes to the assembly of other voltage gated potassium channels (Hopkins *et al*, 1994), and that an inter-subunit interaction between these regions occurs when cysteine residues are introduced in the *Shaker* channel (Schulteis *et al*, 1996). Interactions in the N- and C- terminal domains have also been reported in Kir6.2 (Jones *et al*, 2001). For this, GST constructs of the N- terminal domain of this channel were mixed with various radiolabelled C- terminal fragments. Multiple interaction domains within the C- termini were found, which correlated with regions previously identified as being important for Kir channel assembly and function.

In KirBac1.1, a crystal structure of the closed state has indicated that the intracellular regions can influence gating, and that rearrangement of these domains occurs between the open and closed states of this channel (Kuo *et al*, 2003). This is consistent with the FRET data shown in this chapter, which also shows a possible rearrangement of the intracellular regions upon depolarisation. An inter-subunit interface between the intracellular domains in Kir4.1 and Kir5.1 potassium channels has also been found that has been shown to influence regulation and gating (Casamassima *et al*, 2003). These other studies all indicate intracellular interactions in other channels.

For Kv2.1, C-terminal interactions have previously been shown to be important in driving channel assembly (Bentley *et al*, 1999). However, no direct

studies have previously reported an interaction between the N- and C-terminal regions of Kv2.1. It would therefore be interesting to further demonstrate the C-terminal region, and to further characterise N- and C- terminal interactions of rKv2.1 demonstrated in this chapter.

In conclusion, these results show that for rat Kv2.1, the N- and C-terminal regions interact physically, and rearrange upon depolarisation, which could provide an explanation for how key residues (as discussed in chapter three) in both the N- and C- terminal domains might contribute to the differing activation kinetics of rat and human Kv2.1.

CHAPTER 5

STRUCTURAL ANALYSIS OF RAT Kv2.1 USING ELECTRON MICROSCOPY

5.1 Introduction

Single particle electron microscopy studies have been carried out on the *Shaker* clone, producing a 3D structure at a 25Å resolution (Sokolova *et al,* 2001). The structure consists of a large membrane spanning domain, and a smaller 'hanging gondola' cytoplasmic domain joined by four connectors (Kobertz *et al,* 2000 and see Introduction). The volume of the cytoplasmic domain appeared large enough to accommodate both the N- and C- terminal regions.

In the previous chapter a specific interaction was found between the N- and C- terminal regions of rat Kv2.1, which suggests that the C- terminus is closely associated with the N- terminal region. In this chapter, both wild type rKv2.1 and a mutant with a C-terminal deletion have been expressed and purified, to attempt to create a defined 3D structure using electron microscopy, and thus to determine the location of the C- terminus.

For this, the wild type rKv2.1 channel was transferred to a mammalian expression vector (pMT3) for expression in COS-7 cells. The pMT3 vector has been modified to contain an ID4 tag that when expressed in the same open reading frame as a recombinant protein sequence encodes a fusion tag recognised by ID4 antibodies. This was then used to purify the channel and the C- terminal deleted mutant. An agitoxin binding site (Δ7) was also incorporated into the protein sequences so that a binding assay for agitoxin-2 could be used to investigate whether the purified protein samples were correctly folded. Preliminary single particle electron microscopy was carried out by E. Orlova.

5.2 Results

5.2.1 Construction of rKv2.1 in the pMT3 vector

In order to purify the rKv2.1 protein, the whole channel was cloned into the pMT3 vector containing an ID4 purification tag (sequence of ID4 shown in Fig. 5.1c). For this, the whole of the rKv2.1 channel was first amplified by PCR as described in section 2.4.1. Both the pMT3 vector (containing *Shaker*) and the PCR product were digested with the restriction enzymes *Eco*RI and *Not*I. This produced a fragment of 2646bp for the rKv2.1 PCR product and 5128bp for the pMT3 vector (with the 1920bp *Shaker* fragment discarded). Figure 5.1a shows a 0.7% agarose gel from which fragments were excised and purified (as described in section 2.1.7). The relevant fragments were ligated, transformed and mini-prepped as described in section 2.1.3.

A sample of mini-prepped DNA was sent to Lark for automated DNA sequencing using the pMT3-AS primer (see table 2.12). The complete coding sequence was obtained to check for unwanted amplification errors. An example of the nucleotide sequencing generated and an alignment of this is shown in Fig. 5.1.

5.2.2 Construction of rKv2.1 Δ7 in pMT3

In order to render the rKv2.1 protein susceptible to the toxin agitoxin-2, a Δ7 site was sub-cloned into the rKv2.1 in pMT3, as outlined in section 2.4.2. The Δ7 site contained the following amino acid changes: T355S, L356G, A362N, S363A, I379M, Y380T, and L382V. Both the rKv2.1 Δ7 in Pblu-SK (containing the Δ7 site, Lee *et al*, 2004) and the rKv2.1 in pMT3 were digested with the restriction enzymes *Nru*I and *Bsp*1407I. This produced fragments of 7195bp and 579bp (the latter being discarded) from the rKv2.1 in pMT3. The rKv2.1 Δ7 in Pblu-SK produced a 579bp fragment which contained the Δ7 site and a 5743bp fragment which was then discarded. Figure 5.2a shows a 0.7% agarose gel from which fragments were excised and purified (as described in section 2.1.7).

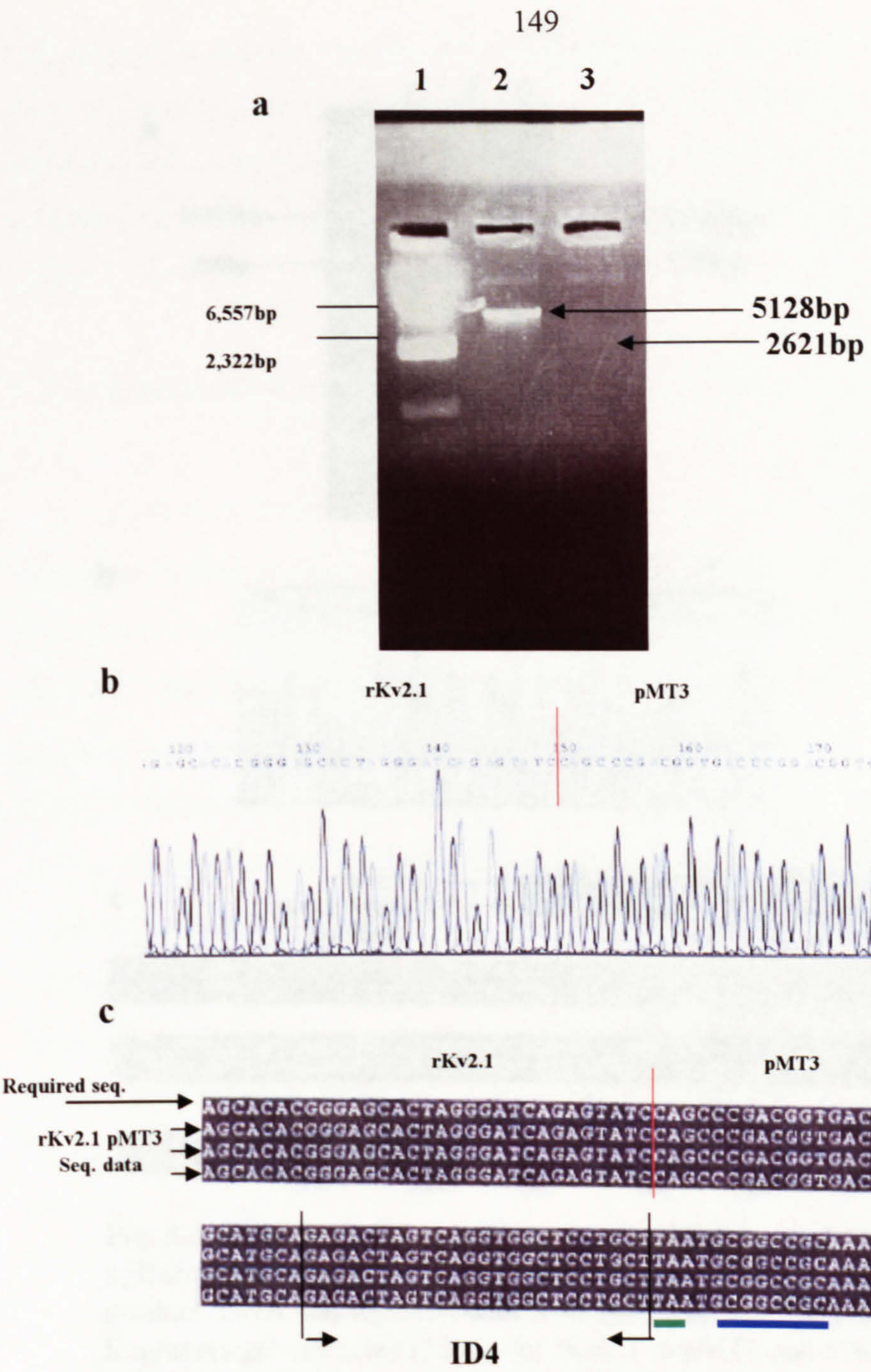

Fig. 5.1 Digestion and sequencing for the rKv2.1 pMT3 clone

a, Restriction digest of Shaker in pMT3 and rKv2.1 PCR product. DNA was digested with *Eco*RI and *Not*I, and the relevant sized fragments gel extracted (5128bp for pMT3 and 2646bp for the rKv2.1 PCR product). Lane 1 contains λ-*Hind*III marker, lane 2 contains the digested gel extracted pMT3 vector and lane 3 contains digested gel extracted PCR product.

b, Sequence electrophoretogram of the rKv2.1 in pMT3 clone. The red line denotes the join from rKv2.1 to the pMT3 vector.

c, The sequence was aligned against the desired chimeric predicted DNA sequence, using ClustalW and Boxshade on-line software. The red line denotes the join from rat to pMT3 vector (containing the pMT3 tag), the green line denotes the stop codon, and the blue line denotes the *Not*I restriction site. Also shown is the sequence of the ID4 tag.

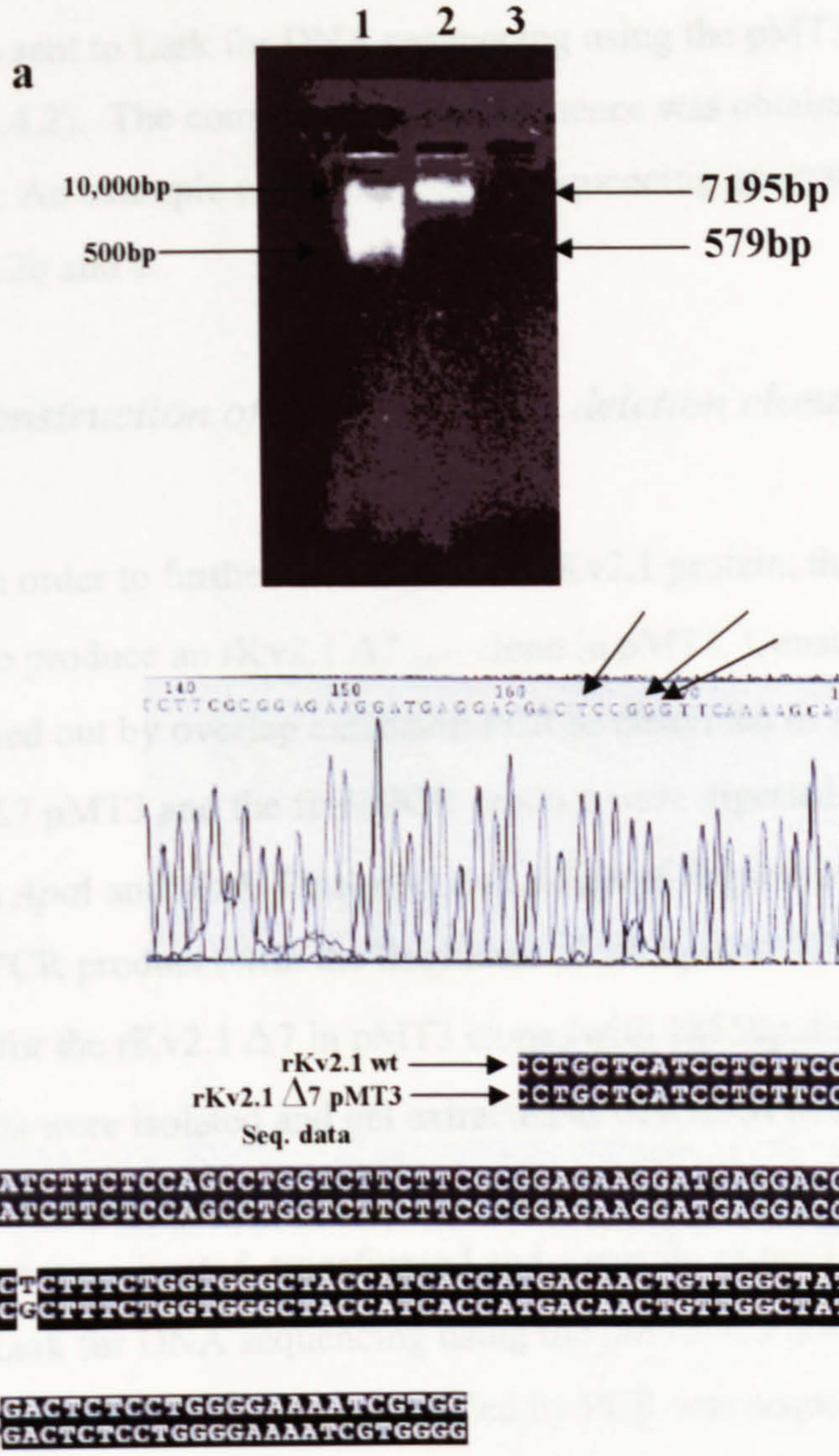

Fig. 5.2 Digestion and sequencing for the rKv2.1 Δ7 pMT3 clone
a, Restriction digest of rKv2.1 in pMT3 and DS-DRK in pBlu SK product. DNA was digested with *Nru*I and *Not*I, and the relevant size fragments gel extracted (7195p for rKv2.1 in pMT3 and 579bp for the DS-DRK Δ 7 product). Lane 1 contains 1kb marker, lane 2 contains the digested gel extracted rKv2.1 pMT3 vector and lane 3 contains digested gel extracted DS-DRK Δ 7.
b, Sequence electrophoretogram of the rKv2.1 Δ 7 in pMT3 clone. The arrows denote three of the changed base pairs.
c, The sequence was aligned against the rKv2.1 wild type DNA sequence, using ClustalW and Boxshade on-line software. Seven amino acids were changed in total. The doted line denotes that the DNA sequence is not continuous.

The relevant fragments were ligated, transformed and a sample of mini-prepped DNA was sent to Lark for DNA sequencing using the pMT3 sequencing primer (section 2.4.2). The complete inserted sequence was obtained to check for errors occurring. An example of the nucleotide sequencing generated for this is shown in Figs. 5.2b and c.

5.2.3 Construction of the C-terminal deletion clone

In order to further investigate the rKv2.1 protein, the C-terminus was deleted to produce an rKv2.1 $\Delta 7_{\text{-no C}}$ clone in pMT3. Construction of this clone was carried out by overlap extension PCR as described in section 2.4.3. Both the rKv2.1 Δ7 pMT3 and the final PCR product were digested with the restriction enzymes *Apa*I and *Not*I. This produced a desired fragment of 532bp for the rKv2.1 PCR product (with the fragments of 592bp and 573bp discarded) and 5919bp for the rKv2.1 Δ7 in pMT3 clone (with 1855bp discarded). The fragments were isolated and gel extracted as described in section 2.1.7. Figure 5.3a shows a gel from which fragments were excised and purified. The relevant fragments were ligated, transformed and a sample of mini-prepped DNA was sent to Lark for DNA sequencing using the pMT3-AS primer (see table 2.12). The region of DNA that was amplified by PCR was sequenced completely to check for unwanted amplification errors. An example of the nucleotide sequencing generated for this from sample 1 is shown in Figs. 5.3b and c.

5.2.4 Protein expression and purification

Both the rKv2.1 Δ7 pMT3 and the rKv2.1 $\Delta 7_{\text{-no C}}$ pMT3 clones were expressed in COS-7 cells, as described in section 2.4.4. Extracted protein was purified on an ID4 column, and samples were run on 10% SDS-PAGE gels (for different times) to confirm purity. Figures 5.4a and 5.5a show Coomassie-stained gels for rKv2.1 Δ7 pMT3 and rKv2.1 $\Delta 7_{\text{-no C}}$ pMT3 protein samples respectively. Lane four in both figures shows the purified protein at the correct size.

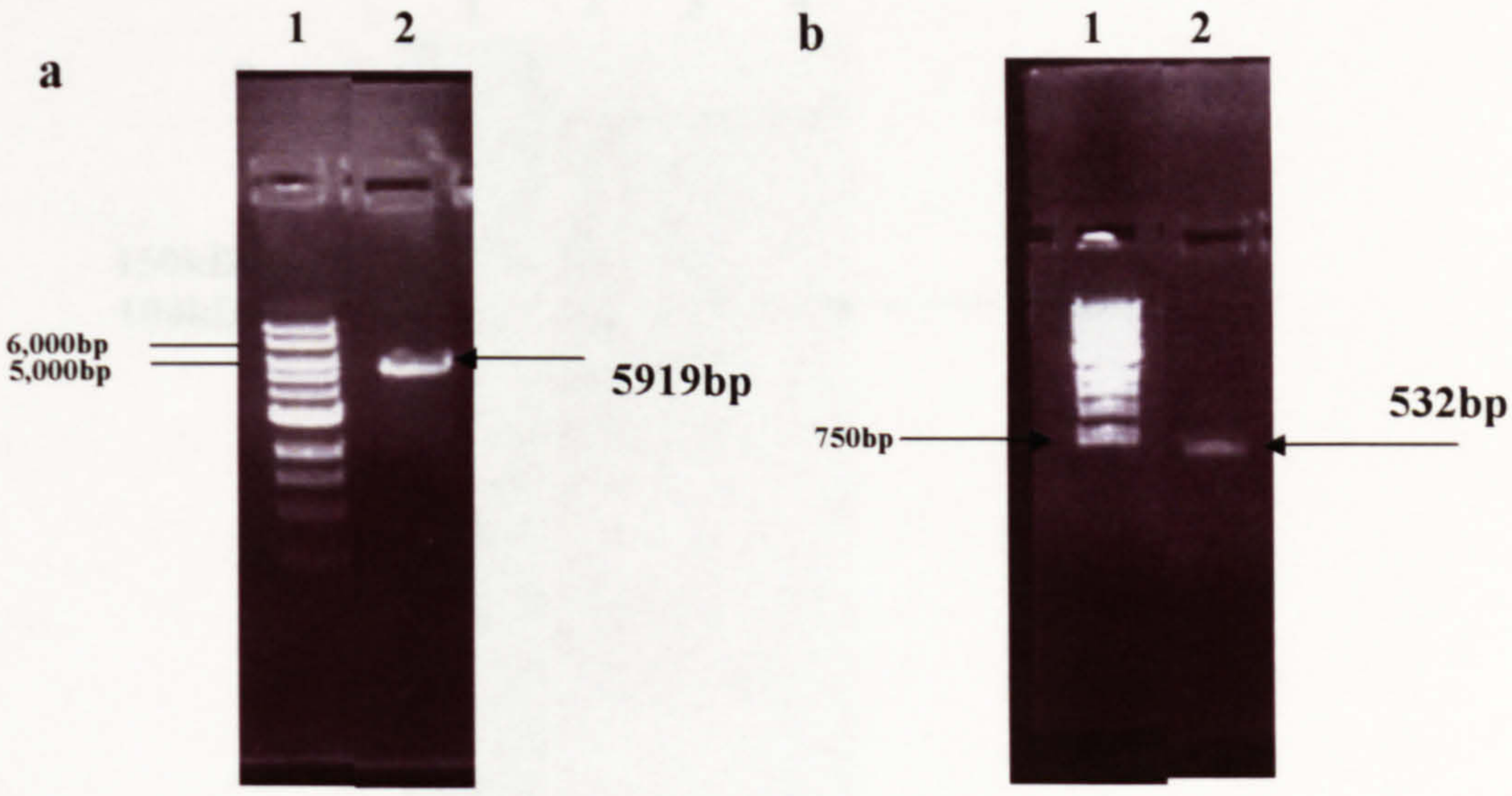

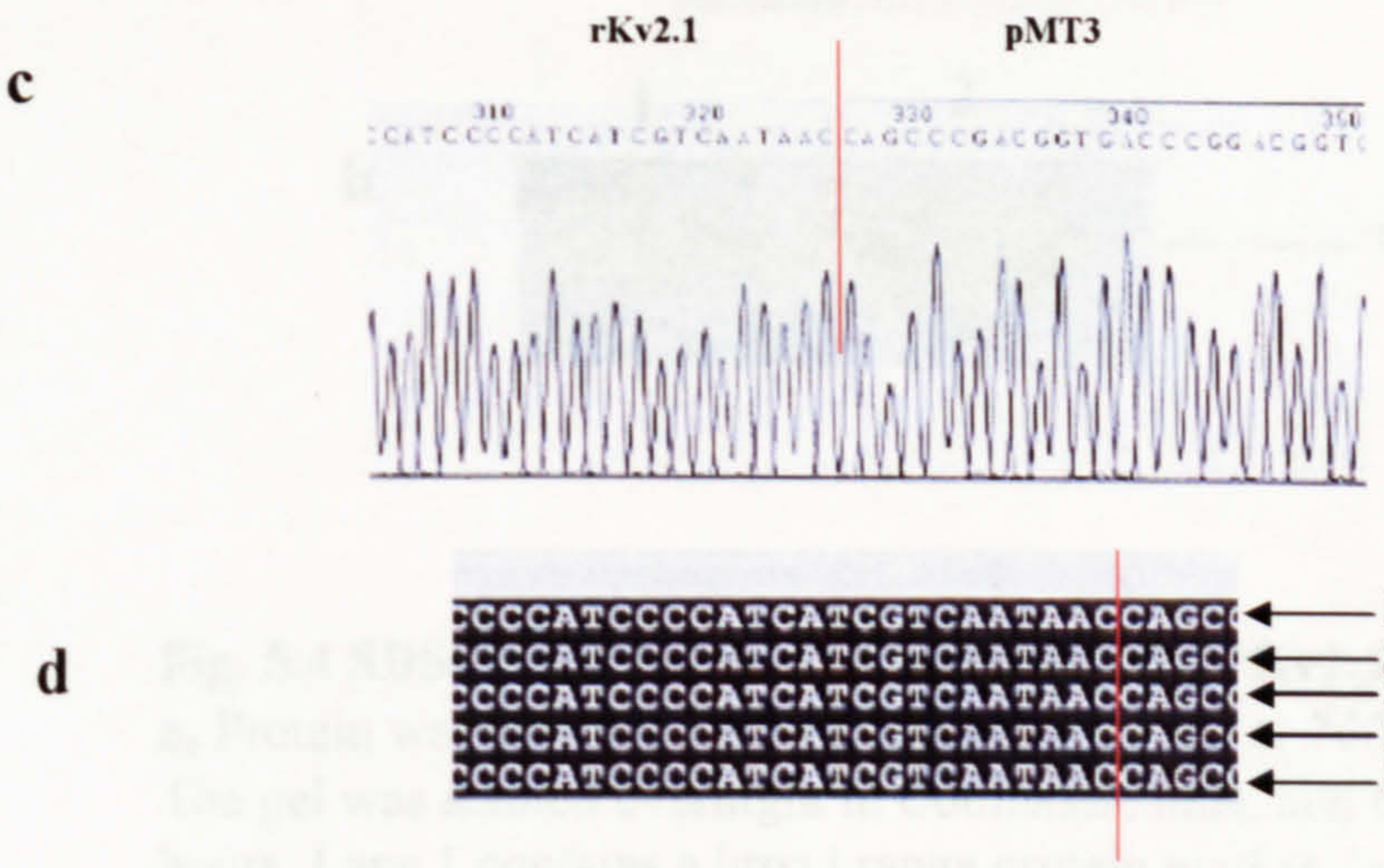

Fig. 5.3 Digestion and sequencing for the rKv2.1 $\Delta 7_{\text{-no C}}$ pMT3 clone
a, Restriction digest of rKv2.1 Δ 7 in pMT3. DNA was digested with *Apa*I and *Not*I, and the relevant size fragment gel extracted (5919p for rKv2.1 Δ 7 in pMT3). Lane 1 contains 1kb marker, lane 2 contains the digested gel extracted rKv2.1 Δ 7 pMT3 vector.
b, Restriction digest of 'no C' PCR product. DNA was digested with *Apa*I and *Not*I, and the relevant sized fragment gel extracted (532bp). Lane 1 contains 1kb marker, lane 2 contains the digested gel extracted PCR product.
c, Sequence electrophoretogram of the rKv2.1 $\Delta 7_{\text{-no C}}$ in pMT3 clone. The red line denotes the end of rKv2.1 S6 domain and the join to pMT3 vector.
d, DNA sequences obtained by sequencing were aligned against the rKv2.1 wild type DNA sequence, using ClustalW and Boxshade on-line software. The red line denotes the end of the S6 domain from rKv2.1 and the join to pMT3 vector.

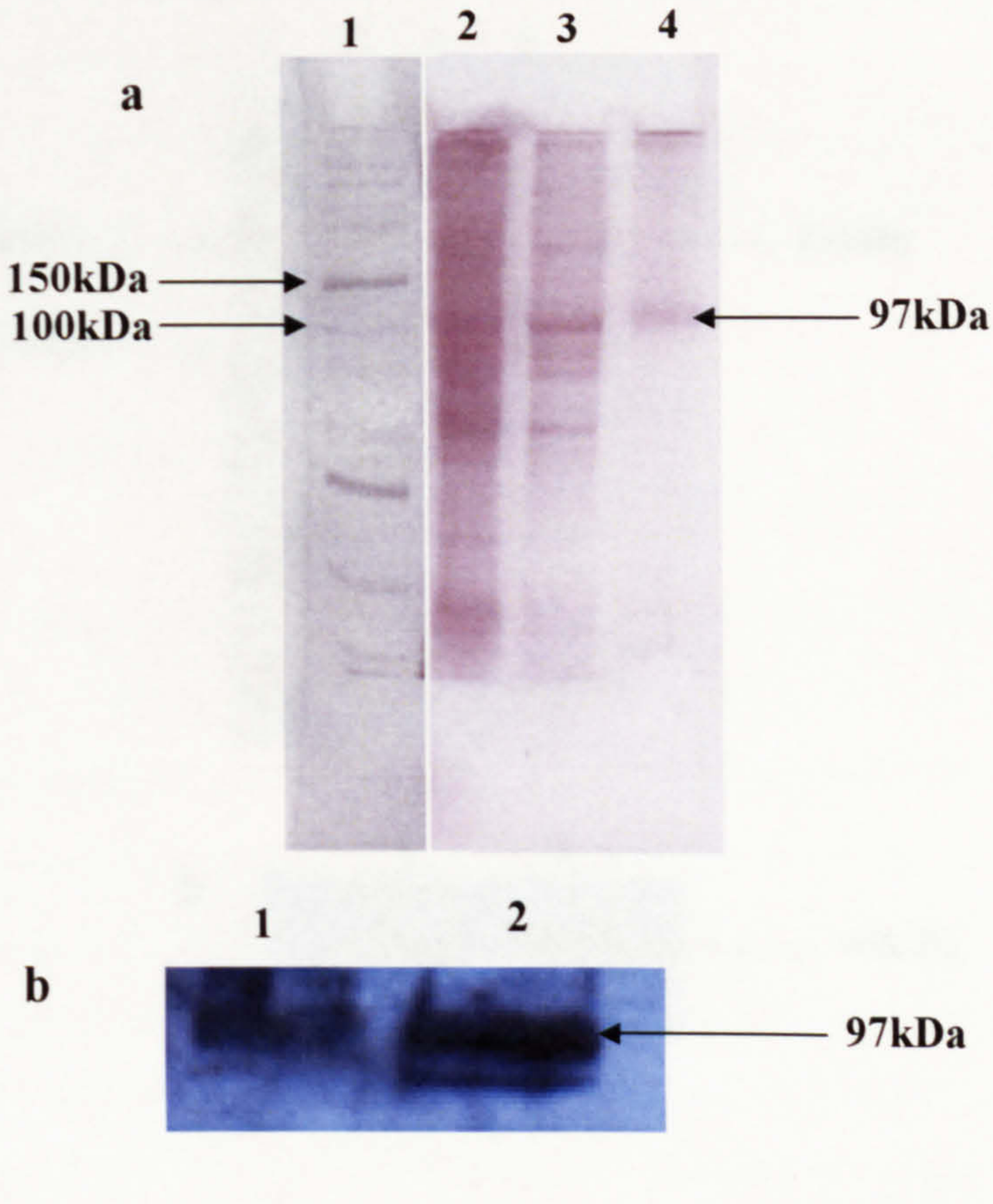

Fig. 5.4 SDS-PAGE gel and Western blot for rKv2.1 Δ7 pMT3.
a, Protein was run on a 10% SDS-denaturing gel at 200V.
The gel was stained overnight in Coomassie blue, and de-stained for 24 hours. Lane 1 contains a broad range protein marker, lane 2 contains the insoluble fraction from transfected COS-7 cells, lane 3 contains the soluble fraction from transfected COS-7 cells and lane 4 contains the purified protein. A band can be seen at the expected size of 97kDa.
b, A Western blot was performed using ID4 antibody to check the presence of the ID4 tag subsequently used for purification, and to check that the tagged protein was purified with the column. Detection was performed using horseradish peroxidase conjugated secondary antibody. A band at the correct size could be seen after 2 hours. Lane 1 shows un-purified protein, and lane 2 shows protein of the correct size after purification.

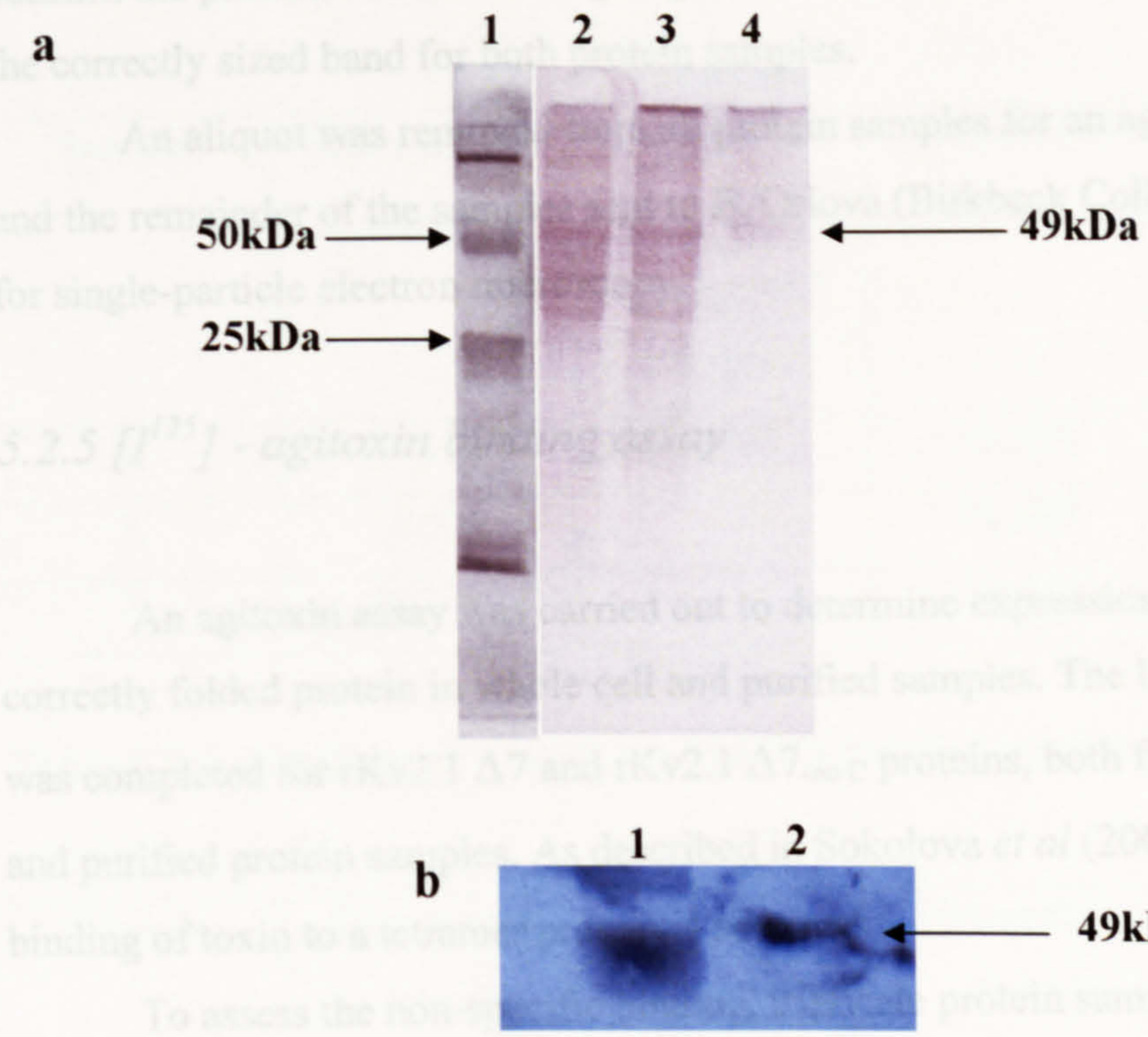

Fig. 5.5 SDS-PAGE gel and Western blot for rKv2.1 $\Delta 7_{\text{-no C}}$ pMT3.
a, Protein was run on a 10% SDS-denaturing gel for 35 minutes at 200V. The gel was stained overnight in Coomassie blue, and de-stained for 24 hours. Lane 1 contains a colour protein marker, lane 2 contains the insoluble fraction from transfected COS-7 cells, lane 3 contains the soluble fraction from transfected COS-7 cells and lane 4 contains the purified protein. A band can be seen at the expected size of 49kDa.
b, A Western blot was performed using ID4 antibody to check the presence of the ID4 tag subsequently used for purification, and to check that the tagged protein was purified with the column. Detection was performed using horseradish peroxidase conjugated secondary antibody. A band at the correct size could be seen after 2 hours. Lane 1 shows un-purified protein, and lane 2 shows protein of the correct size after purification.

A Western blot using an anti-ID4 antibody was then completed to confirm the presence of the ID4 tag. Figures 5.4b and 5.5b show the presence of the correctly sized band for both protein samples.

An aliquot was removed from all protein samples for an agitoxin assay, and the remainder of the samples sent to E. Orlova (Birkbeck College, London) for single-particle electron microscopy.

5.2.5 [I^{125}] - agitoxin binding assay

An agitoxin assay was carried out to determine expression levels of correctly folded protein in whole cell and purified samples. The binding assay was completed for rKv2.1 Δ7 and rKv2.1 $\Delta 7_{\text{-no C}}$ proteins, both for whole cell and purified protein samples. As described in Sokolova *et al* (2003), a 1:1 binding of toxin to a tetramer protein is assumed.

To assess the non-specific binding, triplicate protein samples were first incubated with cold agitoxin to saturate all their toxin binding sites. Hot agitoxin was then added to the mixture and incubated for a further 30 minutes before unbound toxin was removed using a micron filter device. Filters containing the retained Kv2.1-toxin complexes were then counted in a scintillation counter. The average of all three samples is shown in tables 5.1-5.4 as the cold sample.

Triplicate protein samples were then incubated with hot agitoxin for 30 minutes before unbound toxin was removed using micron filter devices. These samples were then counted (named in tables 5.1-5.4 as the hot samples), and the average of the cold samples subtracted to give net counts per minute readings (named the net activity in tables 5.1-5.4).

The net activity values were then used to calculate the amount of active (i.e. toxin binding) protein per sample using the specific activity of the hot toxin. The specific activity was determined by measuring the counts for a specific number of moles of radioactive material, and 1 count per minute was found to equate to 43.4 attomoles of toxin. Tables 5.1 to 5.4 show the results obtained.

Table 5.1 Agitoxin assay - rKv2.1 Δ7 pMT3 whole cell results.

Sample	Hot sample (cpm)	Cold sample (cpm) average of 3 samples	Net activity (cpm)	pmols toxin-binding activity per sample
1	32,133	10,935	21,198	0.92
2	32,624		21,689	0.94
3	40,751		29,816	1.294

Table 5.2 Agitoxin assay - rKv2.1 Δ7 pMT3 purified protein results.

Sample	Hot sample (cpm)	Cold sample (cpm) average of 3 samples	Net activity (cpm)	pmols toxin-binding activity per sample
1	18,039	11,357	6,682	0.29
2	20,574		9,217	0.40
3	19,191		7,834	0.34

Table 5.3 Agitoxin assay - rKv2.1 $\Delta 7_{\text{-no C}}$ pMT3 whole cell results.

Sample	Hot sample (cpm)	Cold sample (cpm) average of 3 samples	Net activity (cpm)	pmols toxin-binding activity per sample
1	24,406	8,968	15,438	0.67
2	23,714		14,746	0.64
3	24,175		15,207	0.66

Table 5.4 Agitoxin assay - rKv2.1 $\Delta 7_{\text{-no C}}$ pMT3 purified protein results.

Sample	Hot sample (cpm)	Cold sample (cpm) average of 3 samples	Net activity (cpm)	pmols toxin-binding activity per sample
1	14,363	9,063	5,300	0.23
2	15,284		6,221	0.27
3	14,132		5,069	0.22

Table 5.5 Agitoxin assay - total protein in sample, measured in pmoles/plate assayed.

	Whole cell sample: Mean pmols toxin-binding activity per sample	Purified protein sample: Mean pmols toxin-binding activity per sample
rKv2.1 pMT3	1.05±0.12	0.34±0.03
rKv2.1 pMT3-no C	0.66±0.008	0.24±0.015

Table 5.5 shows the mean values for the toxin-binding activity, assayed for whole cell extracts (i.e. before purification) and after purification for the rKv2.1 □7 and rKv2.1 $\Delta 7_{\text{-no C}}$ channels. The expression levels were approximately 50% higher for the wild type rKv2.1 Δ7 pMT3. This is in accordance with similar experiments showing a reduced protein expression with the C- terminal domain deleted in *Shaker* (Sokolova *et al*, 2003). Crucially however, the assay results show that both the rKv2.1 Δ7 and the rKv2.1 $\Delta 7_{\text{-no C}}$ protein were successfully expressed and purified using the methods described, and the correctly folded proteins were made (as indicated by their ability to specifically bind the radiolabelled agitoxin).

5.2.6 Preliminary EM results

Fig. 5.6 shows preliminary single particle images for the full length rat Kv2.1 protein. To generate single particle structures, many more such images need to be obtained and the results analysed. Further additional experiments are being carried out at the moment to this end, and it is hoped that a 3D structure will soon be obtained using 3D reconstruction of this protein.

5.3 Discussion

Both the wild type rKv2.1 and the C- terminal deleted mutant were expressed and purified. The presence of the ID4 tag was confirmed by Western blots. An agitoxin assay was then performed which confirmed that a tetramer protein was expressed and purified for both the wild type rKv2.1 Δ7 and rKv2.1 $\Delta 7_{\text{-no C}}$. In summary, both channels were found to be expressed and correctly folded under these conditions, and deletion of the C- terminus did not prevent folding of the channel.

Protein samples were then sent to E. Orlova for single particle EM studies. As can be seen in Figure 5.6, preliminary images have been obtained. Further images are being taken that should allow single particle imaging in order to obtain a 3D structure. Hopefully it will be possible to visualise the channel protein with and without the C- terminal domain, so as to determine the position of the C- terminus.

Previous work (Sokolova *et al*, 2001) on the potassium *Shaker* channel using single particle EM studies has shown that the four-fold symmetric structure shows a large (membrane spanning) and small (intracellular) domain linked by 2nm long connectors, consistent with the 'hanging gondola' model for the T1 domain proposed by Kobertz *et al* (2000). However, X-ray studies of the T1 domain show that the volume of the T1 domain does not account for the total volume of the intracellular domain (Sokolova *et al*, 2001) and thus suggests the presence of the C- terminal region surrounding the T1 domain.

More recently, a single particle EM structure has been obtained by Sokolova *et al* (2003) for the *Shaker* potassium channel with and without the C-terminus bound to the rat Kvβ2 subunit. The location of the C- terminus was determined, which showed that the C- terminus appears to surround the T1 domain. Regions of interaction consist of the N- terminal part from the T1 domain to the start of the S1 transmembrane segment, and the region of the C-terminus from the end of the S6 transmembrane segment to the C- terminus itself.

Interestingly, for *Shaker*, four negatively charged residues were located within the C-terminal linker at positions, E488, N490, E492 and E493. It is

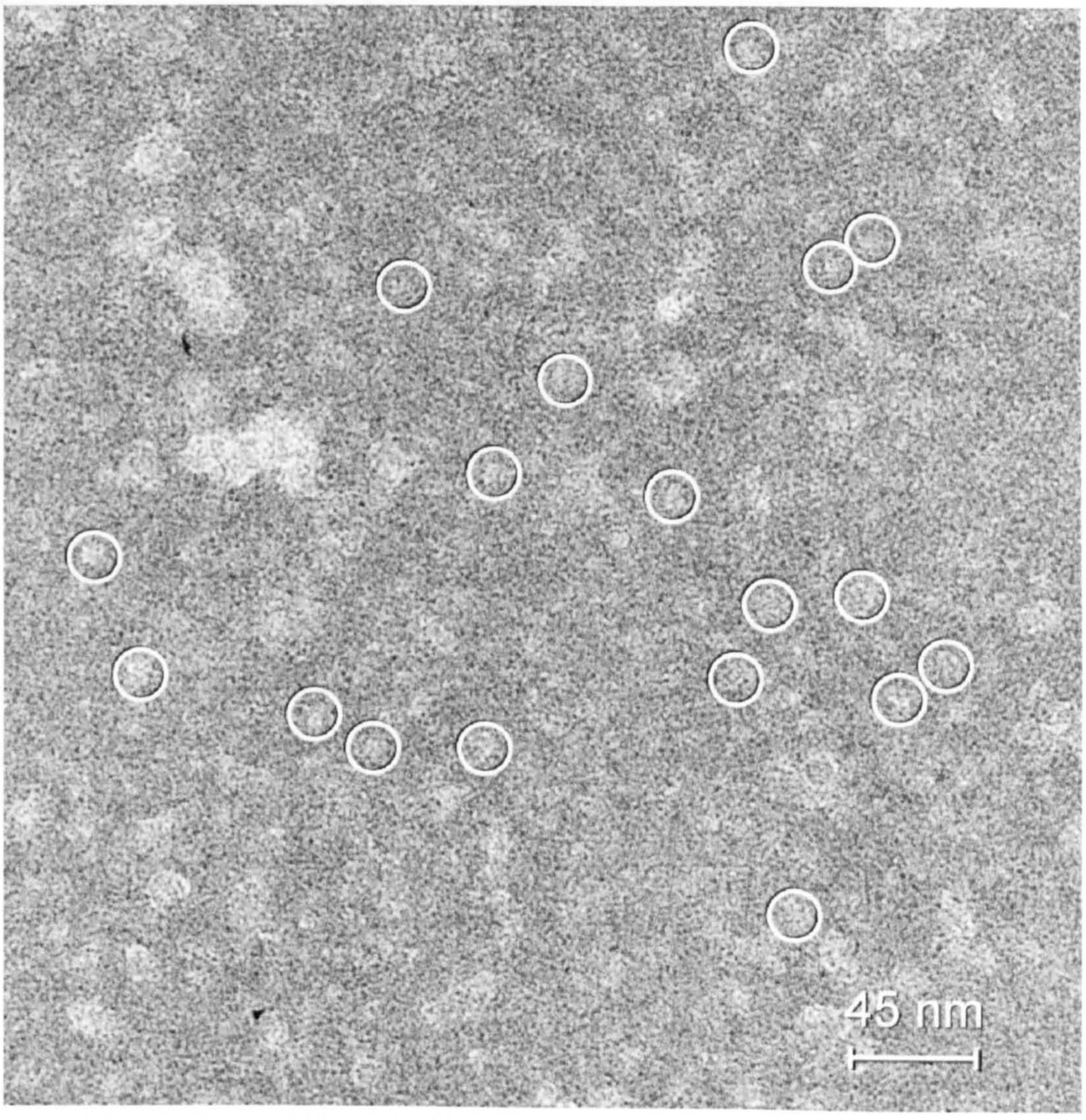

Fig. 5.6 Image of negatively stained full-length rKv2.1 Δ7 complexes.
White circles mark possible rKv2.1 channels. Bar indicates scale (45nm).

thought that these negative residues in the C-terminal linker complement other negative residues in the T1 linker, promoting the passage of positively charged ions (Sokolova *et al*, 2003). In rat Kv2.1 only two negatively charged residues are found at positions equivalent to *Shaker* (residues 488 and 491). Whether the two negative charges in this region of the C-terminal domain of rat Kv2.1 may relate to other residues in the Kv2.1 T1 linker in a similar way to that hypothesised for *Shaker* is as yet unclear.

The *Shaker* channel has previously been shown to be heavily glycosylated, producing an increase in the protein size from 80 to 100kDa upon glycosylation (Sokolova *et al*, 2003). No such shift was found in Kv2.1 in this study, with only one band found upon purification, indicating that Kv2.1 is not glycosylated. Although an (N)-linked glycosylation site is found within the S1-S2 linker in Kv2.1 this site was previously not found to be glycosylated when the rat Kv2.1 channel was expressed in COS-1 cells (Shi *et al*, 1999).

On the basis of structural studies of other Kv channels described above, and the electrophysiological and interaction data described in chapters 3 and 4, the C- terminal region of rat Kv2.1 can be considered as three domains. These consist of the S6 linker region of approximately 50 residues, a Kv2 domain of approximately 250 residues, and the CTA domain of approximately 110 residues (shown schematically in Fig. 3.24 and Ju *et al* (2003)). The CTA domain is predicted to possess several β-strands, as well as hydrophobic regions. It is interesting that this region shows a partial homology across the Kv2 potassium family. The results described in chapter 4 of this thesis show that the C- terminal domain interacts with the T1 domain (N- terminal), which is consistent with recent studies of *Shaker* showing that the C- terminal domain surrounds the T1 domain of this channel (Sokolova *et al*, 2003). It is hoped that in the coming months an EM structure for the Kv2.1 channels described in this chapter will be obtained, so that the structures of the full length and the C- terminal deleted channels can be compared in order to unequivocally reveal the location of the C-terminal domain in Kv2.1 in relation to the T1 domain.

CHAPTER 6

ANALYSIS OF S4 SEGMENT MOVEMENT IN VOLTAGE ACTIVATED CALCIUM CHANNELS USING PCMBS

6.1 Introduction

An outward movement of the S4 region upon depolarisation is thought to lead to opening of voltage dependent ion channels. Although much work has been carried out studying movement of the S4 region upon depolarisation of sodium and potassium channels, no such work has been reported for calcium channels.

The objective of the work described in this chapter was to study the putative voltage-dependent movement of the S4 region of a calcium channel. For this, the accessibility of cysteine residues was investigated using the cysteine-binding reagent parachloromercuribenzenesulfonate (PCMBS) on wild type $Ca_v3.1$, $Ca_v1.2$ and mutant channels. Using site-directed mutagenesis, cysteine residues were introduced into the domain I S4 of the calcium channel chimera CGGG at positions V263, A265, L266, A268, F269, and V271. cRNAs for the mutant channels were injected into *Xenopus laevis* oocytes and currents recorded 4-5 days later using two-electrode voltage clamp technique. PCMBS was perfused onto the expressed channels, and the effects on the current amplitude were examined.

6.2 Results

6.2.1 Effects of PCMBS on wild type calcium channel currents

PCMBS is a highly hydrophilic membrane impermeable reagent, that has previously been shown to react with cysteines in an aqueous environment only (Yan *et al*, 1993). Thus if PCMBS were to react with a channel under depolarising conditions but not at rest, this would suggest that cysteines within the channel moved out of the membrane bilayer as a result of depolarisation, and remained inaccessible at rest.

Firstly it was necessary to test wild type channels, $Ca_v3.1$ and $Ca_v1.2$ (shown schematically in Fig. 6.1), to see if they reacted with PCMBS without engineered cysteines. The corresponding cRNA transcripts were expressed in *Xenopus* oocytes. The oocytes were repetitively depolarised by stepping to –30mV for $Ca_v3.1$, and +10mV for $Ca_v1.2$, from a holding potential of –80mV. While repetitively depolarising, 100μM PCMBS was applied. I/V curves were constructed before and after the application of PCMBS. Barium was used as a charge carrier in all experiments described in this chapter.

Extracellular cysteines which could react with PCMBS are already present in $Ca_v3.1$; indeed there are 14 cysteines located on the extracellular loops. The results in Figs. 6.2 and 6.3 show that PCMBS did react with $Ca_v3.1$; the current was markedly reduced following application of PCMBS. The wild type $Ca_v3.1$ channel was therefore not used in further experiments. In contrast, PCMBS did not appear to react with wild type $Ca_v1.2$, as the current was not significantly affected by the addition of this reagent (Figs. 6.2 and 6.3), which suggests that this channel could be used in cysteine mutagenesis studies of the S4 domain with PCMBS. Further work with a chimeric channel was then done as the investigation was to study $Ca_v3.1$, which was not possible (see above). It is worth noting that there is only one non-conserved cysteine residue found within the extracellular loops in $Ca_v1.2$, compared with seven in $Ca_v3.1$; the rest are conserved or partially conserved within the calcium channel family.

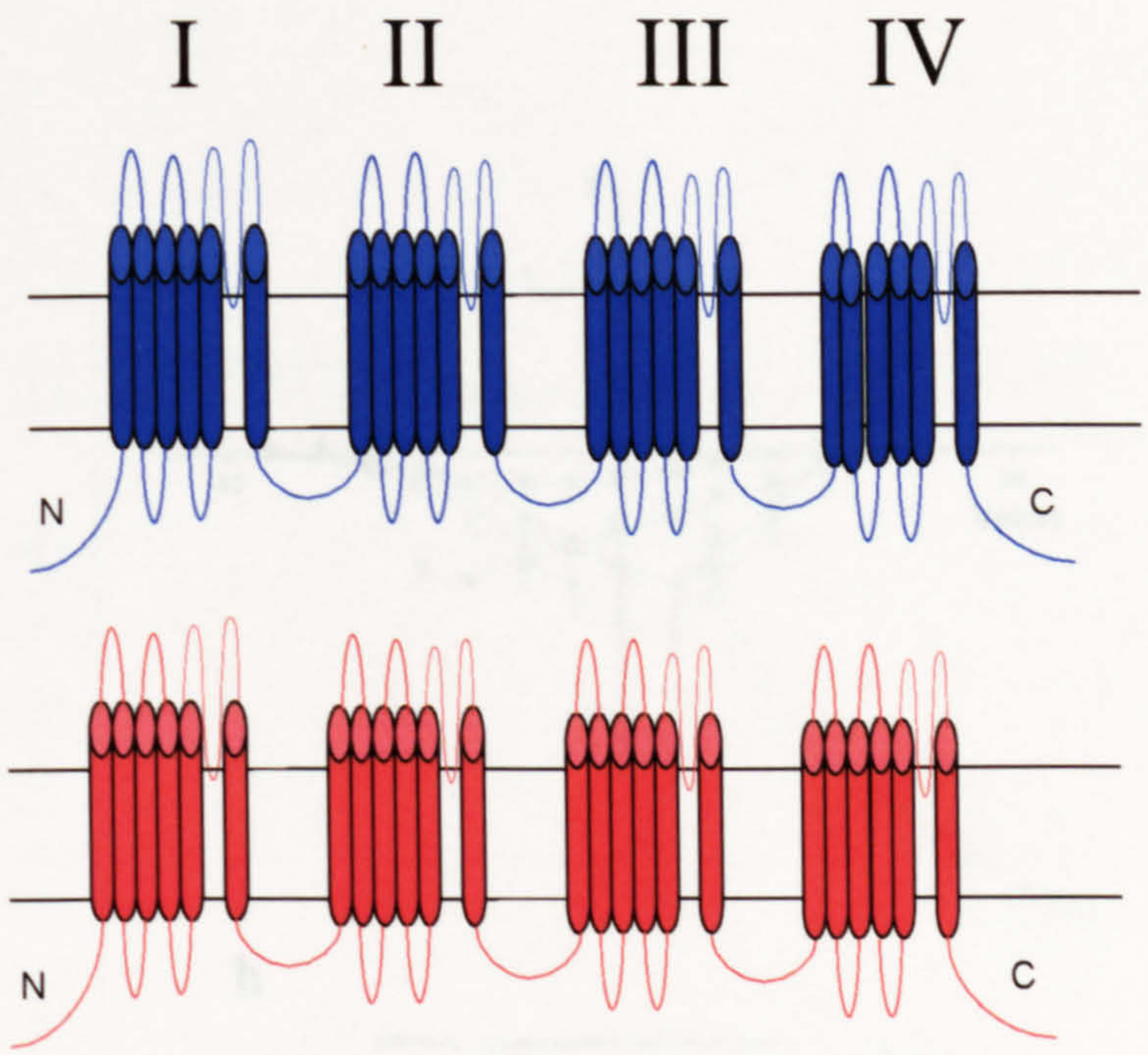

$Ca_v3.1$ (GGGG)

$Ca_v1.2$ (CCCC)

CGGG

GCGG

Fig. 6.1 Schematic structure of wild type $Ca_v3.1$, $Ca_v1.2$ and chimeras.

The four transmembrane domains (I-IV) are represented by four letter codes. GGGG refers to wild type $Ca_v3.1$, and CCCC refers to wild type $Ca_v1.2$. Two chimeras CGGG and GCGG had domains I and II swapped as shown.

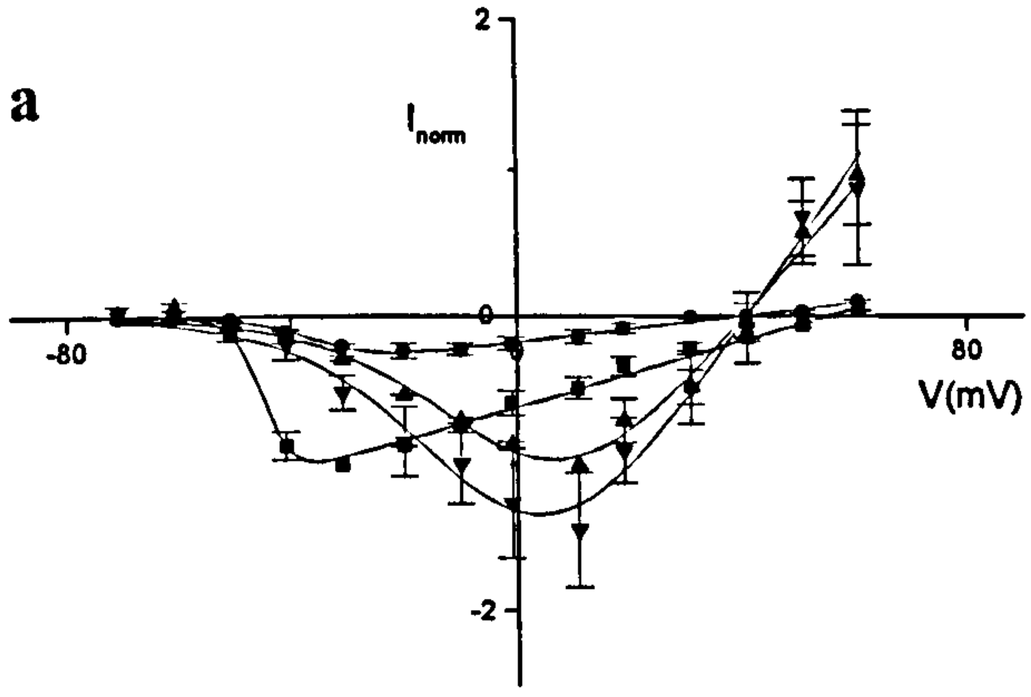

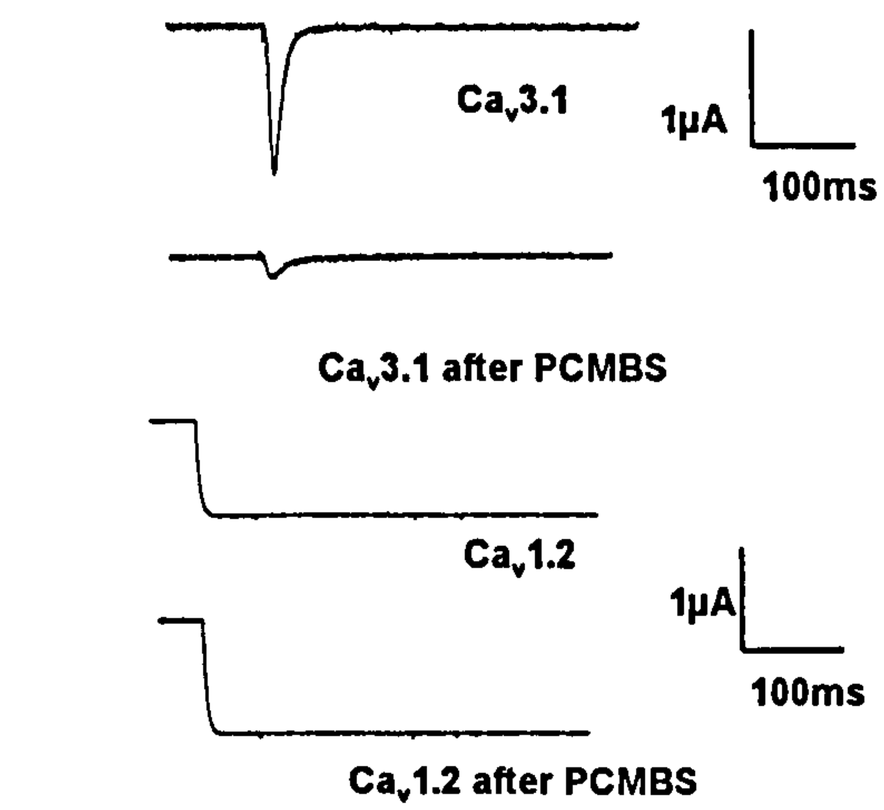

Fig. 6.2 Effect of PCMBS on wild type $Ca_v3.1$ and $Ca_v1.2$.
a, The mean normalised I/V curves for wild type $Ca_v3.1$, before (-1.17±0.04 μA, ■ $n = 4$) and after PCMBS (●, $n = 4$), and wild type $Ca_v1.2$, before (-1.05±0.06 μA, ▲ $n = 5$) and after PCMBS (▼, $n = 5$) are shown. Curves were normalised to the values at -30mV for $Ca_v3.1$ and +10mV for $Ca_v1.2$ before PCMBS.
b, Sample current traces are shown for two cells corresponding to near the maxima of the I/V curves (-30mV for $Ca_v3.1$ and +10mV for $Ca_v1.2$). A holding potential of -80mV was used in all experiments.

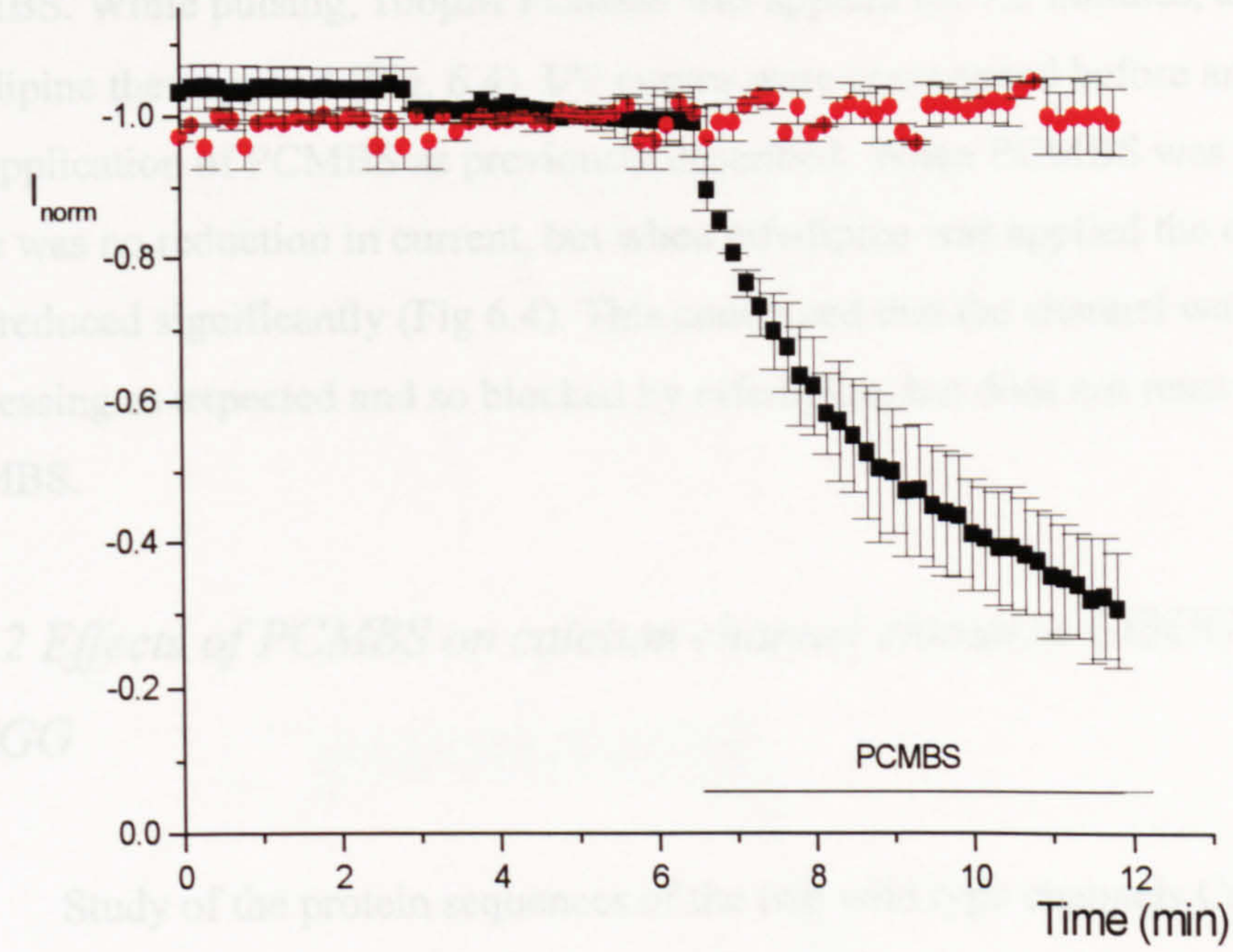

Fig. 6.3 Time course of the effect of PCMBS on wild type $Ca_v3.1$ and $Ca_v1.2$.

Effect of application of PCMBS on wild type $Ca_v3.1$, (■, $n = 4$) and $Ca_v1.2$, (●, $n = 4$) is shown. PCMBS was applied over the time period indicated by the solid line. Cells were repeatedly depolarised stepping to -30mV for $Ca_V3.1$, and +10mV for $Ca_v1.2$ from a holding potential of -80mV (see Methods). Current amplitudes were normalised to -1 with respect to the value measured over the first 4 minutes of the recording, -1.15±0.04 μA for $Ca_v3.1$ and -1.09±0.03 μA for $Ca_v1.2$.

The results shown above would suggest that the conservation of cysteines could be related to whether a channel reacts with PCMBS.

To check that $Ca_v1.2$ wild type channel was expressing correctly, 1μM nifedipine (an L-type specific blocker) was applied after the application of PCMBS. While pulsing, 100μM PCMBS was applied for 7.5 minutes, and nifedipine then applied (Fig. 6.4). I/V curves were constructed before and after the application of PCMBS as previously described. When PCMBS was applied there was no reduction in current, but when nifedipine was applied the current was reduced significantly (Fig 6.4). This confirmed that the channel was expressing as expected and so blocked by nifedipine, but does not react with PCMBS.

6.2.2 Effects of PCMBS on calcium channel chimeras CGGG and GCGG

Study of the protein sequences of the two wild type channels $Ca_v3.1$ 'GGGG', and $Ca_v1.2$ 'CCCC', shows that $Ca_V3.1$ has six more non-conserved cysteines than $Ca_v1.2$; three are present in the extracellular loops of domain I, and one cysteine is present in domain II. Some of these residues may account for the reactivity of $Ca_v3.1$, but not $Ca_v1.2$, with PCMBS. As this study aimed to analyze $Ca_v3.1$, two chimeric channels that had either domains I or II substituted by $Ca_v1.2$, CGGG and GCGG were investigated next.

The chimeric channel CGGG, made by J. Li (shown schematically in Fig. 6.1) was investigated first. Upon the application of PCMBS, no decrease in current occurred (Figs. 6.5 and 6.6). As can also be seen from the current traces, CGGG was high voltage activating like $Ca_V1.2$. The results show that this clone is suitable for further investigation by creating cysteine mutants in the S4 of domain I, as the chimera CGGG is not affected by PCMBS.

In contrast, chimera GCGG, (also made by J. Li, shown schematically in Fig. 6.1) did show a significant decrease in current when PCMBS was applied, (Figs. 6.6 and 6.7). This result is probably due to the three non-conserved cysteine residues still present in domain I of this chimera, which may have reacted with PCMBS. As can also be seen from the current traces, GCGG was

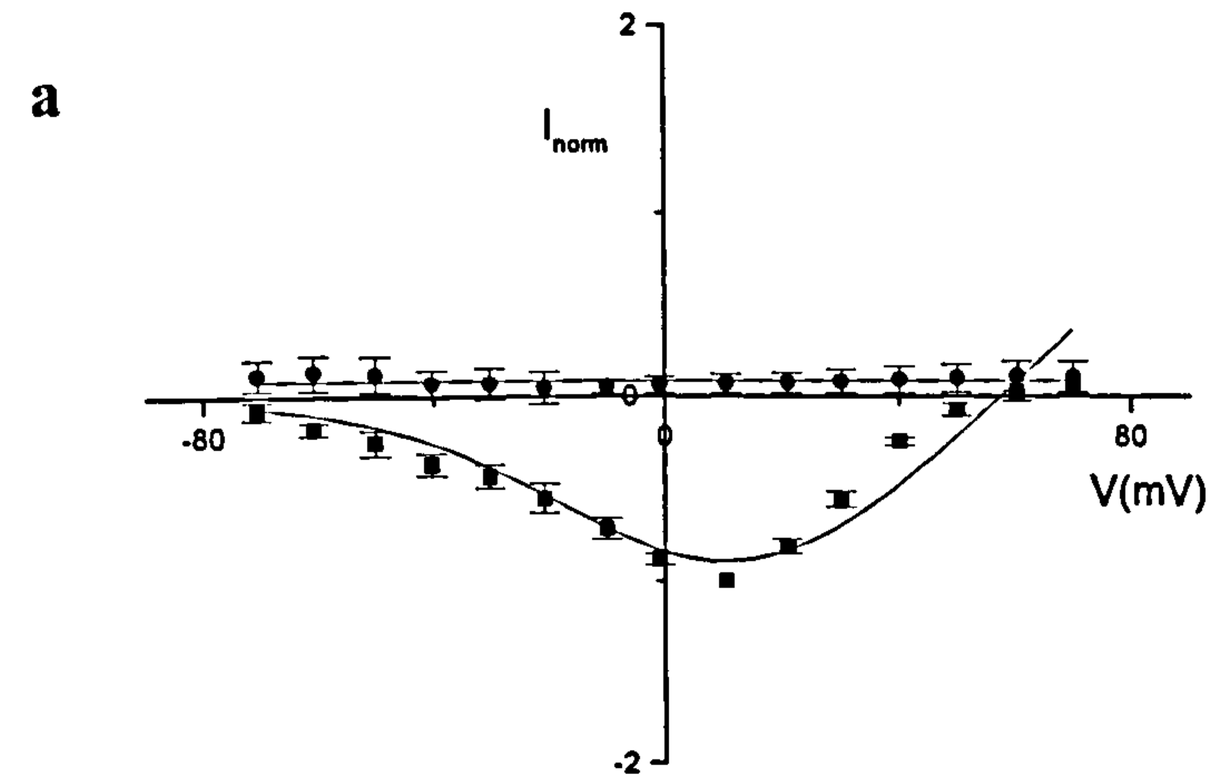

Fig. 6.4 Effect of PCMBS and nifedipine on wild type $Ca_v1.2$.
a, The mean normalised I/V curve for wild type $Ca_v1.2$, before (1.01±0.04 μA ■, *n*=3) and after (●, *n*=3) the addition of PCMBS and nifedipine. Curves were normalised to +10mV as in Fig. 6.2.
b, Oocytes were perfused with 100μM PCMBS (shown by the red bar), and then perfused with nifedipine (1μM) as indicated by the black bar. Cells were repeatedly depolarised to +10mV. Current amplitudes were normalised to -1 with respect to the value measured over the first 4 minutes of the recording (1.05±0.05 μA).

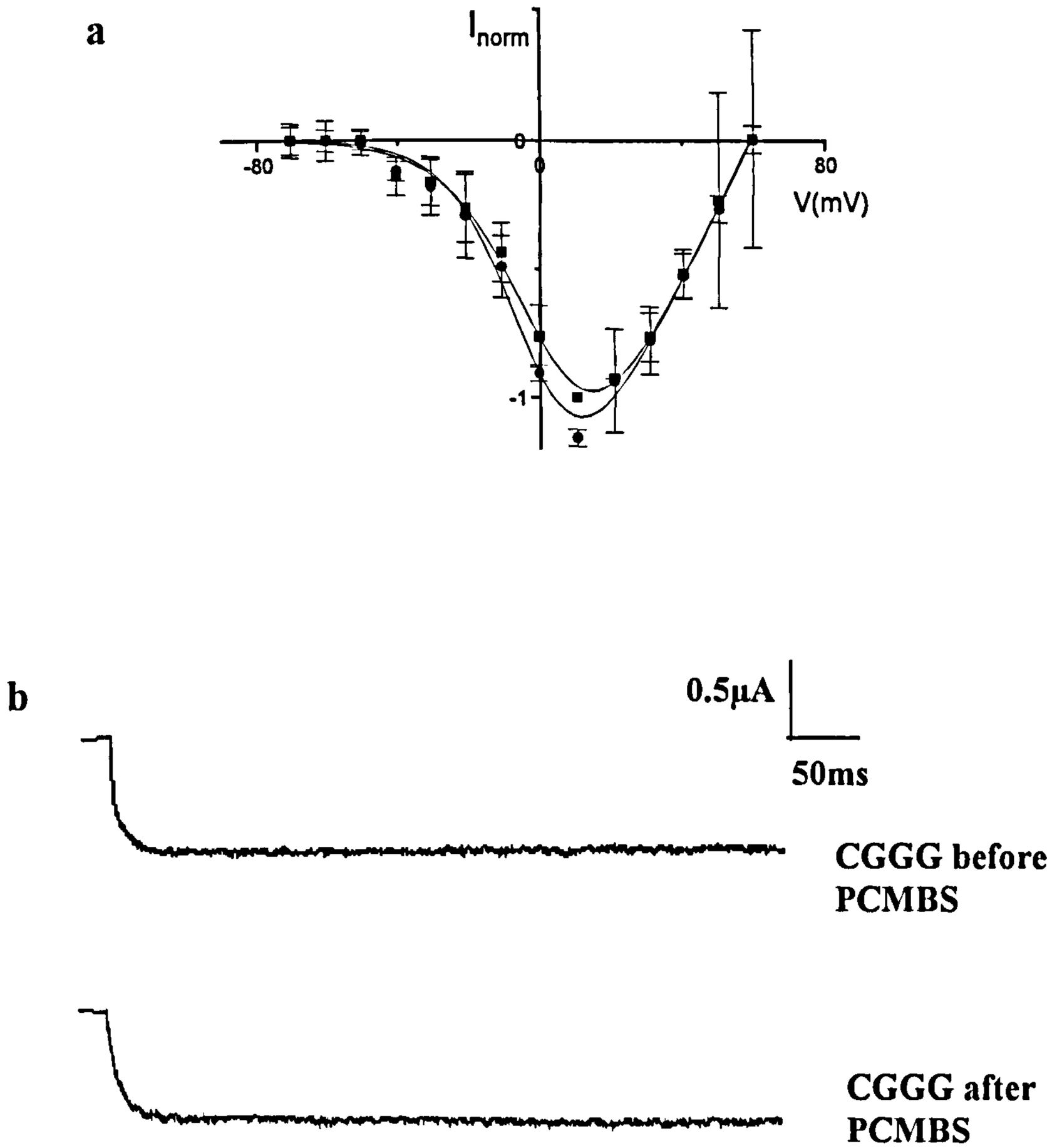

Fig. 6.5 Effect of PCMBS on chimera CGGG.
a, The mean normalised I/V curves for chimera CGGG, before (■, n = 6) and after PCMBS (●, n = 6). Curves were normalised to the current at +10mV before PCMBS (-0.76±0.01 μA).
b, Sample current traces are shown for one cell corresponding to near the maximum of the I/V curve (+10mV). A holding potential of -80mV was used in all experiments.

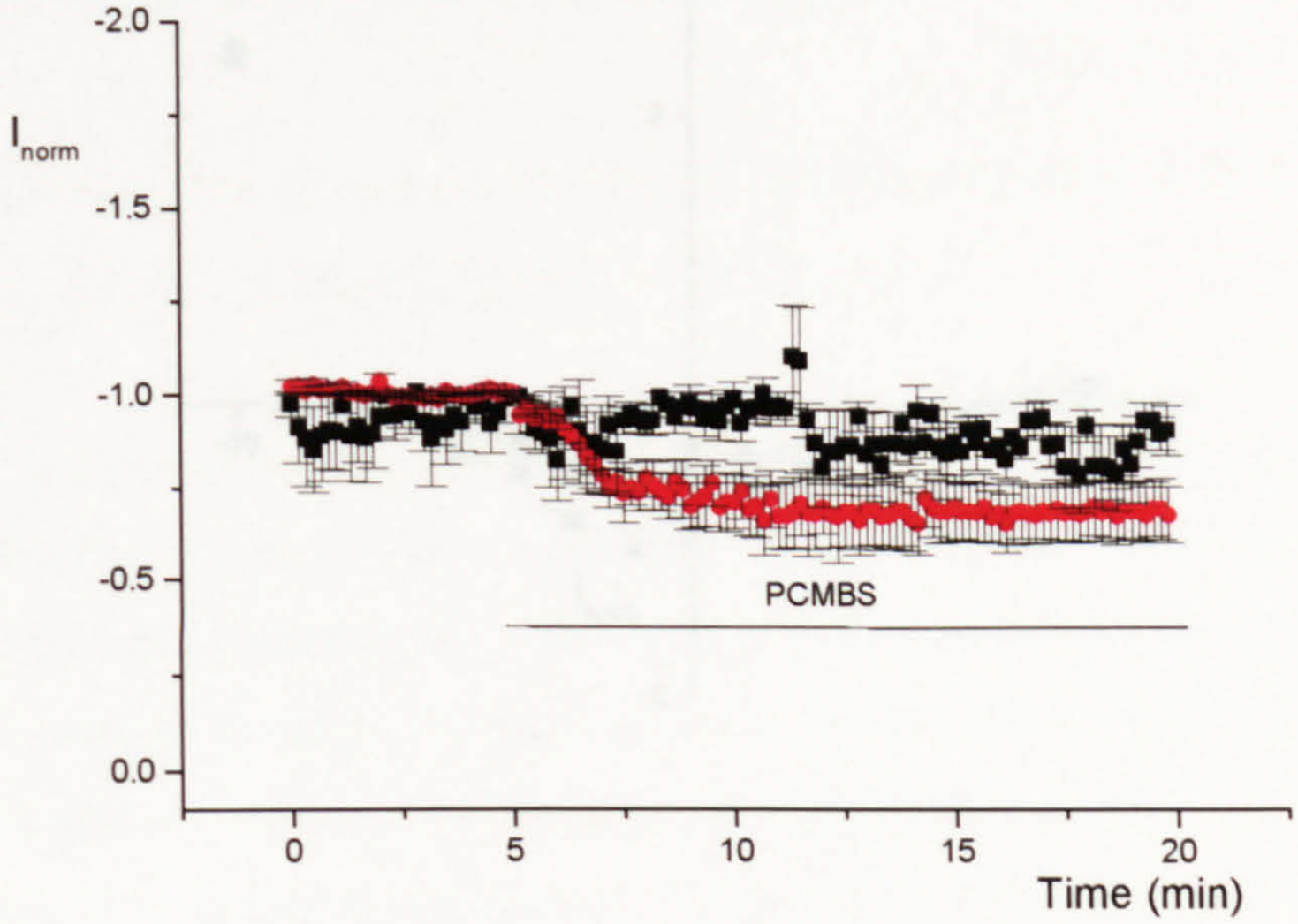

Fig. 6.6 Time course of the effect of PCMBS on chimeras CGGG and GCGG.

The figure shows the effect of application of PCMBS on oocytes injected with cRNA from either CGGG, (■, $n = 6$) or GCGG, (●, $n = 5$). Oocytes were perfused with 100μM PCMBS over the time indicated by the bar. Cells were repeatedly depolarised by stepping to -10mV for GCGG, and +10mV for CGGG from a holding potential of -80mV (see Methods). Current amplitudes were normalised to -1 with respect to the value measured over the first 4 minutes of the recording (-0.4±0.04 μA for GCGG and -0.81±0.03 μA for CGGG) .

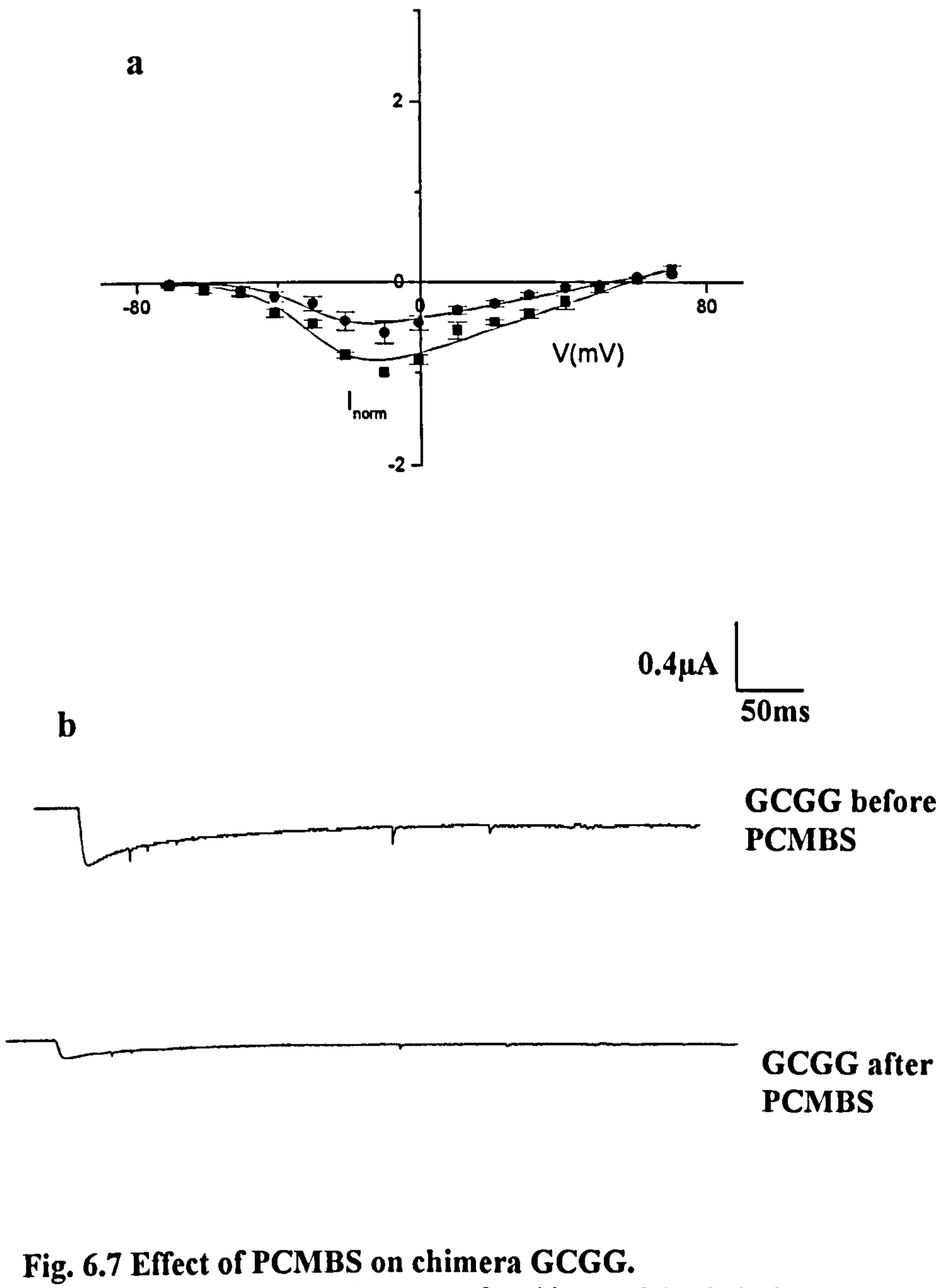

Fig. 6.7 Effect of PCMBS on chimera GCGG.
a, The mean normalised I/V curves for chimera GCGG, before, (■, $n = 5$) and after PCMBS (●, $n = 5$). Curves were normalised to -10mV before PCMBS (-0.4±0.01 µA). The values from -20mV to +30mV inclusive were found to be significantly different ($p<0.05$).
b, Sample current traces are shown for one cell corresponding to near the maximum of the I/V curve (-10mV). A holding potential of -80mV was used in all experiments.

low voltage activating like $Ca_v3.1$. The results for this chimera show that it is not particularly suitable for cysteine mutagenesis, and therefore it was not used again in this analysis.

As chimera CGGG did not react with PCMBS, it was therefore decided to use this clone for this cysteine mutagenesis study.

6.2.3 Generation of domain I CGGG cysteine mutants V263C, A265C, L266C, A268C, F269C, and V271C

In order to characterise the extent of exposure of the S4 segment upon depolarisation, six neutral amino acid residues (V263, A265, L266, A268, F269, and V271, $Ca_v1.2$ numbering) in the S4 region of domain I in chimera CGGG were mutated to cysteine. Positively charged amino acids in the S4 of the CGGG chimera were not changed, as this might be expected to perturb the structure. Mutation of these conserved residues was carried out using the QuikChange™ site-directed mutagenesis method (as described in section 2.1.5). A fragment of the clone containing domain I in pUC18 was used. Site directed mutagenesis was performed only on small fragments of the coding sequence, rather than the entire length, to reduce the possibility of accidentally introducing other, unwanted, mutations. Thermal cycling and *Dpn*I digestion were carried out as described in section 2.1.5. After digestion, products were transformed (as described in section 2.1.1) into *E. coli* and DNA prepared from colonies grown under ampicillin selection by mini-preps (as described in section 2.1.3). Fig. 6.8 shows the results of the automated sequencing indicating that all of the mutants were correctly constructed.

Sections of the constructs containing mutations introduced into the CGGG clone in pUC18 were then sub-cloned into wild type $Ca_v3.1$ (as described in section 2.5.1) using the restriction enzymes *Hind*III and *Xba*I. Fig. 6.9 shows a sample of digested products. In all site-directed mutants made, the smaller domain I fragment (1380bp) was ligated into the larger vector fragment (8609bp). Fig. 6.10 shows a sample of one of the automated sequencing electrophoretograms, indicating that this construct had the correct sequence around the initiation codon.

a

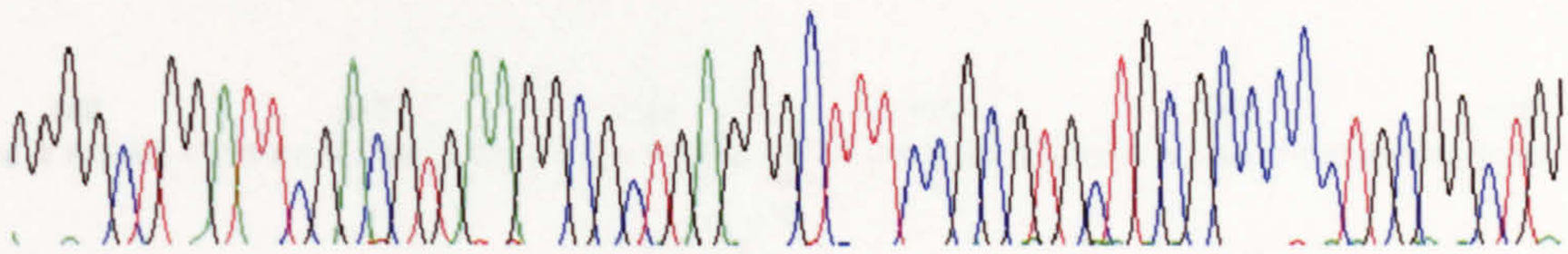

Chimera CGGG

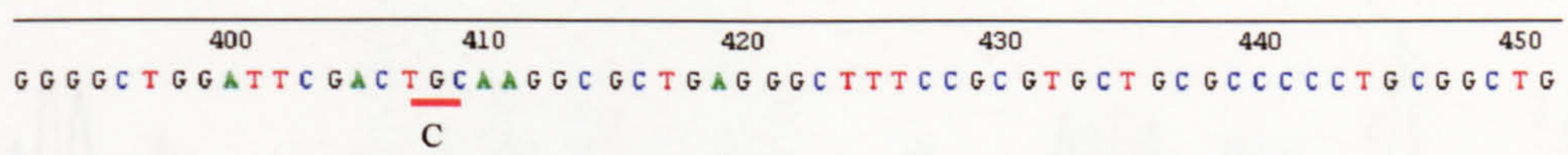

b

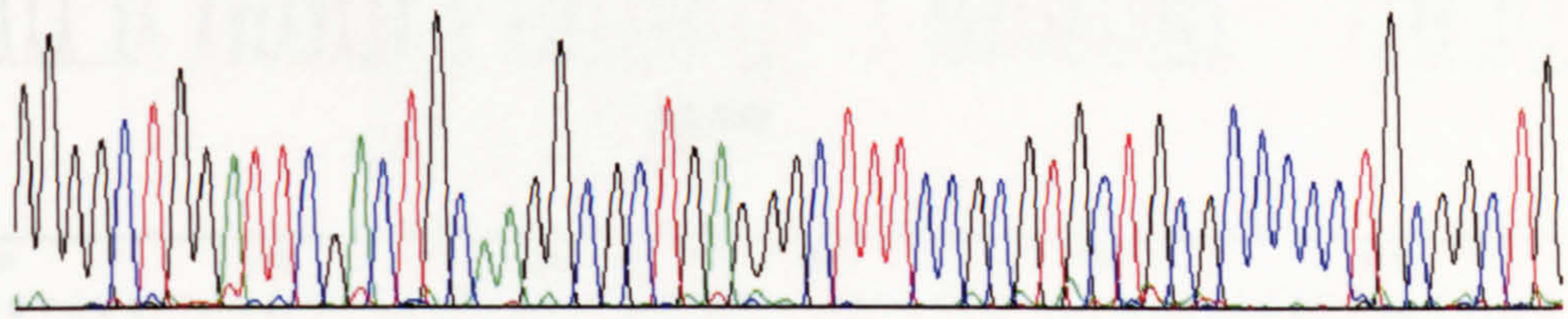

V263C

c

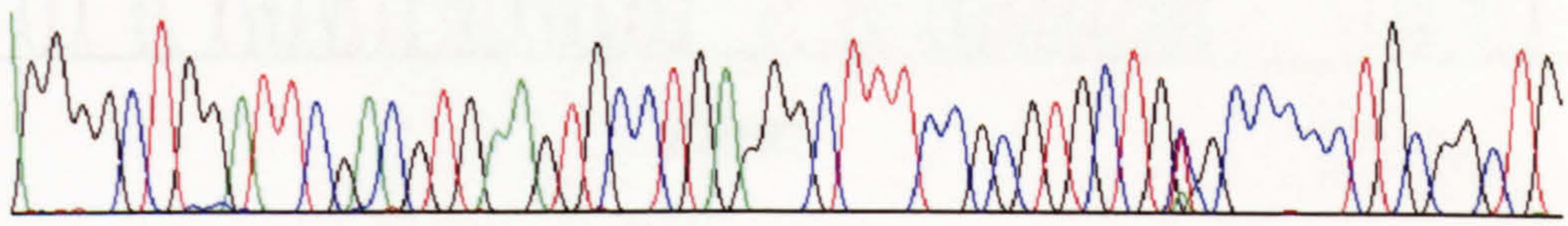

A265C

d

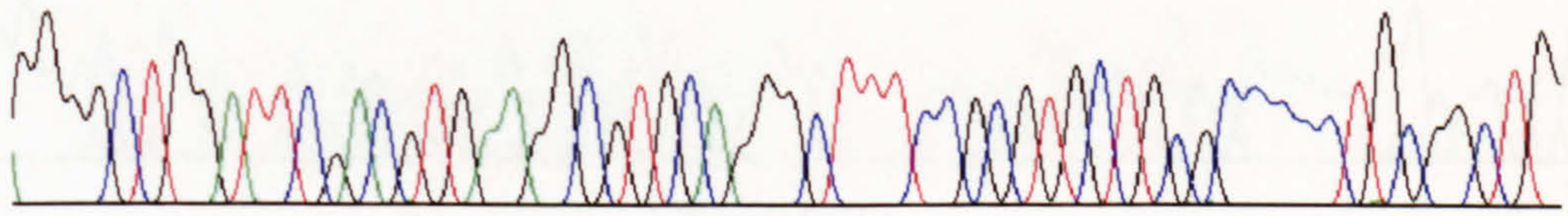

L266C

Fig. 6.8. Electrophoretograms of cysteine mutants.
The figure shows the electrophoretograms of part of the nucleotide sequence for CGGG before mutagenesis (**a**), and for V263C, A265C, and L266C (**b-d**). Mutated codons are shown underlined in red.

660 670 680 690 700 710

G G G G C T G G A T T C G A C G T G A A G G C G C T G A G G T G T T T C C G C G T G C T G C G C C C C C T G C G G C T G

C

e

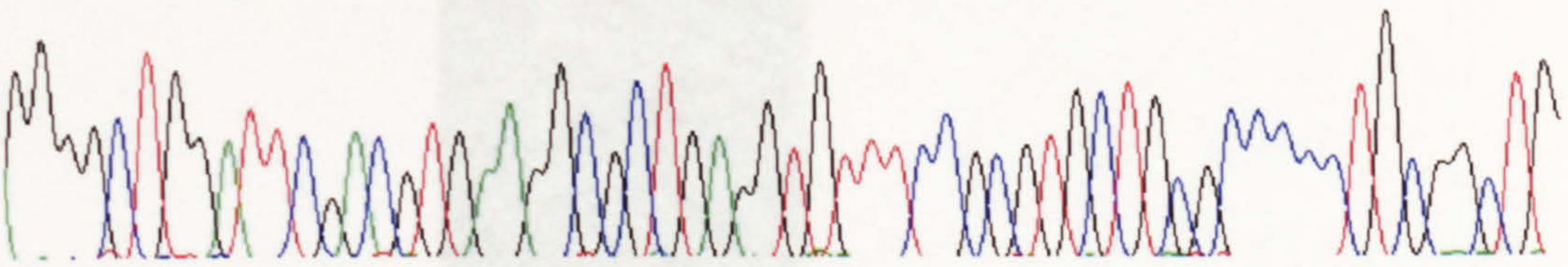

A268C

660 670 680 690 700 710

G G G G C T G G A T T C G A C G T G A A G G C G C T G A G G G C T T G C C G C G T G C T G C G C C C C C T G C G G C T G

C

f

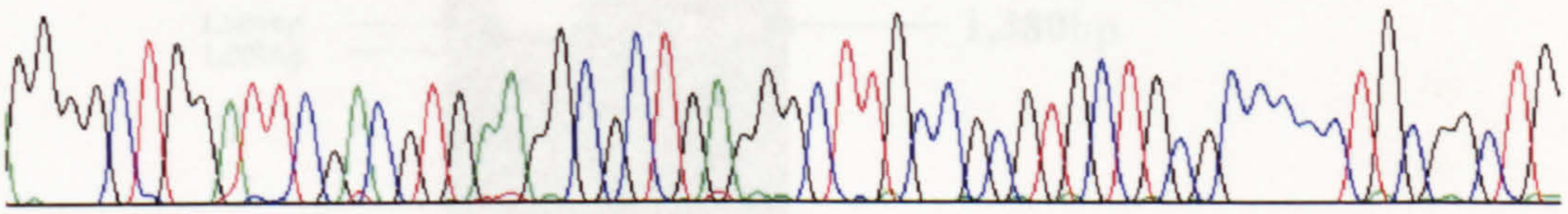

F269C

660 670 680 690 700 710

G G G G C T G G A T T C G A C G T G A A G G C G C T G A G G G C T T T C C G C T G C C T G C G C C C C C T G C G G C T G

C

g

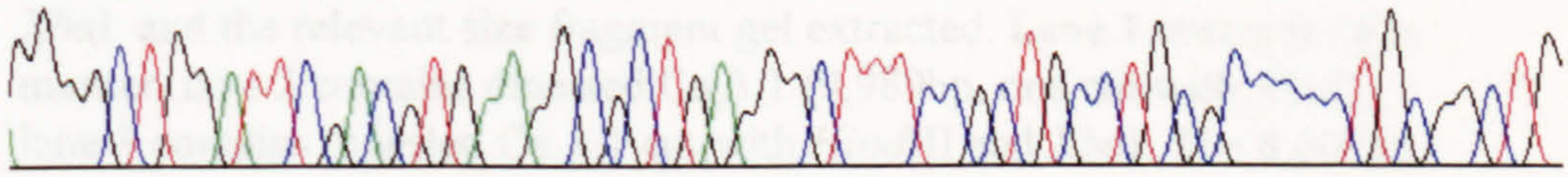

V271C

Fig. 6.8 (continued) Electrophoretograms of cysteine mutants.
The figure shows the electrophoretograms of part of the nucleotide sequence for A268C, F269C, and V271C (**e-g**). Mutated codons are shown underlined in red.

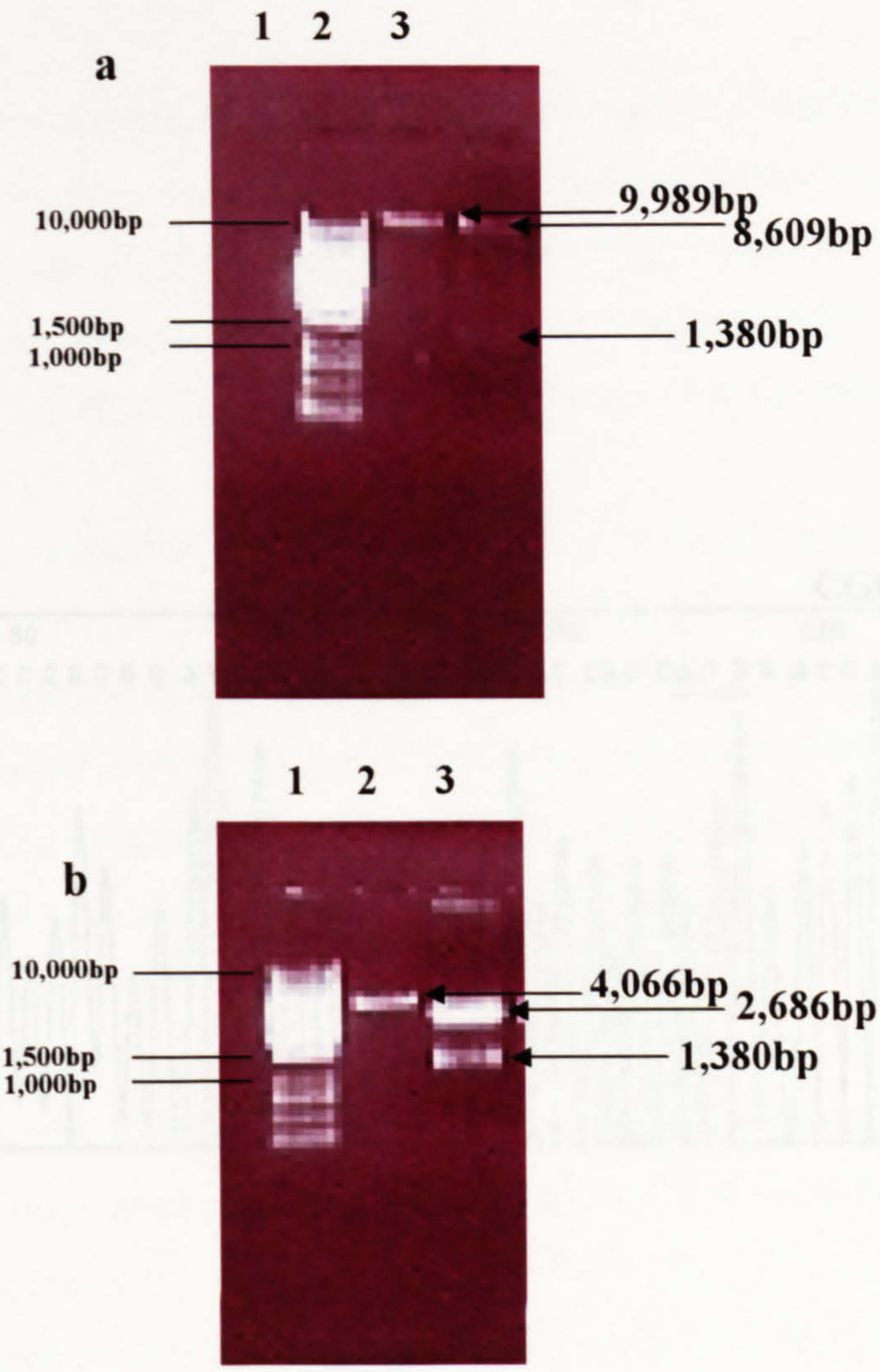

Fig. 6.9 Digestion of $Ca_v3.1$, and domain I (pUC18) DNA.
The fragments were produced by digestion with the restriction enzymes *Hind*III and *Xba*I.
a, Restriction digest of $Ca_v3.1$. DNA was digested with *Hind*III and *Xba*I, and the relevant size fragment gel extracted. Lane 1 contains 1Kb marker, lane 2 contains digested $Ca_v3.1$ (9,989bp, one cut with *Xba*I), lane 3 contains digested $Ca_v3.1$ cut with *Hind*III and *Xba*I. The 8,609bp, fragment was used for subsequent ligation.
b, Restriction digest of cysteine mutantV263C in pUC18. DNA was digested with *Hind*III and *Xba*I, and the relevant size fragment gel extracted. Lane 1 contains 1Kb marker, lane 2 contains digested cysteine mutant (4066bp, one cut with *Xba*I), lane 3 contains digested cysteine mutant cut with *Hind*III and *Xba*I. The 1,380bp fragment was used for subsequent ligation .

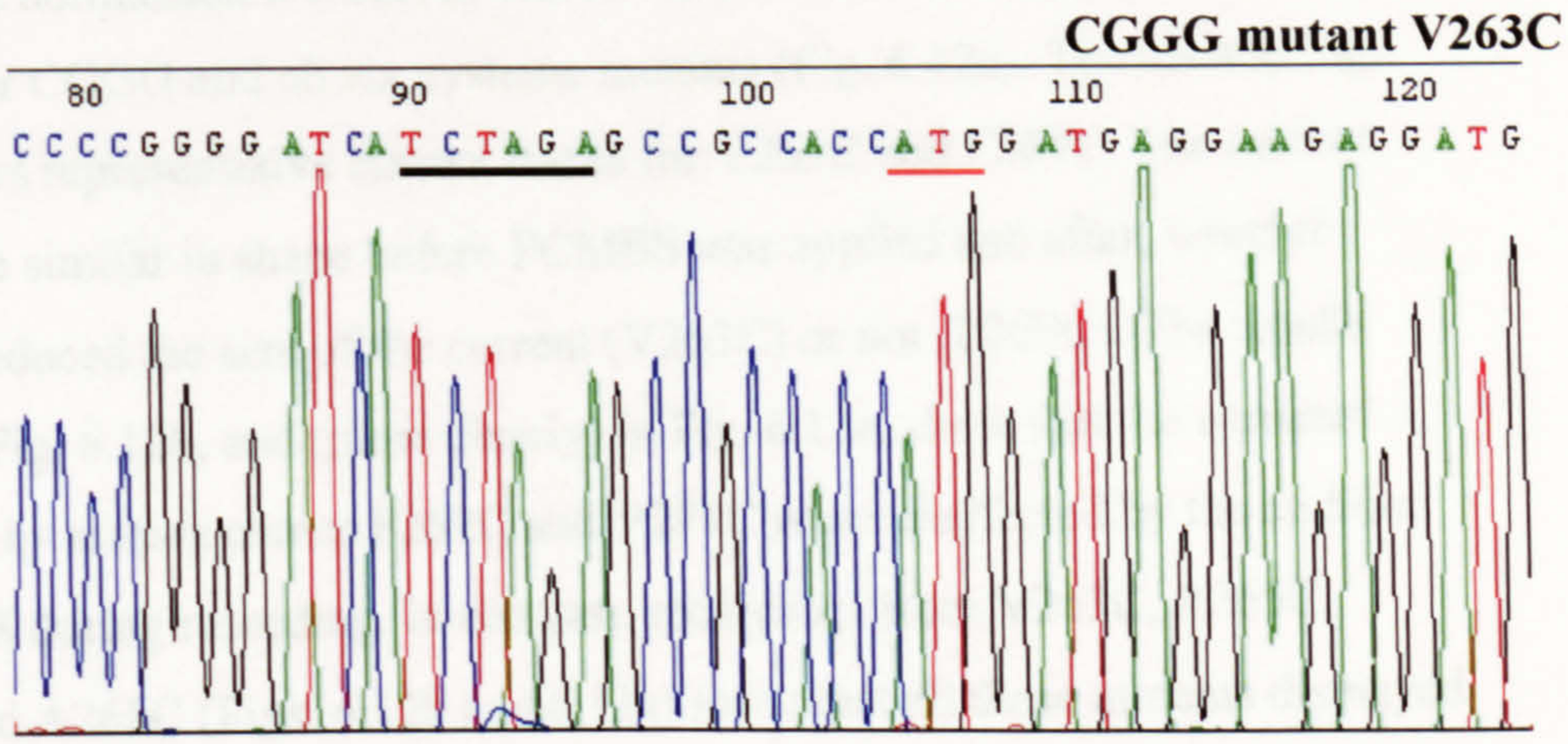

Fig. 6.10 An example electrophoretogram showing part of the nucleotide sequence following the sub-cloning of domain I into $Ca_v3.1$.

Part of a sample sequence of sub-cloned CGGG cysteine mutant V263C. Restriction site used (*Xba*I) is indicated by the black line, and the start codon is indicated by the red line.

6.2.4 Characterisation of S4 cysteine mutant currents

In order to investigate accessibility of the engineered cysteine residues to PCMBS (shown schematically in Fig. 6.11), cRNA was transcribed *in vitro* and injected into *Xenopus* oocytes for whole cell recording of calcium channel currents using the two-electrode voltage clamp technique. PCMBS (100μM) was applied during repetitive stimulation to +10mV from a holding potential of –80mV.

The normalised I/V curves before PCMBS had been applied were similar in shape for CGGG and all six cysteine mutants (Fig. 6.12a). The inset in Fig. 6.12a shows representative current traces for V263C and F269C. The current traces were similar in shape before PCMBS was applied and after, whether PCMBS reduced the size of the current (V263C) or not (F269C). The results shown in Fig. 6.12b, and (more clearly) in Fig. 6.13a, show that the currents expressed by mutant clones F269C and V271C were unaffected by the addition of PCMBS during recording. In contrast, recordings from V263C, A265C, L266C and A268C (Figs. 6.12b and 6.13a) show that all these mutants displayed currents that were rapidly inhibited by PCMBS, and were significantly different from currents before the application of PCMBS (student's t- test, $p<0.05$). This suggests that under these experimental conditions the introduced cysteines were exposed to the extracellular environment. The lack of effect of PCMBS on the F269C and V271C clones suggests that these residues are buried in the tetrameric structure of the channel, and that they remain inaccessible to PCMBS during channel activation. Thus, the accessibility of the S4 region to PCMBS occurs up to and including residue 268, with 269 and 271 remaining buried in the membrane. Interestingly, the rate of onset of the effect of PCMBS was faster for A265C than for V263C, L266C, and A268C (Fig. 6.13b). This suggests that the rate of inhibition did not vary systematically with the depth of the residue in the membrane.

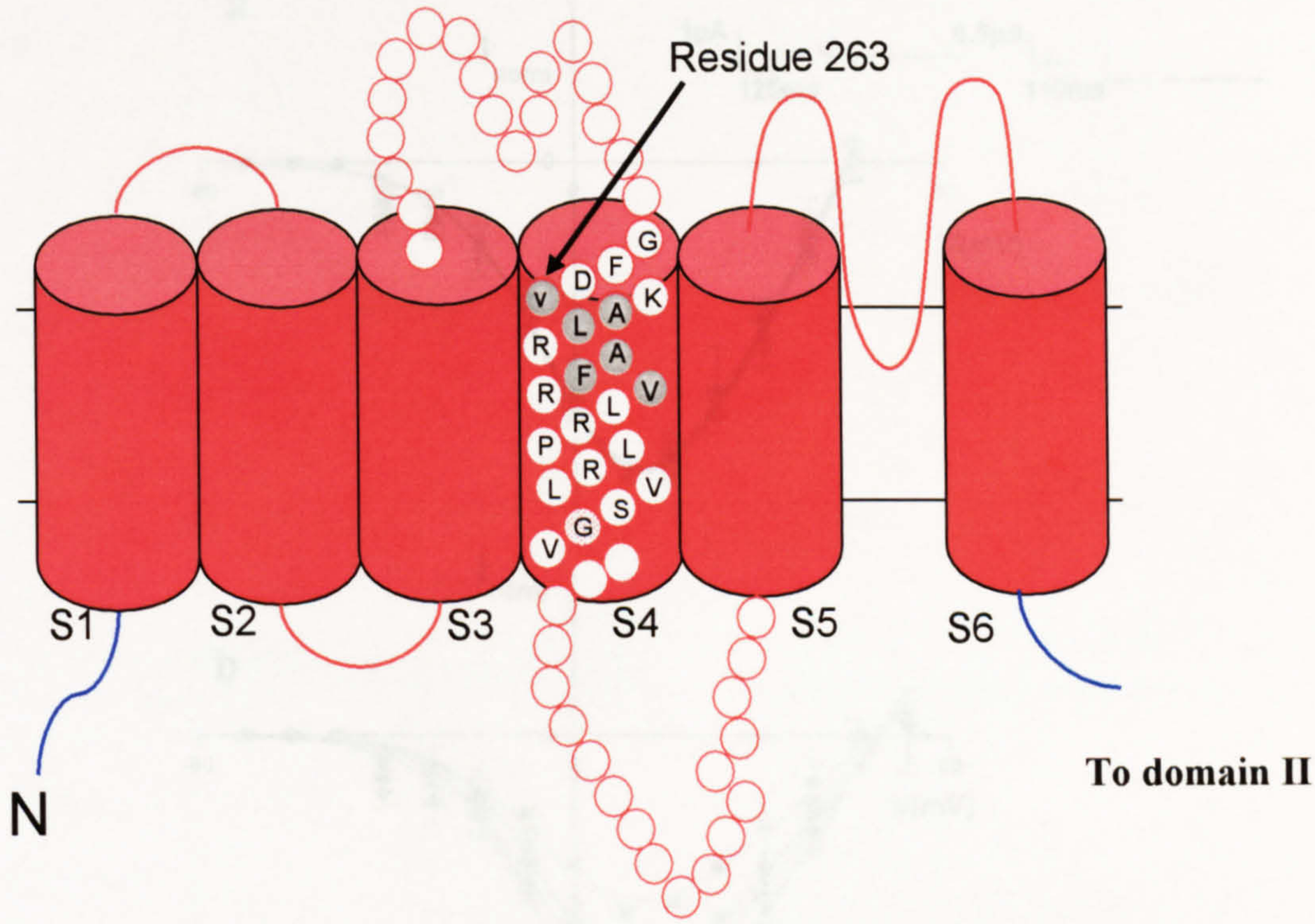

Fig. 6.11 Schematic structure of domain I CGGG.
Proposed membrane topology of CGGG in domain I, showing positions of the cysteine substitutions. The single amino acid code is used, and the hydrophobic segments S1-S6 are shown as cylinders. Amino acids that were changed to cysteine residues are indicated with grey shading. Red colour indicates amino acids from $Ca_v1.2$, and blue indicates amino acids from $Ca_v3.1$.

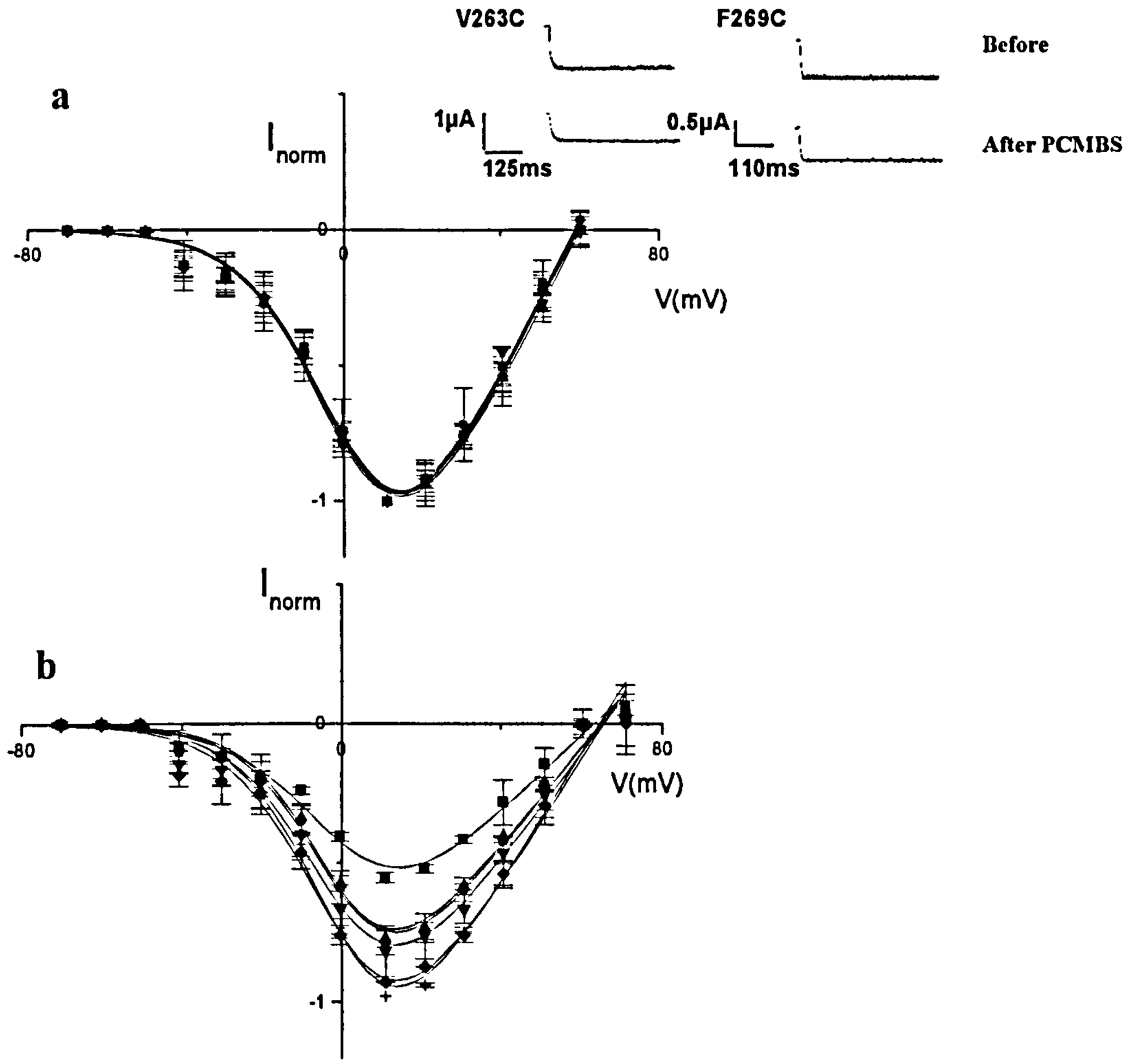

Fig. 6.12 Normalised current-voltage curves showing the effect of PCMBS on calcium channel chimera CGGG and cysteine mutants.

a, The figure shows the normalised I/V curves for the chimera CGGG (■, n = 6), and cysteine mutants V263C (●, n = 3), A265C (▲, n = 4), L266C, (▼, n = 3), A268C (♦, n = 3), F269C (+, n = 4), and V271C (×, n = 3) before the application of PCMBS. Current amplitudes were normalised with respect to the value measured at +10mV: CGGG, -0.76±0.01 μA, V263, -0.94±0.05 μA, A265C, -0.79±0.01 μA, L266C, -0.81±0.06 μA, A268C, -0.91±0.03 μA, F269C, -0.78±0.05 μA, and V271C, -0.72±0.04 μA.

The inset shows representative current traces for V263C and F269C before and after PCMBS. There were no significant differences between the mutants at any data points (student's t-test, $p<0.05$).

b, The figure shows the mean I/V curves for the cysteine mutants V263C (■, n = 3), A265C (●, n = 4), L266C (▲, n = 3), A268C (▼, n = 3), F269C (♦, n = 4), and V271C (+, n = 3) after the application of PCMBS. Currents for mutants V263C, A265C, L266C, and A268C were found to be significantly different from the currents before the application of PCMBS (student's t-test, $p<0.05$).

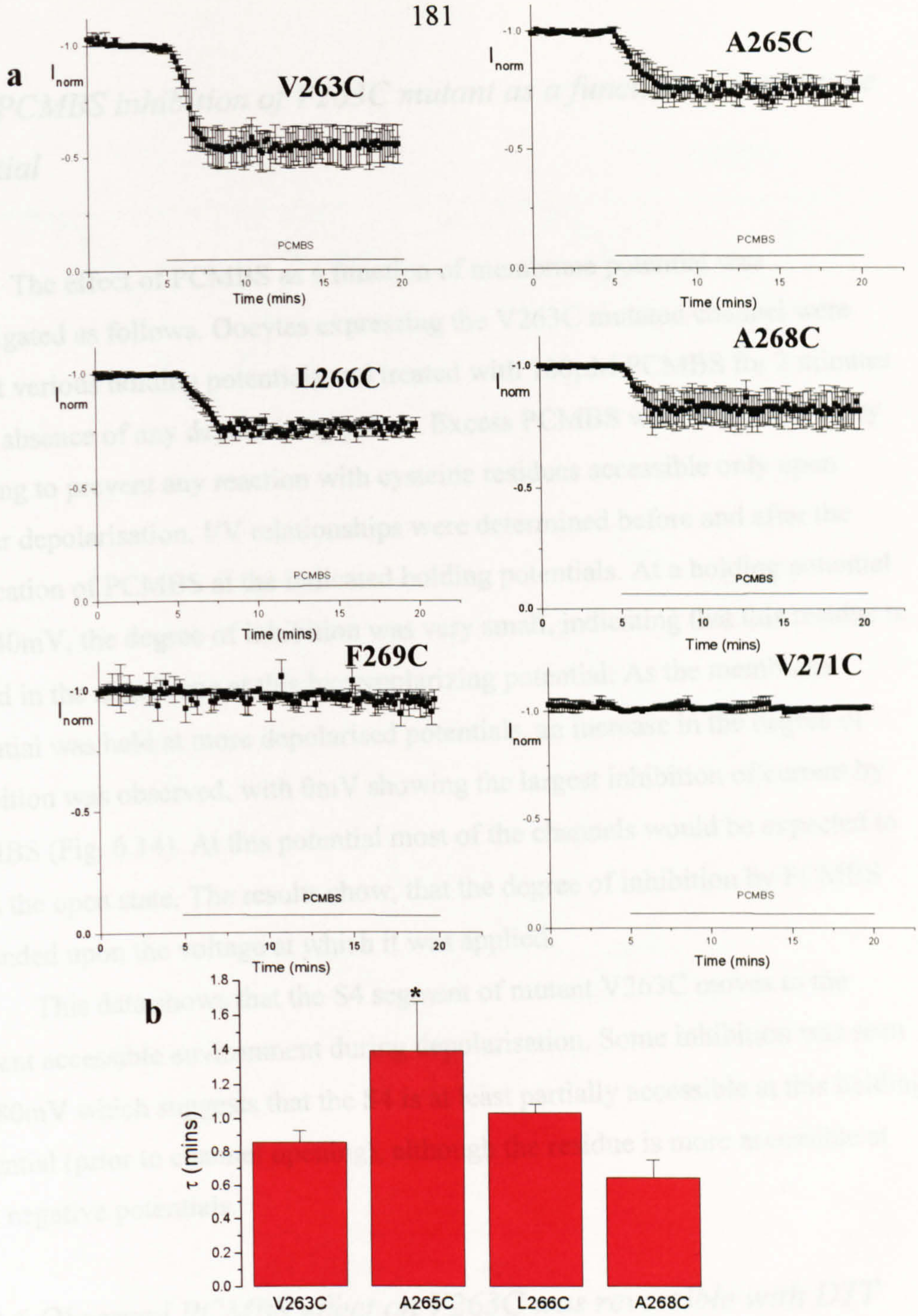

Fig. 6.13 Effect of PCMBS on calcium channel cysteine mutants.

a, Effect of application of PCMBS on calcium currents invoked by repetitive depolarisation of *Xenopus* oocytes expressing mutants V263C ($n = 3$), A265C ($n = 4$), L266C ($n = 3$), A268C ($n = 3$), F269C ($n = 4$), and V271C ($n = 3$). Cells were repeatedly depolarised to +10mV from a holding potential of -80mV. Current amplitudes were normalised with respect to the value measured over the first 4 minutes of the recording: V263C, -0.97±0.05 μA, A265C, -0.83±0.01 μA, L266C, -0.86±0.06 μA, A268C, -0.95±0.03 μA, F269C, -0.81±0.06 μA, and V271C, -0.78±0.08 μA. **b**, Exponential time constant of the time course of inhibition by PCMBS of V263C, A265C, L266C and A268C. *, significant difference between A265C and the other mutants shown (student's t-test, $p<0.05$).

6.2.5 PCMBS inhibition of V263C mutant as a function of membrane potential

The effect of PCMBS as a function of membrane potential was investigated as follows. Oocytes expressing the V263C mutated channel were held at various holding potentials and treated with 100μM PCMBS for 2 minutes in the absence of any depolarising pulses. Excess PCMBS was then removed by washing to prevent any reaction with cysteine residues accessible only upon further depolarisation. I/V relationships were determined before and after the application of PCMBS at the indicated holding potentials. At a holding potential of -140mV, the degree of inhibition was very small, indicating that this residue is buried in the membrane at this hyperpolarizing potential. As the membrane potential was held at more depolarised potentials, an increase in the degree of inhibition was observed, with 0mV showing the largest inhibition of current by PCMBS (Fig. 6.14). At this potential most of the channels would be expected to be in the open state. The results show, that the degree of inhibition by PCMBS depended upon the voltage at which it was applied.

This data shows that the S4 segment of mutant V263C moves to the solvent accessible environment during depolarisation. Some inhibition was seen at –80mV which suggests that the S4 is at least partially accessible at this holding potential (prior to channel opening), although the residue is more accessible at less negative potentials.

6.2.6 Observed PCMBS effect on V263C was reversible with DTT

To investigate whether the inhibitory effect of PCMBS on V263C was due to specific covalent binding to a cysteine residue, the current during repetitive depolarisation to +10mV was first inhibited by adding 100μM PCMBS, followed by the application of 1mM dithiothreitol (DTT), as described in section 2.6.5. As can be seen in Fig. 6.15, DTT reversed the inhibitory effect of PCMBS on mutant V263C. This is consistent with the proposed mechanism of inhibition by PCMBS, i.e. by covalently binding to the cysteine at position 263, a

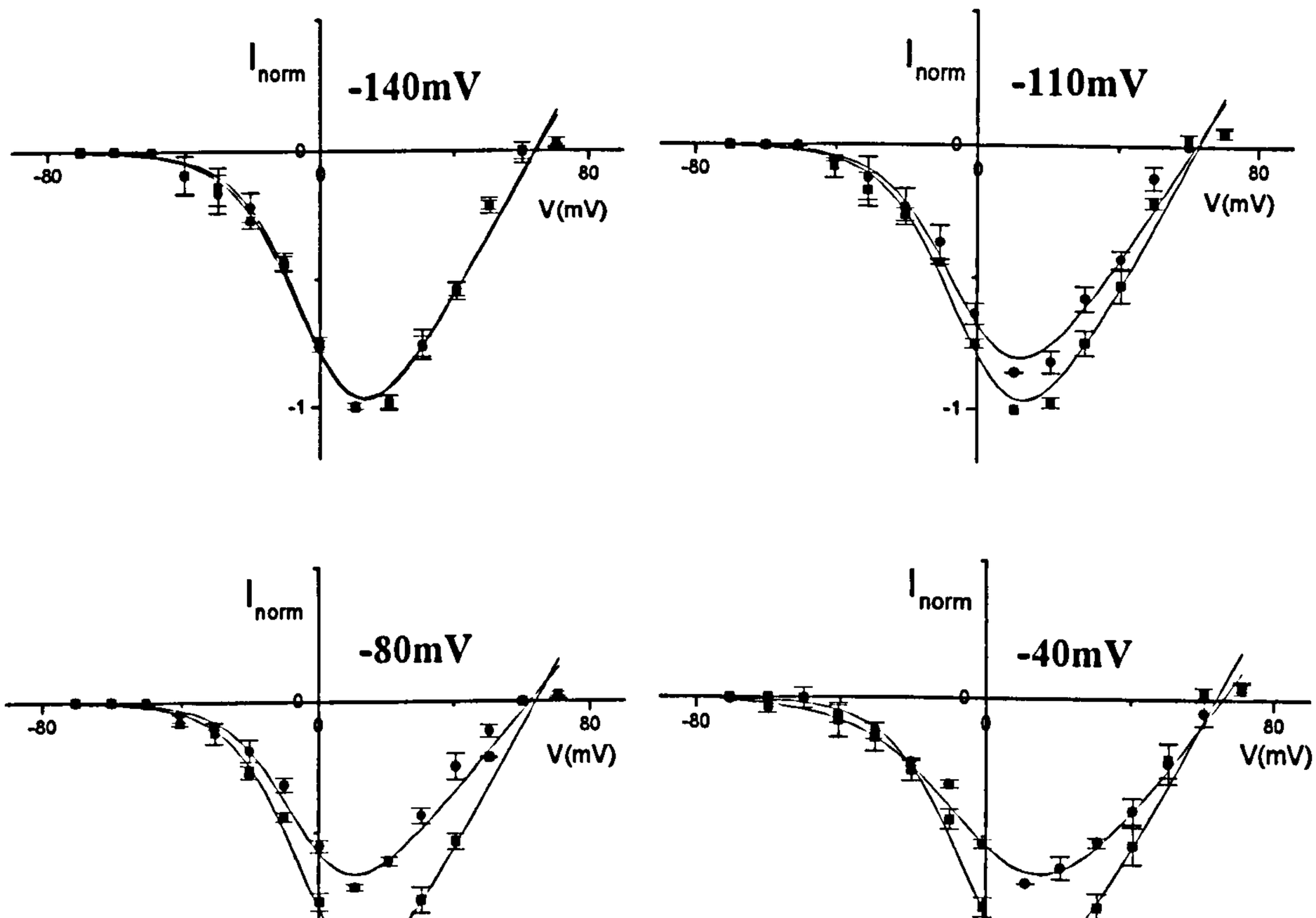

Fig 6.14 Dependence of inhibition of CGGG V263C by PCMBS on holding potential.

Normalised current/voltage (I/V) curves are shown for mutant V263C before (■) and after (●) application of PCMBS (100μM). The reagent was applied in the absence of stimulation at the indicated holding potentials (see Methods) and then unreacted PCMBS removed by washing. Currents were normalised to the value at +10 mV before PCMBS (-140mV, -1.04 ± 0.09 μA, n = 4; -110mV, -0.79 ± 0.08 μA, n = 3; -80mV, -0.74 ± 0.02 μA, n = 5; -40mV, -0.83 ± 0.05 μA, n = 3; 0mV, -1.10 ± 0.08 μA, n = 3) and curves were fitted with the Boltzmann equation.

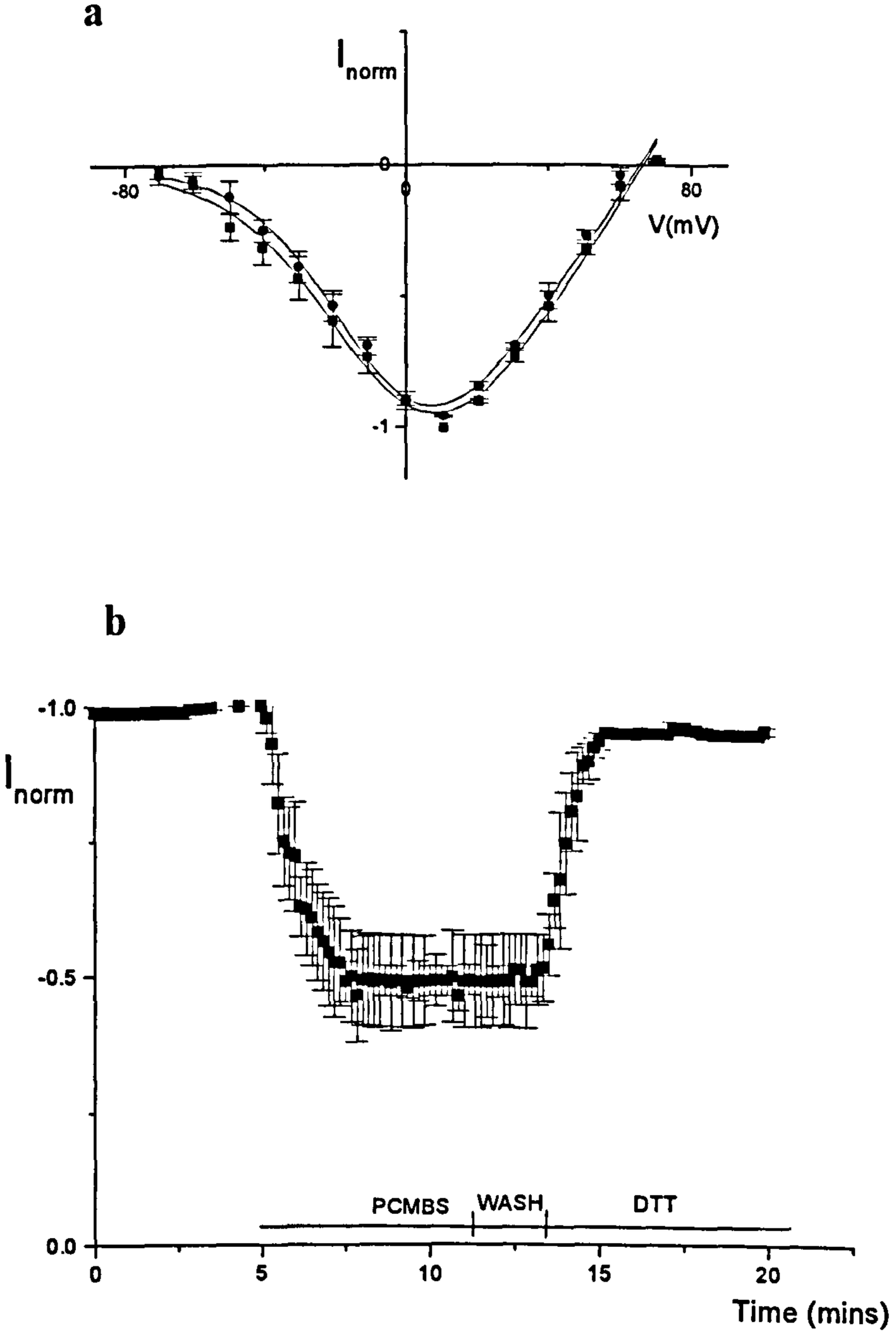

Fig. 6.15 Reversal of inhibition of V263C by PCMBS with dithiothreitol (DTT).

a, Normalised I/V curves are shown for mutant V263C before (■, n = 4) and after (●, n = 4) the application of both PCMBS and DTT. The current was normalised to the initial value (-1.16±0.07 μA).
b, Oocytes expressing the mutant V263C were held at -80mV and stepped to +10 mV repeatedly every 10 s. PCMBS (100μM) was applied for 6 mins, cells were then washed for 2 mins, and DTT (1mM) was applied as indicated. The mean current is shown for 4 oocytes. Current was normalised with respect to the first 5 mins of recording.

reaction that could be reversed by the reducing agent DTT. The nature of the proposed covalent reaction of PCMBS with a cysteine residue is shown in Fig. 6.16.

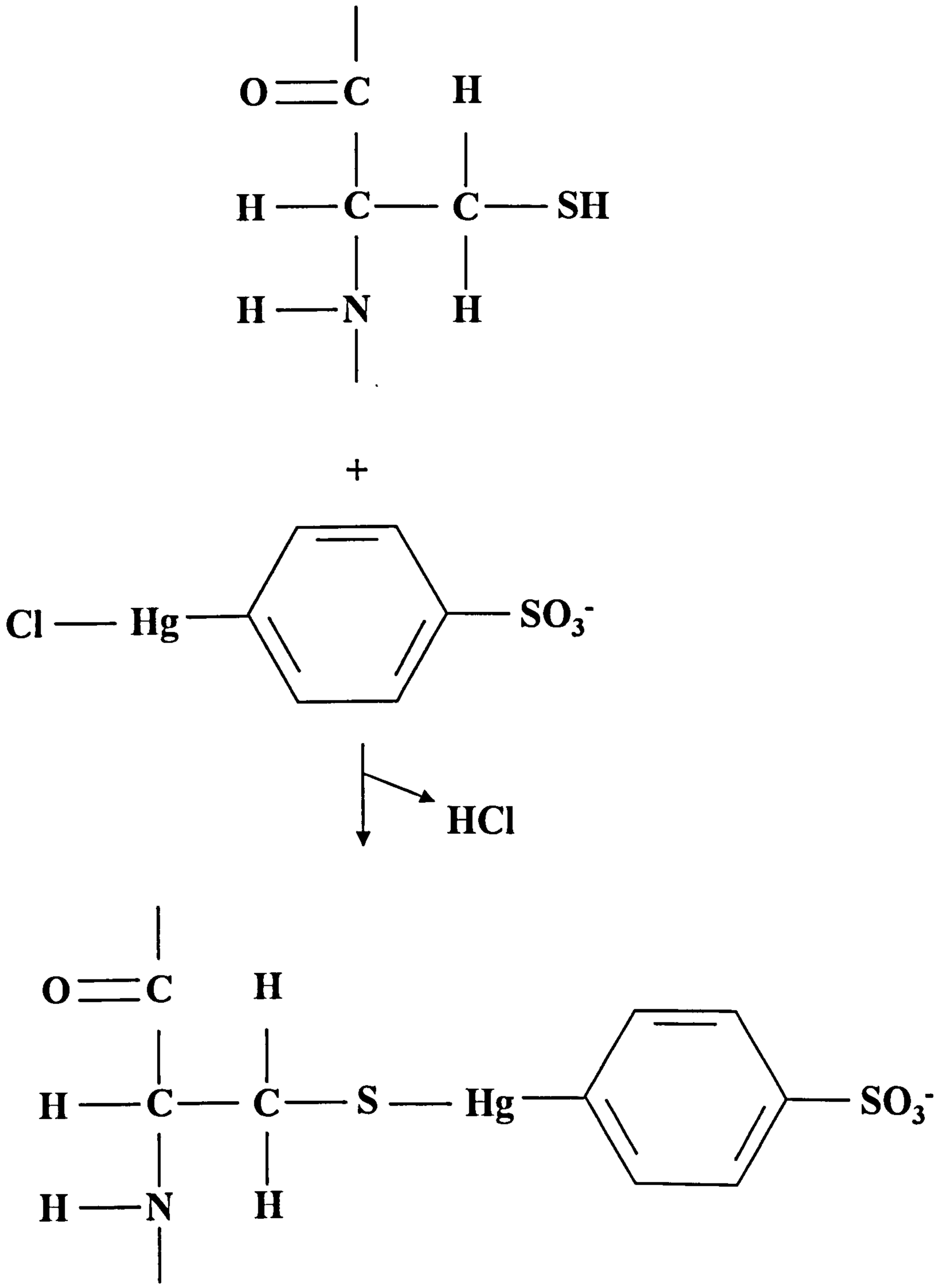

Fig. 6.16 Schematic diagram showing the modification of the side chain of a cysteine residue by the sulphydryl reagent PCMBS.
The membrane impermeable reagent PCMBS can oxidise the free sulphydryl (SH) group on the side chain of the cysteine to form a mixed disulphide and displace an HCl molecule.
Diagram taken from C. Milligan, PhD thesis (2000).

6.3 Discussion

In this chapter, the accessibility to PCMBS of cysteine residues introduced within the S4 segment in domain I of a CGGG calcium chimera was studied. This reagent is known to specifically bind with cysteines in an external solvent-accessible environment. The reaction of a PCMBS molecule with a cysteine molecule is shown schematically in Fig. 6.16.

PCMBS rapidly reduced calcium channel currents mediated by many of the cysteine mutants investigated in this chapter. The effect was shown to be reversible by the use of a reducing agent DTT, but not by washing, indicating specific covalent effects of the reagent on cysteines. The specific nature of this reaction is also indicated by the susceptibility of CGGG to PCMBS only after the introduction of additional cysteine residues.

The results obtained using PCMBS in this study are as follows. Wild type $Ca_v3.1$ and GCGG chimera did react with PCMBS when no additional cysteines were introduced. This was apparently due to non-conserved extracellular cysteines already being present. Indeed, in domain I of $Ca_v3.1$, three non-conserved cysteines are present in the extracellular loops, and one non-conserved cysteine is also present in domain II. In contrast, CGGG chimera (and wild type $Ca_v1.2$) did not react with PCMBS, suggesting that it is cysteines in domain I of $Ca_v3.1$ that react with PCMBS. The lack of susceptibility of CGGG chimera to PCMBS makes it suitable for cysteine accessibility studies with PCMBS. The chimera CGGG was high voltage activating like $Ca_v1.2$, and not low voltage activating like $Ca_v3.1$. It might therefore be assumed that the results shown in this chapter for chimera CGGG could also apply to domain I of the wild type $Ca_v1.2$.

Cysteine residues substituted into the domain I S4 of CGGG in place of V263, A265, L266 and A268 reacted when extracellular PCMBS was applied. In contrast, cysteines substituted in place of residues F269 and V271 did not confer susceptibility to PCMBS. This suggests that under depolarising conditions the S4 segment of domain I in CGGG chimera becomes exposed to the extracellular environment up to and including residue A268, with residues 269 and 271 remaining buried.

This is consistent with the findings of Yusaf *et al* (1996) who used a similar strategy to study the movement of S4 in the potassium *Shaker* channel with PCMBS as a probe. They determined that cysteine substitutions of L358, L361, V363, and L366, but not V367, S376, and G386, render the channel susceptible to extracellular PCMBS upon depolarisation, and so have established the extent of the S4 movement in the *Shaker* channel. Thus residue L366 in the *Shaker* channel represents the last residue of the S4 segment that is exposed, and sequence alignment of *Shaker* and CGGG sequences shows that A268 (in CGGG) and L366 (in *Shaker*) are equivalent (see Fig. 6.17). It can also be seen that the S4 segment is well conserved between the two channels. Taking the membrane boundary as in Gandhi *et al* (2002) (residue 361), this would correspond to an exposure of nine residues in the calcium channels.

However, as it is thought that the S4 lies within a water-filled crevice in potassium channels (e.g. Gandhi *et al* 2002), movement could be less than this, perhaps just up to V263, but certainly involving at least six residues. By comparison with the *Shaker* potassium channel, residues K264, R267, R270 and R273 of this calcium channel are likely to contribute to gating charge measurements when the S4 moves in the calcium channel.

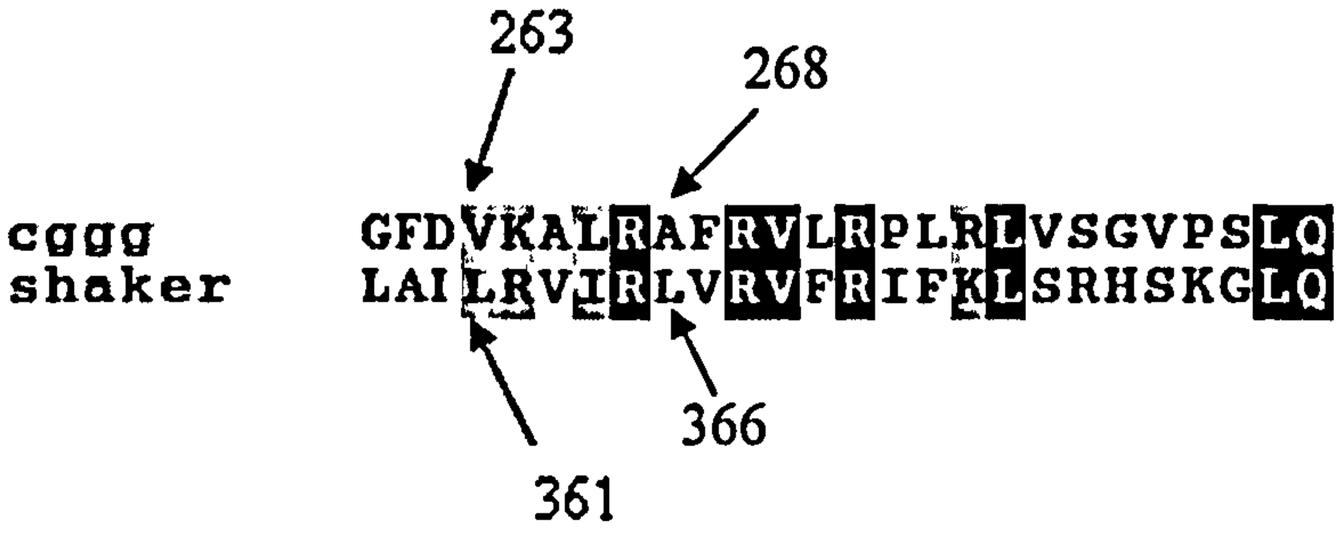

Fig. 6.17 Alignment of CGGG calcium chimera and *Shaker* potassium channel S4 domains.

Overall, it can be seen that the movement of the S4 region in this calcium channel chimera is comparable with that found in potassium channels. Results that we have found for domain I S4 movement in this high-voltage activating chimera may apply also to wild type $Ca_v1.2$; clearly it would also be of interest to

test S4 movement of $Ca_v1.2$ directly and indeed to test S4 movement in domains II, III and IV.

The accessibility to PCMBS of residue V263C was shown to depend upon membrane potential. Thus, whilst residue V263C remains buried in the membrane at very negative potentials, a depolarisation triggers its movement outwards to a position where it might react with PCMBS. The results clearly show an outward movement upon depolarisation to a degree less than that required for ionic flow. This data is consistent with measurements of gating currents of calcium channels, where gating currents occur at more negative potentials than for ionic currents (10mV for $Ca_v3.1$, and 30-40mV for $Ca_v1.2$). These results indicate that the voltage sensor moves at rather similar voltages independent of whether the calcium channel is low voltage activating or high voltage activating (Josephson, 1997, Neely *et al*, 1993, and Lacinova *et al*, 2002).

Two major conclusions can be made from this investigation. Firstly, in CGGG calcium channel chimera, depolarisation results in an outward movement of domain I S4 up to and including residue A268. Secondly, S4 movement has been shown to be voltage dependent, with movement shown at depolarised potentials. It is hoped that future studies will further enhance our understanding of these previously unreported movements of S4 segments within these calcium channels.

CHAPTER 7

SUMMARY OF CONCLUSIONS

7.1 Summary of conclusions

The main aims of this thesis were as follows: to identify key residues, or regions, responsible for the differing activation kinetics between rat and human Kv2.1 potassium channels, to determine how these residues or regions might interact, to determine an EM structure of rat Kv2.1, and to characterise movement of the calcium channel S4 region in response to changes in membrane potential.

The major conclusions to be drawn from these studies are as follows;

- **Chapter 3.** By point mutations and chimeras followed by electrophysiology experiments, it was found that residues in both the N- and C- termini of Kv2.1 potassium channels are important in determining activation kinetics. This is consistent with structural studies that suggest that residues 67 and 75 in the N-terminus appear to be in close proximity to the CTA domain in the C- terminus (residues 740-853).
- **Chapter 4.** GST interaction studies, Biacore surface plasma resonance, and FRET showed that the N- and C- termini of rat Kv2.1 appear to interact physically with each other, suggesting an obvious mechanism by which they could jointly influence reaction kinetics.
- **Chapter 5.** The necessary constructs were made in preparation for EM studies to produce a 3D protein structure. Further electron microscopy and single particle analysis by our collaborators should resolve the structure and thus help further our understanding of ion channel properties at the molecular level.
- **Chapter 6.** By using site directed mutagenesis of a chimeric calcium channel to introduce cysteine residues, S4 channel movement in response to depolarisation was studied using PCMBS. The extent of this movement appears to be similar to that found for potassium channels. S4 movement in this calcium

channel was also found to first occur at voltages considerably more negative than those required for ionic flow; again a similar property to that reported previously for potassium channels.

REFERENCES

References

Abraham, M.R., Jahangir, A., Alekseev, A.E., and Terzic, A. (1999). Channelopathies of inward rectifying potassium channels. *FASEB J.* **13**, 1901-1910.

Adair, B.D., Nunn, R., Lewis, S., Dukes, I.D., Phillipson, L., and Yeager, M. (2005). Structure of the human recombinant Kv2.1 channel at 1.9Å resolution. *Biophysical. J.* (Annual meeting abtracts), 19a

Albrecht, B., Lorra, C., Stocker, M., and Pongs, O. (1993). Cloning and characterization of a human delayed rectifier potassium channel gene. *Receptors and Channels*. **1**, 99-110.

Altier, C., Spaetgens, R.L., Nargeot, J., Bourinet, E., and Zamponi, G.W. (2001). Multiple structural elements contribute to voltage-dependent facilitation of neuronal alpha 1C ($Ca_v1.2$) L-type calcium channels. *Neuropharmacology*. **40**, 1050-1057.

Amberg, G.C., Rossow, C.F., Navedo, M.F., and Santana, L.F. (2004). NAFTc3 regulates Kv2.1 expression in arterial smooth muscle. *J. Biol. Chem.* **279**, 47326-47334.

Ashcroft, F.M. (2000). Ion channels and disease: Channelopathies. Academic Press, Orlando, Florida, USA.

Bauer, C.K., and Schwarz, J.R. (2001). Physiology of Eag K+ channels. *J. Mem. Biol.* **182**, 1-15.

Bentley, G.N., Brooks, M.A., O'Neill, C.A., and Findlay, J.B.C. (1999). Determinants of potassium channels assembly localised within the cytoplasmic C-terminal domain of Kv2.1. *Biochem. et Biophys. Acta*. **1418**, 176-184.

Bezanilla, F and Stefani E. (1994). Voltage-dependent gating of ionic channels. *Annu. Rev. Biophys. Biomol. Struct.* **23**, 819-846.

Bezanilla, F. (2000). The voltage sensor in voltage-dependent ion channels. *Physiol. Rev.* **80**, 555-592.

Bezanilla, F. (2002). Voltage sensor movements. *J. Gen. Physiol.* **120**, 465-473.

Bichet, D., Haass, F.A., and Jan, L.Y. (2003). Merging functional studies with structures of inward-rectifier K+ channels. *Nature. Rev. Neurosci.* **4**, 957-967.

Biel , M., Ruth, P., Bosse, E., Hullin, R., Stuhmer, W., Flockerzi, V., and Hofmann, F. (1990). Primary structure and functional expression of a high voltage activated calcium channel from rabbit lung. *FEBS Lett.* **269**, 409-412.

Bixby, K.A., Nanao, M.H., Shen, N.V., Kreusch, A., Bellamy, H., Pfaffinger, P.J., and Choe, S. (1999). Zn^{2+} binding and molecular determinants of tetramerization in voltage gated K^{+} channels. *Nat. Struc. Biol.* **6**, 38-43.

Broillet, M-C., and Firestein. (1997). β subunits of the olfactory cyclic nucleotide-gated channel form a nitric oxide activated Ca^{2+} channel. *Neuron.* **18**, 951-958.

Brown, D.A. (2000). Neurobiology: the acid test for resting potassium channels. *Curr. Biol.* **10**, R456-459.

Brunet, S., Aimond, F., Li, H., Guo, W., Eldstrom, J., Fedida, D., Yamada, K., and Nerbonne, J.M. (2004). Heterogeneous expression of repolarizing, voltage-gated K+ currents in adult mouse ventricles. *J. Physiol.* **559**, 103-120.

Carbone, E., and Lux, H.D. (1984). A low voltage-activated, fully inactivating Ca channel on vertebrate sensory neurones. *Nature*. **310**, 501-502.

Casamassima, M., D'Adamo, M.C., Pessia, M., and Tucker, S.J. (2003). Identification of a heteromeric interaction that influences the rectification, gating, and pH sensitivity of Kir4.1/Kir5.1 potassium channels. *J. Biol. Chem.* **278**, 43533-43540.

Catterall, W.A. (1995). Structure and function of voltage-gated ion channels. *Annu. Rev. Biochem.* **64**, 493-531.

Cha, A., Snyder, G.E., Selvin, P.R., and Bezanilla, F. (1999a). Atomic scale movement of the voltage-sensing region in a potassium channel measured via spectroscopy. *Nature*. **402**, 809-813.

Cha, A., Ruben, P.C., George Jr, A.L., Fujimoto, E., and Bezanilla, F. (1999b). Voltage sensors in domains III and IV, but not I and II, are immobilized by Na^+ channel fast activation. *Neuron.* **22**, 73-87.

Choe, S., Cushman, S., Baker, K.A., and Pfaffinger, P. (2002). Excitability is mediated by the T1 domain of the voltage-gated potassium channel. *Novartis Found. Symp.* **245**, 169-175.

Clapham, D.E. (2003). TRP channels as cellular sensors. *Nature*. **426**, 517-524.

Coma, M., Vicente, R., Tsevi, I., Grande, M., Tamkun, M.M., and Felipe, A. (2002). Different Kv2.1/Kv9.3 heteromer expression during brain and lung post-natal development in the rat. *J. Physiol. Biochem*. **58**, 195-203.

Consiglio, J.F., and Korn, S.J. (2004). Influence of permeant ions on voltage sensor function in the Kv2.1 potassium channel. *J. Gen. Physiol.* **123**, 387-400.

Cribbs, L.L., Lee, J-H., Yang, J., Satin, J., Zhang, Y., Daud, A., Barclay, J., Williamson, M.P., Fox, M., Rees, M., and Perez-Reyes, E. (1998). Cloning and characterization of α1H from human heart, a member of the T-type Ca2+ channel family. *Circ. Res*. **83**, 103-109.

Cushman, S.J., Nanao, M.H., Jhang, A.W., DeRubeis, D., Choe, S., and Pfaffinger, P.J. (2000). Voltage dependent activation of potassium channels is coupled to T1 domain structure. *Nat. Struc. Biol.* **7**, 403-407.

Dedek, K., and Waldegger, S. (2001). Colocalization of KCNQ1/KCNE channel subunits in the mouse gastrointestinal tract. *Eur. J. Physiol.* **442**, 896-902.

Deschenes, I., and Tomaselli, G.F. (2002). Modulation of Kv4.3 current by accessory subunits. *FEBS Lett.* **528**, 183-188.

Dirksen, R.T., Nakai, J., Gonzalez, A., Imoto, K., and Beam, K.G. (1997). The S5-S6 linker of repeat I is a critical determinant of L-type Ca2+ channel conductance. *Biophys. J.* **73**, 1402-9.

Dolly, J.O., and Parcej, D.N. (1996). Molecular properties of voltage-gated K+ channels. *J. Bioenerg. Biomem.* **28**, 231-253.

Doyle, D.A., Morais, C.J., Pfuetzner, R.A., Kuo, A., Gulbis, J.M., Cohen, S.L., Chait, B.T., and MacKinnnon, R. (1998). The structure and function of the potassium channel: molecular basis of K conduction and selectivity. *Science.* **280**, 69-77.

Doyle, D.A. (2004). Strutural themes in ion channels. *Eur. Biophys. J.* **33**, 175-179.

Drewe, J.A., Verma, S., Frech, G., and Joho, R.H. (1992). Distinct spatial and temporal expression patterns of K+ channel mRNAs from different subfamilies. *J. Neurosci.* **12**, 538-548.

Drysdale, R., Warmke, J., Kreber, R., and Ganetzky, N. (1991). Molecular characterization of eag: A gene affecting potassium channels in *Drosophila melanogaster*. *Genetics.* **127**, 497-505.

Dumont, J. N. (1972). Oogenesis in Xenopus laevis. *Journal of Morphology* **136, 153-179.**

Ellinor, P.T., Yang, J., Sather, W.A., Zhang, J.F., and Tsien, R.W. (1995). Ca2+ channel selectivity at a single locus for high-affinity Ca2+ interactions. *Neuron.* **15, 1121-1132.**

Fedida, D., and Hesketh, J.C. (2001). Gating of voltage-dependent potassium channels. *Prog. Biophs. Mol. Biol.* **75,** 165-199.

Frech, G.C., VanDongen, M.J., Shuster, G., Brown, A.M., and Joho, R.H. (1989). A novel potassium channel with delayed rectifier properties isolated from rat brain by expression cloning. *Nature*. **340,** 642-645.

Gandhi, C.S., and Isacoff, E.Y. (2002). Molecular models of voltage sensing. *J. Gen. Physiol.* **120,** 455-463.

Garcia, J., Nakai, J., Imoto, K., and Beam, K.G. (1997). Role of S4 segments and the leucine heptad motif in the activation of an L-type calcium channel. *Biophys. J.* **72,** 2515-2523.

Glauner, K.S., Mannuzzu, L.M., Gandhi, C.S., and Isacoff, E.Y. (1999). Spectroscopic mapping of voltage sensor movement in the *Shaker* potassium channel. *Nature*. **402,** 813-817.

Gudermann, T., and Flockerzi, V. (2005). TRP as new pharmacological targets. *Naunyn-Sch Arch Pharmacol.* [pub ahead of print].

Guida, S., Trettel, F., Pagnutti, S., Mantuano, E., Tottene, A., Veneziano, L., Fellin, T., Spadaro, M., Stauderman, K., Williams, M., Volson, S., Ophoff, H., Frants, R., Jodice, C., Frontali, M., and Pietrobon, D. (2001). Complete loss of P/Q calcium activity caused by a CACNA1A missense mutation carried by patients with episodic ataxia type 2. *Am. J. Hum. Genet*. **68,** 759-764.

Gulbis, J.M., Zhou, M., Mann, S., and MacKinnon, R. (2000). Strcucture of the cytoplasmic β subunit T1 assembly of voltage dependent K+ channels. *Science*, 289, 123-127.

Heginbotham, L., LeMasurier, M., Kolmakova-Partensky, L., and Miller, C. (1999). Single *Streptomyces lividans* : K+ channels functional asymmetries and sideness of proton activation. *J. Gen. Physiol.* 114, 551-559.

Hille, B. (2001). Ion channels of excitable membranes (Third edition). Sinauer Associates, Inc. Sunderland, Massachusetts, USA.

Hoda, J.C., Zaghetto, F., Koschak, A., and Striessnig, J. (2005). Congenital stationary night blindness type 2 mutations S229P, G369D, L1068P, and W1440X alter channel gating or functional expression of $Ca_v1.4$ L-type Ca2+ channels. *J. Neurosci.* 25, 252-9.

Hodgkin, A.L., and Huxley, A.F. (1952). A quantitative description of membrane current and its application to conduction and excitation in nerve. *J. Physiol. (Lond)* 117, 500-544.

Hofmann, F., Lacinova, L., and Klugbauer, N. (1999). Voltage-dependent calcium channels: from structure to function. *Rev. Physiol. Biochem. Pharmacol.* 139, 33-89.

Hopkins, W.F., Demas, V., and Tempel, B.L. (1994). Both N- and C-terminal regions contribute to the assembly and functional expression of homo and heteromultimeric voltage-gated K+ channels. *J. Neurosci.* 14, 1385-1393.

Horton, R.M., Hunt, H.D., Ho, S.N., Pullen, J.K., and Pease, L.R. (1989). Engineering hybrid genes without the use of restriction enzymes, gene splicing by overlap extension. *Gene (Amst).* 77, 61-68.

Hulme, J.T., Konoki , K., Lin , T.W-C., Gritsenko , M.A., Camp, D.G., Bigelow , D.J., and William A. Catterall. (2005). Sites of proteolytic processing and

noncovalent association of the distal C-terminal domain of $Ca_v1.1$ channels in skeletal muscle. *PNAS.* **102,** 5274-5279.

Islas, L.D., and Sigworth, F.J. (1999). Voltage sensitivity and gating charge in *Shaker* and Shab family potassium channels. *J. Gen. Physiol.* **114,** 723-741.

Jiang, Q-X., Wang, D-N., and MacKinnon, R. (2004). Electron microscope analysis of KvAP voltage-dependent K+ channels in an open conformation. *Nature.* **430,** 806-810.

Jiang, Y., Lee, A., Chen, J., Cadene, M., Chait, B.T., and MacKinnon, R. (2002). Crystal structure and mechanism of a calcium-gated potassium channel. *Nature.* **417,** 515-522.

Jiang, Y., Lee, A., Chen, J., Cadene, M., Chait B.T., and MacKinnon, R. (2002b). The open pore conformation of potassium channels. *Nature.* **417,** 523-526.

Jiang, Y., Lee, A., Chen, J., Ruta, V., Cadene, M., Chait, B. T., and MacKinnon, R. (2003). X-ray structure of a voltage-dependent K+ channel. *Nature.* **423,** 33-41.

Jones, P.A., Tucker, S.J., and Ashcroft, F.M. (2001). Muliple sites of interaction between the intracellular domains of an inwardly recifying potassium channel, Kir6.2. *FEBS Letts.* **508,** 85-89.

Josephson, I.R. (1997). Kinetic components of the gating currents of human cardiac L-type Ca^{2+} channels. *Pflugers Arch.* **433,** 321-329.

Ju M., Stevens, L., Leadbitter, E., and Wray, D. (2003). The roles of N- and C-terminal determinants in the activation of the Kv2.1 potassium channel. *J. Biol. Chem.* **278,** 12769-12778.

Kamb, A., Iverson, L.E., and Tanouye, M.A. (1987). Molecular characterization of *Shaker*, a Drosophila gene that encodes a potassium channel. *Cell*. **50**, 405-413.

Kaupp, U.B., Niidome, T., Tanbe, T., Terada, S., Bonigk, W., Stuhmer, W., Cook, N.J., Kangawa, K., Matsuo, M., Hirose, T., Myata, T., and Numa, S. (1989). Primary structure of the rod receptor cyclic GMP-gated channel. *Nature*. **342**, 762-766.

Kaupp, U.B. (1995). Family of cyclic nucleotide gated ion channels. *Curr. Opin. Neurobiol.* **5**, 434-442.

Kerschensteiner, D., Monje, F., and Stocker, M. (2003). Structural determinants of the regulation of the voltage gated potassium channel Kv2.1 by the modulatory alpha subunit Kv9.3. *J. Biol. Chem*. **278**, 18154-18161.

Ketchum, K.A., Joiner, W.J., Sellers, A.J., Kaczmarek, L.K., and Goldstein, S.A.N. (2002). A new family of outwardly rectifying potassium channel proteins with two pore domains in tandem. *Nature*. **376**, 690-695.

Kharkovets, T., Hardelin, J-P., Safieddine, S., Schweizer, M., El-Amraoui, A., Petit, C., and Jentsch, T.J. (2000). KCNQ4, a K+ channel mutated in a form of dominant deafness, is expressed in the inner ear and the central auditory pathway. *PNAS*. **97**, 4333-4338.

Klugbauer, N., Marais, E., Lacinova, L., and Hofmann, F. (1999). A T-type calcium channel from mouse brain. *Pflugers Arch*. **437**, 710-715.

Kobertz, W.R., and Miller, C. (1999). K+ channels lacking the tetramerization domain: implications for pore structure. *Nat. Struc. Biol.* **6**, 1122-1125.

Kobertz, W.R., Williams, C., and Miller, C. (2000). Hanging gondola structure of the T1 domain in a voltage gated K+ channel. *Biochem*. **39**, 10347-10352.

Koopmann, R., Benndorf, K., Lorra, C., and Pongs, O. (1997). Functional differences of a Kv2.1 channel and a Kv2.1/Kv1.2 S4-chimera are confined to a concerted shift of various gating parameters. *Receptors Channels* **5**, 15-28.

Koopmann, R., Scholle, A., Ludwig, J., Leicher, T., Zimmer, T., Pongs, O., and Benndorf, K. (2001). Role of the S2 and S3 segment in determining the activation kinetics in Kv2.1 channels. *J. Membr. Biol.* **182**, 49-59.

Kreusch, A., Pfaffinger, P.J., Stevens, C.F., and Choe, S. (1998). Crystal structure of the tetramerization domain of the *Shaker* potassium channel. *Nature.* **392**, 945-948.

Kunkel, T.A., Roberts, J.D., Zakour, R.A. (1987). Rapid and efficient site-directed mutagenesis without phenotypic selection. *Methods Enzymol.* **154**, 367-382.

Kuo, A., Gulbis, J.M., Antcliff, J.F., Rahman, T., Lowe, E.D., Zimmer, J., Cuthbertson, J., Ashcroft, F.M., Ezaki, T., and Doyle, D.A. (2003). Crystal structure of the potassium channel KirBac1.1 in the closed state. *Science.* **300**, 1922-1926.

Lacinova, L., Klugbauer, N., and Hofmann, F. (1999). Absence of modulation of the expressed calcium channel alpha subunit by alpha2delta subunits. *J. Physiol.* **516**, 639-645.

Lacinova, L., Klugbauer, N., and Hofmann, F. (2002). Gating of the expressed $Ca_v3.1$ calcium channel. *FEBS Lett.* **531**, 235-240.

Lambert, R.C., Maulet, Y., Mouton, J., Beattie, R., Volsen, S., De Waard, M., and Feltz, A. (1997). T-type Ca2+ current properties are not modified by Ca2+ channel beta subunit depletion in nodosus ganglion neurons. *J. Neurosci.* **17**, 6621-6628.

Larsson, H.P., Baker, O.S., Dhillon, D.S., and Isacoff, E.Y. (1996). Transmembrane movement of the *Shaker* K+ channel S4. *Neuron.* **16,** 387-397.

Leadbitter, E.L. (2002). Activation properties of human and rat forms of a voltage gated potassium channel. (Thesis).

Lee, C.W., Kim, S., Roh, S.H., Endoh, H., Kodera, Y., Maeda, T., Kohno, T., Wang, J.M., Swartz, K.J., and Kim, J.I. (2004). Solution structure and functional characterization of SGtx1, a modifier of Kv2.1 channel gating. *Biochem.* **43,** 890-897.

Lee, J-H., Daud, A.N., Cribbs, L.L., Lacerda, A.E., Pereverzev, A., Klockner, U., Schneider, T., and Peres-Reyes, E. (1999). Cloning and expression of a novel member of the low voltage activated T-type calcium channel family. *J. Neurosci.* **19,** 1912-1921.

Li, J., Stevens, L., and Wray, D. (2004). Roles of molecular regions in determining differences between voltage dependence of activation of $Ca_v3.1$ and $Ca_v1.2$ calcium channels. *J. Biol. Chem.* **279,** 26858-26867.

Liman, E.R., Hess, P, Weaver, F., and Koren, G. (1991). Voltage sensing residues in the S4 region of a mammalian K+ channel. *Nature.* **353,** 752-756.

Lipscombe, D., Helton, T.D., and Xu, W. (2004). L-type calcium channel: the low down. *J. Neurophysiol.* **92,** 2633-2641.

Llinas, R., Sugimori, M., Lin, J.W., and Cherksey, B. (1989). Blocking and isolation of a calcium channel from neurons in mammals and cephalopods utilizing a toxin fraction (FTX) from funnel-web toxin. *PNAS.* **86,** 1689-1693.

Logothetis, D.E., Movahedi, S., Slater, C., Lindpainter, K., and Nadal-Ginard, B. (1992). Incremental reduction of positive charge within the S4 region of a voltage-gated K^+ channel result in corresponding decreases in gating charge. *Neuron.* **8,** 531-540.

Ludwig, J., Weseloh, R., Karschin, C., Liu, Q., Netzer, R., Engeland, B., Stnsfeld, C., and Pongs, O. (2000). Cloning and functional expression of rat eag2, a new member of the ether-a-go-go family of potassium channels and comparison of its distribution with that of eag1. *Mol. Cell. Neurosci.* **16**, 59-70.

McCrossan, Z.A., Lewis, A., Panaghie, G., Jordan, P.N., Christini, D.J., Lerner, D.J., and Abbot, G.W. (2003). MinK-related peptide 2 modulates Kv2.1 and Kv3.1 potassium channels in mammalian brain. *J. Neurosci.* **23**, 8077-8091.

MacKinnon, R. (1991). Determination of the subunit stoichiometry of a voltage-activated potassium channel. *Nature*. **350**, 232-235.

MacKinnon, R. (2003). Potassium channels. *FEBS Letts*. **555**, 62-65.

McRory, J.E., Santi, C.M., Hamming, S.C., Mezeyova, J., Sutton, K.G., Baillie, D.L., Stea, A., and Snutch, T.P. (2001). Molecular and functional characterization of a family of rat brain T-type calcium channels. *J. Biol. Chem.* **276**, 3999-4011.

Michaelevski, I., Chikvashvili, D., Tsuk, S., Singer-Lahat, D., Kang, Y., Linial, M., Gaisano, H.Y., Fili, O., and Lotan, I. (2003). Direct Interaction of target SNAREs with Kv2.1 channel. *J. Biol. Chem*. **278**, 34320-34330.

deMiera, E.C.V-S. (2004). Modification of Kv2.1 currents by the silent Kv10 subunits. *Mol. Brain Res*. **123**, 91-103.

Mikami, A., Imoto, K., Tanabe, T., Niidome, T., Mori, Y., Takeshima, H., Narumiya, S., and Numa, S. (1989). Primary structre and functional expression of the cardiac dihydropyridine-sensitive calcium channel. *Nature*. **340**, 230-233.

Milligan, C. J. (2000). Sulphydyl reagents and potassium channels (Thesis).

Milligan, C.J., and Wray D. (2000). Local movement in the S2 region of the voltage-gated potassium channel hKv2.1 studies using cysteine mutagenesis. *Biophys. J.* 8, 1852-1861.

Minke, B. (1977). Drosophila mutant with a transducer effect. *Biophys. Struct. Mech.* 3, 59-64.

Minor, D.L.Jr., Lin, Y-F., Mobley, B.C., Avelar, A., Jan, Y.N., Jan, L.Y., and Berger, J.M. (2000). The polar T1 interface is linked to conformational changes that open the voltage gated potassium channel. *Cell.* **102**, 657-670.

Minor, D.L. Jr. (2001). Potassium channels: life in the post-structural world. *Curr. Opin. Struct. Biol.* **11**, 408-414.

Misonou, H., Mohapatra, D.P., Park, E.W., Leung, V., Zhen, D., Misonou, K., Anderson, A.E., and Trimmer, J.S. (2004). *Nature neurosci.* **7**, 711-718.

Mitterdorfer, J., Grabner, M., Kraus, R.L., Hering, S., Prinz, H., Glossman, H., and Striessnig, J. (1998). Molecular basis of drug interaction with L-type Ca2+ channels. *J. Bioenerg. Biomembr.* 30, 319-334.

Monteil, A., Chemin, J., Leuranguer, V., Altier, C., Mennessier, G., Bourinet, E., Lory, P., and Nargeot, J. (2000). Specific properties of T-type calcium channels generated by the human α1I subunit. *J. Biol. Chem.* **275**, 16530-16535.

Monteil, A., Chemin, J., Bourinet, E., Mennessier, G., Lory, P., and Nargeot, J. (2000b). Molecular and functional properties of α1G subunit that forms T-type calcium channels. *J. Biol. Chem.* **275**, 6090-6100.

Monticelli, L., Robertson, K.M., MacCallum, J.L., and Tieleman, D.P. (2004). Computer simulation of the KvAP voltage-gated potassium channel: steered molecular dynamics of the voltage sensor. *FEBS Letts.* **564**, 325-332.

Murakoshi, H., Shi, G., Scannevin, R.H., and Trimmer, J.S. (1997). Phosphorylation of the Kv2.1 K+ channel alters voltage-dependent activation. *Mol. Pharmacol.* **52**, 821-828.

Neely, A., Wei, X., Olcese, R., Birnbaumer, L., and Stefani, E. (1993). Potentiation by the β subunit of the ratio of the ionic current to the charge movement in the cardiac calcium channel. *Science*. **262**, 575-578.

Nichols, C.G., and Lopatin, A.N. (1997). Inward Rectifier potassium channels. *Annu. Rev. Physiol.* **59**, 171-191.

Nilius, B., Hess, P., Lansman, J.B., and Tsien, R.W. (1985). A noveL- type of cardiac calcium channel in ventricular cells. *Nature.* **316**, 443-446.

Nishida, M., and MacKinnon, R. (2002). Structural basis of inward rectification: cytoplasmic pore of the G protein-gated inward rectifier GIRK1 at 1.8 Å resolution. *Cell.* **111**, 957-965.

Nowycky, M.C., Fox, A.P., and Tsien, R.W. (1985). Three types of neuronal calcium channel with different calcium agonist sensitivity. *Nature*. **316**, 440-443.

Orlova, E.V., Papakosta, M., Booy, F.P., van Heel, M., and Dolly, J.O. (2003). Voltage-gated K+ channel from mammalian brain: 3D structure at 18Å of the complete $(\alpha)_4(\beta)_4$ complex. *J. Mol. Biol.* **326**, 1005-1012.

Padinjat, R., and Andrews, S. (2004). TRP channels at a glance. *J. Cell. Sci.* **117**, 5707-5709.

Pak, M.D., Vovarrubias, M., Radcliffe, A., and Salkoff, L. (1991). A mouse brain homolog of the drosophila shab K+ channel with conserved delayed-rectifier properties. *J. Neurosci.* **11**, 869-880.

Pal, S., Hartnett, K.A., Nerbonne, J.M., Levitan, E.S., and Aizenman, E. (2003). Mediation of neuronal apoptosis by Kv2.1-encoded potassium channels. *J. Neurosci.* **23**, 4798-4802.

Papazian, D.M., Timpe, L.C., Jan, Y.N., and Jan, L.N. (1991). Alteration of voltage-dependence of *Shaker* potassium channel by mutations in the S4 sequence. *Nature*. **349**, 305-310.

Papazian, D.M., Shao, X.M., Seoh, S.A., Mock, A.F., Huang, Y., and Wainstock, D. (1995). Electrostatic interactions of S4 voltage sensor in *Shaker* K+ channel. *Neuron.* **14**, 1293-1301.

Pascual, J.M., Shieh, C-C., Kirsch, G.E., and Brown, A.M. (1997). Contribution of the NH2 terminus of Kv2.1 to channel activation. *Am. J. Cell Physiol.* **273**, C1849-C1858.

Patel, A.J., Lazdunski, M., and Honore, E. (1997). Kv2.1/Kv9.3, a novel ATP-dependent delayed-rectifier K+ channel in oxygen-sensitive pulmonary artery myocytes. *EMBO J.* **16**, 6615-6625.

Perez-Reyes, E., Cribbs, L.L., Daud, A., Lacerda, A.E., Barclay, J., Williamson, M.P., Fox, M., Rees, M., and Lee, J.H. (1998). Molecular characterization of a neuronal low-voltage activated type calcium channel. *Nature*. **391**, 896-900.

Perez-Reyes, E. (2003). Molecular physiology of low-voltage-activated T-type calcium channels. *Physiol. Rev.* **83**, 117-161.

Planells-Cases, R., Ferrer-Mintiel, A.V., Patten, C.D., and Montal, M. (1995). Mutation of conserved negatively charged residues in the S2 and S3 transmembrane segments of a mammalian K+ channel selectively modulates gating. *PNAS.* **92**, 9422-9426.

Qin, D., Huang, B., Deng, L., El-Adawi, H., Ganguly, K., Sowers, J.R., and El-Sherif, N. (2001). Downregulation of K(+) channel genes expression in type I diabetic cardiomyopathy. *Biochem. Biophys. Res. Commun.* **283**, 549-553.

Qu, Y., Baroudi, G., Yue, Y., El-Sherif, N., and Boutjdir, M. (2005). Localization and modulation of {alpha}1D ($Ca_v1.3$) L-type Ca channel by protein kinase A. *Am. J. Physiol. Heart Circ. Physiol.* **288**, H2123-30.

Robbins, J. (2001). KCNQ potassium channels: physiology, pathphysiology, and pharmacology. *Pharm. & Thera.* **90**. 1-19.

Roberts, S.K. (2003). TOK homologue in *Neurospora crassa*: first cloning and functional characterization of an ion channel in a filamentous fungus. *Euk. Cell.* **2**, 181-190.

Ruby, B., and McBain, C.J. (2001). Kv3 channels: voltage-gated K+ channels designed for high-frequency repetitive firing. *Trends Neurosci.* **24**, 517-526.

Saada N., Dai, B., Echetebu, C., Sarna, S.K., and Palade, P. (2003). Smooth muscle uses another promoter to express primarily a form of human $Ca_v1.2$ L-type calcium channel different from the principal heart form. *Biochem. Biophys. Res. Commun.* **302**, 23-8.

Salinas, M., de Weille, J., Guillemare, E., Lazdunski, M, and Hugnot, J.P. (1997). Modes of regulation of shab K+ channel activity by the Kv8.1 subunit. *J. Biol. Chem.* **272**, 8774-8780.

Salkoff, L. and Jegla, T. (1995). Surfing the DNA databases for K+ channels nets yet more diversity. *Neuron.* **15**, 489-492.

Sanguinetti, M.C., Curran, M.E., Zou, A., Shen, J., Spector, P.S., Atkinson, D.L., and Keating, M.T. (1996). Coassembly of K(V)LQT1 and minK (IsK) proteins to form cardiac I(Ks) potassium channel. *Nature.* **384**, 80-83.

Sambrook, J., Fritish, E.F., and Maniatis, T. (1989). Molecular Cloning – A laboratory manual (Second Edition). Cold Spring Harbour Press, Cold Spring Harbour.

Sano, Y., Mochizuki, S., Miyake, A., Kitada, C., Inamura, K., Yokoi, I., Nozawa, K., Matsushime, H., and Furuichi, K. (2002). Molecular cloning and characterization of Kv6.3, a novel modulatory subunit for voltage-gated K(+) channel Kv2.1. *FEBS Lett.* **512**, 230-234.

Sato, K., Raymond, C., Martin-Moutot, N., Saski, T., Ohtake, A., Minami, T., Van Renterghem, C., Takahashi, M., and Seagar, M.J. (2000). Binding of six chimeric analogs of omega-conotoxin MVIIA and MVIIC to N- and P/Q-type calcium channels. *Biochem. Biophys. Res. Commun.* **269**, 254-256.

Scholle, A., Koopmann, R., Leicher, T., Ludwig, J., Pongs, O., and Benndorf, K. (2000). Structural elements determining activation kinetics in Kv2.1. *Receptors channels*. **7**, 65-75.

Scholle, A., Zimmer, T., Koopmann, R., Engleland, B., Pongs, O., and Benndorf, K. (2004). Effects of Kv2.1 intracellular regions on activation of Kv2.1 channels. *Biophys. J.* **87**, 873-882.

Schulteis, C.T., Nagaya, N., and Papazian, D.M. (1996). Intersubunit interaction between amino- and carboxyl- terminal cysteine residues in tetrameric *Shaker* K+ channels. *Biochem.* **35**, 12133-12140.

Schultz, D., Mikala, G., Yatani, A., Engle, D.B., Illes, D.E., Segers, B., Sinke, R., Weghuis, D.O., Klockner, U., Wakamori, M., Wang, J-J., Melvin, D., Varadi, G., and Schwartz, A. (1993). Cloning, chromosomal localization, and functional expression of the alpha1 subunit of the L-type voltage-dependent calcium channel from normal human heart. *PNAS.* **90**, 6228-6232.

Schultz, J.H., Volk, T., and Ehmke, H. (2001). Heterogeneity of Kv2.1 mRNA expression and delayed recifier current in single isolated myocytes from rat left ventricle. *Circ. Res.* **88**, 438-490.

Seoh, S.A., Sigg, D., Papazian, D.M., and Bezanilla, F. (1996). Voltage sensing residues in the S2 and S4 segments of the *Shaker* K+ channel. (1996). *Neuron.* **16**, 1159-1167.

Shao, X.M., and Papazian, D.M. (1993). S4 mutations alter the single channel gating kinetics of *Shaker* K^+ channel. *Neuron.* **11**, 343-352.

Sharma, N., D'Arcangelo, G., Kleinlaus, A., Halegoua, S., and Trimmer, J.S. (1993). Nerve growth factor regulates the abundance and distribution of K+ channels in PC12 cells. *J. Cell Biol.* **123**, 1835-1843.

Sheets, M.F., and Hanck, D.A. (2002). The outermost lysine in the S4 of domain III contributes little to the gating charge in sodium channels. *Biophys. J.* **82**, 3048-3055.

Shi, G., and Trimmer, J.S. (1999). Differential asparagines-linked glycosylation of voltage-gated K^+ channels in mammalian brain and in transfected cells. *J. Membrane Biol.* **168**, 265-273.

Shi, G., and Soldatov, N.M. (2002). Molecular determinants of voltage-dependent slow inactivation in the Ca2+ channel. *J. Biol. Chem.* **277**, 6813-6821.

Shieh, C-C., Klemic, K. G., and Kirsch, G.E. (1997). Role of the transmembrane segement S5 on gating of voltage-dependent K+ channels. *J. Gen. Physiol.* **109**, 767-778.

Shrivastava, I.H., Durell, S.R., and Guy, H.R. (2004). A model of voltage gating developed using the KvAP channel crystal structure. *Biophys. J.* **87**, 2255-2270.

Sidach, S.S., and Mintz, I.M. (2000). Low-affinity blockade of neuronal N-type Ca channels by the spider toxin omega-agatoxin-IVA. *J. Neurosci.* **20**, 7174-7182.

Sirois, J.E., Lei, Q., Talley, E.M., Lynch, C., and Bayliss, D.A. (2000). The TASK-1 two pore domain K+ channel is a molecular substrate for neuronal effects of inhalation anesthetics. *J. Neurosci.* **20**, 6347-6354.

Snutch, T.P., Tomlinson, W.J., Leonard, J.P., and Gilbert, M.M. (1991). Distinct calcium channels are generated by alternative splicing and are differentially expressed in the mammalian CNS. *Neuron*. **7**, 45-57.

Sokolova, O., Kolmakova-Partensky, L., and Grigorieff, N. (2001). Three-dimensional structure of a voltage gated potassium channel at 2.5nm resolution. *Structure*. **9**, 215-220.

Sokolova, O., Accardi, A., Gutierrez, D., Lau, A., Rigney, M., and Gigorieff, N. (2003). Conformational changes in the C terminus of *Shaker* K+ channel bound to the rat Kvβ2-subunit. *PNAS*. **100**, 12607-12612.

Sokolova, O. (2004). Structure of cation channels, revealed by single particle electron microscopy. *FEBS Lett*. **564**, 251-256.

Talavera, K., Janssens, A., Klugbauer, N., Droogmans, G., and Nilius, B. (2003). Pore structure influences gating properties of the T-type Ca2+ channel alpha 1G. *J. Gen. Physiol*. **121**, 529-540.

Tsien, R.W., Ellinor, P.T., and Horne, W.A. (1991). Molecular diversity of voltage-dependent Ca2+ channels. *Trends Parmacol. Sci*. **12**, 349-354.

Tsuk, S., Michaelevski, I., Bentley, G.N., Joho, R.H., Chikvashvili, D., and Lotan, I. (2004). Kv2.1 channel activation and inactivation is influenced by physical interactions of both syntaxin 1A and the t-SNARE complex with the C-terminus of the channel. *Mol. Pharmacol*. **3**, [ahead of print].

VanDongen, A.M.J., Frech, G.C., Drewe, J.A., Joho, R.H., and Brown, A.M. (1990). Alteration and restoration of K+ channel function by deletions at the N- and C-termini. *Neuron.* **5**, 433-443.

Vergara, C., Latorre, R., Marrion, N.V., and Adelman, J.P. (1998). Calcium activated potassium channels. *Curr. Opin. Neurobiol.* **8**, 321-329.

Wang, Q., Curran, M.E., Splawski, I., Burn, T.C., Millholland, J.M., VanRaay, T.J., Shen, J., Timothy, K.W., Vincent, G.M., de Jager, T., Svhwartz, P.J., Toubin, J.A., Moss, A.J., Atkinson, D.L. Landes, G.M., Connors, T.D., and Keating, M.T. (1996). Positional Cloning of a novel potassium channel gene: KVLQT1 mutations cause cardiac arrhythmias. *Nat. Genet.* **12**, 17-23.

Wei, X., Neely, A., Lacerda, A.E., Olcese, R., Stefani, E., Perez-Reyes, E., and Birnbaumer, L. (1994). Modification of Ca2+ activity by deletions at the carboxyl terminus of the cardiac alpha 1 subunit. *J. Biol. Chem.* **269**, 1635-1640.

Wes, P.D., Chevesich, J., Jeromin, A., Rosenberg, C., Stetten, G., and Montell, C. (1995). TRPC1, a human homolog of a Drosophila store-operated channel. *PNAS.* **92**, 9652-9656.

Westenbroek, R.E., Anderson, N.L., and Byers, M.R. (2004). Altered localization of $Ca_v1.2$ (L- type) calcium channels in nerve fibers, schwann cells, ondontoblasts, and fibroblasts of tooth pulp after tooth injury. *J. Neurosci. Res.* **75**, 371-383.

Wilson, G.G., O'Neill, C.A., Sivaprasadarao, A., Findlay, J.B., and Wray, D. (1994). Modulation by protein kinase A of a cloned rat brain potassium channel expressed in Xenopus oocytes. *Pflugers Arch.* **428**, 186-193.

Wong, W.H., Hurley, K.M., and Eatock, R.A. (2004). Differences between the negatively activating potassium conductance of mammalian cochlear and vestibular hair cells. *JARO.* **5**, 270-284.

Wu, S.N. (2003). Large-conductance Ca2+- activated K+ channels: physiological role and pharmacology. *Curr. Med. Chem.* **10**, 649-661.

Yamada, Y., Chen, X., Kobayashi, T., Kamada, Y., Nagashima, M., Tsutsuura, M., Seki, S., Yamakage, M., Namiki, A., and Tohse, N. (2002). A truncated splice variant of KCNQ1 cloned from rat heart. *Biochem. Biophys. Res. Comm.* **294**, 199-204.

Yan, L., Figueroa, D.J., Austin, C.P., Liu, Y., Bugianesi, R.M., Slaughter, R.S., Kaczorowski, G.J., and Kohler, M.G. (2004). Expression of voltage-gated potassium channels in human and rhesus pancreatic islets. *Diabetes*. **53**, 597-607.

Yan, R-T., and Maloney, P.C. (1993). Identification of a residue in the translocation pathway of a membrane carrier. *Cell.* **75**, 37-44.

Yang, J., Ellinor, P.T., Sather, W.A., Zhang, J.F., and Tsien, R.W. (1993). Molecular determinants of Ca2+ selectivity and ion permeation in L-type Ca2+ channels. *Nature.* **366**, 158-61.

Yang, W-P., Levesque, P.C., Little, W.A., Conder, M.L., Ramakrishnan, P., Neubauer, M.G., and Blanar, M.A. (1998). Functional expression of two KvLQT1-related potassium channels responsible for an inherited idiopathic epilepsy. *J. Biol. Chem.* **273**, 19419-19423.

Yost, C.S. (1999). Potassium channels: Basic aspects, functional roles, and medical significance. *Anaesthesiol.* **90**, 1186-1203.

Yus-Najera, E., Munoz, A., Salvador, N., Jensen, B.S., Rasmussen, H.B., Defelipe, J., and Villarroel, A. (2003). Localization of KCNQ5 in the normal and epileptic human temporal neocortex and hippocampal formation. *Neurosci.* **120**, 353-364.

Yusaf, S.P., Wray, D., and Sivaprasadarao, A. (1996). Measurement of the movement of the S4 segment during the action of a voltage-gated potassium channel. *Eur. J. Physiol.* **433,** 91-97.

Zagotta, W.N., Hoshi, T., Dittman, J., and Aldrich, R.W. (1994). *Shaker* potassium channel gating transitions in the activation pathway. *J. Gen. Physiol.* **103,** 279-319.

Zhang, H., Bhattachatjee, A., Hu, F., Zhang, M., Goswami, T., Wang, L., Wu, S., Berggren, P.O., and Li, M. (2000). Cloning of a T-type Ca2+ channel isoform in the insulin-secreting cells. *Diabetes*. **49,** 59-64.

Zhang, J.F., Ellinor, P.T., Aldrich, R.W., and Tsien, R.W. (1994). Molecular determinants of voltage-dependent inactivation in calcium channels. *Nature*. **372,** 97-100.

Zhu, X.R., Wulf, A., Schwarz, M., Isbrandt, D., and Pongs, O. (1999). Characterization of human Kv4.2 mediating a rapidly-inactivating transient voltage-sensitive K+ current. *Receptors Channels*. **6,** 387-400.

Zitron, E., Kiesecker, C., Luck, S., Kathofer, S., Thomas, D., Kreye, V.A., Ki, J., Katus, H.A., Schoels, W., and Karle, C.A. (2004). Human cardiac inwardly rectifying current Kir2.2 is upregulated by activation of protein kinase A. *Cardiovasc. Res.* **63,** 520-527.